



# University of HUDDERSFIELD

## University of Huddersfield Repository

Berberkic, Sanjin

Measurement of small signal variations using one-dimensional chaotic maps

### Original Citation

Berberkic, Sanjin (2014) Measurement of small signal variations using one-dimensional chaotic maps. Doctoral thesis, University of Huddersfield.

This version is available at <http://eprints.hud.ac.uk/id/eprint/23737/>

The University Repository is a digital collection of the research output of the University, available on Open Access. Copyright and Moral Rights for the items on this site are retained by the individual author and/or other copyright owners. Users may access full items free of charge; copies of full text items generally can be reproduced, displayed or performed and given to third parties in any format or medium for personal research or study, educational or not-for-profit purposes without prior permission or charge, provided:

- The authors, title and full bibliographic details is credited in any copy;
- A hyperlink and/or URL is included for the original metadata page; and
- The content is not changed in any way.

For more information, including our policy and submission procedure, please contact the Repository Team at: [E.mailbox@hud.ac.uk](mailto:E.mailbox@hud.ac.uk).

<http://eprints.hud.ac.uk/>

# **Measurement of Small Signal Variations Using One-Dimensional Chaotic Maps**

**Sanjin Berberkic**

**BEng, MSc**

**A thesis submitted to the University of Huddersfield  
in partial fulfilment of the requirements for  
the degree of Doctor of Philosophy**

**July 2014**

# Abstract

A novel electronic signal Measurement System (MS) based on one-dimensional chaotic maps (Logistic Map (LM) and Tent Map (TM)) has been developed, analysed and tested. Firstly, an in-depth theoretical analysis of each map was performed using MATLAB based computation, and the results demonstrated that the high sensitivity, to initial conditions, of each map was suitable for small signal change detection and measurement. A new 3D representation of chaos map output for varying initial input was also developed allowing the suitability of any one-dimensional chaotic map to be determined.

An electronic implementation of the chaotic maps, using low noise and low cost components was developed along with a feedback and a series based MS. The implementations were tested and the experimental results demonstrate a matching within  $\pm 1\%$ , between theory and the electronic implementations, both maps exhibiting behaviour identical to the theoretical maps, ranging from fixed point stability, periodicity and chaos.

Each map implementation was tested separately and as part of a complete MS and the results reveal that the proposed measurement technique can detect and measure input signals changes as low as  $5\ \mu\text{V}$  over a  $10\ \text{V}$  input range, which yields a greater resolution than a MS using an 20 bit Analogue to Digital Converter (ADC) over the same input range.

The main advantage of the presented MS is that the accuracy of the measurement is independent of the input range which is not the case with classical approach to

measurement based on conditioning circuitry followed by an ADC as the minimum detectable change is directly proportional to the input range.

# Acknowledgements

I would like to express my gratitude towards my main supervisor Peter Mather for helping me in bringing this work to a conclusion, his guidance and support during my research and particularly his help during the writing of this thesis are invaluable. I would also like to express my deepest appreciation to Violeta Holmes for helping me, not only during my Ph.D. but during all my studies at Huddersfield University. I would also like to thank Roger Bromley for all the interesting discussions about chaos and many other subjects.

Beside my supervisors, I have also had valuable help from Chris Daykin during countless laboratory sessions and from Paul Glendinning during my visits to Manchester University.

During all the time spent working on this thesis I had the chance of meeting and working with great people that helped me in numerous ways, in particular I would like to thank Maythem, Tim, Yousif and Hussam for being great colleagues and friends, Anthony and Karim for being great housemates and for all the fun we have had in the last 4 years.

Finally, I would like to thank my family for supporting me throughout all my studies; my sister Nadja for being my best friend, my father Alija for his financial support and for providing me with countless bottles of “Prangijaš”, my girlfriend Yasmine for supporting me when I needed her the most and my mother Jelena for being the best mother. This thesis is dedicated to them.

# Contents

Abstract.....	2
Acknowledgements.....	4
List of Figures.....	10
List of Tables .....	14
Glossary of Terms and Symbols.....	15
Acronyms.....	15
Symbols .....	16
1 Introduction.....	19
1.1 Background .....	19
1.2 Chaos and Measurement .....	20
1.3 Aims and Objectives .....	23
1.4 Original Work .....	24
1.5 Document Structure .....	26
2 Theory and Literature Review .....	27
2.1 Classic Methods of Measurement.....	27
2.1.1 Conditioning Circuitry.....	29
2.1.2 Data Acquisition .....	33
2.1.3 Measurement Method Summary.....	37
2.2 Chaos.....	38

2.3	Discrete One-dimensional Chaotic Maps .....	40
2.3.1	The Logistic Map.....	41
2.3.2	The Tent Map .....	49
2.3.3	The Bit Shift Map .....	52
2.3.4	Summary.....	54
2.4	Applied Chaos.....	55
2.4.1	Electronic Implementation of Chaos .....	55
2.4.2	Chaos in Cryptography .....	57
2.4.3	Chaos Based ADCs.....	58
2.4.4	Chaos Based Measurement System .....	62
2.5	Lyapunov Exponent .....	63
2.5.1	Lyapunov Exponent Estimation .....	65
2.6	Conclusion .....	67
3	Proposed Signal Measurement Technique.....	69
3.1	Quantifying Input Signal Change .....	72
3.1.1	Measurement Errors.....	75
3.2	System with Feedback .....	84
3.2.1	System with Feedback Experimental Setup .....	84
3.3	Series System .....	86
3.3.1	Series System Experimental Setup .....	86
3.4	Conclusion .....	87

4	Measurement System Implementation .....	90
4.1	One-Dimensional Maps Implementation .....	90
4.1.1	Logistic Map Implementation.....	90
4.1.2	Tent Map Implementation .....	95
4.2	Measurement System Implementation.....	99
4.2.1	Feedback System Implementation .....	99
4.2.2	Series System Implementation .....	103
4.3	Conclusion .....	104
5	Performance Analysis of Implemented Chaotic Maps .....	106
5.1	Transfer Characteristic .....	107
5.2	Logistic Map Transfer Characteristic .....	108
5.3	Tent Map Transfer Characteristic .....	109
5.4	Bifurcation Diagram .....	110
5.4.1	Logistic Map Bifurcation Diagram.....	110
5.4.2	Tent Map Bifurcation Diagram .....	112
5.5	Time Series .....	113
5.5.1	Logistic Map Time Series.....	114
5.5.2	Tent Map Time Series .....	115
5.6	Lyapunov Exponent .....	116
5.6.1	Logistic Map Lyapunov Exponent .....	118
5.6.2	Tent Map Lyapunov Exponent .....	119

5.7	Noise Measurement.....	121
5.7.1	Logistic Map Noise Measurement.....	123
5.7.2	Improved Logistic Map Implementation .....	126
5.7.3	Tent Map Noise Measurement.....	131
5.8	Conclusion .....	132
6	Measurement System Results .....	133
6.1	Divergence Between Two Signals .....	134
6.1.1	Logistic Map.....	134
6.1.2	Tent Map.....	141
6.2	Divergence Against Input Signal Range .....	145
6.2.1	Logistic Map.....	145
6.2.2	Tent Map.....	146
6.3	Divergence Against Input Signal Change .....	147
6.3.1	Logistic Map.....	148
6.3.2	Tent Map.....	149
6.4	Conclusion .....	150
7	Discussion.....	152
8	Conclusion and Further Work .....	156
8.1	Conclusion .....	156
8.2	Further Work.....	158
	References.....	159

Appendices .....	166
List of Appendices:.....	166
Appendix A.....	167
Appendix B.....	168
Appendix C.....	171
Appendix D.....	175
Appendix E.....	184
Appendix F.....	186
Appendix G.....	214
Appendix H.....	216

# List of Figures

Figure 1-1 Simplified Block Diagram of a Chaos Based MS .....	23
Figure 2-1 Block Diagram of the Elements Composing a Measurement System .....	27
Figure 2-2 Equivalent Input Noise Voltage of a TL071 Operational Amplifier (Texas-Instruments, 2005).....	32
Figure 2-3 Analogue Signal Sampled Using 4 bit and 5 Bit ADCs .....	34
Figure 2-4 Undetected Input Signal Variations Due to Limited ADC Resolution.....	36
Figure 2-5 Transfer Characteristic of the Logistic Map .....	42
Figure 2-6 Computed Bifurcation Diagram of the Logistic Map .....	43
Figure 2-7 Bifurcation Diagram of the Logistic Map from $r = 3.4$ to $r = 3.5$ .....	44
Figure 2-8 Bifurcation Diagram of the Logistic Map from $r = 3.5$ to $r = 3.6$ .....	45
Figure 2-9 Bifurcation Diagram of the Logistic Map for $r = 3.8$ to $r = 3.9$ .....	45
Figure 2-10 Behaviour of the Logistic Map for Different Values of $r$ .....	46
Figure 2-11 Sensitivity to Initial Conditions of the Logistic Map For A $10^{-4}$ Change.....	48
Figure 2-12 Sensitivity to Initial Conditions of the Logistic Map For A $10^{-7}$ Change.....	48
Figure 2-13 Sensitivity to Initial Conditions of the Logistic Map For A $10^{-15}$ Change.....	49
Figure 2-14 Tent Map Transfer Characteristic .....	50
Figure 2-15 Tent Map Bifurcation Diagram.....	51
Figure 2-16 Bit Shift Map Transfer Characteristic .....	53
Figure 2-17 High Sensitivity to the Initial Conditions of the Bit Shift Map .....	54

Figure 2-18 Working Principle of the ADC Based on the Bit Shift Map.....	59
Figure 2-19 Tent Map Based ADC.....	60
Figure 2-20 Variation of the Lyapunov Exponent for the Logistic Map.....	64
Figure 2-21 Lyapunov Exponent Estimation Using the Prediction Error Method.....	66
Figure 3-1 Flowchart of the 3D Divergence Graph.....	70
Figure 3-2 Sensitivity to Initial Conditions of the Logistic Map for $r=4$ .....	71
Figure 3-3 Divergence of the TM for the Entire Input Range.....	72
Figure 3-4 LM divergence Graph With Set Threshold for a $\Delta$ of 0.0001.....	73
Figure 3-5 Divergence Between Two Samples.....	74
Figure 3-6 $\Delta$ Estimation Error.....	77
Figure 3-7 Two Inputs with Identical Output Values.....	78
Figure 3-8 Two Identical Time Series From Two Different Inputs.....	78
Figure 3-9 Number of Nulls for Different Values of $N$ .....	80
Figure 3-10 Width of a Null for an Input Change of $100\mu V$ .....	80
Figure 3-11 Delta Estimation Error Against Number of Iterations.....	81
Figure 3-12 Delta Estimation Error VS Amount of Divergence for Different $\Delta$ .....	83
Figure 3-13 Delta Estimation Error for Different Values of the Parameter $\mu$ .....	83
Figure 3-14 Block Diagram of the Presented Iterated System.....	85
Figure 3-15 Series System Block Diagram.....	87
Figure 4-1 Block Diagram of the LM Implementation.....	92
Figure 4-2 Simplified Schematic of the Modified LM.....	93
Figure 4-3 Block Diagram of the TM Implementation.....	96
Figure 4-4 Construction of the TM Transfer Characteristic.....	97
Figure 4-5 Schematic of the Proposed Implementation of the TM.....	97
Figure 4-6 Schematic of the Feedback System for Map Iteration.....	102

Figure 4-7 Control Signals for the Iterated Measurement System .....	102
Figure 4-8 Block Diagram of the Series System .....	104
Figure 5-1 Transfer Characteristic Measurement Setup.....	107
Figure 5-2 Measured VS Theoretical Logistic Map Parabola.....	108
Figure 5-3 Measured VS Theoretical Tent Map Characteristic.....	109
Figure 5-4 Measured Bifurcation Diagram of the LM .....	111
Figure 5-5 Computed LM Bifurcation Diagram.....	112
Figure 5-6 Tent Map Experimental Bifurcation Diagram .....	113
Figure 5-7 Logistic Map Experimental Time Series .....	115
Figure 5-8 Tent Map Experimental Time Series .....	116
Figure 5-9 Logistic Map Time Series for $r = 3.35$ .....	117
Figure 5-10 Prediction Error for a Non-Chaotic Time Series .....	117
Figure 5-11 Estimation of the Lyapunov Exponent From the Prediction Error .....	118
Figure 5-12 Tent Map Lyapunov Exponent Estimation .....	120
Figure 5-13 Measured Noise Floor of the HP 3562A DSA.....	122
Figure 5-14 Measured Noise of the LM .....	125
Figure 5-15 One-Quadrant Precision Analogue Multiplier .....	127
Figure 5-16 Noise of the One-Quadrant Multiplier .....	129
Figure 5-17 Simplified Schematic of the Improved LM .....	129
Figure 5-18 Noise of the Improved LM .....	130
Figure 5-19 Noise of Previous Implementation VS Improved Implementation.....	130
Figure 5-20 Noise of the TM Implementation.....	131
Figure 6-1 Time Series and Divergence for a $500\mu\text{v}$ Change. ....	135
Figure 6-2 Divergence for Two Different Input Changes. ....	136
Figure 6-3 LM Multiple Runs for a Fixed Input.....	138

Figure 6-4 Use of the “Noise Band” to Measure the Sensitivity of the LM.....	138
Figure 6-5 Multiple Time Series For Different Input Samples .....	140
Figure 6-6 Noise Band at Iteration 8 for Different Input Samples .....	141
Figure 6-7 Divergence Between Two Time Series With a 200 $\mu$ V Change .....	142
Figure 6-8 Experimental Divergence of the LM for a Change of 500 $\mu$ V: (a) and (b) for the Entire Input Range. (c) and (d) for a Range Limited to 0.1-0.9.....	146
Figure 6-9 Experimental Divergence of the TM for a 200 $\mu$ V Change for the Entire Input Range.....	147
Figure 6-10 Logistic Map Divergence VS Change .....	149
Figure 6-11 Measurement Error VS Change for the Series Implementation of the TM Based MS .....	150

# List of Tables

Table 5-1 Estimated and Theoretical Lyapunov Exponent for the LM.....	119
Table 5-2 Estimated and Theoretical Lyapunov Exponent for the TM.....	120
Table 5-3 Equivalent Noise Bandwidth Coefficient.....	123
Table 5-4 Noise for Components Used in the LM Implementation. ....	125
Table 6-1 Practical and Computed Divergence .....	137
Table 6-2 TM Change Measurement with Feedback System.....	143
Table 6-3 TM Change Measurement with Series System .....	144
Table A-1 Signal Change Estimation Error.....	167
Table A-2 Identical Time Series For Two Different Input Values.....	167

# Glossary of Terms and Symbols

## Acronyms

$\mu\text{C}$	Microcontroller
1D	One Dimensional
1Q	One Quadrant
3D	Three Dimensional
ADC	Analogue to Digital Converter
BSM	Bit Shift Map
BZ	Belousov–Zhabotinsky
CMOS	Complementary Metal Oxide Semiconductor
CSV	Comma-Separated Values
DAQ	Data Acquisition Device
DSA	Dynamic Signal Analyser
FPGA	Field Programmable Gate Array
FSR	Full Scale Range
GPIB	General Purpose Interface Bus
IC	Integrated Circuit
LCD	Liquid Cristal Display
LE	Lyapunov Exponent
LM	Logistic Map
LPF	Low Pass Filter
LSB	Least Significant Bit

MS	Measurement System
Op-amp	Operational amplifiers
PLL	Phase Lock Loop
ppm	parts per million
rms	root mean square
S/H	Sample and Hold
SD	Spectral Density
SS	Spread Spectrum
TM	Tent Map
USB	Universal Serial Bus

## Symbols

$\alpha$	Position of a potentiometer
$\Delta$	Difference between two input signals
$\delta$	Divergence between two time series at a given iteration
$\lambda$	Lyapunov exponent
$\mu$	Parameter of the Tent Map
$\sigma$	Parameter of the Bit Shift Map
$\varphi$	Parameter of a chaos map
A	Analogue input signal
B	Noise bandwidth
b	Binary number
D	Digital output signal
<b>D</b>	Number of Nulls in section 3.1

$E$	Thermal noise voltage
$f$	Function
$f'$	Derivative
$f_{\text{high}}$	Highest frequency
$f_{\text{low}}$	Lowest frequency
$f_{\text{Nyquist}}$	Nyquist frequency
$f_{\text{OverSampling}}$	Sampling rate required for oversampling
$K$	Noise bandwidth coefficient
$k$	Boltzmann constant
$k$	Number of time steps used for the estimation of the Lyapunov Exponent in section 2.5
$M$	Resolution of an ADC
$N$	Number of possible digital values of the output of an ADC
$Q$	Voltage step size (LSB)
$R$	Resistor
$R$	Chaos map input range in section 3.1
$r$	Parameter of the Logistic Map
$Ref$	Reference voltage
$T$	Absolute temperature
$V$	Voltage
$V_{\text{FSR}}$	Full scale voltage of the input of an ADC
$V_{\text{in}}$	Input voltage
$V_n$	Voltage noise
$V_{\text{out}}$	Output voltage

$V_{\text{refHI}}$	Highest analogue value and the input of an ADC
$V_{\text{refLOW}}$	Lowest analogue value at the input of an ADC
$x_n$	State of a chaos map at iteration n
$y^n$	Starting point of Lyapunov exponent calculation
$y^{nn}$	Closest neighbour of the point $y^n$

# 1 Introduction

## 1.1 Background

Measurement of physical quantities is essential in the majority of technical devices as almost every electronic system requires the magnitude of one or more parameters to be determined in order to perform specific tasks. The quantity and quality of signal measurement required for systems have grown drastically with the advance of technology. For example, modern cars, although performing the same task as the older models are fitted with an increasing number of sensors to enhance user comfort and safety; the measured parameters can range from critical; engine temperature, collision detection and oil level to less critical; ambient temperature and seat position. For some applications, the improvement in measurement quality (accuracy, precision) represents the main factor to the overall system performance; this can be the case in pollutant, earthquake or explosive detection etc., where the sensitivity and accuracy of a system is critical.

In order to measure any physical variable a Measurement System (MS) is required. With the increasing need for high accuracy systems, the ability to detect small amplitude changes of a given parameter has become a key factor. Low level signal parameter change measurement is challenging due to practical limitations such as interferences from external sources, sensor limitations, in terms of accuracy, and other errors inherent to the electronic circuitry (limited resolution, noise generated by the components).

As MS are designed to achieve improved performances in terms of sensitivity and accuracy, the overall complexity of the system is increased which generally increases the overall cost. In a classical approach to a MS, the physical quantity being measured is converted to a proportional electric signal (voltage or current) and adapted to a given system value range before being digitalised using an Analogue to Digital Converter (ADC). This general method gives satisfactory results in the majority of cases but becomes inefficient when small input signal changes have to be detected over a large input range, as the minimum detectable change is directly proportional to the resolution of the ADC being used. This means that higher resolutions ADCs which are generally more expensive are required to determine small parameter changes thus increasing the overall cost of the system. To palliate the loss of resolution with increased input signal range, a specific MS has to be used with resolution independent from the input range. In this thesis, a chaos based MS has been developed and tested for the purpose of eliminating the need for expensive ADCs when a small change of input signal has to be detected over a large input range.

## **1.2 Chaos and Measurement**

Chaos as a means of measurement is generally perceived to be counterintuitive as the essence of chaos is the inability to predict the future state of a system with absolute certainty. Starting from the second half of the 20<sup>th</sup> century the study of chaos has brought a new insight on a phenomenon that was long believed to be random uncorrelated variations (noise), namely the high sensitivity to initial conditions. The phenomenon was observed in various fields ranging from economics: the evolution

of cotton prices, biology: the evolution of population of foxes and meteorology: the evolution of weather conditions (G.L.Baker and J.P.Gollub, 1990).

The high sensitivity to initial conditions was first mentioned by French mathematician Henri Poincaré in 1890; while studying a three-body problem where the motion of three bodies has to be determined at any particular point in time from initial data (individual mass, position and velocity). Poincaré showed that the motion of the bodies is highly sensitive to initial conditions. The significance of this discovery remained unnoticed until 1961 when the mathematician and meteorologist Edward Lorenz observed a similar phenomenon while running weather prediction algorithms on a computer (Gleick, 1988). After evaluating a weather prediction model for many hours, Lorenz wanted to confirm the results by rerunning the simulation, but in order to shorten the time required for the simulation Lorenz entered a result from a printout table from the middle of the original dataset. Limiting the result to three decimal places, Lorenz assumed that the rounding error would be insignificant. The results obtained from the second run were at first similar to the initial simulation before diverging completely. Lorenz then realised that the weather prediction model was highly sensitive to initial conditions and that a small change between two starting conditions produced, after a number of iterations, completely different results. This discovery changed meteorology as Lorenz concluded that accurate weather prediction for long periods of time is subsequently impossible. The impact of his discovery wasn't limited to meteorology, but also influenced other scientific fields where similar phenomena were observed and led to the creation of a new science named: "*chaos theory*" (Ingraham, 1991). Sometimes referred to as the "butterfly effect", this phenomenon is the main feature of chaotic systems. The name of the phenomenon came from the title of a talk given

by Edward Lorenz in 1972: “*Does the flap of a butterfly’s wings in Brazil set off a tornado in Texas?*” (Lorenz, 1972).

As opposed to stochastic (non-deterministic) systems where the behaviour is randomly affected by external forces (noise), the behaviour of a chaotic system is deterministic and is part of its inherent dynamics. What may appear as noise is in fact following simple rules yet exhibiting complex behaviour. Contrary to a stochastic process where the following data cannot be predicted but only guessed using statistical analysis, the following data of a chaotic system can be predicted and the accuracy of the prediction can be infinite if the initial values of the chaotic system are known with infinite accuracy. To relate that to the weather models used in meteorology, the weather could be accurately predicted for years if the model and the initial data used (i.e. temperature, wind speeds, pressure etc.) were infinitely accurate with infinite number of points (Ingraham, 1991).

In this work the fundamental idea is to reverse the process of the high sensitivity to initial conditions and use simple mathematical expressions which exhibit chaotic behaviour to measure small variation of input signals. If a small change of starting conditions produces a large change at a later stage, the process can be reversed and the large change at a given time can be used to accurately determine a small change in the starting conditions.

The simplified block diagram in Figure 1-1, shows how a chaos based MS can be structured. The physical variable is first converted into a usable electric signal before being fed to a chaotic map, which takes advantage of the high sensitivity to initial conditions to detect small variations of the input signal. This enables the MS to detect small variations of the physical quantity being measured.

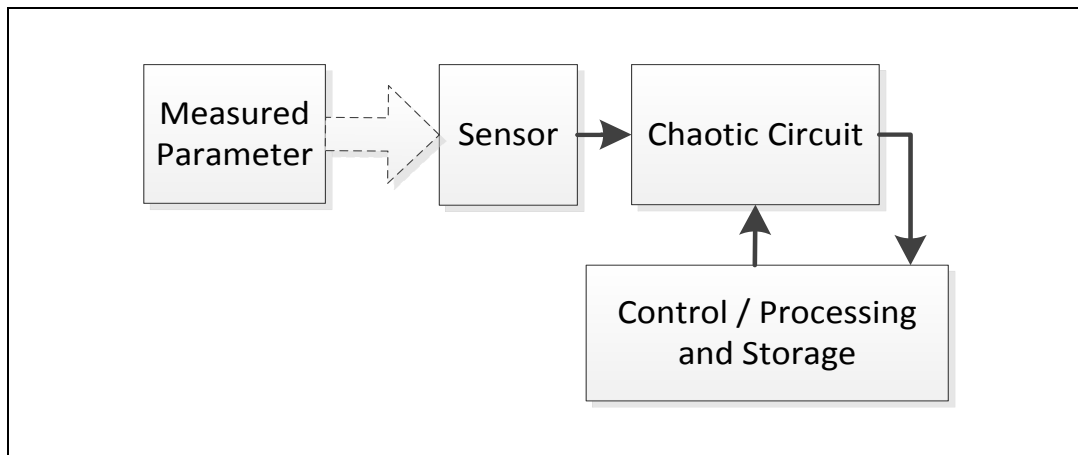


FIGURE 1-1 SIMPLIFIED BLOCK DIAGRAM OF A CHAOS BASED MS

The simplest mathematical models exhibiting chaotic behaviour are referred to as chaotic maps. Chaotic maps have been implemented electronically for various applications such as; practical approach to the study of chaotic phenomena, cryptography and algorithmic ADCs. Chaotic maps can be multidimensional or One-Dimensional (1D); all maps exhibit high sensitivity to initial conditions with the main difference being the number of parameters defining the map. Single parameter (1D) chaotic maps are ideal for electronic implementation due to the general simplicity of the circuitry required to implement the maps resulting in lower overall cost and reduced inherent system noise.

### 1.3 Aims and Objectives

The aim of the present work was to analyse, design, implement and assess a chaos based MS that can detect and measure small electric signal changes independently of the input range. The objectives fulfilled during this work were as follow:

- **Identify the suitable chaotic function to be implemented as part of a MS**

One-dimensional (1D) chaotic maps were analysed using computation. The possible use of the chaotic maps for signal measurement was evaluated with MATLAB

simulation and a method to quantify the input signal change was proposed for two chaotic maps: Logistic and Tent Map.

- **Implement the chaotic functions and compare the characteristics with theory**

The two selected chaotic maps were implemented electronically: although some electronic implementations of one-dimensional chaotic maps are available in literature (Campos-Cantón et al., 2009, Eguchi et al., 2000, Suneel, 2006) the proposed implementations were designed for this specific application in order to reduce the noise and obtain a viable MS by increasing the sensitivity of the system. The electronic implementations performance characteristics were compared with those of the theoretical maps to ascertain the accuracy and correlation between the theory and the practical implementations.

- **Build the MS and assess the performance**

A new method of signal measurement using chaotic maps was proposed. The performance of the designed MS was assessed and the maps were compared to find the solution that produces the most advantageous performance in terms of signal detection and measurement.

## **1.4 Original Work**

The fundamental basis of the work presented in this thesis is original and has led to a patent application: British Patent Application n° 1309585.4. The main areas of original contribution are:

- Analysis of the high sensitivity to initial conditions of two 1D chaotic maps with the use of MATLAB computation software.
- A novel three-dimensional (3D) representation of the divergence between two closely located starting conditions, for the entire input range of 1D chaotic maps has been developed. This will enable the high sensitivity of any 1D chaotic map to be analysed. The MATLAB code developed for this purpose can be used for any further work associated with the “*butterfly effect*” of 1D chaotic maps. The use of the developed 3D representation is not limited to measurement and electronics as the high sensitivity to initial conditions is present in many fields such as neurology, meteorology and biology.
- New electronic implementations of the two selected 1D chaotic maps, specifically designed for the measurement of small signal variations, have been developed, characterised and optimised. The proposed circuit implementations could also be used for any application requiring chaotic behaviour.
- Two topologies of the measurement system have been proposed with the associated hardware and software and the differences between the two methods were assessed.
- A means of detecting or quantifying the magnitude of input signal change was proposed for each map. Two methods were developed; a calibration method for the Logistic Map and a mathematical method for the Tent Map.

## 1.5 Document Structure

This document is structured in the following manner:

- In the second chapter the classical method of measurement is presented and the main sources of error are identified, this is then followed by an introduction to chaos, one dimensional chaotic maps and high sensitivity to initial conditions of chaotic systems. Methods and techniques used to identify actual chaotic behaviour are introduced, finally the chapter is concluded with the application of chaos in electronics in general and particularly in ADCs and measurement systems.
- The 3<sup>rd</sup> chapter explains the proposed technique for the realisation of a novel measurement system which utilises the high sensitivity to initial condition associated with chaotic systems.
- Following the explanation of the proposed signal measurement technique, the 4<sup>th</sup> chapter focuses on the implementation of the chaotic one-dimensional maps and the chaos based measurement system.
- Chapter 5 assesses the electronic implementations developed in the previous chapter by comparing practical results with theoretical behaviour of each map.
- In chapter 6 the measurement capability of the proposed MS is evaluated with practical measurements in order to assess the overall performance.
- Finally the results obtained in chapters 5 and 6 are discussed in chapter 7
- In the last chapter the author suggests some possible further work followed by a conclusion about the overall achievements.

# 2 Theory and Literature Review

The traditional techniques used to measure physical quantities are initially presented, followed by the main sources of errors associated with Measurement Systems (MS). An introduction to “chaos” is then presented followed by One-Dimensional (1D) chaotic maps and the techniques used to evaluate whether the behaviour achieved in a practical system is truly chaotic. Finally, a review of chaos applied in electronics, communications and Analogue to Digital Converters (ADC) is presented.

## 2.1 Classic Methods of Measurement

The typical MS is generally composed of several elements in order to convert a physical variable into a measured value that can be displayed or utilised by an electronic system, as shown in Figure 2-1 (Dyer, 2001, Morris, 2001).

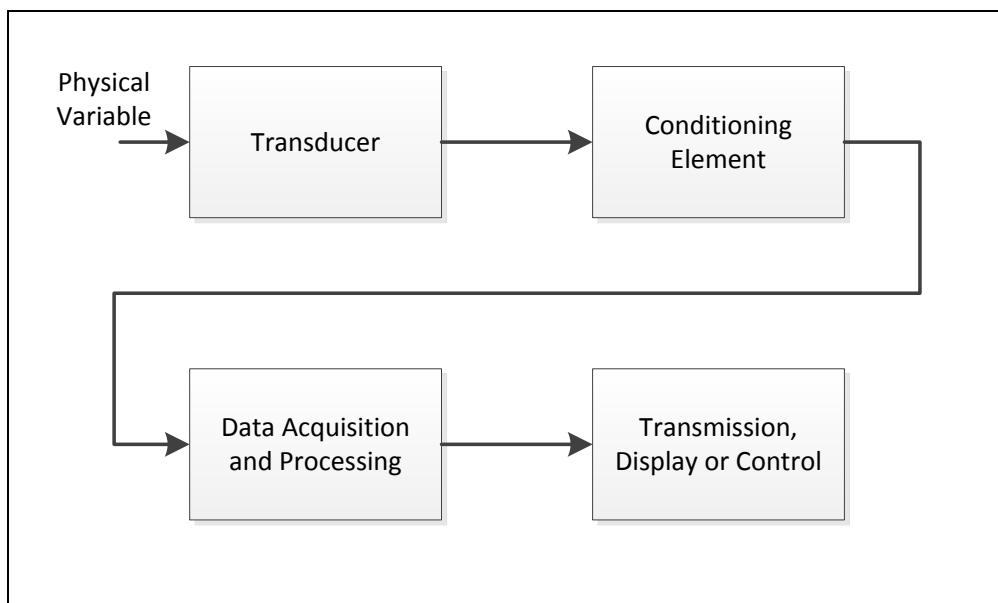


FIGURE 2-1 BLOCK DIAGRAM OF THE ELEMENTS COMPOSING A MEASUREMENT SYSTEM

- Transducer: common to most MSs, usually generates an analogue output proportional to the physical parameter being measured; covered by the following definition. A transducer is a device which provides a usable output in response to a specific physical quantity (Norton, 1969). Some examples of transducers are: Piezoelectric sensors for vibration measurement, Hall Effect sensors for magnetic field measurement, thermocouple probes for temperature measurement, ultra sound sensors for distance measurement etc. Transducers are an essential part of a MS as the physical parameter being measured has to be converted to an electric signal before undergoing conditioning (Morris, 1993, Neubert, 1975).
- Variable conditioning element: adapts the signal provided by the transducer to a suitable format, for example the Piezoelectric transducer generates an electrical charge in response to mechanical movement, the electric charge cannot be displayed directly, used to control a system or stored in memory. Thus, the charge has to be conditioned / converted to a proportional voltage or a current that can be exploited by the following stage of the MS. The conditioning circuitry is generally specifically designed for a given transducer (Morris, 2001).
- Data acquisition and processing: in most modern MS the data obtained from the conditioning circuitry is converted into a digital format. This allows the data processing, display and storage with the use of Microcontrollers ( $\mu\text{C}$ ) or computers (Schmid, 1970). In order to convert the signal from the analogue to the digital domain the quantisation is performed by an Analogue to Digital Converter (ADC). ADCs are mainly characterised by resolution which can range from 1-bit to more than 30 bits. The resolution of the ADC indicates

the number of discrete values (digital values) it can produce over the range of analogue values which means that the accuracy of the MS is dictated by the resolution of the ADC as any variations lower than one digital step of the ADC will be undetectable by the MS (Morris, 2001, Dyer, 2001).

- Transmission, display or control: once the data is processed, the system can either transmit the data, display for direct visualisation, store, or control a variable in the case of a control system. The practical limit of sensitivity for any MS is determined by specific factors such as the sensor sensitivity, the intrinsic noise of the circuitry and the resolution of the ADC used for the digitalisation of the signal (Morris et al., 2012).

The performances of the transducers are inherent to the construction of the transducer and are generally independent of the other sections of the MS such as the conditioning circuitry and the ADC. The transmission, display or control section doesn't influence the overall performance of the MS as no additional information is created during that process where the information is transmitted in order to be accessible to the user or used to control a system. The following sections will discuss the parts of the MS that affect the performance of the MS to detect small variation of the input signal, this will be followed by a discussion on the conditioning circuitry and the limits to measurement set by the noise which is inherent in all electronic circuitry used for signal conditioning, followed by the limitations of the ADC.

### **2.1.1 Conditioning Circuitry**

The conditioning circuitry, as defined in the previous section is used to adapt the signal originating from a transducer to a format that can be digitalised by an ADC. The signal is converted to a voltage with a range scaled to the input range of the

ADC used within the MS. The conditioning circuitry inevitably adds noise and errors to the analogue signal which limits the overall MS performance as data can be corrupted by the noise. For this reason, the conditioning circuitry requires rigorous design and the use of high performance, low noise components adapted to the required performance of the MS. In many applications the conditioning circuitry is composed of amplifiers, with each component generating inherent noise, which in turn reduces the performance of the MS. The theoretical limit for a MS in terms of performance is set by the thermal noise of the resistors used in the circuit (Keithley-Instruments, 2004, Lax et al., 2006) as any signal variation lower than the thermal noise will be below the noise floor and therefore undetectable by the system. It is important to avoid the use of high value resistors (R) as the root mean square (rms) thermal noise voltage (E) is determined by the expression (2-1) known as Johnson noise (Horowitz and Hill, 1989) so that for a given temperature, the thermal noise is proportional to the value of the resistor.

$$E = \sqrt{4kTRB} \quad (2-1)$$

Where k is the Boltzmann's constant ( $1.38 * 10^{-23}$ J/K ), T is the absolute temperature in Kelvin (K) and B is the noise bandwidth in Hz.

Although, the theoretical measurement limit of any physical parameter is set by the thermal noise the main source of noise in most circuitry is generally due to the active components such as Operational amplifiers (Op-amps). Op-amp noise is determined by three main components: shot (current) noise, voltage noise, and thermal noise (Texas-Instruments, 2009, Horowitz and Hill, 1989). The shot and voltage noise are

specific to a particular Op-amp model, whilst the thermal noise is set by the resistors used to set the gain of the Op-amp.

- Current noise: current noise is converted to voltage noise when flowing through a resistor. Ideally, to minimise the effects of current noise the source resistors should be kept to a low value. An Op-amp with low voltage noise can have a high current noise which can generate proportionally more noise if the source impedance is not minimised.
- Voltage noise: Input voltage noise is bandwidth dependent and measured in  $\text{nV}/\sqrt{\text{Hz}}$ . The voltage noise is always referred to the input which means that the noise is multiplied by the Op-amp gain. The voltage noise dominates in most cases where the source impedance is low as the thermal noise and current noise will be negligible in comparison.
- Source resistors: The resistors connected to the Op-amp generally contribute significantly to the overall noise content. The first component is the Johnson noise of the resistor as shown in expression (2-1), and secondly the resistor can generate additional noise through the conversion of the Op-amp current noise to voltage noise, which can dominate the overall noise value if the impedance of the resistor is high.

The characteristic of the Op-amp noise (this is the case for voltage noise and current noise) is composed of two main sections; a flat region where the noise is constant over frequency, this region is referred to as white noise region and a region where the noise is inversely proportional to the square root of the frequency, commonly referred to as  $1/f$  noise. The main characteristic of interest in Figure 2-2 is the ‘corner’ frequency where the  $1/f$  noise and the white noise are equivalent. Thus it

can be observed that for frequencies lower than the corner frequency the overall noise is dominated by 1/f noise and above by the thermal noise. A lower corner frequency means that the Op-amp has lower overall noise; this is typically the case for low frequency applications.

The graph in Figure 2-2 represents the equivalent voltage noise at the input of the TL071 Op-amp (Texas-Instruments, 2005); this allows the noise at the output of any Op-amp based amplifier to be calculated by multiplying the noise for a given bandwidth by the gain of the Op-amp.

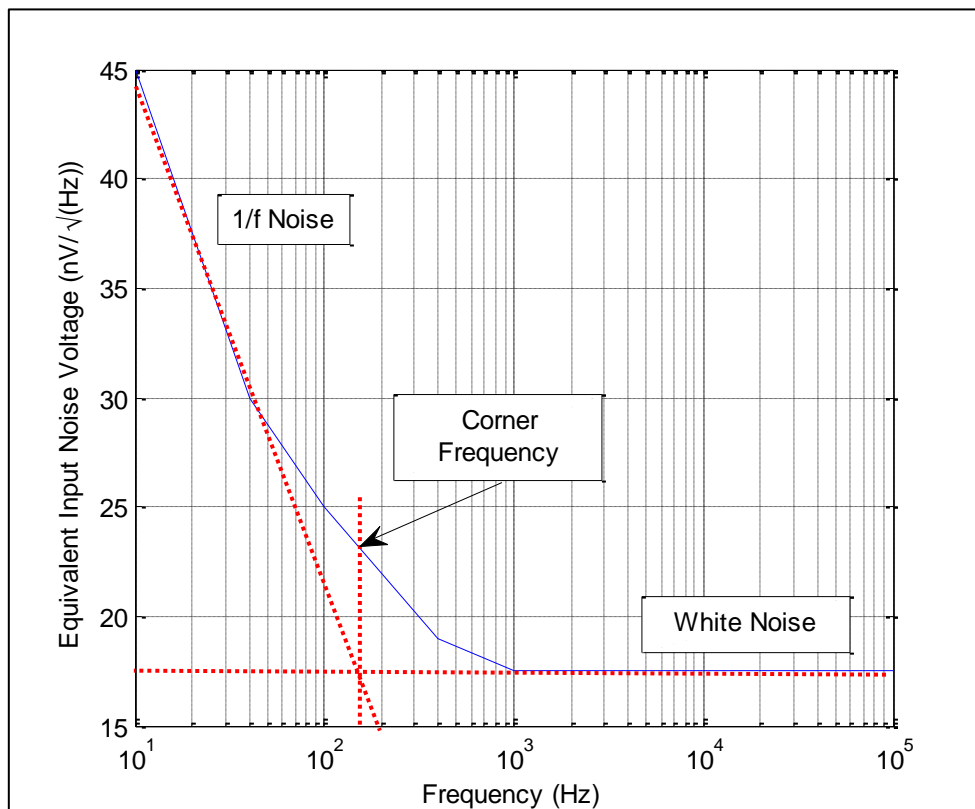


FIGURE 2-2 EQUIVALENT INPUT NOISE VOLTAGE OF A TL071 OPERATIONAL AMPLIFIER (TEXAS-INSTRUMENTS, 2005)

All sources of noise present at the output of the conditioning circuitry are referred to as the ‘noise floor’; which is the overall inherent noise, thus any input signal above the noise floor can be identified and conversely any input signal below the noise floor (lower amplitude) will be concealed by the noise, which will make the

measurement challenging as the system will be unable to differentiate between the noise and the signal.

In addition to noise, other errors are created by the conditioning circuitry such as offset voltages, offset voltage drifts or gain errors. Just as noise, the offsets are generally specified in the datasheets of different Op-amps and the use of low offset Op-amps is required for high accuracy MS. To maintain a low gain error, the common practise is to use resistors with minimal tolerance and/or trimming potentiometers.

The gain of amplifiers composing the conditioning circuitry should be set to match the ADC input range whilst avoiding over amplification, which can lead to additional errors (saturation of the amplifier or a signal out of the ADC input range)

As identified in this section, the conditioning circuitry is a critical part of any MS and requires careful design in order to minimise the noise and errors introduced by different components. The next element that composes the classic MS is the data acquisition which will be discussed in the following section.

### **2.1.2 Data Acquisition**

The data acquisition is an essential element of the MS as the analogue signal has to be converted to digital data in order to allow processing. The data quantisation is generally performed using an Analogue to Digital Converter (ADC). The ADC is used to convert analogue signals to discrete time digital values, thus the overall accuracy of the MS is highly dependent of the ADC performance (Razavi, 1995). An ADC produces a digital output  $D$ , as a function of the analogue input  $A$  as shown by expression (2-2).

$$D = f(A) \quad (2-2)$$

Whilst the input can take an infinite number of values within the specified input range of the ADC, the output of the ADC is limited to a restricted number of digital values (codes) set by the resolution of the ADC. Thus an ADC must convert each input value to an output code which is an approximation of the input. The ADC conversion of an analogue signal is illustrated in Figure 2-3 (Plassche, 1994), where the input voltage is sampled using a 4 bit and a 5 bit ADC. Due to the higher resolution, the 5 bit ADC has a lower voltage step ( $Q$ ) as defined by expression (2-3), which allows a more accurate representation of the input signal. Figure 2-3 also shows that a greater ADC resolution (number of bits) will yield a more accurate digital representation of the analogue input signal.

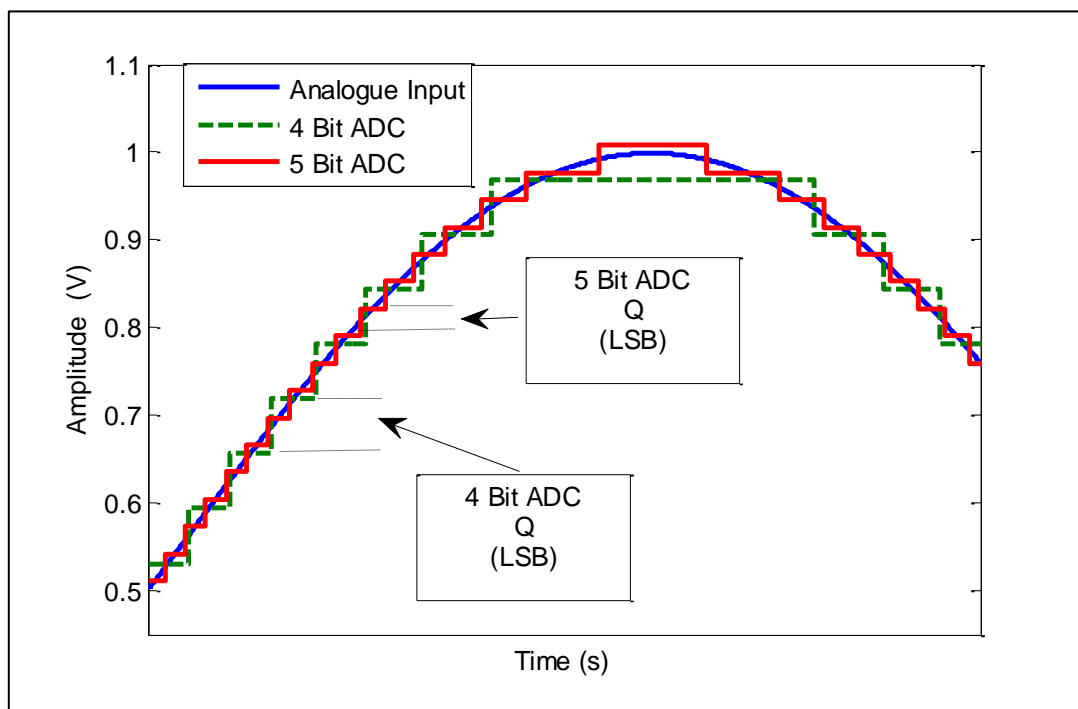


FIGURE 2-3 ANALOGUE SIGNAL SAMPLED USING 4 BIT AND 5 BIT ADCS

The accuracy of an ADC is directly linked to the voltage step  $Q$ , which is the minimal voltage change required at the input of the ADC for the output to change by

1 binary value, known as the Least Significant Bit (LSB). The voltage step can be calculated using expression (2-3) and illustrated in Figure 2-3.

$$Q = \frac{V_{FSR}}{N} \quad (2-3)$$

Where  $V_{FSR}$  is the Full Scale Range input voltage, determined by expression (2-4) and  $N$  is the number of digital values that the ADC output can take for a range of analogue values at the input and is defined by expression (2-5).

$$V_{FSR} = V_{refHI} - V_{refLOW} \quad (2-4)$$

Where  $V_{refHI}$  is the highest analogue value and  $V_{refLOW}$  the lowest analogue value at the input of the ADC.

$$N = 2^M \quad (2-5)$$

Where  $M$  is number of bits representing the resolution of the ADC.

For an ADC to detect an input signal change, and thus yield a digital output change, the value of  $Q$  needs to be of lower amplitude than the input signal change whilst ensuring that the  $V_{FSR}$  remains large enough for the given application. This can be an issue for high accuracy applications requiring extensive input ranges (Craig, 1995). Figure 2-4 illustrates this problem; a varying analogue signal is applied at the input of an ADC. In cases where the variations in the input signal are smaller than the  $Q$  of the ADC the output code generated by the ADC remains constant, which means that the MS is unable to detect the signal variations.

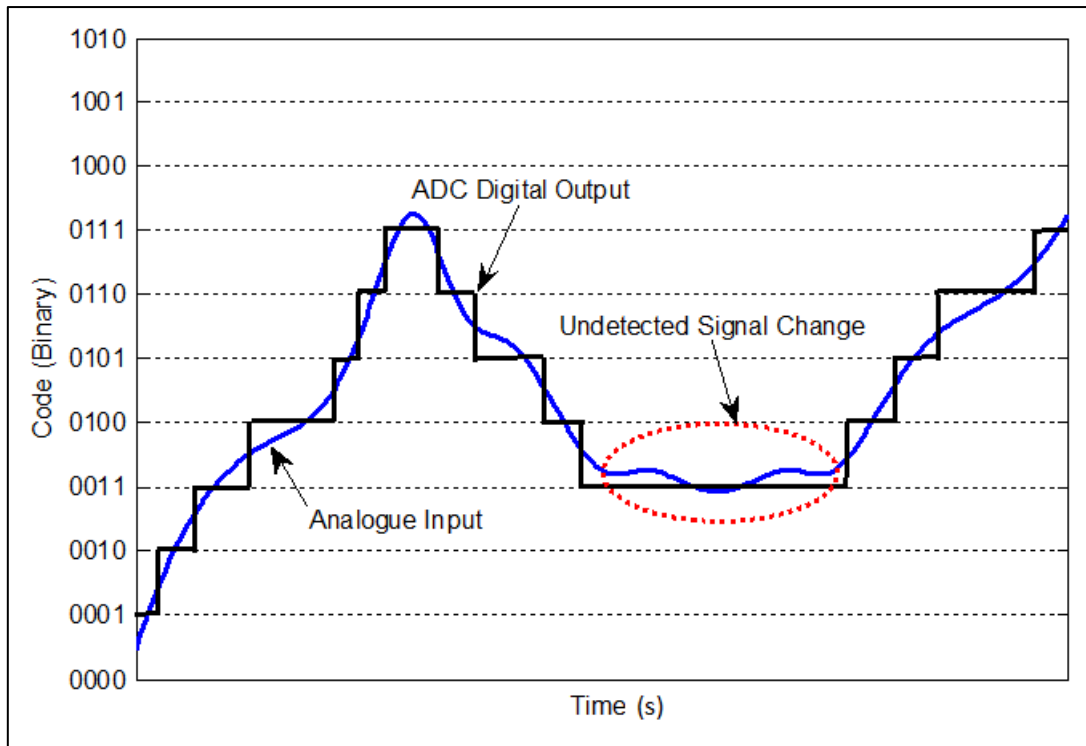


FIGURE 2-4 UNDETECTED INPUT SIGNAL VARIATIONS DUE TO LIMITED ADC RESOLUTION

The solution to this problem is to use an ADC with a higher resolution value which will increase the cost as the price is proportional to the resolution of the ADC which will also require resistors with lower tolerances and higher performance op-amps for the conditioning of the signal thus further increasing the price of the MS. The change of ADC often requires the redesign of the MS (hardware and/or software). Another possibility is the use of a techniques called oversampling that has been developed to increase the resolution of ADCs (ATMEL, 2005). This method involves taking multiple samples of the input signal to obtain an increased resolution via algorithms implemented in software. The main issue with the oversampling is the high penalty on the sampling rate, as a result the minimum sampling rate required for the over sampling technique is significantly higher than the Nyquist frequency as shown in expression (2-6).

$$f_{\text{OverSampling}} = 4^n \cdot f_{\text{Nyquist}} \quad (2-6)$$

Where  $n$  is the additional number of bit of resolution.

Additionally the input signal must contain enough noise to toggle the LSB of the ADC in order for the oversampling technique to work. In cases where the input signal is containing low level of noise; artificial noise must be added to the input signal which requires additional circuitry.

The problem of limited ADC resolution within a MS is further illustrated by the following example:

A MS equipped with a 10 Bit ADC used to detect a 0.1 mV change in the input signal over a voltage range of 0 V to 10 V. Applying expressions (2-5)  $N = 1024$ , which for a  $V_{FSR}$  of 10 V, yields a  $Q$  of 9.7 mV. In this case the ADC is unable to detect a 0.1 mV signal change as the minimum signal change required to modify the output of the ADC is 9.7 mV. Thus a 18 bit ADC is required.

### **2.1.3 Measurement Method Summary**

In the classic approach to MS the main sources of errors have been identified; in the conditioning circuitry, a particular attention should be given to the noise of each component in order to optimise the performance of the MS. Similarly, the selection of the ADC is paramount and the resolution of the ADC should be selected in relation to the amount of signal variation to be measured.

In cases where a MS, capable of detecting small variations over an extended input range is required, the use of a high resolution ADC is essential, which will

drastically increase the overall cost of the MS and in some cases require an unrealistically high resolution (>32 bit).

After highlighting the sources of errors associated with the conditioning circuitry and the limitations in terms of performance associated with the use of ADCs, the next section will introduce the subject of chaos and show where it has been implemented in electronic systems. Finally, the next section will also demonstrate how chaotic behaviour can be used in a MS as a means of detecting small signal variations over a large input range, thus addressing the issue of ADC resolution and input signal range previously identified.

## **2.2 Chaos**

Chaos behaviour can be observed in any nonlinear system that exhibits irregularity and unpredictability as well as high sensitivity to initial conditions commonly known as the “*butterfly effect*”(Ingraham, 1991). Although, being deterministic (non-random) and sometimes following simple equations chaotic systems can display complex behaviour which, significantly never repeats. Chaos can be observed in simple mechanical systems such as the motion of a pendulum, it also materialises everywhere in nature, from the turbulences of a water flow to the evolution of populations (Gleick, 1988). When studying dynamical systems in 1913 Henri Poincaré noted that in some cases a really small change in initial condition can produce a disproportionately large change at the output of the system, which makes prediction impossible as the initial conditions of a practical system can never be known with absolute accuracy (G.L.Baker and J.P.Gollub, 1990). Real interest in the subject of chaos started in 1963 with the publication by the meteorologist and

mathematician Edward Norton Lorenz of the paper called “*Deterministic Nonperiodic Flow*” in which the author shows a simplified convection model and concluded that the sensitivity to the initial conditions makes the long term weather prediction impossible (Lorenz, 1963).

The mathematical models with chaotic behaviour referred to as “*chaotic maps*” can be separated using two main criteria; the time domain (continuous or discrete) and the number of space dimensions (one, two or three dimensional).

Contrary to continuous maps where the evolution of the map is described using differential equations, discrete time maps are not continuous time functions and the solutions of the map can be calculated with the use of iteration, which makes the computation resource requirements significantly lower.

The number of dimensions of a chaotic map defines the number of parameters present within the map. From that aspect, one-dimensional (1D) maps are the simplest form of chaotic maps as only one parameter is used in the map which thus makes the calculation and implementation relatively simple.

Combining the two criteria of classification of chaotic maps, it can be concluded that the discrete 1D maps are more suited to electronic system implementation due to the ease of computation of discrete maps and the low complexity of single parameter 1D maps.

The next section will thus discuss three different 1D maps which have relatively simple structures and detail the behaviour of each.

## 2.3 Discrete One-dimensional Chaotic Maps

Discrete 1D chaotic maps also called 1D difference equations or 1D iterated maps are the simplest mathematical expressions that exhibit chaotic behaviour. For this reason 1D maps are often used in the study and application of chaos. 1D maps are mathematical expressions that model the evolution through iteration of a single variable. A typical one-dimensional map is of the form shown in equation (2-7).

$$x_{n+1} = f(\varphi, x_n) \quad (2-7)$$

Where  $x_n$  is the state of the system at iteration  $n$ ,  $x_{n+1}$  is the state of the system at iteration  $n+1$  and  $\varphi$  is a parameter which can vary from map to map and in some cases the value of which can lead the map to chaotic behaviour.

The relative simplicity of discrete 1D chaotic maps makes them an ideal means of applying chaos, thus discrete 1D maps have been implemented electronically to obtain means of practically studying chaos (Suneel, 2006, Campos-Cantón et al., 2009). Discrete 1D maps are also used in different fields, such as biology to describe biological systems; this is particularly the case for the Logistic Map (LM) which has been used as a discrete-time demographic model for population modelling in resource limited environments (May, 1976). In medicine, 1D chaotic maps have been used to model neurons as it has been shown that neurons can exhibit chaotic behaviour (Harth, Zeller et al., 1995). In chemistry, 1D maps have been used to analyse chemical reactions such as the Belousov–Zhabotinsky (BZ) reaction (R. H. Simoyi, 1982) or more recently as an abstract model for evolution (Usychenko, 2011). Discrete 1D maps have also been used in information processing systems such as artificial neural networks (Nozawa, 1992, Song et al., 2007), communication

encrypting where the high sensitivity to initial condition is exploited to encrypt data (Kocarev and Jakimoski, 2001, Martinez-Nonthe et al., 2012), electronic logic gates (Murali et al., 2005) and random number generation (Cristina et al., 2012, Kanso and Smaoui, 2009, Nejati et al., 2012, Luca et al.). All these applications show that discrete 1D maps are powerful tools used for modelling and information processing. More details about applied chaos are available in section 2.4.

In the following sections three commonly studied, discrete 1D chaotic maps are presented; the Logistic Map, the Tent Map and the Bit Shift Map. To analyse the behaviour of each chaotic map, two approaches were taken; the bifurcation diagram and the time series. The bifurcation diagram shows the behaviour of the map for different values of the map parameter and thus illustrating which parameter values cause a map to exhibit chaotic behaviour. The time series enables an analysis of the behaviour of the map for a fixed parameter value allowing a visual analysis of the complex behaviour.

### **2.3.1 The Logistic Map**

The Logistic Map (LM), given by the difference equation (2-8) was initially introduced as a discrete-time demographic model by the biologist Robert May to model the population of rabbits and foxes (May, 1976). The LM is analogous to the logistic equation created by the mathematician Pierre François Verhulst (Miner, 1933) and is a discrete 1D nonlinear map with the transfer characteristic shown in Figure 2-5.

$$x_{n+1} = rx_n(1 - x_n) \quad x_n \in [0,1] \quad (2-8)$$

Where  $x_n$  is the present state of the LM,  $x_{n+1}$  is the next state and  $r$  is the parameter of the LM that can be set to a value from 0 to 4.

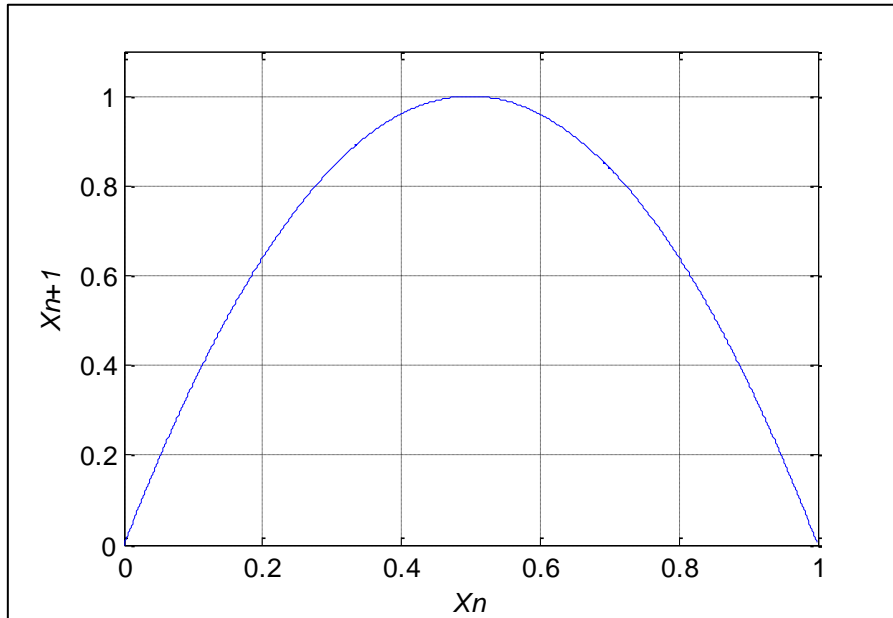


FIGURE 2-5 TRANSFER CHARACTERISTIC OF THE LOGISTIC MAP

The simplicity of the LM combined with complex behaviour makes the LM the ideal example of how relatively simple mathematical models can exhibit chaotic behaviour.

A commonly used technique to demonstrate that a map displays chaotic behaviour is the bifurcation diagram which displays the behaviour of the map for variations of the parameter  $r$ .

- ***Bifurcation Diagram***

The bifurcation diagram generated for the LM, using MATLAB, is given in Figure 2-6, with the map being iterated 10000 times for every value of  $r$  from 0 to 4. It can be observed that for  $0 \leq r \leq 1$  the output remains at zero and for  $0 \leq r \leq 3$  the output is constantly increasing. The first output signal oscillations appear for  $r > 3$

where the output starts to oscillate between two fixed points. At approximately  $r = 3.448$  the first period doubling occurs, as shown in Figure 2-7 (expanded region of Figure 2-6), the output is now oscillating between 4 points. The period doubling is an important feature of the LM and is referred to as the “*route to chaos*”. This feature is not only inherent to the LM but it can be observed in other maps and chaotic systems (G.L.Baker and J.P.Gollub, 1990). The next period doublings are visible in Figure 2-8 which is an expanded region of the full bifurcation diagram, and occurs at 3.543 and at 3.564 respectively. As  $r$  increases the period doublings get closer until an infinite number of bifurcation is reached at approximately 3.569, finally leading to chaos.

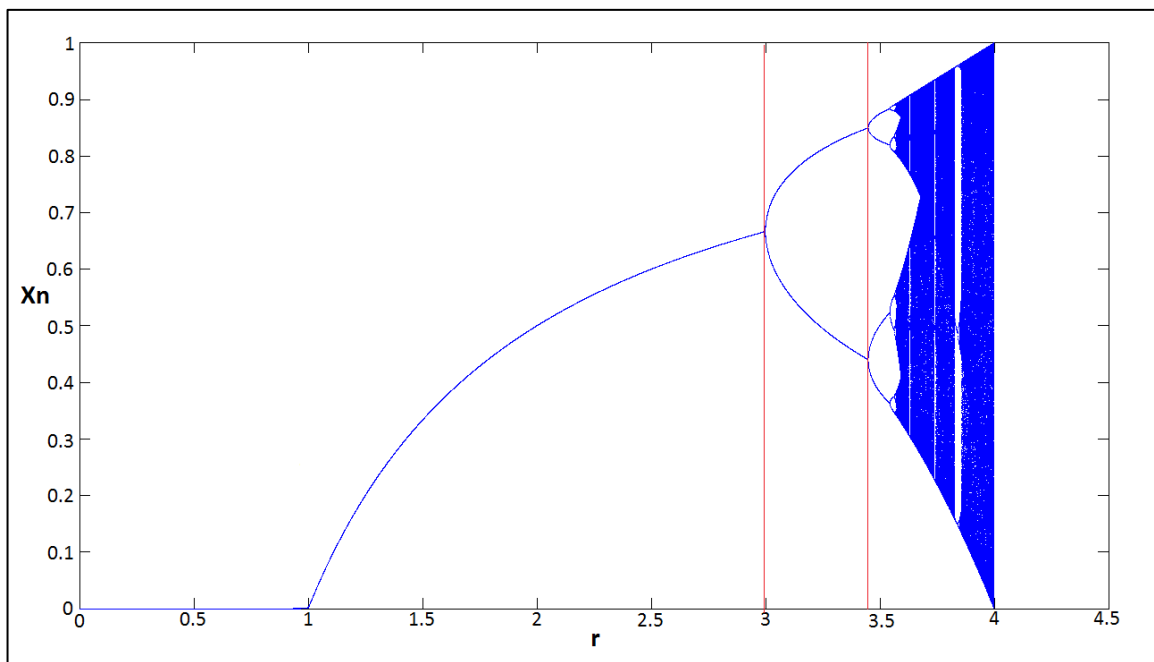


FIGURE 2-6 COMPUTED BIFURCATION DIAGRAM OF THE LOGISTIC MAP

Although the LM behaves chaotically after a given value of the parameter  $r$  is reached, the chaotic behaviour stops for periodic gaps named *windows of periodicity* in which the output exhibits periodic oscillations, as shown in the bifurcation diagram Figure 2-9. As  $r$  is increased from 3.82 towards 3.83 the output leaves chaos and goes back to periodicity, once  $r$  reaches approximately 3.841 the period

doubling starts again and the map proceeds to exhibit chaotic behaviour again at approximately 3.842. As  $r$  is further increased, the output remains chaotic and occupies more of the output range until the output takes up the entire output range at  $r = 4$ . If the value of  $r$  is greater than 4 the output of the LM will diverge to minus infinity and will no longer exhibit chaotic behaviour. This phenomenon is often referred to as “*exiting condition*” or “*extinction*” in reference to population modelling (Miner, 1933).

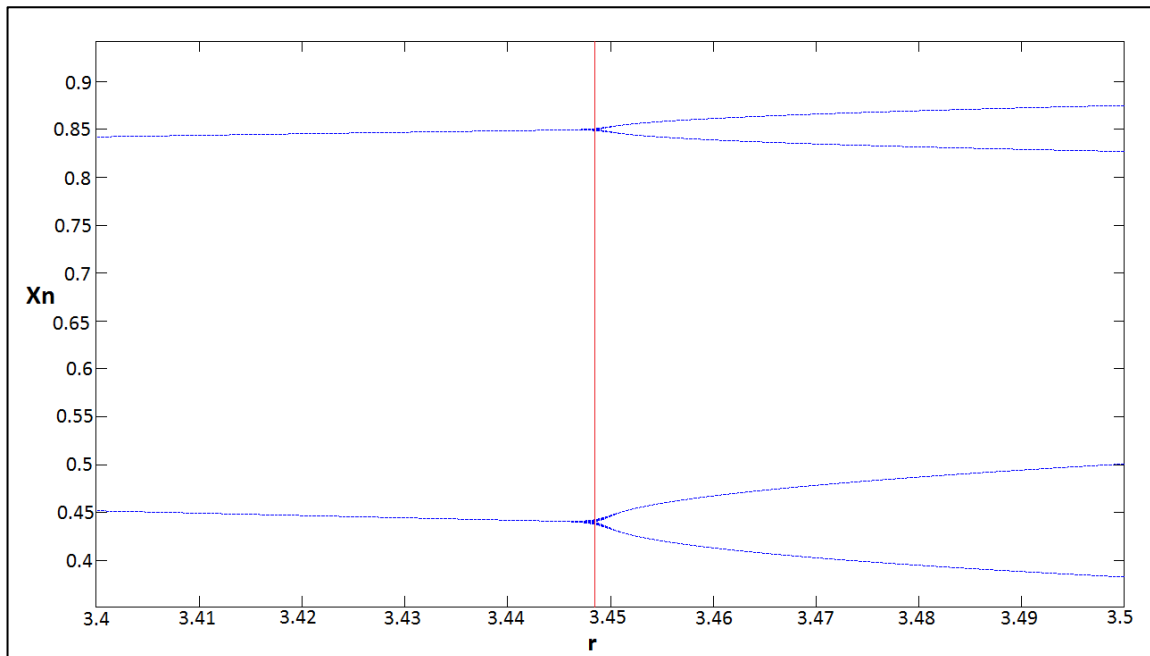


FIGURE 2-7 BIFURCATION DIAGRAM OF THE LOGISTIC MAP FROM  $R = 3.4$  TO  $R = 3.5$

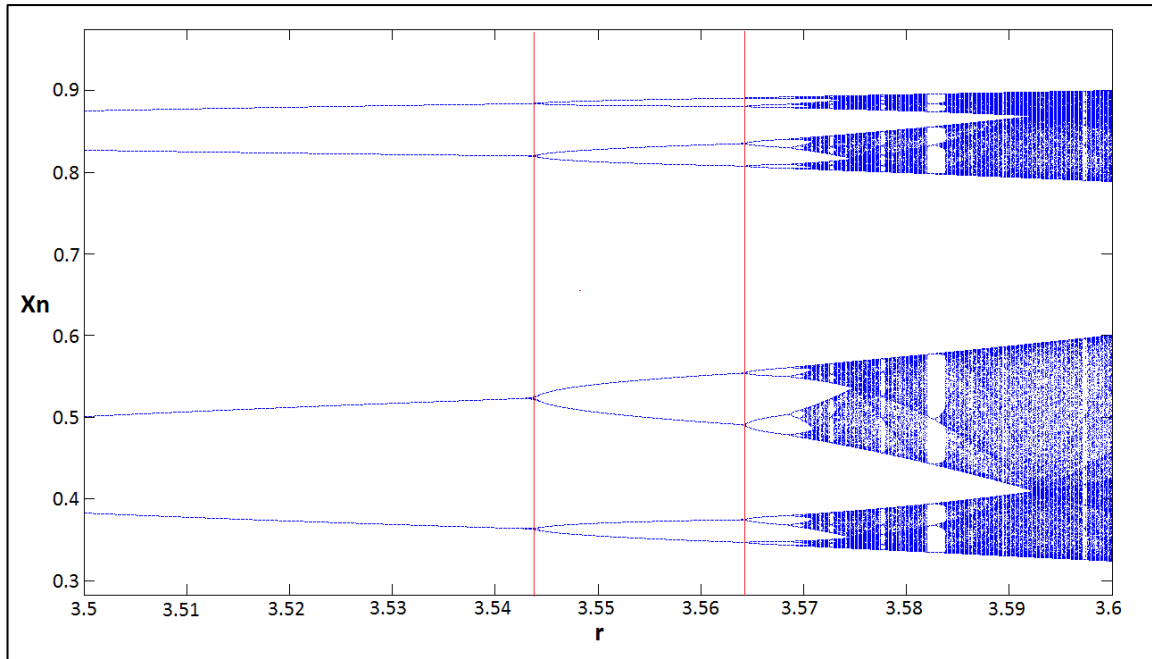


FIGURE 2-8 BIFURCATION DIAGRAM OF THE LOGISTIC MAP FROM R =3.5 TO R =3.6

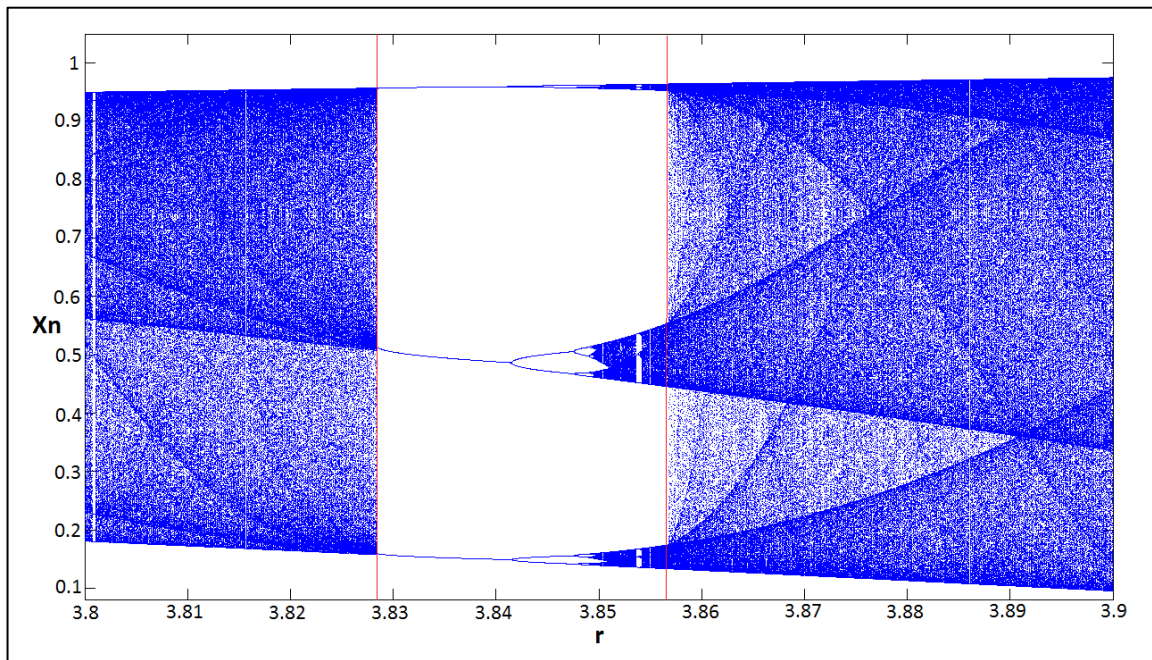


FIGURE 2-9 BIFURCATION DIAGRAM OF THE LOGISTIC MAP FOR R =3.8 TO R =3.9

- ***Time Domain Analysis***

An analogous analysis of the LM behaviour can be accomplished in time domain by displaying the output of the map for a given number of iterations and by varying the

parameter  $r$ . Figure 2-10 shows four different graphs plotted for different values of  $r$ . The Y axis represents the output  $x_n$  of the LM against the number of iterations on the X axis. In Figure 2-10(a)  $r$  is set to 2.2, it can be observed after three iterations that the output settles to a constant value, this result is consistent with the bifurcation diagram shown in Figure 2-6. As  $r$  is increased to 3.3 the output starts to oscillate between two values as displayed in Figure 2-10(b), and oscillates between four points in Figure 2-10(c), as  $r$  is set to 3.52 which further validates the behaviour observed in the bifurcation diagram. Finally, in Figure 2-10(d)  $r$  is set to 3.8 and the random-like evolution of the time series shows that the LM behaves chaotically. At  $r = 4$  the output occupies the entire output range while for values of  $r$  greater than 4 the map no longer exhibits chaotic behaviour and reaches an exiting condition.

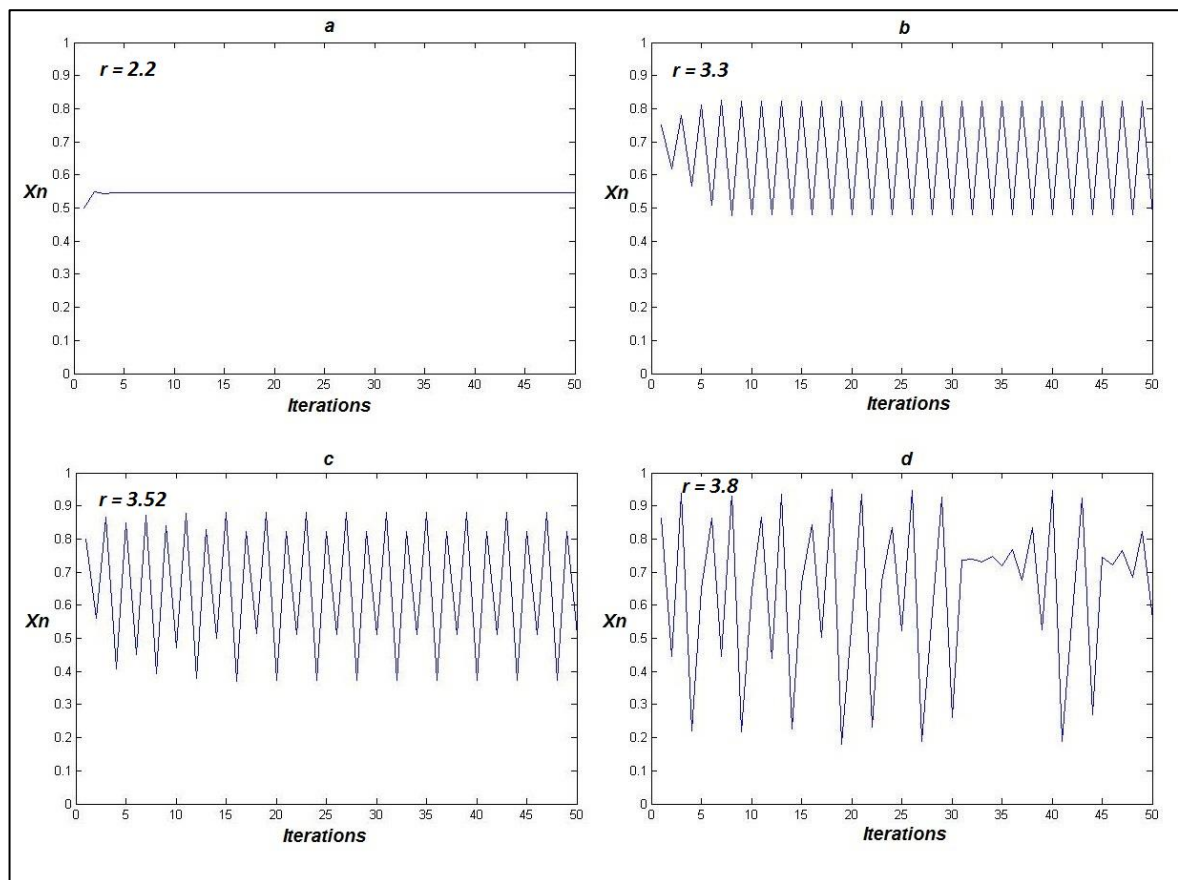


FIGURE 2-10 BEHAVIOUR OF THE LOGISTIC MAP FOR DIFFERENT VALUES OF  $r$

- ***High Sensitivity to Initial Conditions***

As previously stated, the main characteristic of chaos is the high sensitivity to initial conditions, which can be analysed using simulations. Firstly, the map is iterated for a given input and the values of  $x_n$  are stored to obtain a signature representing the input, then a relatively small change is applied to the input and the map is reiterated with the results of the two signatures being subtracted to obtain the difference, enabling the point of divergence to be ascertained. In Figure 2-11 the input  $x$  is set to 0.6, the parameter  $r$  is set to 3.8 in order for the LM to behave chaotically, and the map is iterated 50 times (shown as plot a1). The same process is performed once again but with a small change of 0.0001 added to the input  $x$  and represented by plot a2. The results of the iterations are then subtracted and displayed as (a0). It can be observed that from iteration 1 to iteration 11 the two signatures are very close in amplitude. The divergence between the two signals is visible at iteration 8 and the divergence grows exponentially after this point. In Figure 2-12 the change between the two input values is reduced to  $10^{-7}$ , with the point of divergence being observed after 23 iterations, which demonstrates that the number of the iteration at which the two time series diverge is larger for smaller difference of initial conditions of the LM. This is further demonstrated in Figure 2-13 where the change in initial conditions is as small as  $10^{-15}$  and the two signals diverge after a greater number (approximately 68) of iterations. Although there is a pattern between the iteration when the divergence occurs and the amount of change it is impossible to extrapolate a relationship between the amount of change and the iteration number using this analysis, due to the fact that the analysis is performed for a single input rather than a full input range. An extensive analysis of the high sensitivity to initial condition of the TM using a novel computational analysis is presented in Chapter 3.

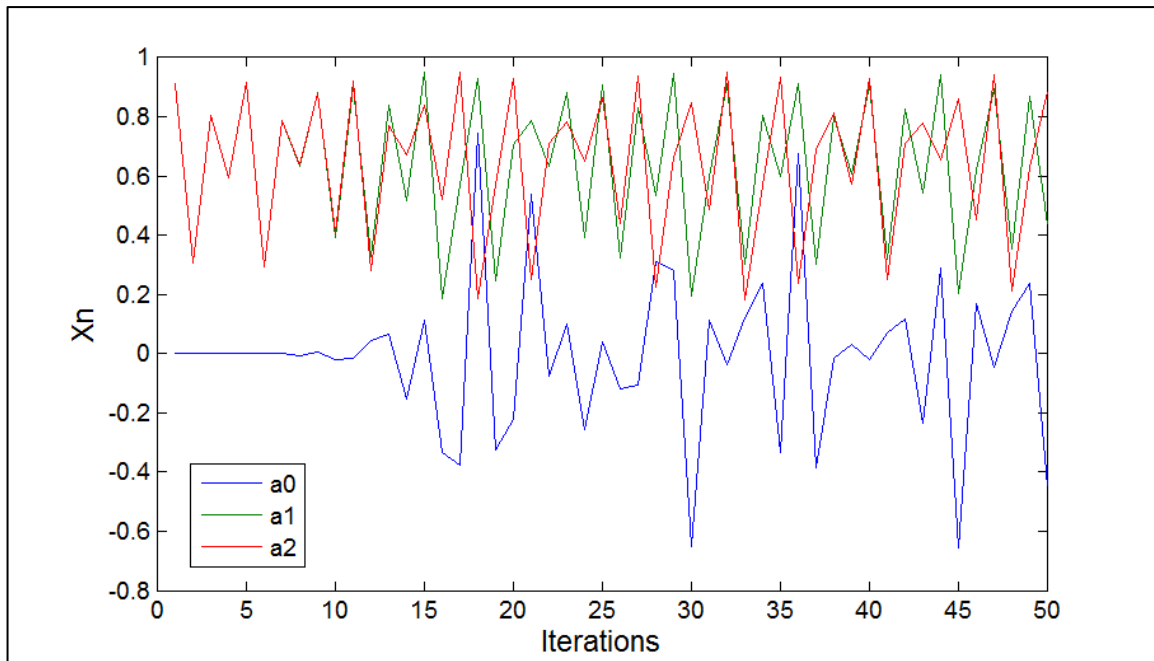


FIGURE 2-11 SENSITIVITY TO INITIAL CONDITIONS OF THE LOGISTIC MAP FOR A  $10^{-4}$  CHANGE.

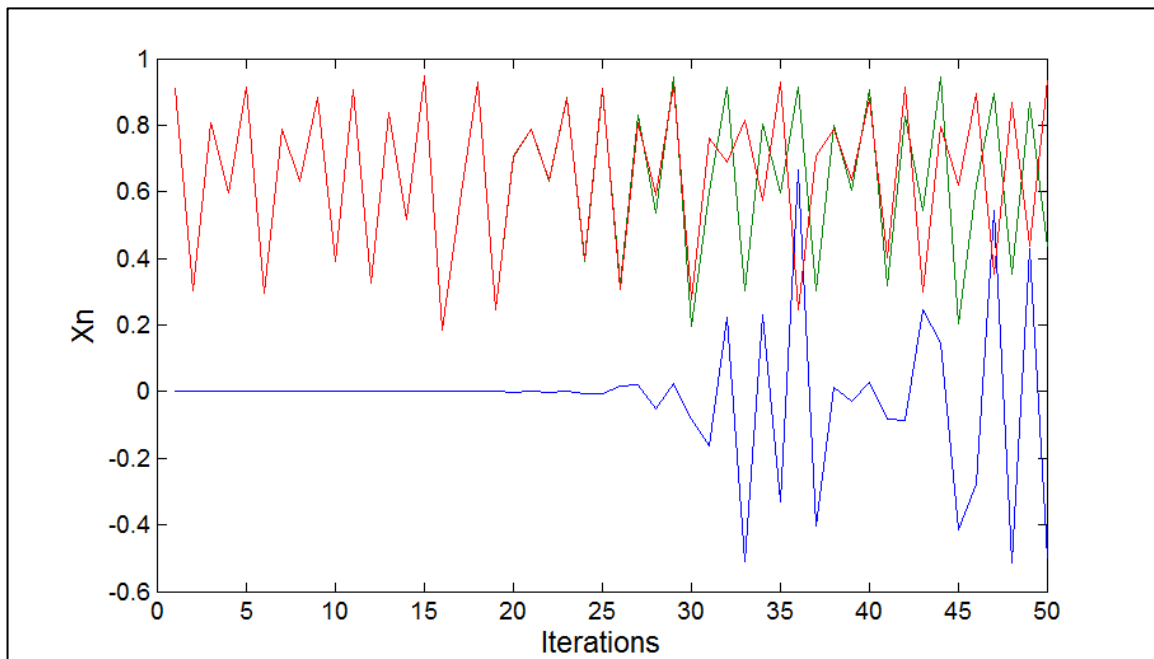


FIGURE 2-12 SENSITIVITY TO INITIAL CONDITIONS OF THE LOGISTIC MAP FOR A  $10^{-7}$  CHANGE.

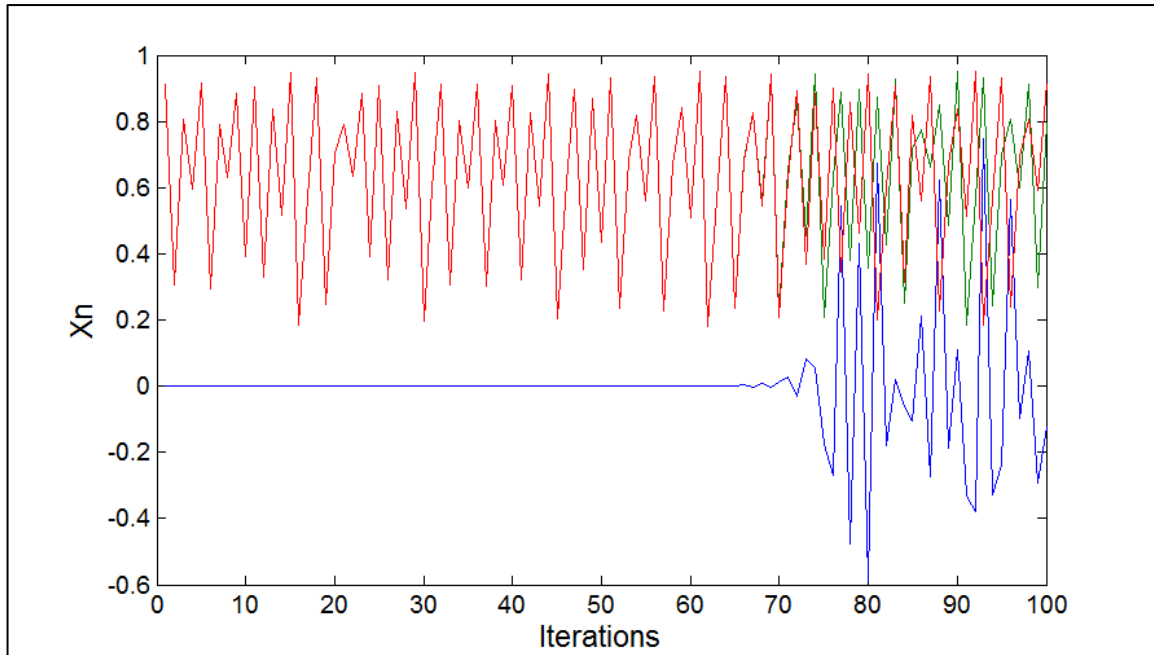


FIGURE 2-13 SENSITIVITY TO INITIAL CONDITIONS OF THE LOGISTIC MAP FOR A  $10^{-15}$  CHANGE.

The theoretical behaviour of the LM was explained by analysing the time domain behaviour, the bifurcation diagram and the chaotic proprieties. This was mainly performed using MATLAB simulations to compute and present the different aspects of the LM. The next section will focus on another discrete 1D chaotic map, namely the Tent Map (TM), as it is relatively simple to implement and just as with the LM, it exhibits chaotic behaviour.

### 2.3.2 The Tent Map

The TM is a piecewise linear function composed of two straight lines contained within the interval  $[0,1]$  yet the TM exhibits complex behaviour including periodicity and chaos (G.L.Baker and J.P.Gollub, 1990). The TM function is given by equation (2-9) where the parameter  $\mu$  sets the slope / gradient of the lines and can be varied anywhere within the interval 1 to 2. The effect of the value of  $\mu$  will be

discussed further in this chapter. The TM was named after its tent-like triangle transfer characteristic shown in Figure 2-14.

$$x_{n+1} = \begin{cases} \mu x_n & \text{for } x_n < \frac{1}{2} \\ \mu(1 - x_n) & \text{for } x_n \geq \frac{1}{2} \end{cases} \quad (2-9)$$

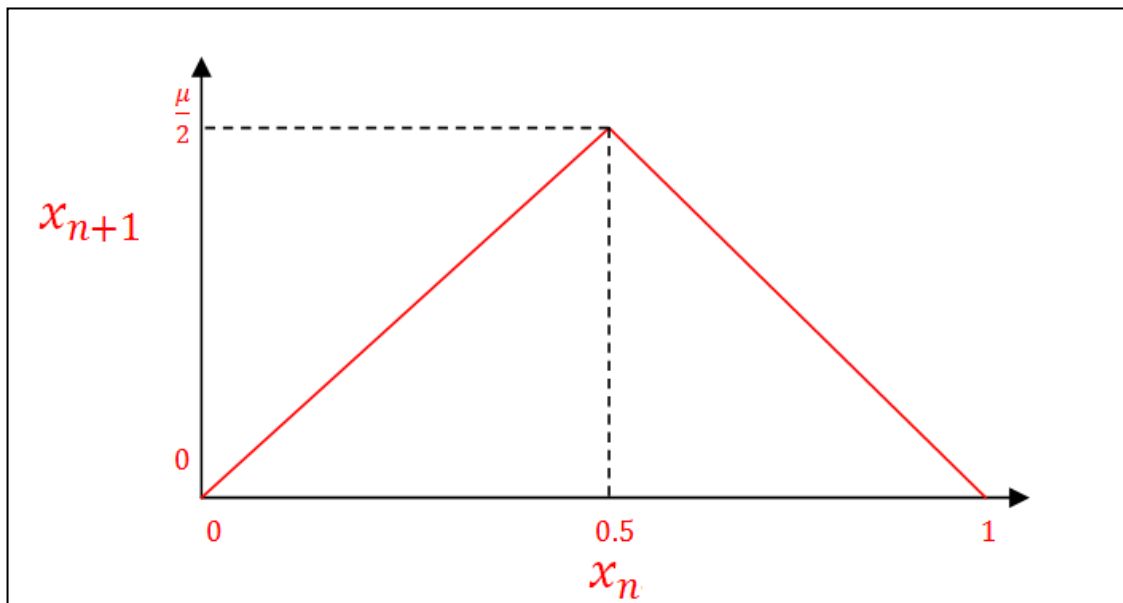


FIGURE 2-14 TENT MAP TRANSFERT CHARACTERISTIC

- ***Bifurcation Diagram of the Tent Map***

The bifurcation diagram of the TM is shown in Figure 2-15, where the behaviour of the TM is set with the parameter  $\mu$ . As the parameter  $\mu$  is increased from 1 to 2 the TM displays a complex behaviour ranging from fixed point stability to periodicity and finally chaos. The bifurcation diagram shows successive branches similar to the period doubling cascade of the LM (from  $\mu = 1$  to 1.42), rather than being single lines the outlines of the TM are chaotic attractors bounded within a subset of the interval  $[0,1]$ , this interval is sometimes referred to as *Orbit* (Lynch, 2004). As the parameter  $\mu$  is increased towards 2 the output swing increases in range until the

entire  $[0,1]$  interval is taken. Unlike the LM the bifurcation diagram of the TM does not exhibit any windows of periodicity which makes it even more suitable for applications where chaotic behaviour needs to be maintained. Ideally, the parameter  $\mu$  should be set to 2 as this is the point where the sensitivity to initial condition of the TM is highest (Lynch, 2004). A problem arises in practical implementation when setting  $\mu$  at exactly 2, as a small amount of noise could produce an exiting condition in which case the TM will no longer behave chaotically as  $\mu$  or the input signal are outside the limits due to the noise. This situation can be avoided by setting  $\mu$  close to 2 with a margin greater than the noise of the practical implementation. For example if the parameter is set to 1.99, a margin of 0.01 (which is in most cases greater than the noise present in practical implementation as discussed later in section 5.7) will insure that the TM remains highly sensitive to initial conditions whilst preventing any exiting conditions.

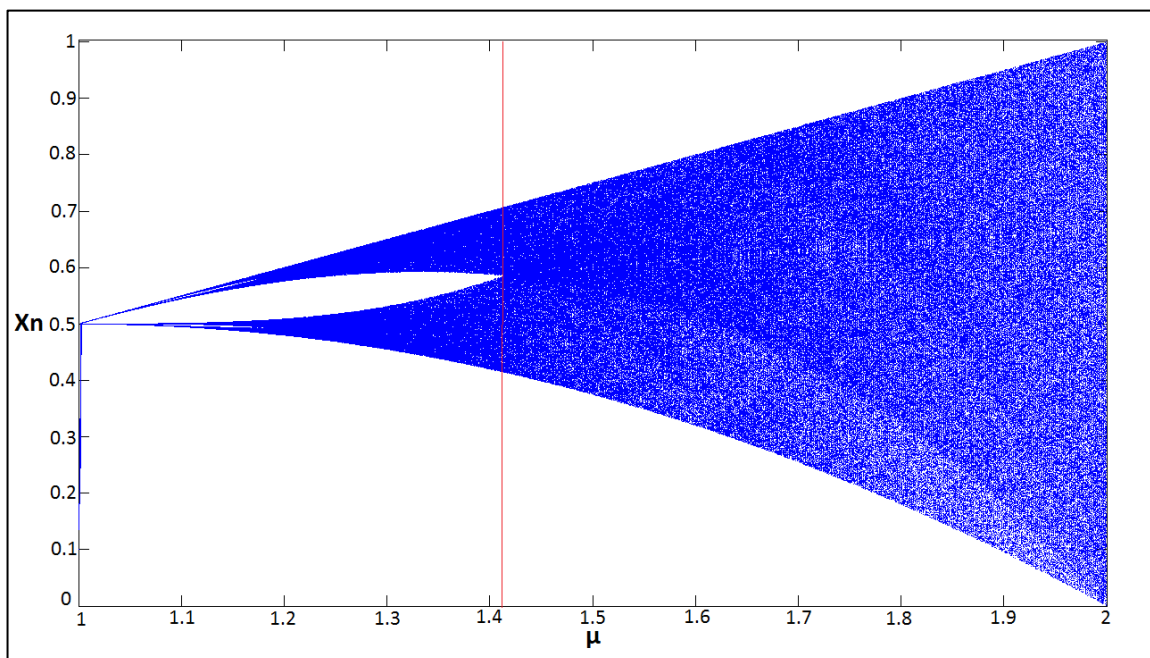


FIGURE 2-15 TENT MAP BIFURCATION DIAGRAM

- ***Time Domain Behaviour and High Sensitivity to Initial Conditions***

The TM and the LM are topologically conjugate which means that the behaviour of both maps is similar under iteration (Alligood et al., 1997). The time domain behaviour of the TM being similar to that of the LM, hence the time domain analysis is not shown in this thesis.

Similarly, because of the analogous behaviour under iteration between the TM and the LM the high sensitivity to initial conditions of the TM produces results comparable to the LM shown in section 2.3.1, with further analysis carried out in Chapter 3.

### **2.3.3 The Bit Shift Map**

The Bit Shift Map (BSM) sometimes referred to as Bernoulli map or Doubling map is a discrete piecewise-linear 1D chaotic map expressed by equation (2-10) with a transfer characteristic shown in Figure 2-16. Contrary to the TM and the LM where the parameter of the map can be varied, the parameter of the BSM is a constant set to two. The name of the BSM comes from the fact that if the input of the map is written in binary form, after each iteration, the output is obtained by shifting the bits to the right and replacing the last bit on the left by a zero. From this feature it can be observed that the simulation of the BSM using computation is problematic as the rounding of the computer will eventually cause any input number to produce a zero after a given number of iterations as the binary expansion will be limited in length, this is not an issue when it comes to practical implementation as the values present at the input will always be irrational (infinite binary expansion). Similarly to the TM and the LM, the BSM needs an accurate setting of the parameter  $\sigma$  to two in

order to avoid exiting conditions. Due to a fixed value of the parameter  $\sigma$ , a bifurcation diagram cannot be obtained.

$$x_{n+1} = \sigma x_n \text{ mod } 1 \quad (2-10)$$

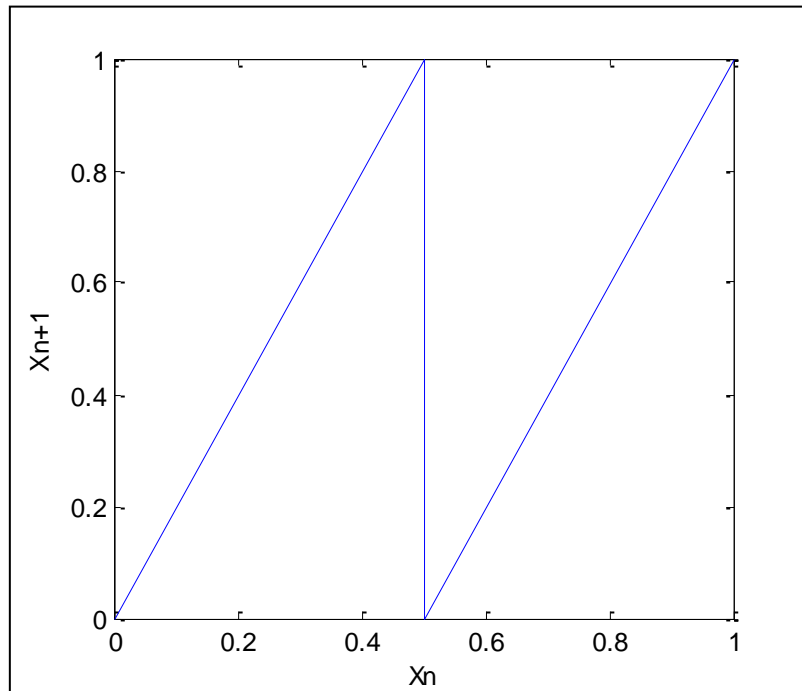


FIGURE 2-16 BIT SHIFT MAP TRANSFER CHARACTERISTIC

- ***Time Domain Behaviour and High Sensitivity to Initial Conditions***

In time domain, the output of the BSM takes the entire output range in the interval  $[0,1]$  which is the case for the TM for  $\mu = 2$  and for the LM when  $r = 4$ . To demonstrate the high sensitivity to the initial conditions of the BSM, four time series were computed using MATLAB. Firstly, an input signal was iterated through the BSM followed by a signal with an added difference ( $\Delta$ ) of 0.001. The two time series are shown in Figure 2-17 (plot a1) and the divergence between them is displayed in plot a2. It can be seen that the time series are divergent approximately at iteration 8. Two additional time series were computed but this time with  $\Delta$  of 0.0000001 as

shown in (b1). The divergence between the two time series is shown in (b2) which occurs after approximately 17 iterations demonstrating that the divergence between two time series occurs later when  $\Delta$  is reduced.

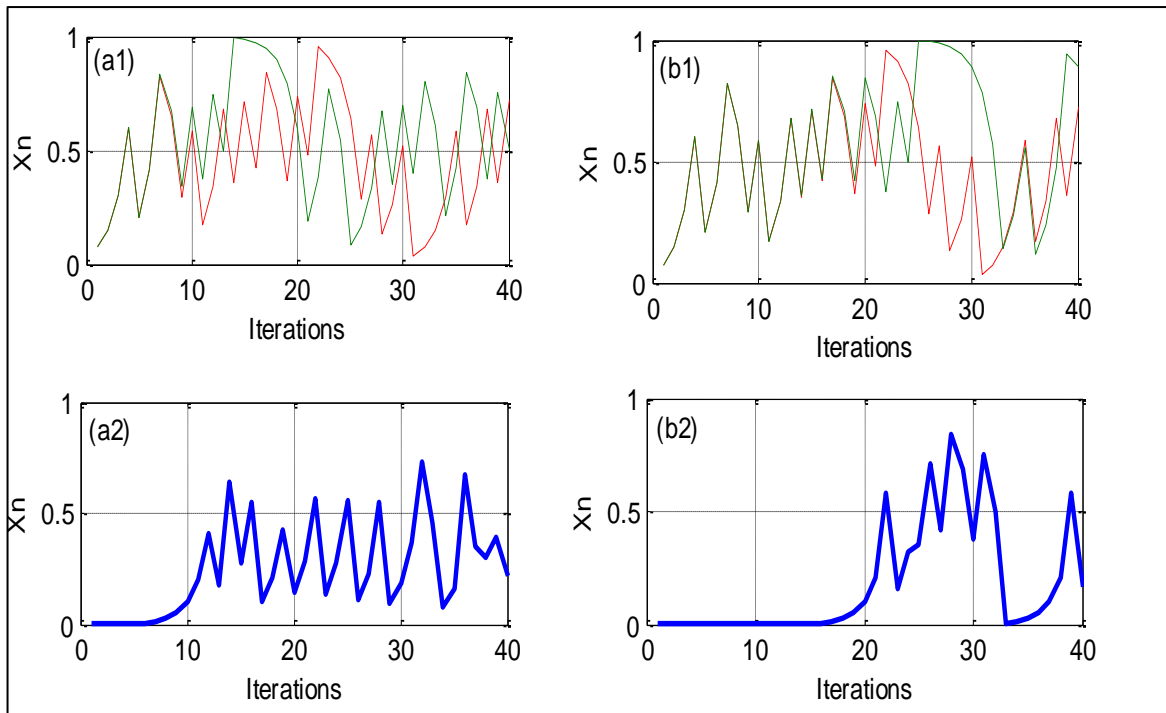


FIGURE 2-17 HIGH SENSITIVITY TO THE INITIAL CONDITIONS OF THE BIT SHIFT MAP

### 2.3.4 Summary

The investigation of three discrete 1D chaotic maps has shown that all maps, despite having a simple characteristic equation, exhibit chaotic behaviour and indicates that the time/iteration of divergence between two neighbouring starting points is proportionally linked to the amount of change between the two points.

In addition to the similarity between the BSM and the TM, the BSM requires an accurate parameter setting which is not the case for the LM and the TM where the parameters can be varied within a given region without systematically leading to exiting conditions. In practical implementations, the noise and component tolerances

limit the accuracy at which the parameter can be set. In that aspect the LM and TM are superior to the BSM for the purposes of this work.

Since the BSM is a piecewise linear map similarly to the TM, the BSM will not be considered for implementation in the present thesis, as the work will be focused on the LM and the TM in order to evaluate the different characteristics.

The next section will focus on a means of ascertaining chaotic behaviour in dynamical systems, this presented technique will be used further in this work to identify chaotic behaviour in electronic implementations.

## **2.4 Applied Chaos**

Chaos has been applied across a variety of disciplines, which is particularly the case for one-dimensional maps, due to the relative simplicity which makes them particularly suitable for electronic implementations.

### **2.4.1 Electronic Implementation of Chaos**

One-dimensional (1D) chaotic maps have been used in electronics as random number and noise generators (Díaz-Méndez et al., 2009, Katz et al., Tanaka et al., 2000, Vázquez-Medina et al., 2009, Kanso and Smaoui, 2009, Nejati et al., 2012, Callegari et al., 2005). The output of chaotic circuits occupies the entire output interval in a random-like manner with a relatively flat spectrum response which makes the 1D maps suitable for random number and white noise generators. For example, Díaz-Méndez et al. (2009) have developed and simulated an analogue electronic implementation of the Logistic Map (LM); the spectral density and the statistical distribution exhibited by the circuit were similar to that for white noise

which proves that the LM can be used as a noise generator. The implementations available in literature for this purpose are using Complementary Metal Oxide Semiconductor (CMOS) technology to simplify the integration in a single Integrated Circuit (IC), for example, Tanaka et al. (2000) have successfully implemented noise generators based on both the LM and the TM in a single IC. The results obtained are similar to the noise generator proposed by Díaz-Méndez et al. (2009) and demonstrate the noise like characteristic of the spectral distribution of the electronic implementations. Another noise generator was proposed by Leonardo et al. (2012), but this time rather than using analogue circuitry to generate analogue noise, the authors have implemented a TM based digital noise generator using a Field-Programmable Gate Array (FPGA). A variation of the TM was implemented in order to generate a 13 bit representation of a random natural number, the resources required in the FPGA were limited to 3 multipliers and 2 adder modules. The results obtained demonstrate that the 1D map based noise generator performs as expected and that the statistical distribution is uniformly spread.

In Murali et al. (2005) a 1D chaos map was used for an experimental realisation of a logic gate, although the experiment was successful the main purpose was to prove that 1D map can be used as basic computational elements. In another instance, chaos has been used to improve the capture range of a Phase Lock Loop (PLL); where an external modulating input was used to set the unlocked PLL into a chaotic regime that overlaps the original capture range. The chaos inducing modulation was then turned off, allowing the original dynamics of the PLL to capture the signal. (Bradley, 1993).

Many electronic implementations of chaotic 1D maps are available in literature with the main purpose being the practical approach to the analysis and study of chaos

with no specific application given by the authors (Campos-Cantón et al., 2009, Eguchi et al., 2000, Suneel, 2006, Edang et al., 2011, Hernandez et al.).

## **2.4.2 Chaos in Cryptography**

Communication systems are used to transmit a message (information) from a transmitter to a receiver; before transmitting, the message should be formatted for suitable transmission and encrypted if the security of the transmission is of concern.

The broad spectrum of the chaotic maps used to create random number and noise generators can also be used to design Spread-Spectrum (SS) communication systems. In SS communications, the power of the signal is spread out over a wide frequency band to avoid narrowband interference. The security is increased since the carrier signal is no longer a single spike in the frequency spectrum, making it electronically difficult to monitor and detect. A proposed chaos based system was used as a SS code on the transmitter and receiver end in order to spread the bandwidth of the transmitted signal, effectively increasing the signal robustness to noise and signal jamming (Setti et al., 2002).

In Kocarev (2001) the similarities between classical cryptography systems and the high sensitivity to initial condition of chaotic system are shown. For this reason, chaos has also been used to create cryptographic algorithms, for example a method using the LM has been proposed in literature to simplify the design of chaos based cryptographic systems along with a step by step procedure for designing cryptographic systems using chaotic maps (Kocarev and Jakimoski, 2001). In another paper an optical chaos based secure communication system has been designed using a discrete implementation of the LM, incorporating a pulse position

modulation scheme together with the LM chaotic map to encrypt the signal (Singh and Sinha, 2010).

Additional instances of chaos being used for communication or cryptography include but are not limited to, image encryption (Pareek et al., 2006, Patidar et al., 2009) and analysis of cellular neural networks behaviour (Zou and Nossek, 1993).

### **2.4.3 Chaos Based ADCs**

Chaos has been applied to measurement and particularly to implementation of ADCs, where the ADCs created using chaotic maps are named algorithmic ADCs which rely on the piecewise-linear characteristic of 1D maps to double and fold the signal on each iteration. Algorithmic ADCs generate either a binary or a Gray-code representation of the sampled analogue signal, with the binary ADCs being based on the Bit Shift Map (BSM) while the Gray-code ADC are based on the TM (Kennedy, 1995).

- ***Bit Shift Map ADC***

The BSM can be used as an ADC as the output is a binary expansion of the sampled analogue signal. To do so a comparator is added at the output of the function so that the output is compared against a reference signal. If the signal is higher than the reference the output of the comparator is set to 1, else the output is set to 0. After each of the iterations the LSB, that has been generated, is shifted by 1 to the right and the remaining is iterated through the map to generate the next bit. This process is repeated N times until a N bit binary expansion is obtained. The input analogue voltage is then expressed as shown in expression (2-11).

$$V_n = 0.b_1b_2b_3\dots \equiv \sum_{N=1}^{\infty} 2^{-N} b_N \quad (2-11)$$

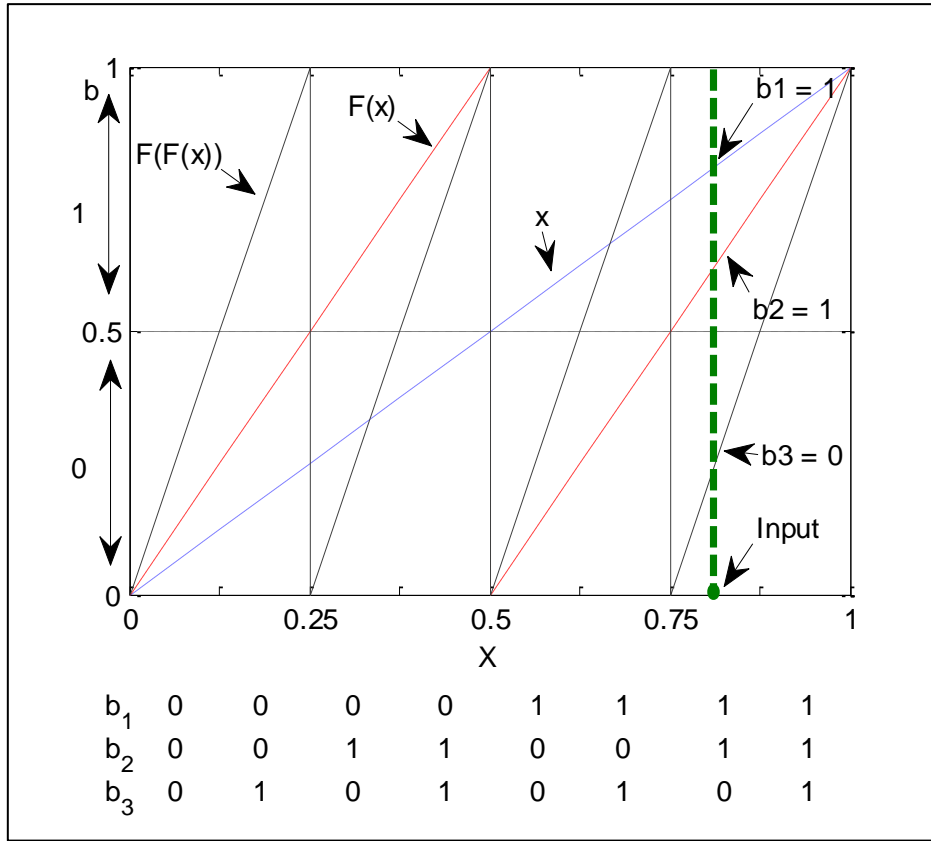


FIGURE 2-18 WORKING PRINCIPLE OF THE ADC BASED ON THE BIT SHIFT MAP

Figure 2-18 illustrates the working principle of the algorithmic ADC based on the BSM Map. Each iteration adds one binary digit that represents the input voltage  $V_n$  (Kennedy, 1995, Kapitaniak et al., 2000). For example if the value of the input voltage is between 0.75 and 0.875 the first bit  $b_1$  will be set to 1 as the input  $x$  is higher than the threshold of 0.5 the second bit  $b_2$  will also be set to 1 as  $F(X)$  is greater than the threshold. Finally the third bit  $b_3$  is set to 0 as  $F(F(X))$  is lower than the threshold. ADCs based on the BSM have been implemented in literature (Qingdu and Qifeng, 2012).

- **Tent Map ADC**

Similarly to the BSM the TM can be used to create an ADC which generates a Gray-code expansion of the analogue input signal. After each iteration the output of the TM circuit is compared to a 0.5 threshold. If the output is lower than the threshold the bit is set at 1, else the bit is set at 0. After each iteration the bits are shifted to the left. This process is shown graphically in Figure 2-19.

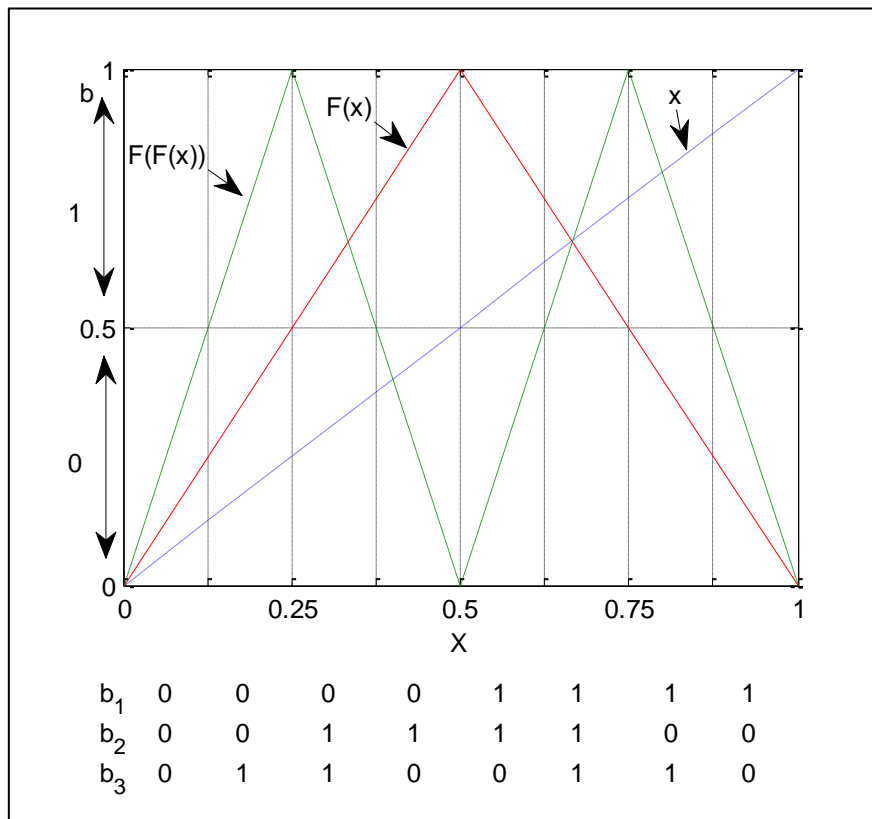


FIGURE 2-19 TENT MAP BASED ADC

Gray-code algorithmic ADCs implemented using the TM are considered superior in term of performance to binary-code ADCs (implemented using the BSM). This is due to the fact that only one bit is changing at any time in a Gray-code ADC for an input signal change equivalent to 1 LSB. In a binary ADC a signal change around the threshold voltage (0.5 V) can cause many bits to change in cascade which can introduce transient errors that are difficult to correct (Arayawat et al., 2008). Another

advantage of the ADCs based on the TM is the improved tolerance to offset error compared to BSM based ADCs (Signell, 2005, Signell et al., 1997); this is due to the fact that in a BSM ADC the offset errors are always amplified with a positive gain which produces an accumulation of the offset errors. Alternatively, in the TM based ADC the amplification is switching between positive and negative gain which reduces the offset errors allowing a design of an ADC with improved resolution compared to BSM based ADCs. Gray-code ADCs have been implemented with different architecture such as voltage-mode where the ADC circuitry is dealing with voltages (Arayawat et al., 2008) and current-mode where the signals propagating through the ADC are currents rather than voltages which allows for a simplified Integrated Circuit (IC) implementation (Pouliquen et al., 1991, Wilamowski et al., 2006, Chaikla et al., 2006).

- **Summary**

Algorithmic ADCs produce accurate results only if the parameters that define the maps behaviour are precisely set; in the case of the TM the parameter  $\mu$  should be set to exactly 2 and the voltage reference for the threshold to 0.5. If any error is introduced to the parameters the error will grow exponentially and coding errors will appear (Kapitaniak et al., 2000, Kennedy, 1995). If the parameter  $\mu$  is set to exactly 2 (required) a small amount of noise can set the parameter to  $\mu > 2$ , which will cause the map to diverge to 0 (exiting condition). The algorithmic ADCs generate accurate results if the components are ideal and noiseless and the parameters set accurately. This explains the low resolution of the ADCs developed using this technique. Wilamowski et al. (2006) proposed a TM based current-mode ADC with an IC implementation with limited resolution of 5 bits. A similar ADC architecture was used by Lu (2011) to design and simulate a 10 bit ADC. In general, chaos based

ADC are limited to a maximum of 12 bits (Keng and Salama, 1994, Hai et al., 2010) which makes them impossible to use for application where an extended input range combined with the ability to detect small variation of input signal is required.

#### **2.4.4 Chaos Based Measurement System**

A limited number of chaos based MS are available in literature; in fact the author is aware of only two main methods of measurement based on chaos (Chernukha, 1996, Hu and Liu, 2010, Wang et al., 1999). Wang et al. (1999) have shown that a chaotic Duffing oscillator can be used to detect weak signals and that the system was immune to noise. The parameters of the chaotic Duffing oscillator are set so that the oscillator operates near a bifurcation point. If any weak signal is added to the system, the oscillator will leave the chaotic region and go into a region where it will alternate between chaos and non-chaos. The length of time spent in the non-chaotic state is then used to approximate the weak signal present within the system. This principle was used to increase the sensitivity of a metal detector; due to the high sensitivity to sinusoidal signals and the immunity to noise the chaotic Duffing oscillator allows the faster detection of small metal particles present in food (Hu and Liu, 2010). The drawback of the proposed system is that it can only be used for detection of sinusoidal signals as the amplitude of the detected signal cannot be accurately quantified due to the oscillator having only two states: chaotic or periodic.

The second method presented by Chernukha (1996) which the author refers to as “*synergic measurement method*” two chaotic systems based on the LM and a chaotic oscillator are presented in order to improve the measurement accuracy of sensors parameters. The chaotic circuit is connected between the sensors and the ADC to provide conditioning circuitry with improved performance over the conventional

approach. The physical parameter being measured modifies a given parameter of a sensor, which in turn varies a parameter of the chaotic circuit. Because of the high sensitivity to the initial condition of the chaotic system this results in a significant change at the output of the chaotic system, allowing the MS to detect small variations of the measured parameter. The drawback of the proposed method is the increased amount of samples required to increase the accuracy as the author states that approximately 500 samples are required to improve the resolution by 2 bits. Unfortunately, other publications written by the same author that fully explains the above method are not accessible in English. Despite interesting theoretical and simulation results the two methods mentioned above have not been implemented and remain theoretical.

## 2.5 Lyapunov Exponent

The Lyapunov Exponent (LE), named after the Russian mathematician Aleksandr Mikhailovich Lyapunov, is used to estimate the sensitivity to initial conditions (i.e. the degree of chaotic behaviour) in chaotic systems (G.L.Baker and J.P.Gollub, 1990). The LE of a map indicates the rate at which two initial states diverge after a given number of iterations and can be calculated using the expression (2-12).

$$\lambda = \lim_{n \rightarrow \infty} \frac{1}{n} \sum_{i=0}^{n-1} \ln|f'(x_i)| \quad (2-12)$$

Where  $\lambda$  is the LE,  $n$  the iteration number and  $f'(x_i)$  the derivative of the chaotic map. If the LE value of a map is negative two neighbouring points will converge and

the map will not exhibit chaotic behaviour, if the LE is positive two neighbouring points will diverge exponentially and the map is highly sensitive to initial condition and thus chaotic. This makes the LE the ideal tool to ascertain the presence of chaos in a given dynamical system.

To demonstrate the use of the LE as a means of ascertaining the presence of chaos, Figure 2-20 shows the LE for the LM as function of the parameter  $r$ . As  $r$  is increased from 0 to 3.569 the LE remains negative which is expected as the bifurcation diagram shows that the TM is not chaotic. At  $r$  values above 3.569, the LE becomes positive showing that the map is chaotic. Finally, in the range where  $3.569 < r \leq 4$  the LE is mainly positive with some areas where the LE goes below 0 due to the windows of periodicity as explained in section 2.3.1 and illustrated in Figure 2-9.

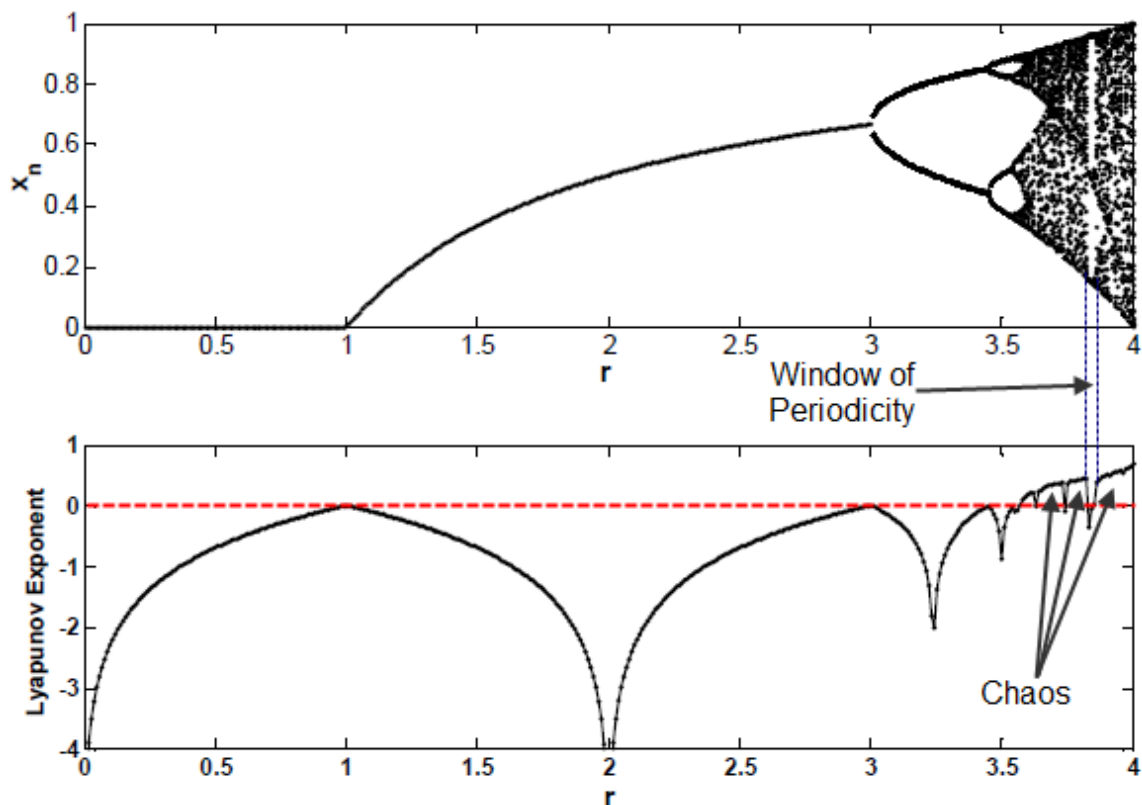


FIGURE 2-20 VARIATION OF THE LYAPUNOV EXPONENT FOR THE LOGISTIC MAP

The following section will explain how the LE can be used to ascertain the presence of chaos for experimental data which will allow the test of electronic implementations developed further in this work, to be performed.

### 2.5.1 Lyapunov Exponent Estimation

In order to estimate the LE from an experimentally obtained time series, different methods should be used as the parameters and the nature of the chaotic system cannot be known accurately. The method used to estimate the LE from the time series is a direct method proposed by Rosenstein et al. (1992) based on the modified Wolf algorithm (Wolf et al., 1985) developed in (Sato et al., 1987, J.Kurths and H.Herzel, 1987) and uses the average exponential growth of the prediction error between two neighbouring points. The expression of the prediction error is given by equation (2-13) (Parlitz, 1998). For more in depth details, the mathematics behind the algorithm can be found in the original paper proposed by Rosenstein (1992). According to (Rosenstein et al., 1992, Wolf et al., 1985) to increase accuracy, a longer time series is required.

$$p(k) = \frac{1}{Nt_s} \sum_{n=1}^N \log_2 \left( \frac{\|y^{n+k} - y^{nn+k}\|}{\|y^n - y^{nn}\|} \right) \quad (2-13)$$

Where  $y^{nn}$  is the closest neighbour of the point  $y^n$ ,  $k$  is the number of time steps used for the estimation of the LE and  $n$  in the iteration number.

After calculating the prediction error from the experimental data it is plotted and the exponential region is used to approximate the LE by measuring the slope of the linear part of the graph. If the slope is negative the separation between the two

neighbouring point is not exponential and the system is not chaotic, alternatively if the slope is positive the separation is exponential, which indicates a high sensitivity to initial conditions i.e. chaos.

An example of the LE estimation from a prediction error is shown in Figure 2-21, where the slope of the line shows the theoretical LE of the chaotic time series, whilst the practical LE can be approximated using the linear region of the estimated LE curve. This method will be used later in the work to ascertain the presence of chaos in the proposed electronic implementation of the chaotic maps.

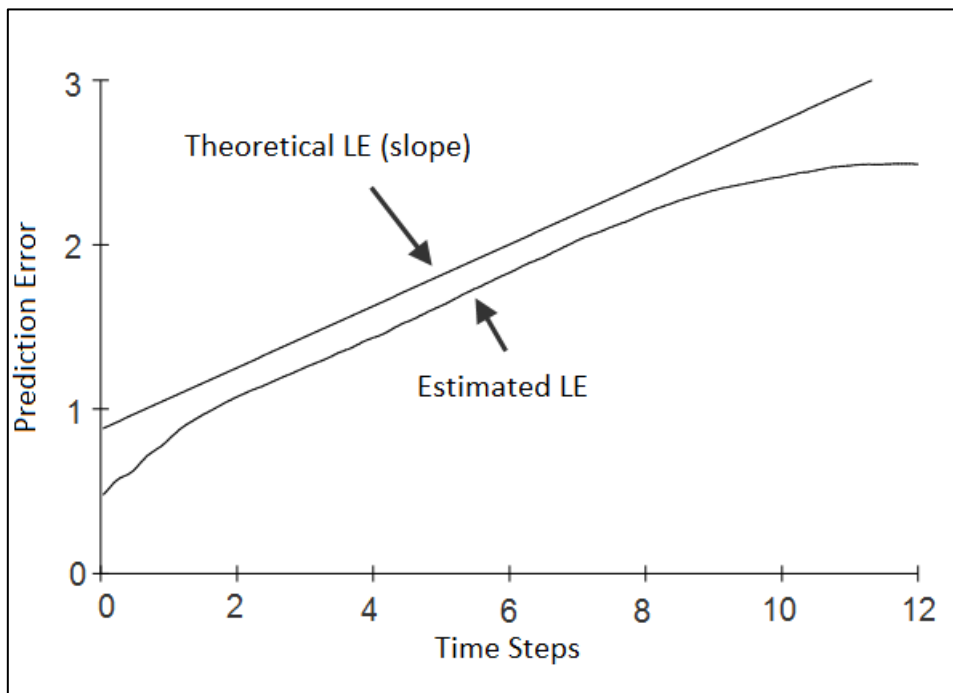


FIGURE 2-21 LYAPUNOV EXPONENT ESTIMATION USING THE PREDICTION ERROR METHOD

The theoretical LE for the LM when the parameter  $r$  is set to 4 is equivalent to the BSM LE and the TM LE when the parameter  $\mu = 2$  and is equal to 0.693 (J.-P. Eckmann and D. Ruelle, 1985).

## 2.6 Conclusion

This chapter introduced the structure of MS and reviewed the limitations inherent to conditioning circuitry and ADCs. An introduction to chaos followed by a review of two 1D chaotic maps was shown, with the typical behaviour being evaluated using bifurcation diagrams and time domain analysis. The next section of the chapter focused on applied chaos and particularly on the use of chaos in electronics; ADCs and measurement systems. The main source of error that limits the performance of chaos based ADCs were evaluated to be the inaccuracy of the parameters and threshold voltages within the implemented system. The chapter was concluded by an explanation of the high sensitivity to initial condition of chaotic maps and the use of Lyapunov Exponent (LE) to determine the presence of chaos from the analysis of experimental data.

From the literature review carried out in this chapter the following has been concluded:

- Classical measurement systems are limited by the sensor performance, the noise of the conditioning circuitry and the performance of the ADC. As the range of the input signal increases the sensitivity of the system decreases due to the quantisation of the ADC (step size).
- Chaos has been used in electronics and particularly in algorithmic ADCs; the performance of which are limited due to parameter and threshold errors.
- Two theoretical measurement systems based on chaotic circuits have been presented in literature without practical implementation.

The next chapter will introduce a novel measurement technique based on the high sensitivity to initial conditions of one-dimensional chaotic maps that can be used to measure small variations of input signals utilising a low resolution ADC. The proposed technique is not reliant on the need for highly accurate parameter values and the sensitivity to signal change is independent of the input range.

# 3 Proposed Signal Measurement Technique

The proposed Measurement System (MS), based on a one-dimensional (1D) chaotic map, uses the high sensitivity to initial condition, as presented in the previous chapter, to measure small input signal changes. The technique differs from a conventional approach to signal measurement by quantifying the difference between two signals rather than determining the absolute value of a sample. This enables the accurate detection and measurement of small input signal changes which is totally independent of input signal range. In the previous chapter the analysis of a single input with different signal changes was performed in order to demonstrate that the moment (iteration) of divergence between the two input time series (signals) was apparently inversely proportional to the amount of change. In order to ascertain the feasibility of the proposed MS, the fundamental requirement for the linearity of divergence needed to be evaluated for a given change throughout the entire input range. The linearity of divergence is not verifiable with a single divergence graph as given previously (Figure 2-11), which shows only the divergence between two time series representing two samples. In order to visualise the divergence over the full normalised input range (0 to 1) a Matlab simulation has been carried out to generate the 3D graph that illustrates the divergence between the time series throughout the entire input range. The developed Matlab code used to generate the 3D graphs is available in Appendix B. This novel 3D visualisation technique allows the analysis of the high sensitivity to initial conditions of any chaotic map throughout the entire input range, which makes it a powerful tool for the study of chaotic maps.

The simulation was performed by taking 10000 input sample points evenly spaced throughout the entire input range. The maps were iterated and each time series obtained was subtracted from time series, for the same points plus a given signal change ( $\Delta$ ). The divergence for each sample was then displayed to produce a 3D graph, as shown in Figure 3-2 for the Logistic Map (LM). The flowchart of the algorithm used to generate the 3D graph is show Figure 3-1.

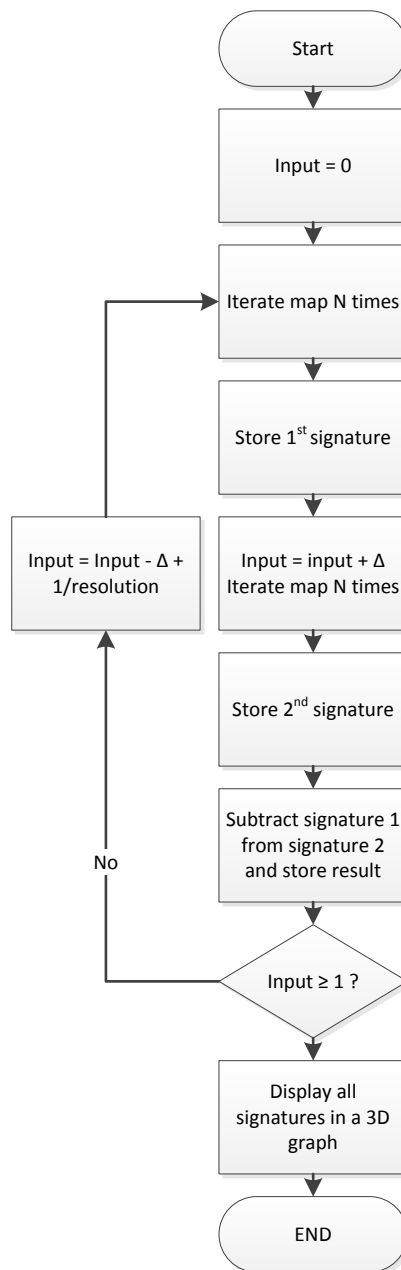


FIGURE 3-1 FLOWCHART OF THE 3D DIVERGENCE GRAPH

The parameter  $r$ , given in equation (2-8) for the LM, was set to 4 (chaotic region) and a change ( $\Delta$ ) of 0.0001 was applied for every input value. The graph shows that whilst being relatively linear the divergence varies between inputs. Any signal lying in the range of 0 to 0.1 and 0.9 to 1 will diverge earlier (iteration 3 to 5) than signals in the range of 0.1 to 0.9 ; this issue can be avoided by only utilising the region 0.1-0.9 of the normalised input range. Additional graphs showing different view angles for different values of  $\Delta$  are shown in Appendix B.

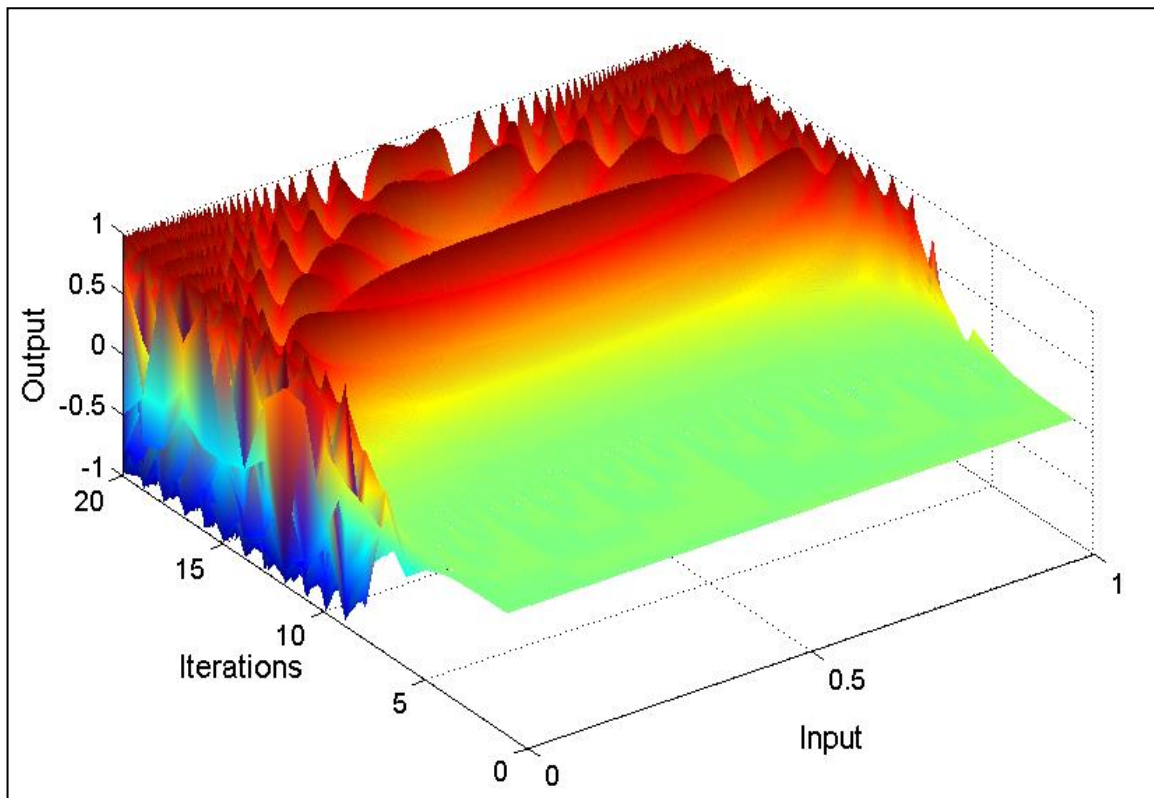


FIGURE 3-2 SENSITIVITY TO INITIAL CONDITIONS OF THE LOGISTIC MAP FOR R=4.

In order to determine the difference in the sensitivity to the initial conditions for the TM based system, the 3D divergence graphs shown in Figure 3-3 was produced in the same manner as the LM based graph. The divergence of the TM is linear throughout the entire input range, for a TM parameter  $\mu$  set to 1.99 (chaotic region) and a change of 0.0001 applied for 10000 points throughout the whole input range.

The two graphs (Figure 3-3 (a) and (b)) represent the same data viewed from different angles where the divergence is visible from iteration 6 for any input value. In this aspect the TM is more suitable for the design of the small signal change detection MS as the full input range can be utilised. Additional 3D graphs are available in Appendix C presenting the behaviour of the TM to different values of  $\Delta$ .

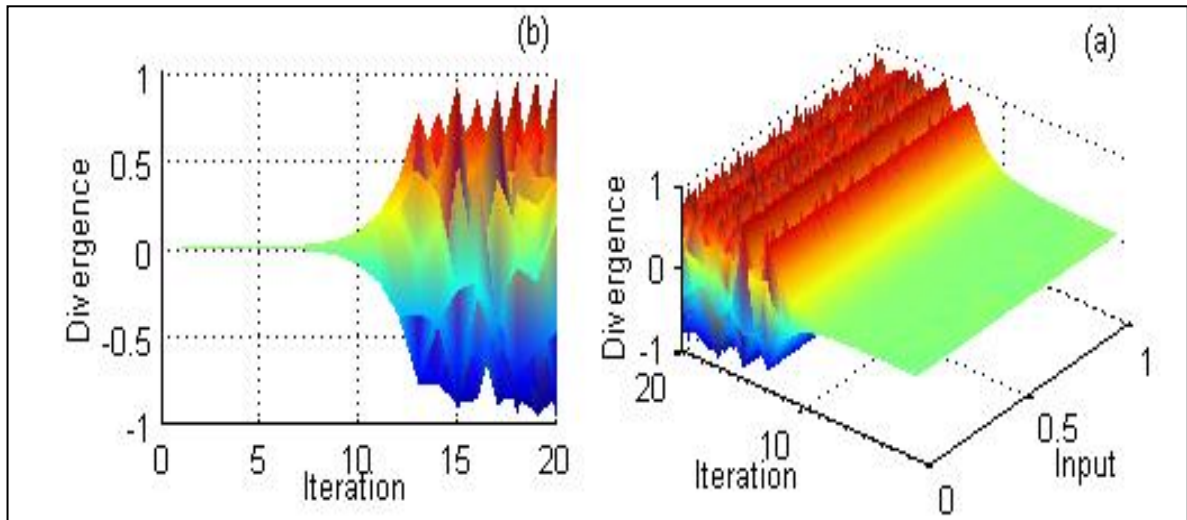


FIGURE 3-3 DIVERGENCE OF THE TM FOR THE ENTIER INPUT RANGE

### 3.1 Quantifying Input Signal Change

The LM and TM implementations are both capable of detecting small variations of input signals, but in order to define a viable measurement system the amount of change between the two signals should be quantifiable. To quantify the amount of change between two input signals when using the LM, a threshold has to be set on the amount of divergence at a given iteration. Thus the iteration sample at which the threshold is reached is used to determine the amount of change between the two samples. The calibration can be performed using the 3D divergence graph previously developed as shown in Figure 3-4. When  $\Delta$  is varied the threshold is reached at

different iteration numbers, by using the relationship between  $\Delta$  and the number of iterations when the threshold is reached the system can estimate the change between two input signals.

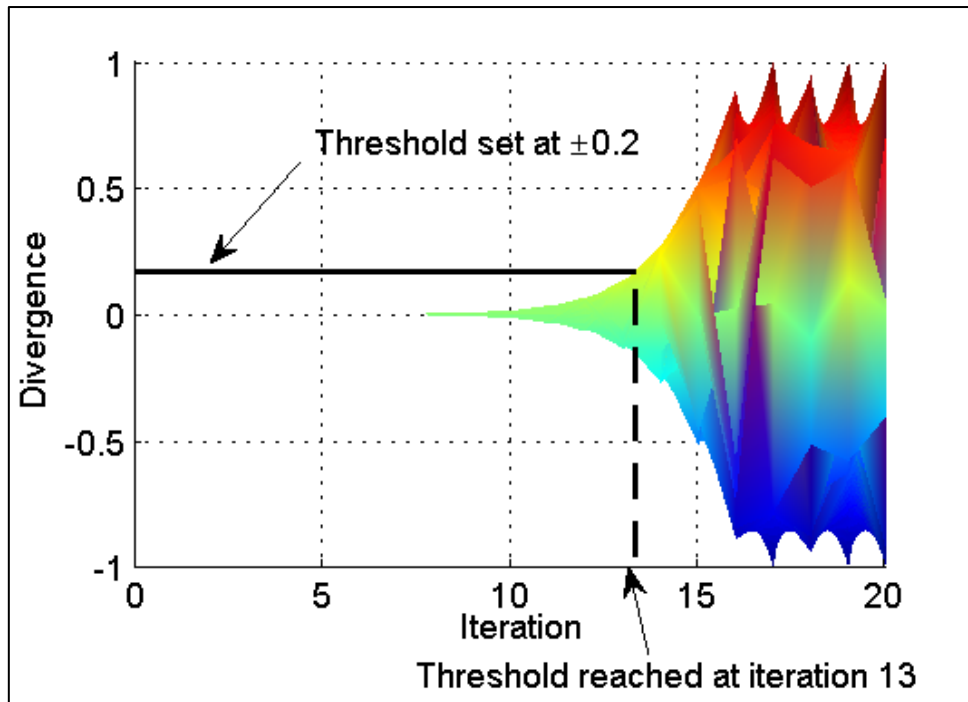


FIGURE 3-4 LM DIVERGENCE GRAPH WITH SET THRESHOLD FOR A  $\Delta$  OF 0.0001

The disadvantage of this method is that the threshold has to be defined using simulation and calibration techniques. However, this requirement is removed when the TM is used since the simple piecewise linear characteristic of the map means that the difference between two input signals can be calculated for the divergence at a given iteration using the formula given by expression (3-1).

$$\Delta = \frac{\delta}{\mu^N} \quad (3-1)$$

Where  $\Delta$  is the amount of change between the two input signals,  $\delta$  is the divergence between the two time series at iteration  $N$  and  $\mu$  is the parameter of the TM. The equation has been derived using the following process:

The gain of the TM is set by the parameter  $\mu$ , the amplification factor, which means that the total amplification after  $N$  iterations is  $\mu^N$ . Thus, if two input values, separated by a difference ( $\Delta$ ) are separately iterated through the map, the  $\Delta$  will also be amplified by  $\mu^N$ . Hence to determine the value of  $\Delta$  between two signals, the divergence  $\delta$  at a given iteration  $N$  should be divided by the overall gain obtained through the iteration process.

To illustrate the process of calculating  $\Delta$ , the parameter  $\mu$  was set to 1.99, a random input was taken and the time series was displayed in Figure 3-5. The dotted green and blue lines show the values for the original input and input with an added  $10 \mu\text{V}$  change respectively. The divergence between the two time series is represented by the red full line.

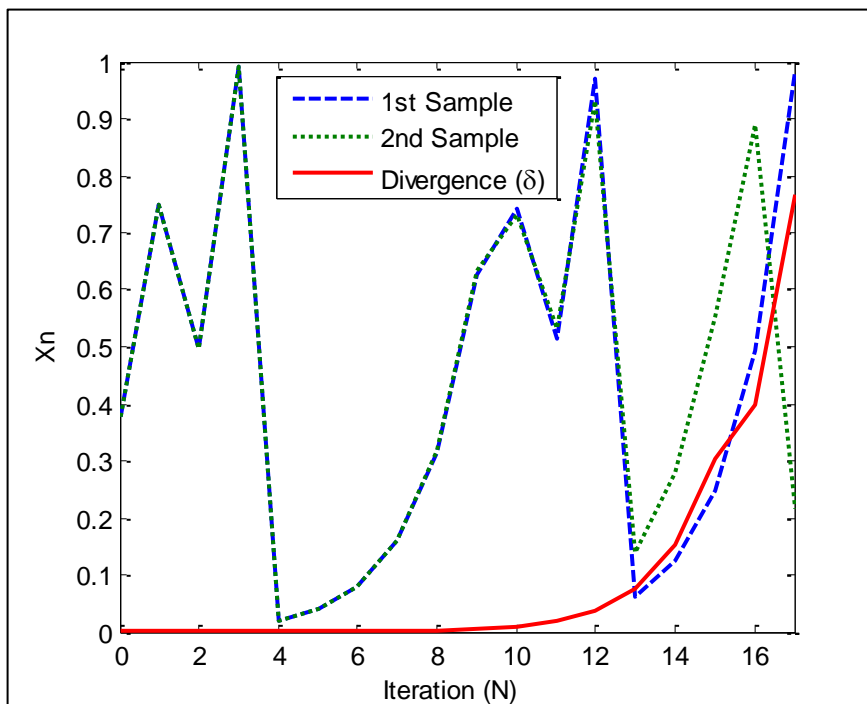


FIGURE 3-5 DIVERGENCE BETWEEN TWO SAMPLES

With an ideal MS, the difference between two signals could be estimated with an unlimited accuracy, however, in practical applications different errors and noise will

limit the performance of the proposed MS. The following section will identify all the errors associated with the chaos based measurement system and the impact of each error will be quantified.

### 3.1.1 Measurement Errors

The errors inherent to the proposed MS have been identified as being associated with the following aspects:

- Errors due to the resolution of the ADC: As shown in the previously section, the estimation of the difference between two input signals is performed using the divergence between the signatures representing the signals. The resolution of the ADC will introduce errors ( $\pm \frac{1}{2}$  step size) as the output of the chaotic map is sampled after each iteration to produce the signatures (time series).
- Errors due to the TM symmetry: The TM being symmetrical, some errors are possible when two signals are symmetrically placed on each side of the TM triangle transfer characteristic.

In addition to the sources of errors shown above, the following aspects of the measurement process have been identified as possible further sources of errors:

- Error due to the number of iteration: The measurement should be taken after a given number of iteration to avoid the loss of information due to the folding of the chaotic map. This will allow an accurate estimation of  $\Delta$ .
- Error due to the amount of divergence between two signatures: Similarly to the number of iterations, the divergence between two signatures used to

estimate  $\Delta$  is important to reduce measurement error as the folding of the map can produce significant errors.

In this section, the sources of errors are analysed and the optimal values for the number of iterations and the amount of divergence are calculated in order to obtain an accurate measurement by minimising measurement errors.

- **Errors due to ADC resolution**

With unlimited number of decimals the calculated  $\Delta$ , using expression (3-1), will match the real  $\Delta$  but in real applications, the data used for the estimation of  $\Delta$  will be limited in terms of accuracy by the resolution of the ADC used within the MS. The error between the simulated  $\Delta$  and the  $\Delta$  calculated, taking into account the resolution of the ADC is shown in Figure 3-6. The sample was limited to 3 decimal places to take into account the restricted resolution of the ADC (10 bit), used to sample the signals in the practical implementation. The error as a percentage of the estimated value of  $\Delta$ , is displayed with the dotted line while the error in volts is shown using a full line. For the first 6 iterations the divergence ( $\delta$ ) being smaller than one LSB of the ADC the calculation yields  $\Delta = 0$  which meant that the system is unable to calculate  $\Delta$  (change undetectable by the ADC). At iteration 7,  $\delta$  is greater than 1 LSB and therefore large enough to be measured by the ADC; the  $\Delta$  is calculated with an error of 19.1%. The error decreased significantly as the number of iterations increased, this is due to the  $\delta$  being considerably greater than the LSB of the ADC. By iteration 13 the error has reduced to less than 1% and reaches the lowest value at iteration 15 with an error of -0.02% representing an error of only 2 nV for a  $\Delta$  of 10  $\mu$ V. After iteration 15 the folding of the TM causes the measurement of the divergence to be inaccurate due to the error increase. The data

used to create Figure 3-5 and Figure 3-6 is available in Table A-1 in Appendix A. These results demonstrate that a  $\Delta$  of 10  $\mu\text{V}$  could be detected to within  $\pm 2$  nV using the proposed technique utilising a low resolution ADC.

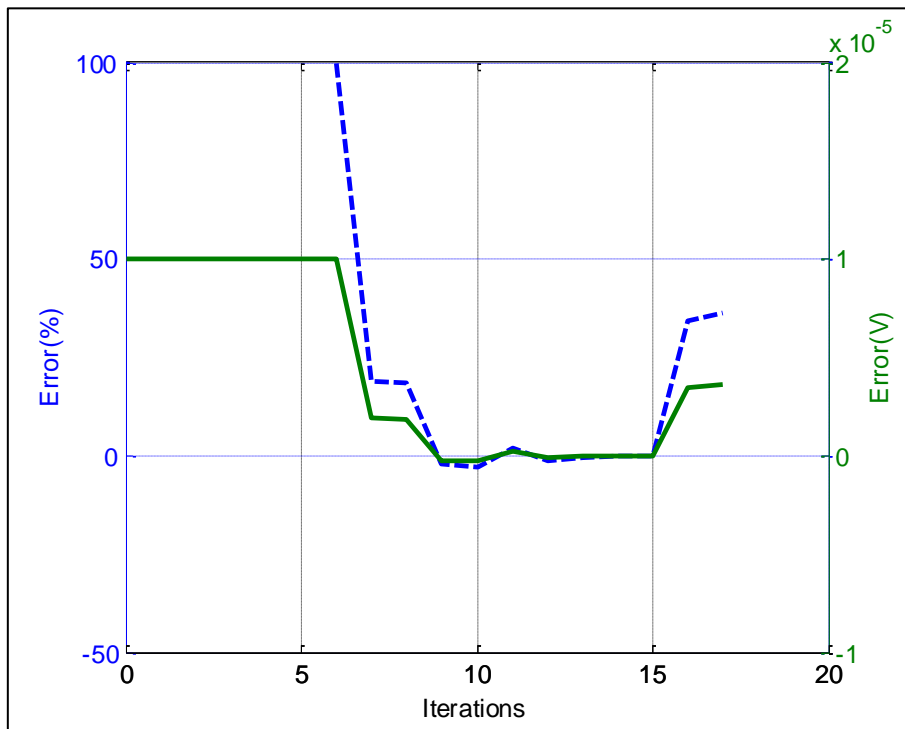


FIGURE 3-6  $\Delta$  ESTIMATION ERROR

- **Errors due to the Tent Map symmetry**

Given the symmetrical nature of the TM, two different input signals that are equidistant from of the peak of the TM triangle will produce identical time series. For example, the input value 0.49 and the input value 0.51 will produce the same time series and only the first values (the initial input value) are different, given by equation (4-9) and illustrated in Figure 3-7. The two time series for  $\mu = 2$  are shown in Figure 3-8, the data used to produce the graph is available in Appendix A, Table A-2. Although the two inputs are separated by 0.02, the two time series are identical from iteration 1 meaning that the divergence will not occur (in a noiseless system).

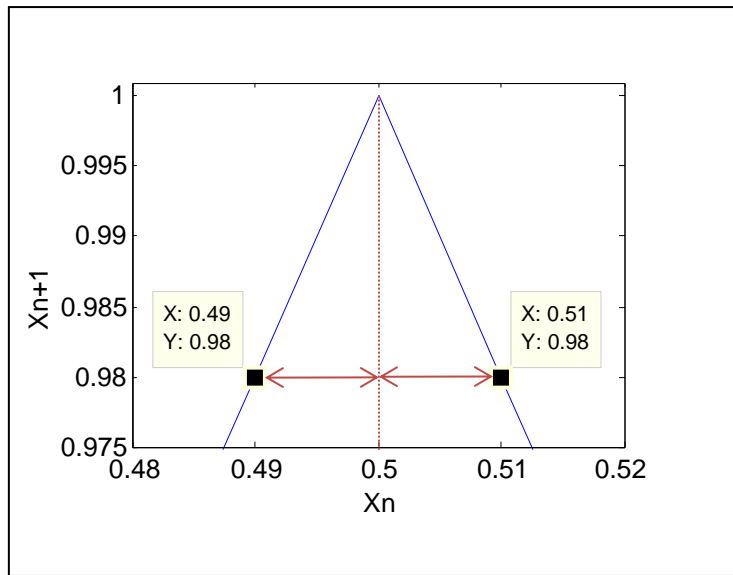


FIGURE 3-7 TWO INPUTS WITH IDENTICAL OUTPUT VALUES

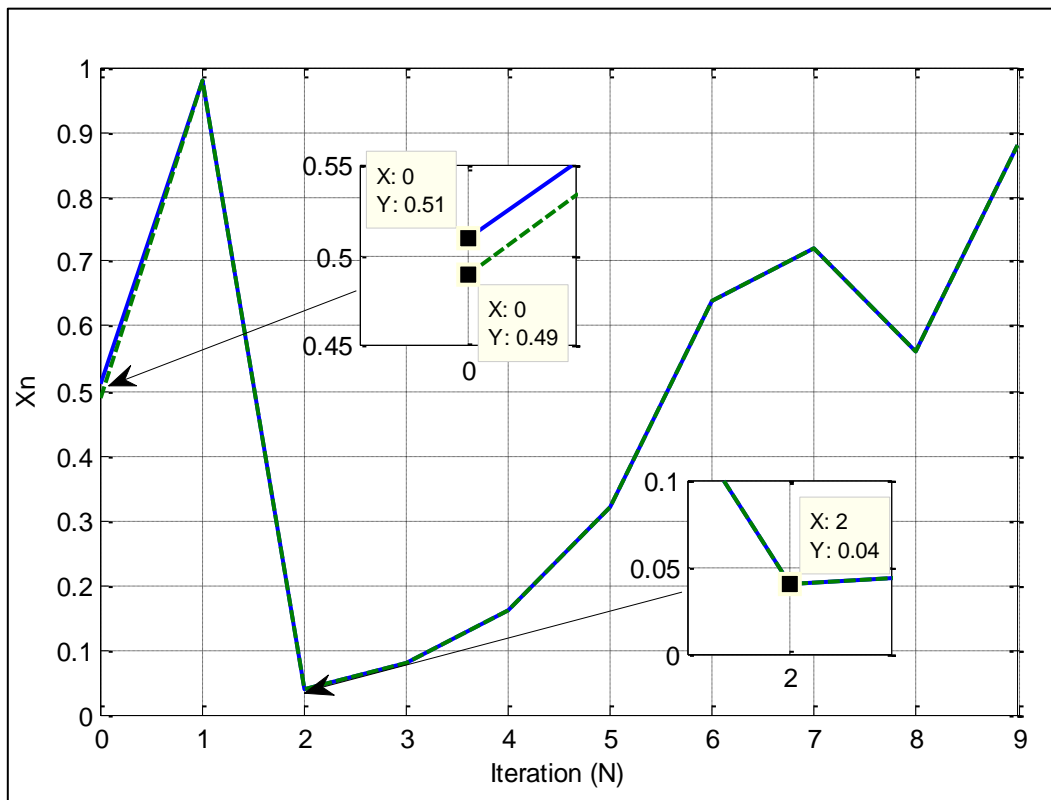


FIGURE 3-8 TWO IDENTICAL TIME SERIES FROM TWO DIFFERENT INPUTS

This feature of the TM behavior can cause errors in the estimation of  $\Delta$ , however Matlab was used to compute the divergence  $\delta$  at iteration  $N$  for a fixed change  $\Delta$

throughout the entire input range. This allowed the effect on the estimation of  $\Delta$  to be analysed. In Figure 3-9 the amount of divergence  $\delta$  is shown for iteration 1, 2, 3 and 6 for a  $\Delta$  of  $50 \mu V$ . A point of significant reduction in divergence  $\delta$ , which will be referred to as “Null” (D) is visible in iteration 1 then the number of nulls increases with the number of iterations following expression (3-2).

$$D = 2^n - 1 \quad (3-2)$$

The width of the null is equal to the amount of change  $\Delta$  at the input as shown in Figure 3-10, where  $\Delta$  was set to  $100 \mu V$ . The fact that the width of a null is equal to the change between two input signals, the probability of being at a null can be calculated using expression (3-3).

$$P(\text{Null}) = \frac{\Delta D}{R} * 100 \% \quad (3-3)$$

Where R is the input range,  $\Delta$  the input change and D the number of nulls for a given iteration N.

From expression (3-3), in order to minimise the probability of being at a null, D should be decreased by reducing the number of iteration whilst the input range R should be maximized. For a  $\Delta$  of  $100 \mu V$  the probability P(Null) is 0.06% when the measurement is taken at iteration 6. As shown in Figure 3-8, the null occurs when the time series reach a value close to one which on the next iteration (iteration 2 in Figure 3-8) generates values close to zero. This pattern can be used by the MS to

detect the presence of nulls in the measurement and thus compensate and identify the signal change more accurately given further investigation.

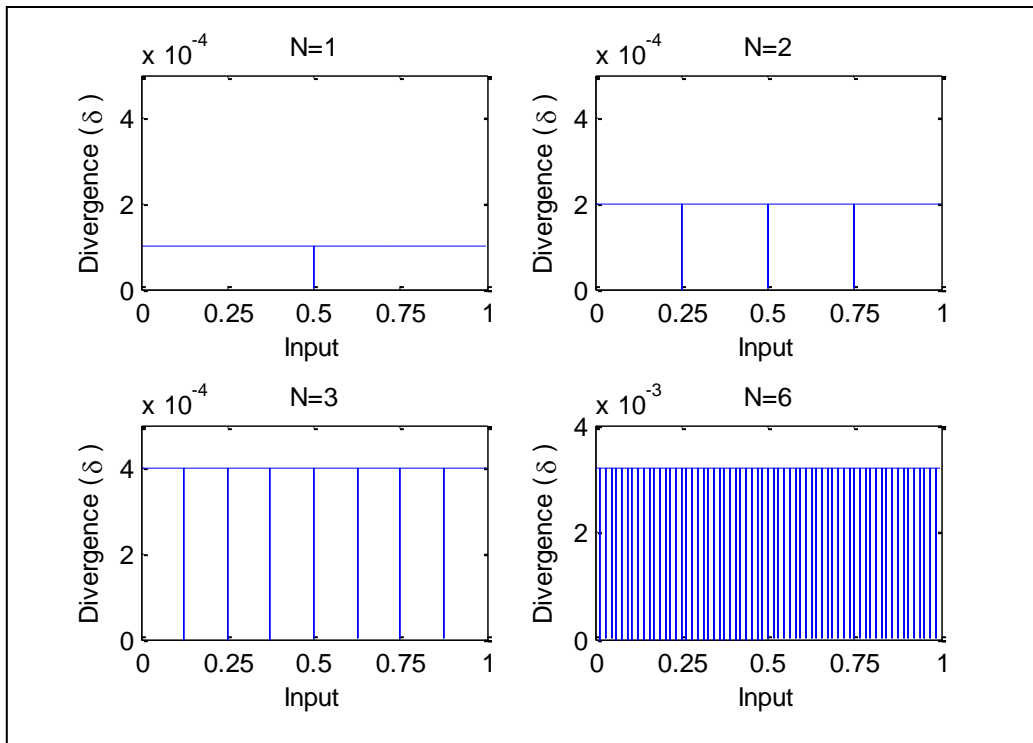


FIGURE 3-9 NUMBER OF NULLS FOR DIFFERENT VALUES OF N

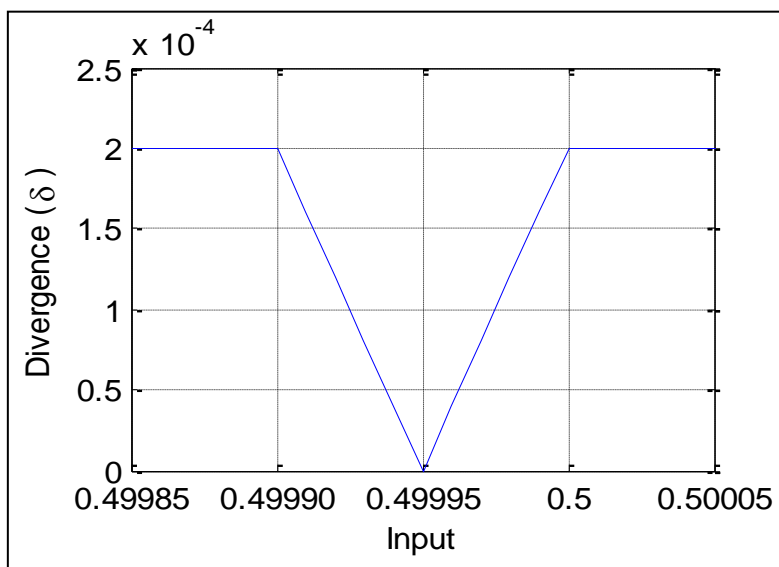


FIGURE 3-10 WIDTH OF A NULL FOR AN INPUT CHANGE OF  $100\mu V$

- **Errors associated with the number of iterations**

The number of iterations performed by the system is directly linked with the accuracy of the measurement: Figure 3-11 shows error magnitude in the calculation of  $\Delta$  against the iteration number for different values of  $\Delta$ . As expected the lower the difference ( $\Delta$ ) between two inputs the higher the iteration ( $N$ ) required to determine  $\Delta$  with an acceptable degree of accuracy. For a change of  $10 \mu\text{V}$  the error decreases to an acceptable 1% at iteration 13. It takes 10, 9 and 8 iterations to reach the same level of accuracy for a change of  $50 \mu\text{V}$ ,  $100 \mu\text{V}$  and  $200 \mu\text{V}$  respectively. Furthermore for a change of  $0.5 \text{ mV}$   $\Delta$  can be estimated to within 0.5% from iteration 1 as the change ( $\Delta$ ) can be detected with the ADC without any iteration.  $\Delta$  can be estimated with an error of less than 0.02% even when the time series used for the calculation are sampled with an ADC that limits the values to 3 decimals. The accuracy of the  $\Delta$  estimation is independent of the amount of change between the input signals.

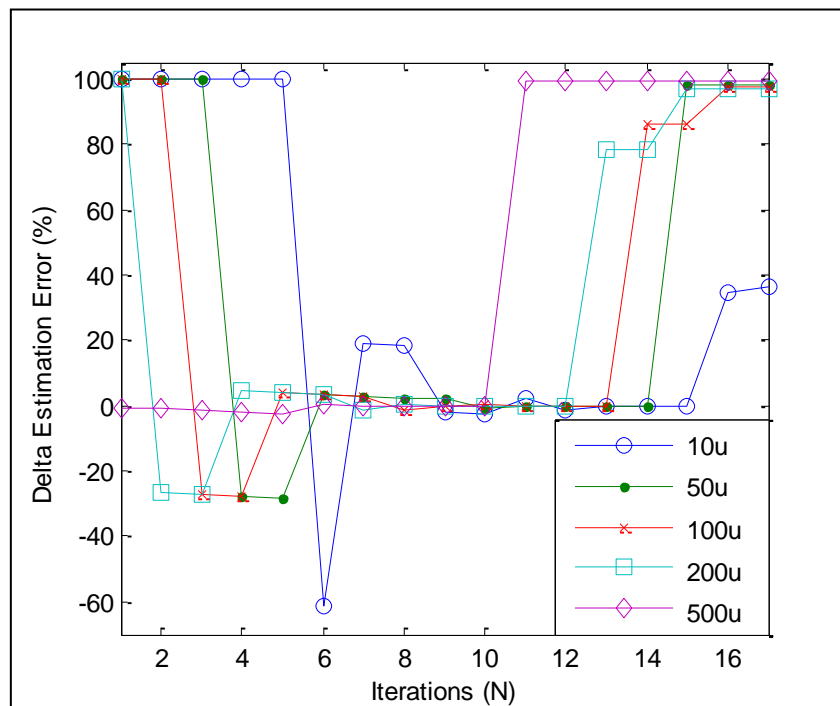


FIGURE 3-11 DELTA ESTIMATION ERROR AGAINST NUMBER OF ITERATIONS

As shown in expression (3-1), to estimate  $\Delta$  the MS requires three parameters; the value of the TM parameter  $\mu$ , the iteration number  $N$  and the value of the divergence between the two samples at any given  $N$ . In the case of an autonomous MS, the system should be able to determine the measurement, which is closest to the actual value of  $\Delta$ , yielding the highest accuracy possible. For this reason, an analysis to determine when the MS should estimate  $\Delta$  has been carried out showing the errors associated with each parameter.

- **Errors due to the amount of divergence between two signatures**

The following analysis graph (a) in Figure 3-12 shows the error in estimating  $\Delta$  against the amount of  $\delta$  between the two time series for different values of  $\Delta$ . If  $\delta$  is below 0.03 the error is greater than  $\pm 1\%$  and as  $\delta$  increases towards 0.3 the error decreases to less than  $\pm 0.1\%$ . Finally, above 0.3 the folding of the TM occurs and  $\delta$  increases again. The graph (b) Figure 3-12 shows an enlarged section of the “low error area” demonstrating that the lowest error is achieved when  $\delta$  is in the interval [0.2-0.3]. This value can be used to configure the MS to estimate  $\Delta$  as soon as  $\delta$  enters the low error interval.

In Figure 3-13 the effect of the parameter  $\mu$  on the estimation of  $\Delta$  is shown. The parameter  $\mu$  was initially set to 1.99 and varied with a  $\pm 0.001$  change to simulate any error that can arise in the real electronic implementations, between the desired set value of the parameter  $\mu$  and the real value. Sample difference ( $\Delta$ ) was set to 50  $\mu\text{V}$  and the effect on the estimation error was simulated: it appears that in the low error interval the error on the estimation of  $\Delta$  remains within  $\pm 0.5\%$ , which corresponds to an estimated  $\Delta$  of 50  $\mu\text{V} \pm 0.25 \mu\text{V}$ .

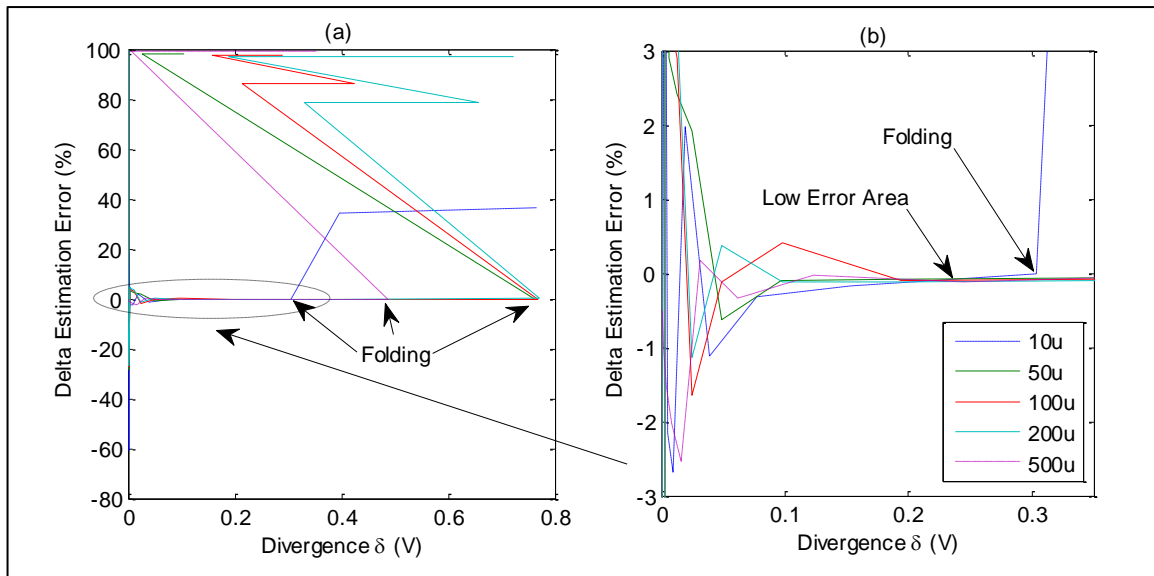


FIGURE 3-12 DELTA ESTIMATION ERROR VS AMOUNT OF DIVERGENCE FOR DIFFERENT  $\Delta$

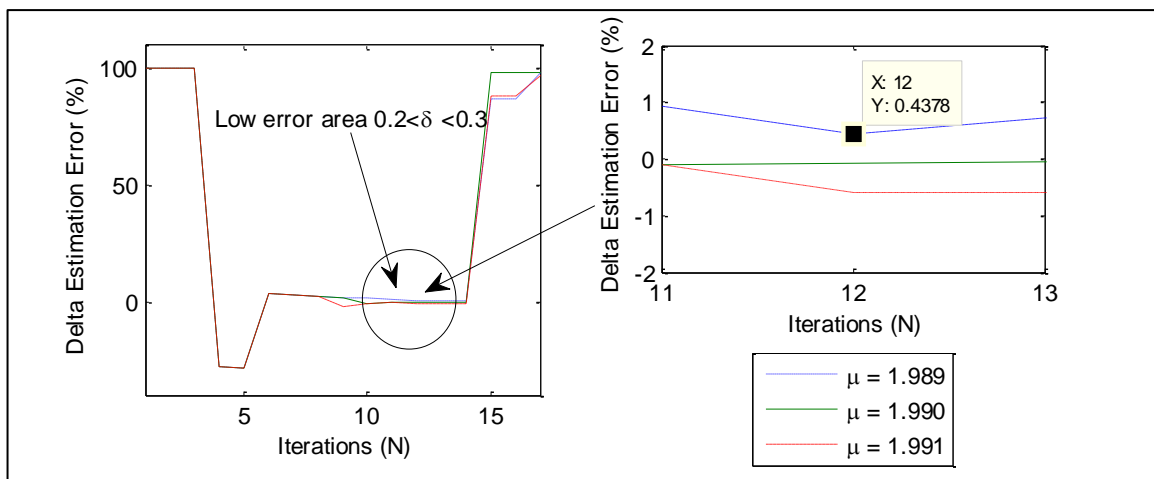


FIGURE 3-13 DELTA ESTIMATION ERROR FOR DIFFERENT VALUES OF THE PARAMETER  $\mu$

A trade-off has to be achieved between the accuracy of the measurement and the probability of reaching a “null”, which will make the estimation inaccurate. If the estimation is performed once  $\delta$  reaches 50 mV the error on the estimation of  $\Delta$  will remain lower than  $\pm 1\%$  so that for a range of 10 V the probability of reaching a null will be 0.5%. Although the probability of obtaining a “null” is not zero, the MS can identify when a null occurs as the output value of the TM is close to zero.

In this section, the mechanism of quantifying the change of input signal was discussed and a new means of measuring small variations of input signal using one-dimensional (1D) chaotic maps was proposed followed by the analyses of sources of measurement errors associated with the proposed system. Finally, the error analysis enables the optimal number of iterations and amount of divergence to be determined and used by the MS in order to obtain an accurate estimation of the input signal change. The next section will show the different topologies used for the proposed MS.

## **3.2 System with Feedback**

In order for the MS to enable successive iterations to be performed, through an electronic implementation, feedback is generally utilised.

### **3.2.1 System with Feedback Experimental Setup**

The individual maps were placed in a feedback system to allow iterations and data storage, as shown in Figure 3-14. The sampling frequency was set to 100Hz. The system operates as follows:

- The system samples the 1<sup>st</sup> input and iterates the chaotic map (N iterations); the result of every iteration is converted to a digital word and stored developing a signature or data set related to the input sample.
- A 2<sup>nd</sup> input is sampled and iterated, converted and stored (2<sup>nd</sup> signature).
- The signature (data set) for the first sample is then subtracted from the signature (data set) for the 2<sup>nd</sup> sample.

- The resulting difference signature obtained is then used to determine the amplitude of the change between the two successive samples, as the number of iterations, before the two signatures diverge, is proportional to the relative difference between the samples.
- The sample difference is measured and not the absolute value.
- The data storage and the subtraction are all performed by a microcontroller ( $\mu\text{C}$ ).

The system implementation and technical details are explained in section 4.2.1.

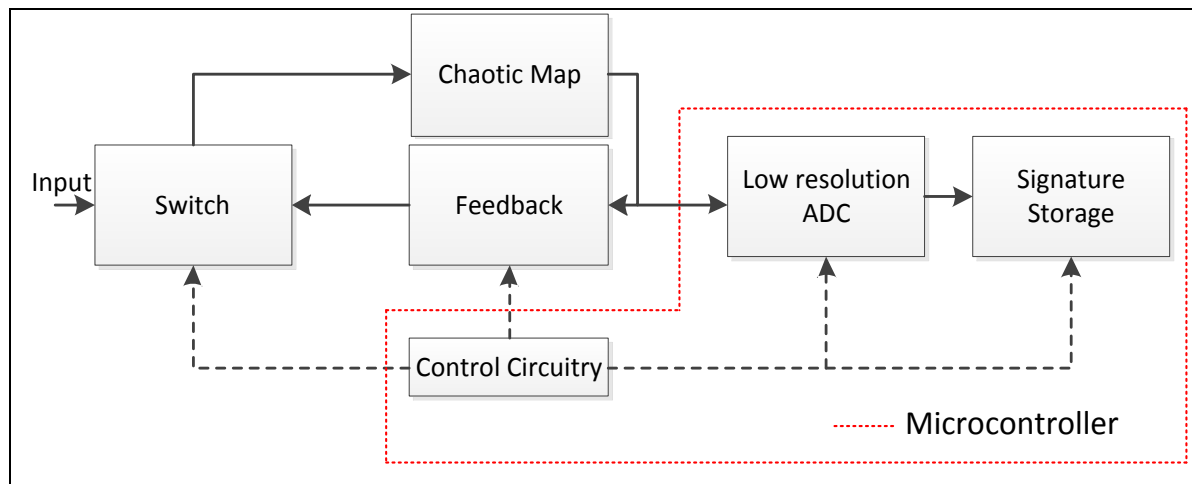


FIGURE 3-14 BLOCK DIAGRAM OF THE PRESENTED ITERATED SYSTEM

The configuration given in Figure 3-14 has been used to assess the performance of the chaotic maps and as the main implementation of the MS. The series implementation has been used to demonstrate that higher levels of sensitivity can be achieved by eliminating the errors generated due to the feedback process.

## 3.3 Series System

In the series system feedback circuitry is not required as the signal is propagated through consecutive chaotic maps implementation, which enables faster response times due to the removal of the need for clocking and eliminates errors generated by the feedback circuitry (sample and hold errors). The main drawback of the series system compared to the iterated system is that the circuitry required to perform a given number of iteration is larger and increases with the number of maps placed in series. Also the number of calculations (series propagation) is set by hardware which prevents any software modifications of the number of iterations.

### 3.3.1 Series System Experimental Setup

The series system operates in a similar way as the iterated system, the main difference is that the central circuitry is required to route the output of each map to the ADC via multiplexing. In Figure 3-15 a block diagram of a series system with three identical chaotic maps is illustrated. The block diagram has been limited to only 3 maps for clarity. The series system works as follows:

- The 1<sup>st</sup> measurement is taken by sampling the output of each map starting with map A and continues through to C. This is performed sequentially by multiplexing the analogue input being sampled in software.
- The data obtained from sampling the output of each map is used to form a signature (data set) for the 1<sup>st</sup> signal sample.
- The same procedure is performed for the next input signal sample.

- The signature from the first sample is then subtracted from the 2<sup>nd</sup> sample signature.
- The modulus of the result obtained is then used to determine the difference between the two samples, as the number of iterations, before the two signatures diverge, or the amount of divergence after N iterations is proportional to the relative difference between the samples.
- The sample difference is measured and not the absolute value.
- The data storage and the subtraction are all performed by a Microcontroller ( $\mu\text{C}$ ).

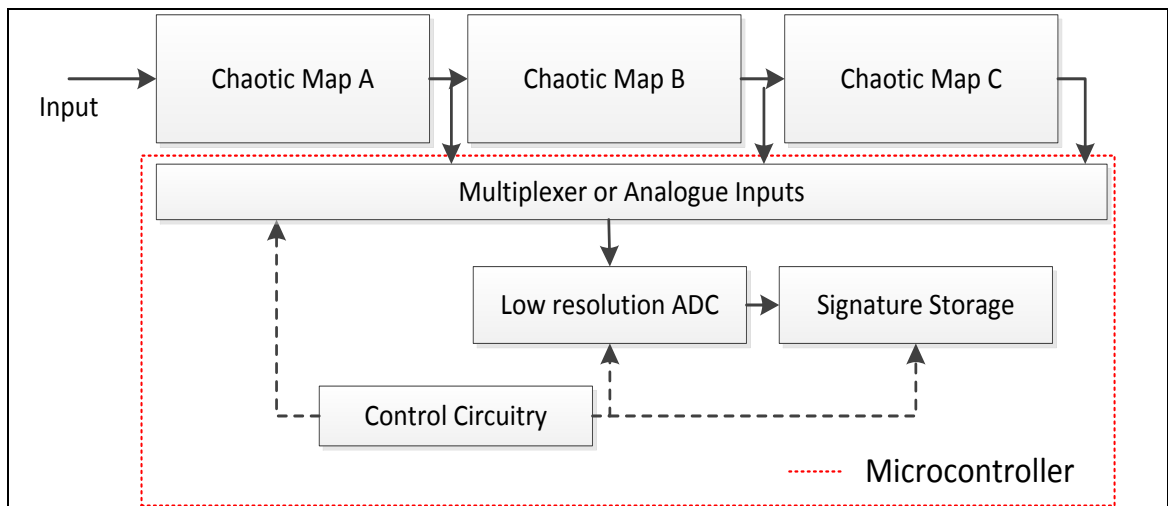


FIGURE 3-15 SERIES SYSTEM BLOCK DIAGRAM

### 3.4 Conclusion

This chapter analysed how the high sensitivity to initial conditions of one-dimensional chaotic maps can be used for the measurement of small signal changes. The working principle of the proposed technique was defined and analysed with the following significant points identified:

- A novel way of visualising the divergence of one-dimensional chaotic maps was proposed using a three dimensional (3D) graph, developed specifically for this application.
- From the 3D representations of the divergence for the LM and the TM it was determined that the TM yielded a relatively linear response throughout the entire input range. Whereas the input range of the LM has to be limited to avoid early divergence due to non-linearity near the extremities of the input range as illustrated in Figure 3-2 and Figure 3-3.
- A method of quantifying the change between two input samples has been proposed in expression (3-1), which is related to the number of iterations and the size of signature divergence.
- The sources of errors associated with the proposed system have been identified and the impact of each error has been assessed and methods of minimising the errors have been proposed.
- The analysis has also shown that “nulls” (point of lower divergence) can appear on the response of the TM around the threshold voltage.
- The number of nulls presents over the entire input range and the probability of reaching a null during a measurement have been expressed by equations (3-2) and (3-3) respectively. The probability of reaching a null during a measurement has been identified as iteration dependent.
- A method of identifying when nulls occur has been presented to avoid flawed measurements.

Finally two possible implementations of a chaos based MS were proposed which are based on the feedback and series system.

The following chapter will discuss the practical implementation of the proposed maps and the overall MS.

# 4 Measurement System Implementation

This chapter focuses on the electronic implementation of the Measurement System (MS) proposed in Chapter 3. Firstly, an electronic implementation of the Logistic Map (LM) and the Tent Map (TM) are proposed followed by the full implementation of the two MS topologies; feedback and series.

## 4.1 One-Dimensional Maps Implementation

This section will discuss the electronic implementation of the LM and the TM, which are two of the simplest mathematical expressions exhibiting chaotic behaviour making them ideal for electronic implementation. As the circuitry required to implement the maps is relatively simple, a low noise implementation is achievable, which is paramount for MS.

### 4.1.1 Logistic Map Implementation

For the design and implementation of the LM; the initial step was to investigate an electronic circuit based on the implementation available in literature (Suneel, 2006). The electronic circuitry was then assessed to ascertain that the system exhibits the characteristics and behaviour identified in the theoretical LM model. Subsequently, the behaviour was established by collecting systems measurements to obtain the LM parabola, the bifurcation diagram and the time series.

The prototype of the LM was implemented using readily available low cost electronic components as shown in Figure 4-2. The LM equation implemented is the modified version to enable an input range of 0 V to 10 V instead of the normalised 0 V to 1 V input range of the classic LM given in expression (2-8). The modified LM shown in equation (4-1) is identical to the original LM the only difference being the scaling factor.

$$x_{n+1} = r_s x_n (10 - x_n) \quad (4-1)$$

Where  $r_s$  can vary from 0 to 0.4 which is equivalent to a variation of  $r$  from 0 to 4 in the classic LM shown in equation (2-8).

Scaling up the LM does not change the behaviour but solely the input and output range which allows the Measurement System (MS) to detect variation of input signal over a wider input range. In order to obtain the expression in equation (4-1), using electronic circuitry, three main circuit blocks were used as shown in Figure 4-1; one subtractor and two multipliers. The first multiplier (multiplier (A)) multiplies the input by the parameter  $r_s$  to obtain  $r_s x_n$ . The subtractor subtracts the input from a 10 V reference to obtain  $(10 - x_n)$ . Finally, the second multiplier (B) multiplies the results from the previous blocks to generate the modified LM expression (4-1).

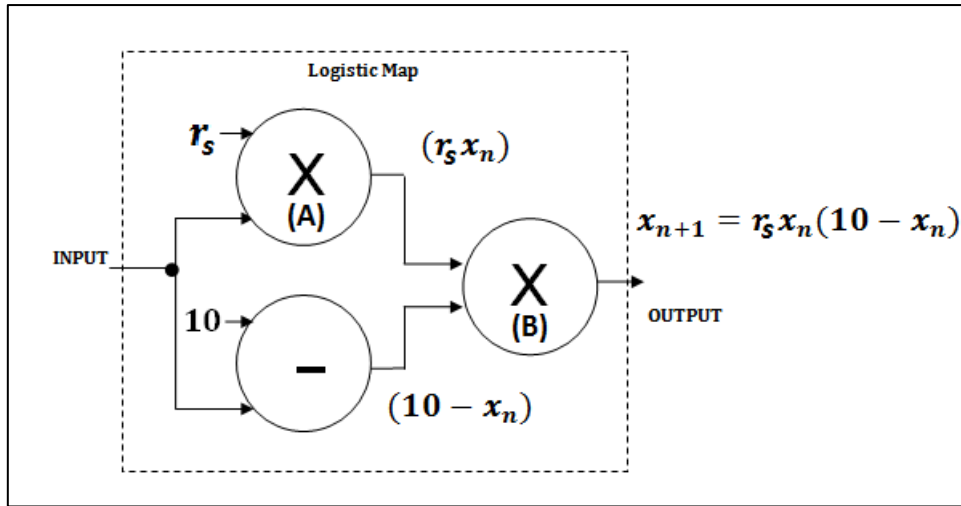


FIGURE 4-1 BLOCK DIAGRAM OF THE LM IMPLEMENTATION

Figure 4-2 shows the circuit diagram of the proposed implementation; which uses three OP27 operational amplifiers (Analog-Devices, 2003) and one AD633JN analogue multiplier (Analog-Devices, 2012) along with several passive components. The passive components used for power supply decoupling and noise filtering are omitted from the schematic to keep the schematic clear. The 10 V reference voltage was produced using a low noise AD587 voltage reference IC (Analog-Devices, 2007); not shown in the simplified schematic. The full schematic is shown in Appendix G and some notes regarding the selection of components are available in Appendix H.

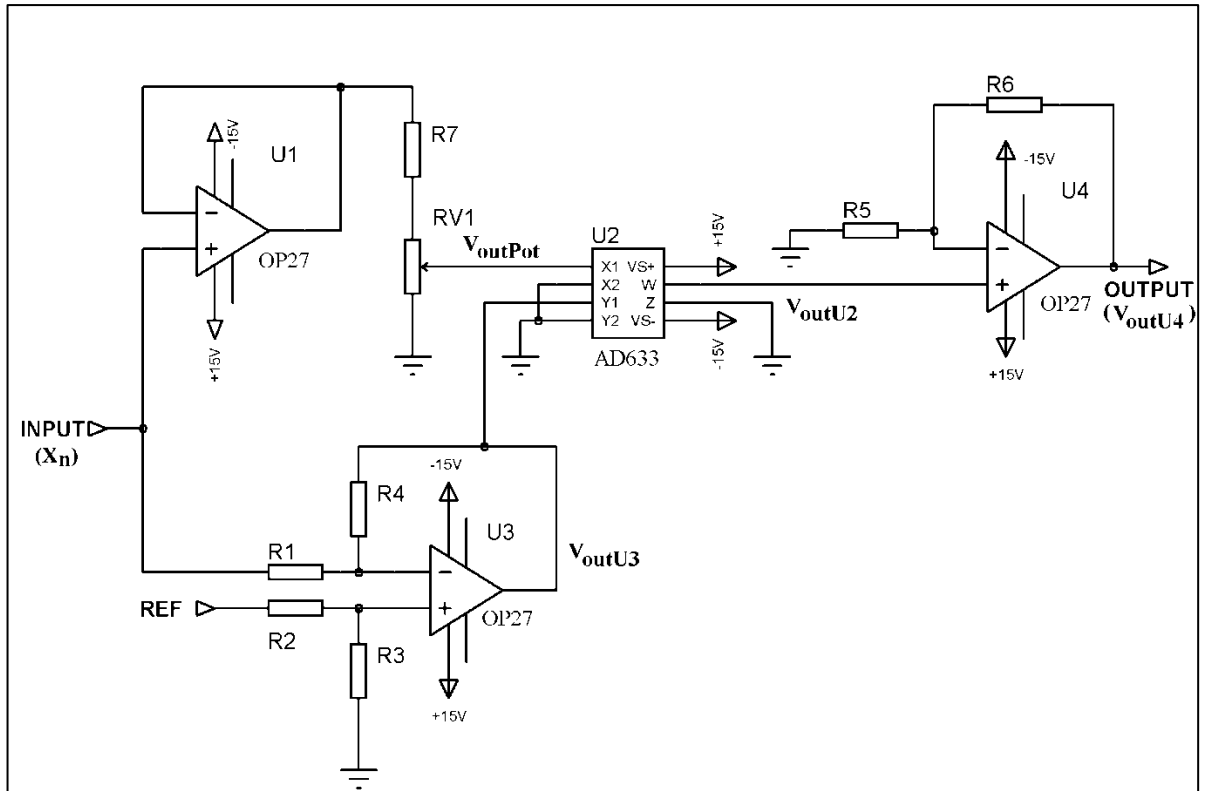


FIGURE 4-2 SIMPLIFIED SCHEMATIC OF THE MODIFIED LM.

In Figure 4-2, U1 is an op-amp configured as a unity gain buffer to insure that R7 and RV1 are not loading the input ( $x_n$ ). The input ( $x_n$ ) is scaled by the constant  $r_s$  set by the potential divider configuration R7 and RV1 following the expression (4-2);  $r_s$  can be set anywhere between 0 and 0.4 by varying the position of RV1.

$$V_{outPot} = x_n \frac{\alpha RV1}{R7 + RV1} = r_s x_n \quad (4-2)$$

Where  $\alpha$  is a variable representing the position of the potentiometer ranging from 0 (minimum) to 1 (maximum). U3 is an operational amplifier configured as a difference amplifier with a transfer function given by the expression (4-3).

$$V_{outU3} = Ref \left( \frac{(R4 + R1)R3}{(R3 + R4)R1} \right) - x_n \left( \frac{R4}{R1} \right) \quad (4-3)$$

The resistors R1 to R4 are set to identical values so that the signal at the inverting input of U3 is subtracted from the signal at the non-inverting input. Hence, in this case the expression (4-3) can be simplified to the expression (4-4), with the reference voltage (Ref) set to 10 V.

$$V_{out_{U3}} = 10 - x_n \quad (4-4)$$

The outputs from U1 and U3 are multiplied using an AD633JN analogue multiplier IC (U2). With a transfer function according to the manufacturer datasheet (Analog-Devices, 2012) given in expression (4-5).

$$V_{out_{U2}} = \frac{(X1 - X2)(Y1 - Y2)}{10} + Z \quad (4-5)$$

In the LM implementation, X2, Y2 are connected to ground since the inputs of the multiplier are single ended (not differential). Z is also connected to ground as no offset is required. This simplifies the expression (4-5) to the expression (4-6).

$$V_{out_{U2}} = \frac{X1 Y1}{10} \quad (4-6)$$

The input X1 is connected to  $V_{out_{Pot}}$  and the input Y1 to  $V_{out_{U3}}$ , which yields the expression (4-7).

$$V_{out_{U2}} = \frac{r_{x_n}(10 - x_n)}{10} \quad (4-7)$$

Since the internal circuitry of the AD633JN multiplier (U2) divides the output by 10,  $V_{out_{U2}}$  is amplified by U4, configured as a non-inverting amplifier with a gain set to

10, in order to obtain the modified LM. The transfer characteristic of the overall circuit is expressed by (4-8).

$$V_{out_{U4}} = V_{out} = \left( \frac{r_{x_n}(10 - x_n)}{10} \right) \left( 1 + \frac{R6}{R5} \right) \quad (4-8)$$

Resistors R6 and R5 are set to obtain a gain of 10 which gives the final transfer characteristic of the whole circuit to match the modified LM as expressed in (4-1).

In this section an electronic implementation of the modified LM was presented; using readily available components the transfer characteristic obtained is identical to the modified LM expression in (4-1). The full schematic of the LM implementation is shown in Appendix G. Contrary to other implementations available in literature such as the circuit presented by Suneel (2006) the proposed implementation uses a single multiplier which simplifies the circuit and reduces the inherent noise as discussed further in section 5.7.

### 4.1.2 Tent Map Implementation

The TM circuit was also constructed using readily available low noise components; the block diagram of the proposed TM implementation is shown in Figure 4-3 and is constructed using four main circuit blocks; level shifter, half wave rectifier, amplifier and adder. The input to the circuit is propagating through two paths shown as (1) and (2). Path (1) is composed of an amplifier to create the line shown as (1). Path (2) is composed of the level shifter and half wave rectifier to create the transfer function shown as (2) in Figure 4-4. This section of the circuit implements the 0.5 V threshold voltage (set by the reference voltage) required to generate the overall transfer characteristic of the TM; the two transfer characteristics obtained from (1) and (2)

are inverted and added to obtain the overall transfer characteristic of the TM. The schematic of the proposed implementation is shown in Figure 4-5. Some components are omitted to simplify the schematic. The full schematic is available in Appendix G along with note regarding the components selection in Appendix H.

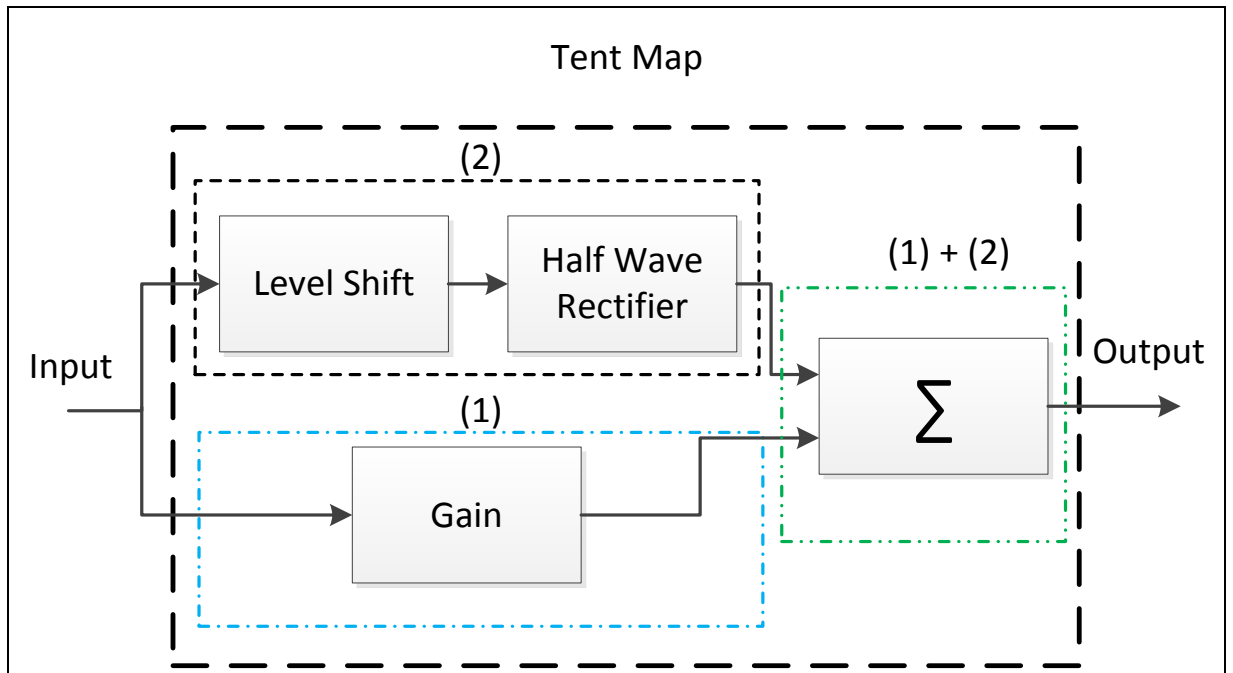


FIGURE 4-3 BLOCK DIAGRAM OF THE TM IMPLEMENTATION

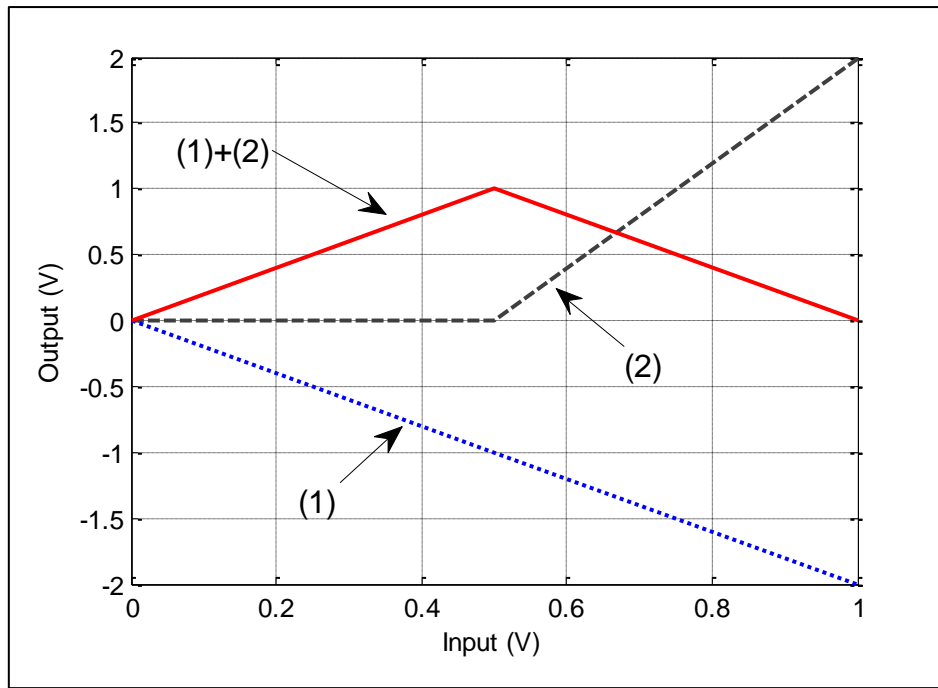


FIGURE 4-4 CONSTRUCTION OF THE TM TRANSFER CHARACTERISTIC

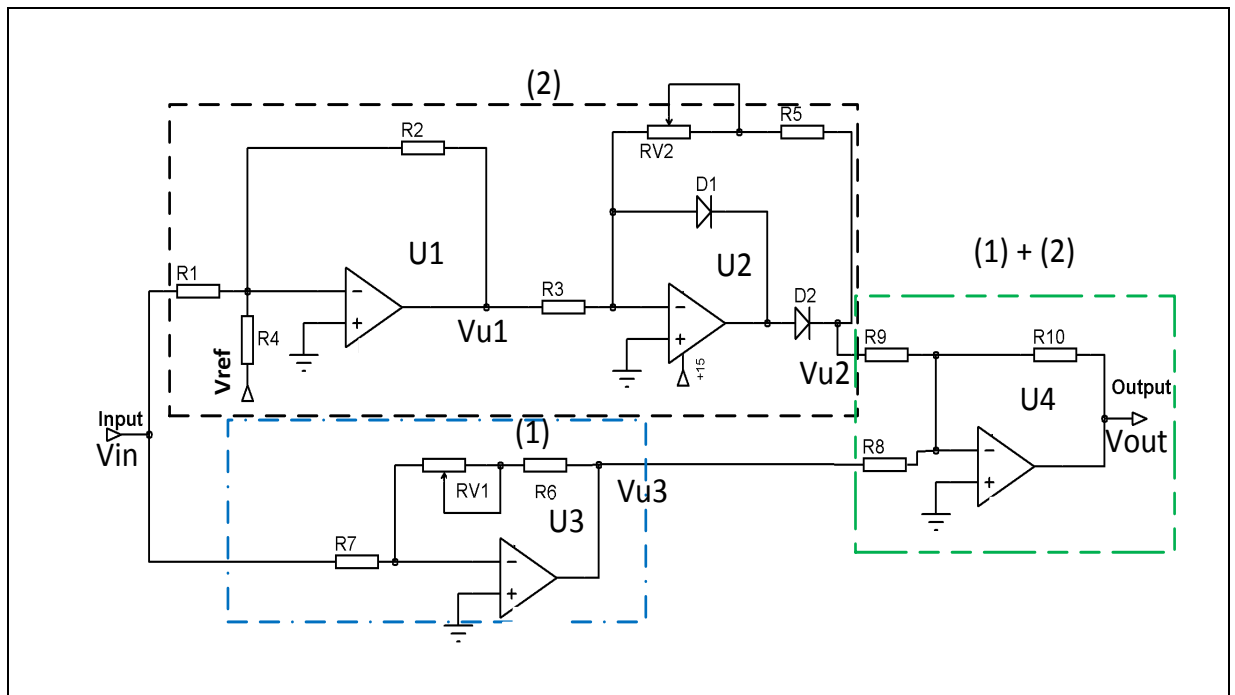


FIGURE 4-5 SCHEMATIC OF THE PROPOSED IMPLEMENTATION OF THE TM

The upper branch of the circuit (shown as (2) in Figure 4-3 and Figure 4-5) is composed of two blocks constructed around the level shifter (U1) and the half wave rectifier (U2) in Figure 4-5. The input signal is applied to a summing amplifier (U1)

to shift by an amount equal to  $V_{ref}$ . The resistor values  $R_1$ ,  $R_2$  and  $R_4$  are identical so that the transfer function can be expressed as (4-9).

$$V_{U1} = -(V_{in} + V_{ref}) \quad (4-9)$$

The output of the half wave rectifier constructed around  $U_2$  has two conditions; when the input is greater than 0 V the output is 0 V and when the input is below 0 V the output is inverted and amplified by a gain set using  $R_{V2}$ ,  $R_5$  and  $R_3$ . Because of the shifting introduced by the previous stage ( $U_1$ ) the threshold is moved from 0 V to  $-V_{ref}$  giving an overall response expressed by equation (4-10).

$$V_{U2} = \begin{cases} \left| -\frac{\alpha R_{V2} + R_5}{R_3} V_{U1} \right| & \text{for } V_{U1} < 0 \\ 0 & \text{for } V_{U1} > 0 \end{cases} \quad (4-10)$$

For the lower path (1) the transfer function given by equation (4-11) is achieved using an inverting amplifier with the gain set by  $R_{V1}$ ,  $R_6$  and  $R_7$ .

$$V_{U3} = -\frac{\alpha R_{V1} + R_6}{R_7} V_{in} \quad (4-11)$$

Paths (1) and (2) are summed using the summing amplifier constructed around  $U_4$  as expressed in (4-12).

$$V_{U4} = -(V_{U2} + V_{U3}) \quad (4-12)$$

Finally, substituting expressions (4-10) and (4-12) for  $V_{U2}$  and  $V_{U3}$  respectively gives expression (4-13).

$$V_{U4} = \begin{cases} - \left( \left| -\frac{\alpha RV2 + R5}{R3} V_{U1} \right| + \frac{(-\alpha RV1 + R6)}{R7} V_{in} \right) & \text{for } V_{in} > -V_{ref} \\ \frac{\alpha RV1 + R6}{R7} V_{in} & \text{for } V_{in} < -V_{ref} \end{cases} \quad (4-13)$$

Where R3 and R5 are set to obtain a gain close to -2, while the resistors R6 and R7 are set to obtain a gain of approximately 4. Inverting and adding the two gains (from paths (1) and (2)) gives a gain of -2 on the second half of the TM characteristic. RV1 and RV2 are used to vary the gains of the two paths (1) and (2) respectively in order to set the parameter of the TM. The reference voltage was produced using a low noise ADR130 voltage reference IC (Analog-Devices, 2013); not shown in the simplified schematic. Vref is set to -0.5 V which gives the original expression of the TM shown in expression (4-14).

$$x_{n+1} = \begin{cases} \mu x_n & \text{for } x_n < \frac{1}{2} \\ \mu(1 - x_n) & \text{for } x_n \geq \frac{1}{2} \end{cases} \quad (4-14)$$

After implementing the LM and the TM the next section will discuss the implementation of the two different topologies of Measurement System (MS).

## 4.2 Measurement System Implementation

In this section the feedback and series measurement system (MS) are implemented.

### 4.2.1 Feedback System Implementation

The working principle of the feedback system was explained in section 3.2.1 and was implemented electronically as per the block diagram presented in Figure 3-14,

the schematic implementation is shown in Figure 4-6. The system design was divided into three sections; a switch between the input and the feedback, a feedback path and the control and storage circuitry. The control circuitry, ADC and memory, are all embedded within a PIC32MX460L  $\mu\text{C}$ : on a Mikroelektronika LV32MX v6 development board, and programmed using Microchip MPLAB environment along with a C32 compiler. A graphic Liquid Crystal Display (LCD) with touch screen provides a graphical user interface by displaying the state of the system. Appendix H discusses the requirements of the  $\mu\text{C}$ . For the digital outputs and analogue inputs the following configuration was used:

- Two digital outputs are used to control the switching between the input and the feedback.
- Further digital outputs are used to control the sample and hold circuitry of the feedback and to discharge (reset) the sample and hold capacitors before the next sample is taken.
- An analogue input was used to sample the chaotic map output and convert to digital data using the internal 10 bit ADC.

The sampled data was stored in the internal memory and transferred to an external USB memory in a Comma-Separated Values (CSV) format to allow the data to be analysed and displayed using MATLAB.

The switching and the sampling process were implemented as follows:

- The Switching circuit block (A) between the input and the feedback (B) was implemented using the DG211 analogue switch IC (Maxim, 2006). The DG211 being a normally closed switch, a logic "0" closes the switch whilst a logic "1" opens the switch.

- The feedback block (B) was implemented with two LF198 Sample and Hold (S/H) circuits (U6, U7) along with two low leakage 0.1  $\mu\text{F}$  capacitors to reduce errors in the feedback path. The switches SW1 and SW2 are used to connect and disconnect the input or the feedback to the input of the chaotic map using pins RC2 and RC3 of the  $\mu\text{C}$ .
- The S/Hs are controlled via the  $\mu\text{C}$  pins (RC4 and RC5). The S/H capacitors were selected to provide low leakage and low dielectric absorption error (Texas-Instruments, 2000). The dielectric absorption can produce significant errors by offsetting the following sample (Analog-Devices, 2008). In addition to the use of polypropylene capacitors, to eliminate any errors due to remaining charge in the S/H capacitors two N-channel MOSFETS (Q1 and Q2) were connected in parallel with C1 and C2 to provide full discharge of the capacitors. A comparator (U1) is used to drive Q1 and Q2, as  $\mu\text{C}$  output pins are unable to drive the MOSFETs directly due to insufficient output voltage. After each series of iterations, before the next input is fed to the chaotic map the  $\mu\text{C}$  triggers the comparator and switches on the MOSFETs, C1 and C2 are short-circuited which removes any remaining charge.

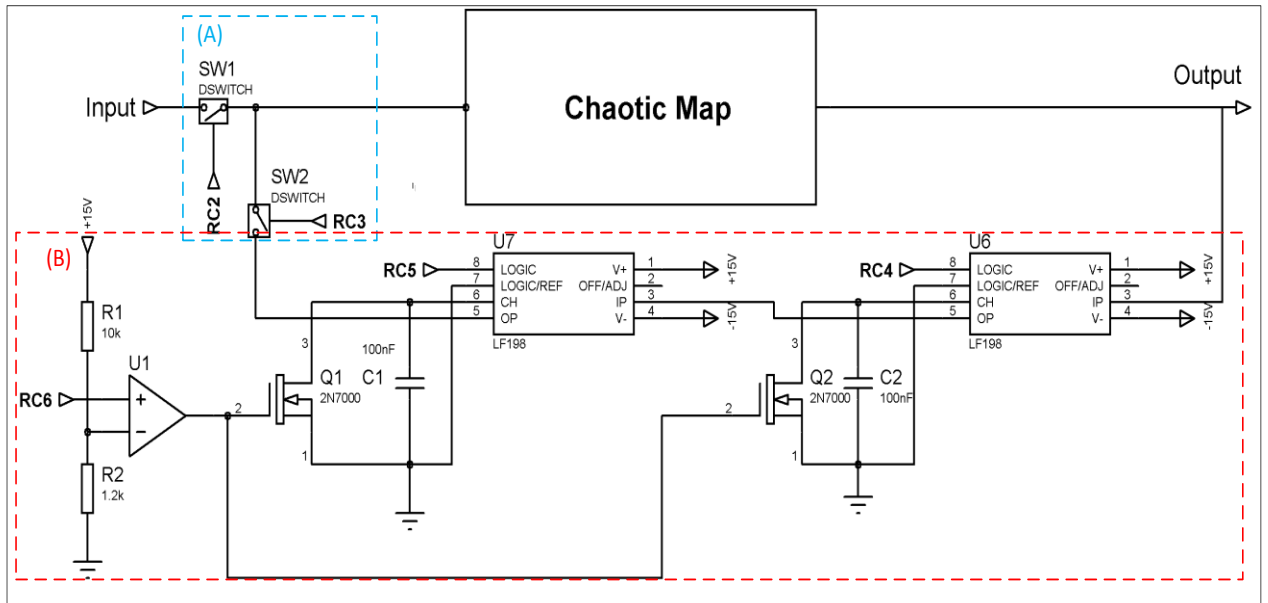


FIGURE 4-6 SCHEMATIC OF THE FEEDBACK SYSTEM FOR MAP ITERATION

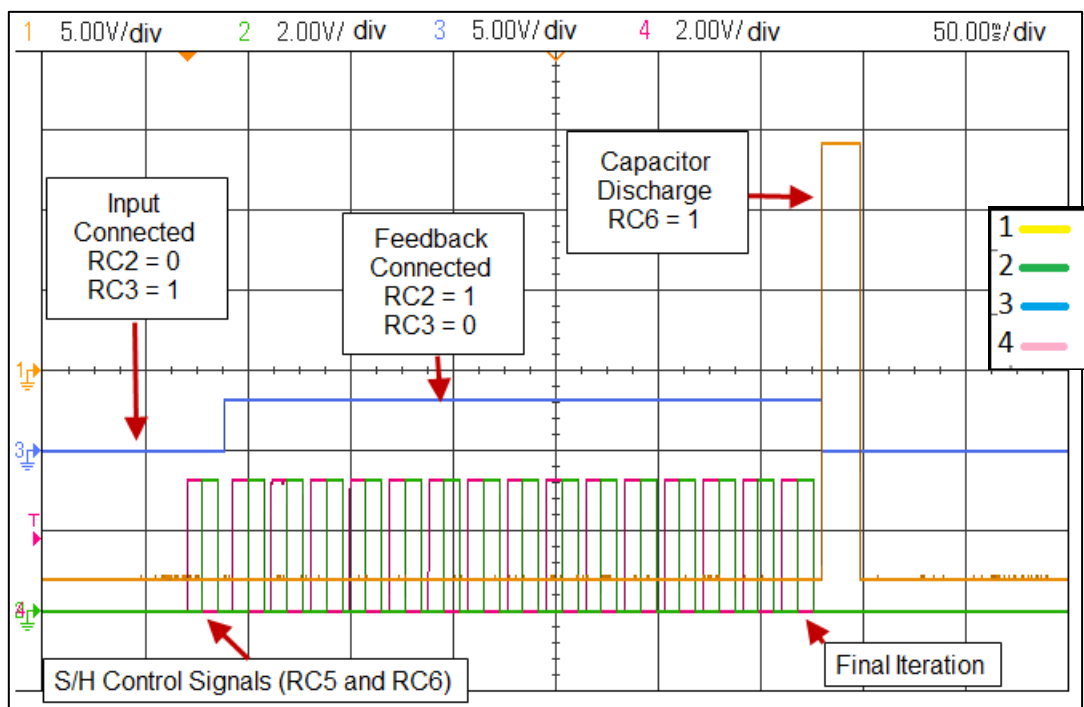


FIGURE 4-7 CONTROL SIGNALS FOR THE ITERATED MEASUREMENT SYSTEM

The signals of a typical run of the iterated MS are shown in the oscilloscope screen capture in Figure 4-7. The signal number is shown on the left hand side of the graph while the scale for each signal (in volts per division) is displayed at the top. Signals

(2) and (4) represent the control signals for the S/H (RC4 and RC5) respectively. Signal (3) is used to control the switching between the input and the feedback (RC2); RC3 is not represented as it is the opposite of RC2. Finally, signal (1) represents the output of the comparator U1 (RC6). The iterative process follows the steps described below:

- Firstly the input is connected to the chaotic map and the resultant output signal is stored in the capacitors by sending a pulse to the S/Hs with RC4 then RC5.
- The input is then disconnected before the feedback is connected to the chaotic map.
- After a delay specified for the signal to propagate through the map circuit the output signal is stored in the S/H capacitors. The pulses for the S/Hs are repeated N times which generate the iterations.
- After each iteration the output signal is sampled, digitised and stored in the internal memory of the  $\mu\text{C}$ . Once the set number of iterations N is reached the input is reconnected and the feedback disconnected.
- The MOSFETS are activated to remove any remaining charge from the capacitors.
- The MS is then ready for the next measurement.

## **4.2.2 Series System Implementation**

In the series implementation no switching of feedback is required; the input of the system and the outputs of each map are connected to a separate analogue input of the ADC as shown in Figure 4-8. The development board and the  $\mu\text{C}$  used to perform the ADC function and the measurement are the same as for the feedback system as

shown in section 4.2.1. The schematic of the given map is copied and connected in series as shown in the block diagram of the series implementation in Figure 4-8: the actual schematic of the series system is not shown due to its simplicity. The  $\mu\text{C}$  used has 16 analogue inputs which mean that the MS is able to perform up to 16 measurements of chaos map outputs, without an additional multiplexer. The propagation of the signal is not controlled by the  $\mu\text{C}$  as the signal propagates freely through each map. The signature is constructed by sampling the output of each map.

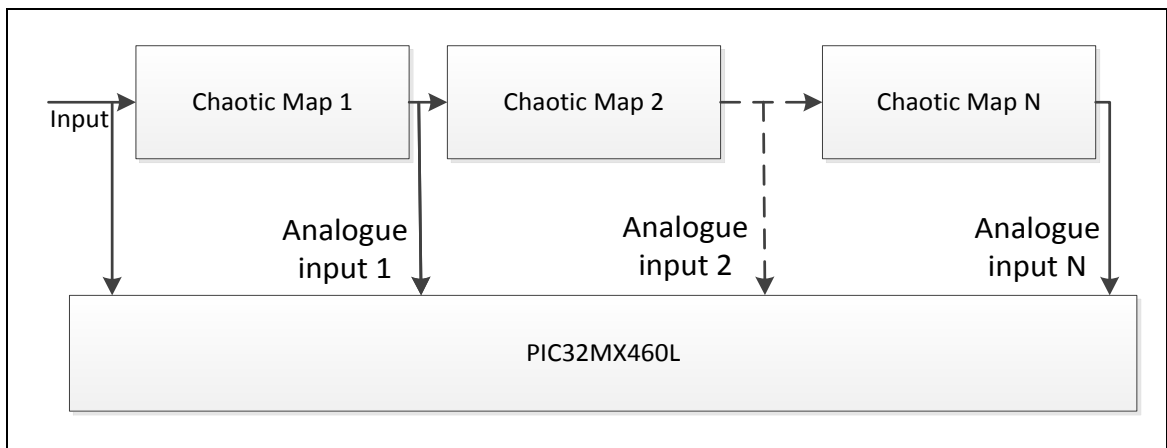


FIGURE 4-8 BLOCK DIAGRAM OF THE SERIES SYSTEM

### 4.3 Conclusion

The first section of this chapter focused on the practical implementation of two one-dimensional chaotic maps, the Logistic and the Tent map respectively. The design process was undertaken to develop an electronic system based on the mathematical expression of each map; to do so, a block diagram was produced followed by the electronic implementation of the maps. The transfer function of each functional block was used to analyse the overall transfer characteristic of the proposed implementation and to ascertain the matching accuracy between the presented circuit and the associated mathematical expression.

High performance, yet readily available components were used to obtain a circuit that yields increased overall MS performance, by reducing the overall noise whilst avoiding expensive and hard to source components.

The second section explains the implemented feedback and series MS. The feedback system requires switching circuitry and S/Hs for the iterations whereas the series system requires multiple identical implementation of the map circuitry which creates a relatively cumbersome MS if a large number of stages are required.

The following chapter will assess the performance of the developed implementations.

# 5 Performance Analysis of Implemented Chaotic Maps

This chapter focuses on the performance analysis of the LM and the TM. To assess the performance, the electronic implementations will be compared to the theoretical maps using the following measurements:

- **Transfer characteristic:** this will assess the accuracy of the practical implementation compared to the theory (transfer characteristic).
- **Bifurcation diagram:** the bifurcation diagram will allow the behaviour of the proposed implementations to be visualised for variations of the map parameter. The bifurcation diagram obtained practically for each map should match the theoretical bifurcation diagrams shown in section 2.3 and exhibit all the characteristic of the theoretical maps ranging from single point stability, periodicity and chaos.
- **Time series:** the time series will be measured and analysed to demonstrate the behaviour over time of the proposed hardware implementations.
- **Lyapunov Exponent:** the data of the time series will be used to estimate the Lyapunov Exponent (LE) of the maps. The estimation of the LE from the experimental time series will allow the chaotic nature of the proposed implementations to be ascertained.
- **Noise measurement:** the noise measurement will be used to quantify the amount of noise inherent to each implementation. This is critical to any MS

as the magnitude of the noise components will determine the performance limit of the MS in terms of signal change that can be accurately determined.

## 5.1 Transfer Characteristic

To obtain the transfer characteristic of each map, the input of the electronic chaos map implementation under test was connected to a signal generator which was set to produce a sinusoid voltage signal. A DC offset was applied to enable the signal to swing between 0 and the highest voltage of the chaos map input range, which corresponds to a 10 V pk-pk input signal with a 5 V offset for the LM and a 1 Vpk-pk input signal with a 0.5 V offset for the TM. A Data Acquisition Device (DAQ) from National Instruments NI 6254 (National-Instruments, 2007) with 16 bit resolution was used to sample the input and output of the circuit. The setup for the measurement is illustrated in Figure 5-1.

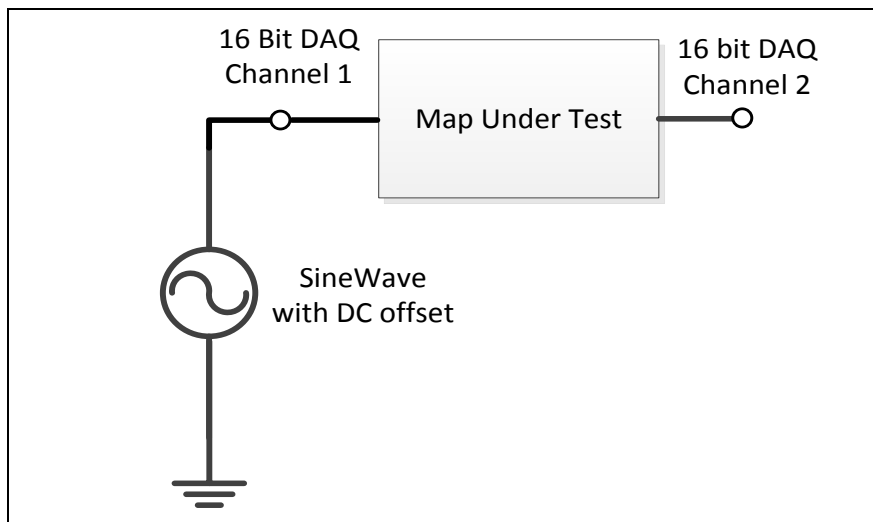


FIGURE 5-1 TRANSFER CHARACTERISTIC MEASUREMENT SETUP.

The DAQ software was used to retrieve the data from the two channels as a Comma-Separated Values (CSV) file which was then plotted using Matlab and compared to

the ideal transfer characteristic of each map to measure the error between the practical and the computed ideal characteristic.

## 5.2 Logistic Map Transfer Characteristic

The experimental data was plotted to obtain a graph of the input signal versus the output, which represents the transfer characteristic of the electronic implementation.

The theoretical parabola representing the LM for  $r = 4$  (normalised) was plotted on the same graph to enable a comparison between the two plots, shown in Figure 5-2(a). With the two plots being closely matched, no significant differences were observed, hence for this reason the error between the practical results and the theoretical parabola is measured and displayed separately in Figure 5-2(b).

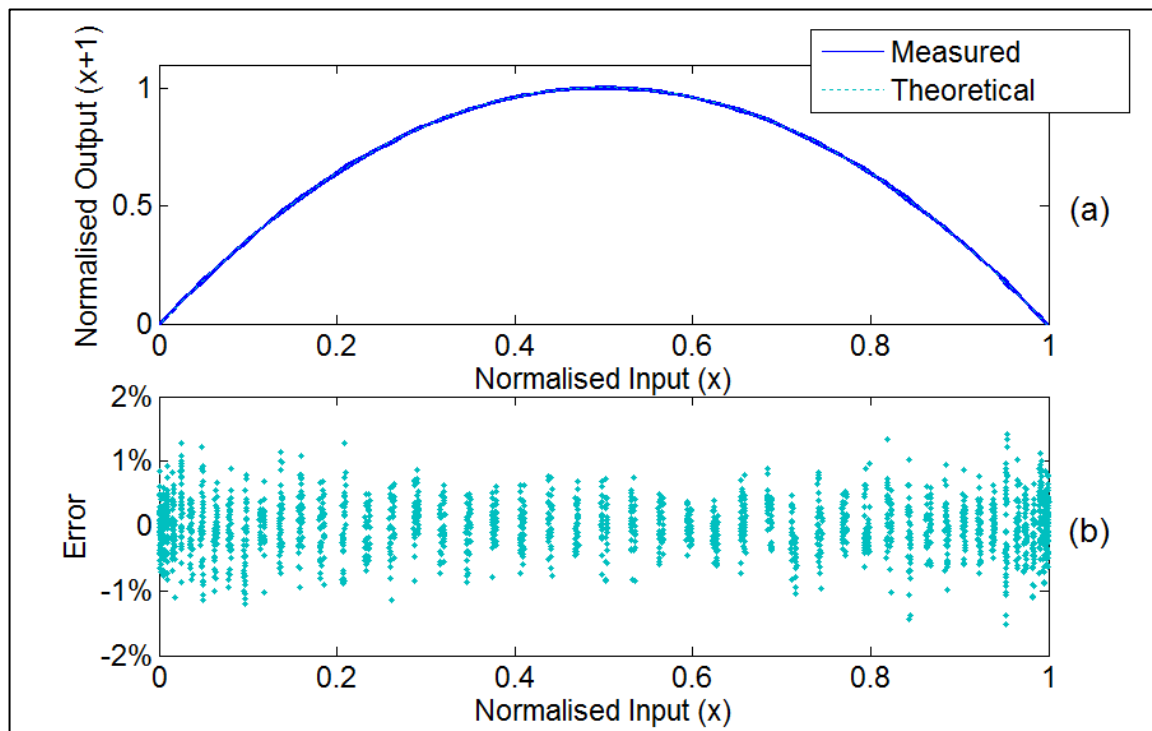


FIGURE 5-2 MEASURED VS THEORETICAL LOGISTIC MAP PARABOLA.

From Figure 5-2(b) it can be noted that the maximum error in the LM practical results is 1.5% and that the majority of the errors are contained within a  $\pm 1\%$  band,

which demonstrates the accurate fit between the measured characteristic and the theory. The fact that the transfer characteristics are closely matched proves that the electronic implementation of the LM designed in section 4.1.1 is performing as defined by the LM equation as in expression (2-8).

### 5.3 Tent Map Transfer Characteristic

The parameter  $\mu$  (from equation (2-9)) was set as near to the value of 2 as could be achieved and the measured transfer characteristic is shown in Figure 5-3 (a) along with the computed ideal transfer characteristic of the TM. The error between the two graphs representing the mismatch between the ideal characteristic and the measured characteristic was obtained by subtracting the ideal characteristic from the measured characteristic. The error given in Figure 5-3 (b) contained within  $\pm 1\%$  across the whole input range which once again demonstrates the close fit of the practical implementation to that specified by the theory.

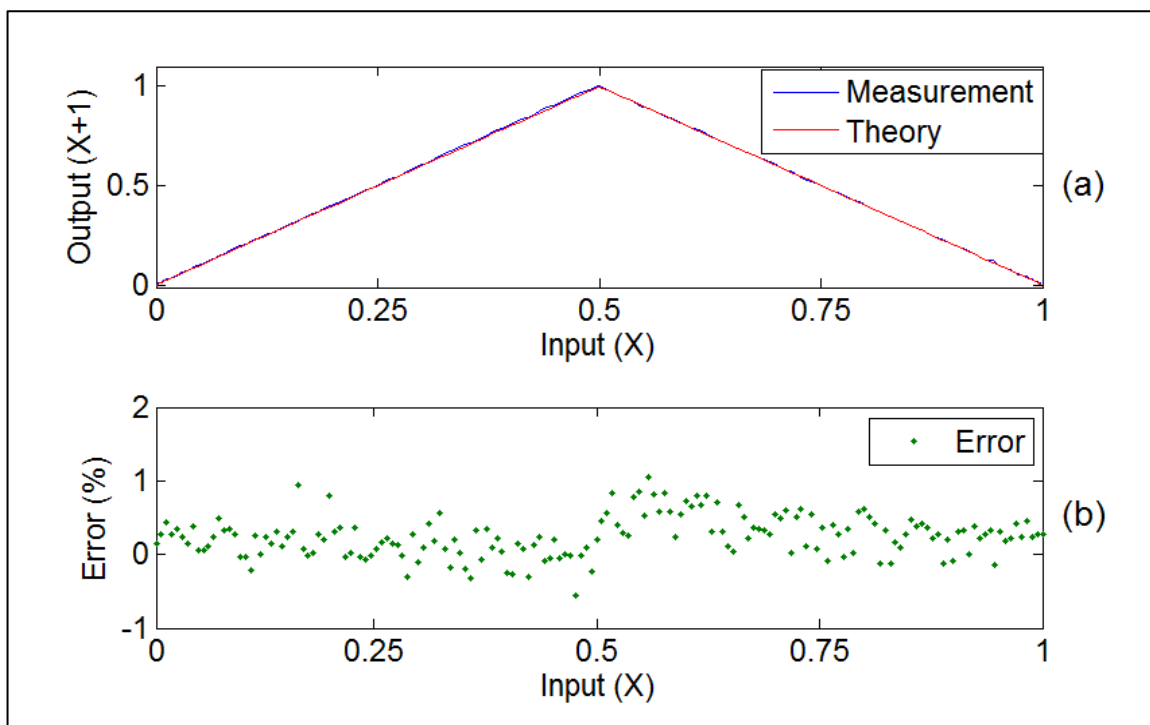


FIGURE 5-3 MEASURED VS THEORETICAL TENT MAP CHARACTERISTIC

## 5.4 Bifurcation Diagram

The Bifurcation diagram, as discussed in section 2.3, illustrates the behaviour of a chaos map for different values of the associated scaling parameter. For every value of the scaling parameter the map under test was placed into the feedback system as presented in section 3.2 and iterated 100 times. The first 10 iterations were discarded in order to display the long term behaviour of the map and remove any initial transient values. The map was iterated using a  $\mu\text{C}$  board and the output was measured using the internal 10 bit ADC. Finally the measurement of each iteration was stored as a CSV file and displayed using MATLAB. The bifurcation diagram obtained experimentally was compared with the computed bifurcation diagram of each map to quantify the matching between the practical electronic implementation and the theory.

### 5.4.1 Logistic Map Bifurcation Diagram

The bifurcation diagram of the electronic implementation of the LM shown in Figure 5-4 is indicating all the characteristics of the theoretical map ranging from fixed point stability, periodic oscillations and chaos. The parameter  $r$  (in equation (2-8)) was varied from 2 to 4 (normalised) by increments of 0.05. Figure 5-5, shows the theoretical bifurcation diagram of the LM computed using MATLAB. The practical data is closely related to the data generated by computation, with the main difference being the unclear bifurcation from fixed point to 2 point oscillation at about  $r = 2.9$ . As described in (Erguler and Stumpf, 2008) the effect of noise on the behaviour of the LM is visible on the bifurcation diagram in a way that the bifurcation points become "blurred". This effect is clearly visible on the transition between single point

stability and periodic oscillations. An additional effect of noise on the LM behaviour is the possibility that the system theoretically diverges to  $\pm\infty$  which can be triggered when the parameter  $r$  is set to exactly 4. However, in a practical system, noise can increase the input signal to exceed the input range, which can lead to an exiting condition. In this work the parameter  $r$  was set close to 4 but not exactly 4 in order to use the chaotic behaviour of the LM whilst avoiding exiting conditions.

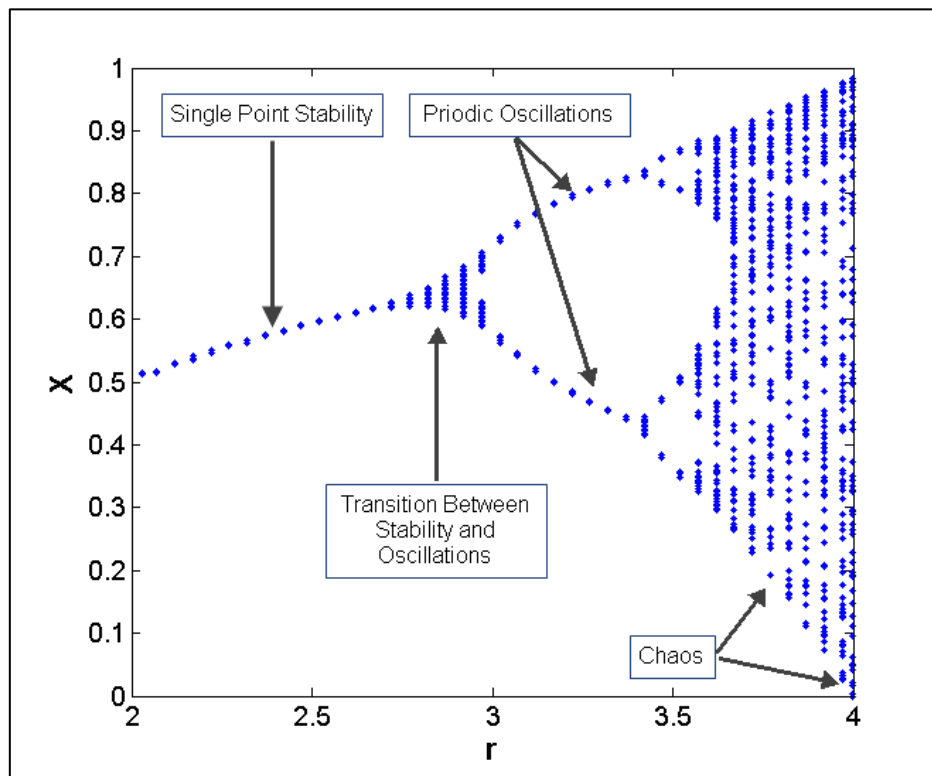


FIGURE 5-4 MEASURED BIFURCATION DIAGRAM OF THE LM

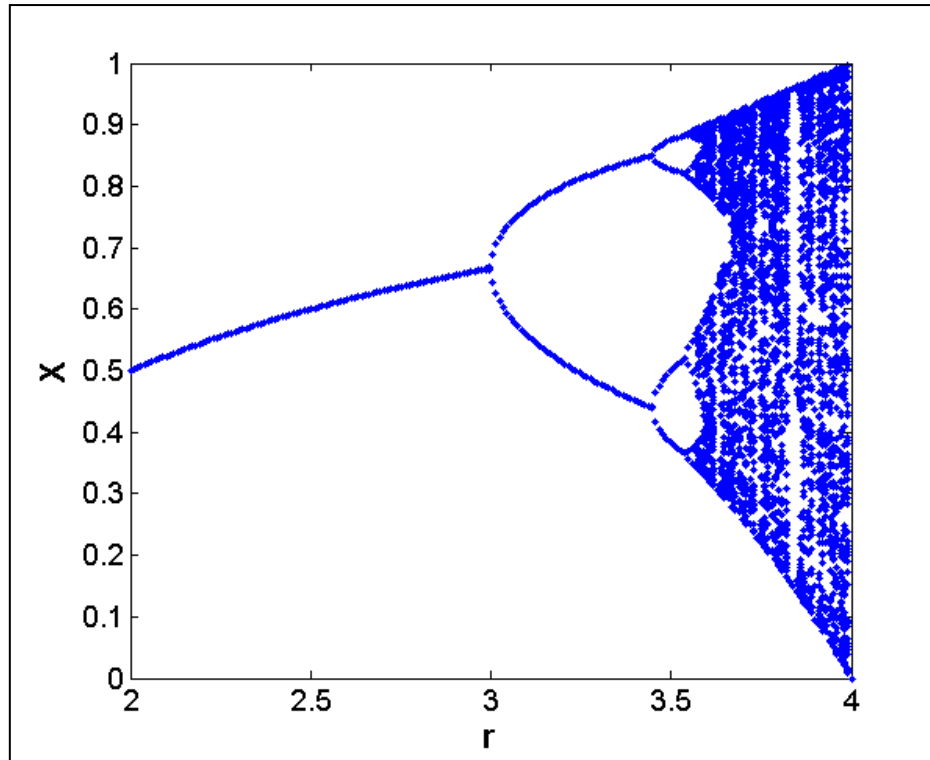


FIGURE 5-5 COMPUTED LM BIFURCATION DIAGRAM

### 5.4.2 Tent Map Bifurcation Diagram

The proposed implementation of the TM was designed to operate with a parameter  $\mu$  set to 2 or close to 2. For this reason it is impossible to vary  $\mu$  throughout the whole input range. The values for the resistors and potentiometers were selected to enable the parameter  $\mu$  to be varied from 1.945 to 2, and resulted in the practical limitation which restricted the measurement range of the parameter  $\mu$ ; the partial bifurcation diagram is shown in Figure 5-6(b). The TM was iterated 100 times, the first 10 samples were removed to suppress any transient response and keep the long term behaviour. As expected from the theoretical bifurcation diagram shown in Figure 5-6(a) when the parameter  $\mu$  is set to 2 the range of the output signal occupies the entire output. The amplitude of the output signal decreases as the parameter  $\mu$  is reduced from 2 to 1.995 and further reduces as the parameter  $\mu$  is decreased towards

1.94. The experimental results are consistent with the theoretical bifurcation diagram.

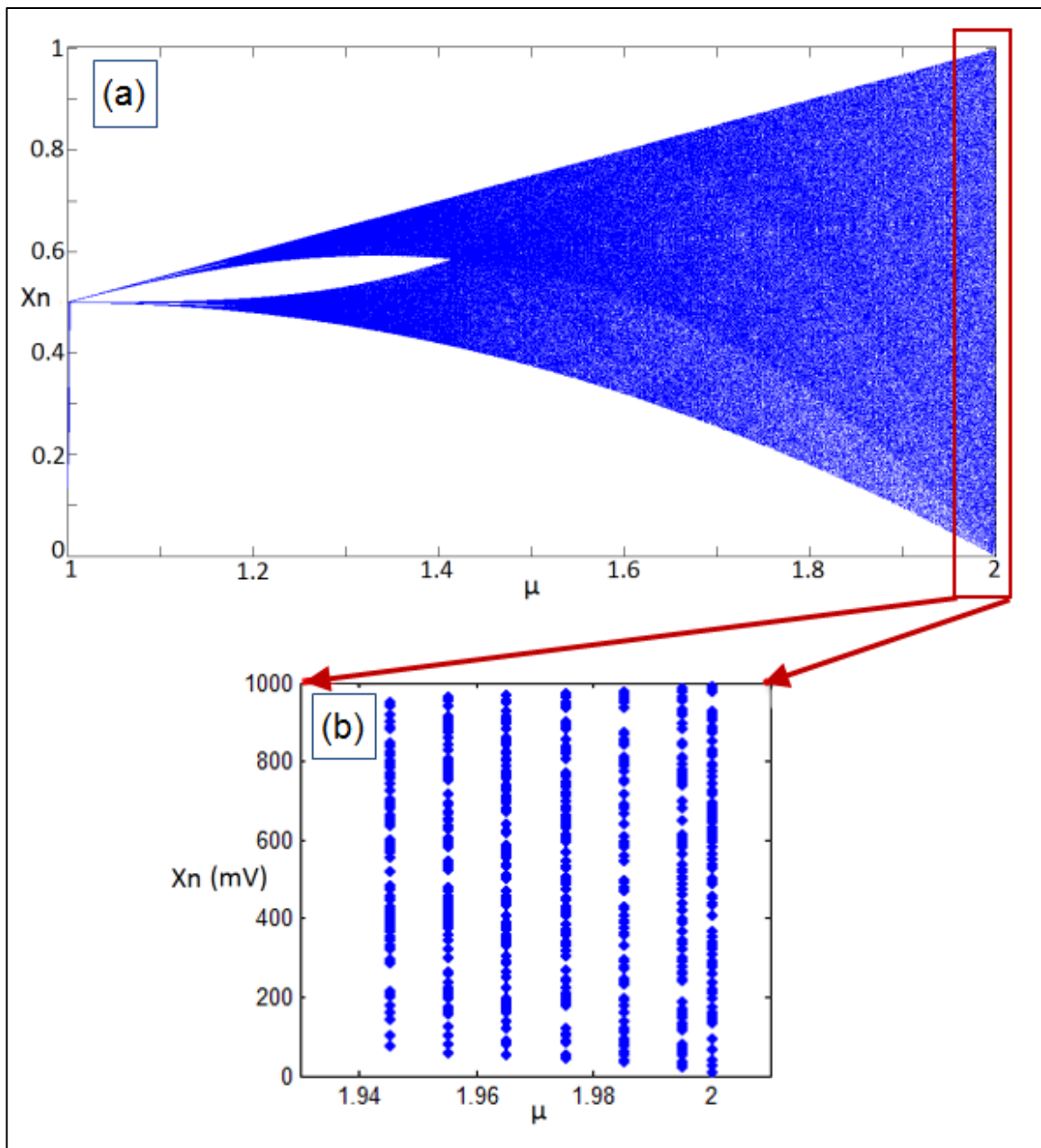


FIGURE 5-6 TENT MAP EXPERIMENTAL BIFURCATION DIAGRAM

## 5.5 Time Series

The time series of chaotic maps displays the evolution of the output signal over a given number of iterations  $N$ . The value of the parameter ( $\mu$  for the LM and  $r$  for the TM) sets the behaviour of the maps. The output could be stable, periodic or chaotic

as explained in section 2.3.1. To generate the time series, each map was placed in the feedback system presented in section 3.2. The input of the map under test was connected to the KROHN-HITE 511 DC voltage reference/calibrator which provides a stable and accurate DC voltage (see Appendix E). The output of the KROHN-HITE 511 was set to an arbitrary value within the input range of the map under test and the map iterated multiple times. The output after each iteration was sampled using a 10 bits ADC available in the  $\mu\text{C}$ , and the data stored as a CSV file and displayed using MATLAB. The parameter of the map under test was set to a value that allows chaotic behaviour and the obtained time series used to ascertain the presence of chaos, first visually and then through the use of Lyapunov Exponent (LE).

### **5.5.1 Logistic Map Time Series**

The parameter  $r$  is set to 3.99 (0.399 for the modified map) so that the behaviour of the map would exhibit chaos; Figure 5-7 shows the experimental time series obtained from the electronic implementation of the LM with the output showing non periodic behaviour and is contained between 1 and 0. This result is consistent with the bifurcation diagram of the system shown in Figure 5-5.

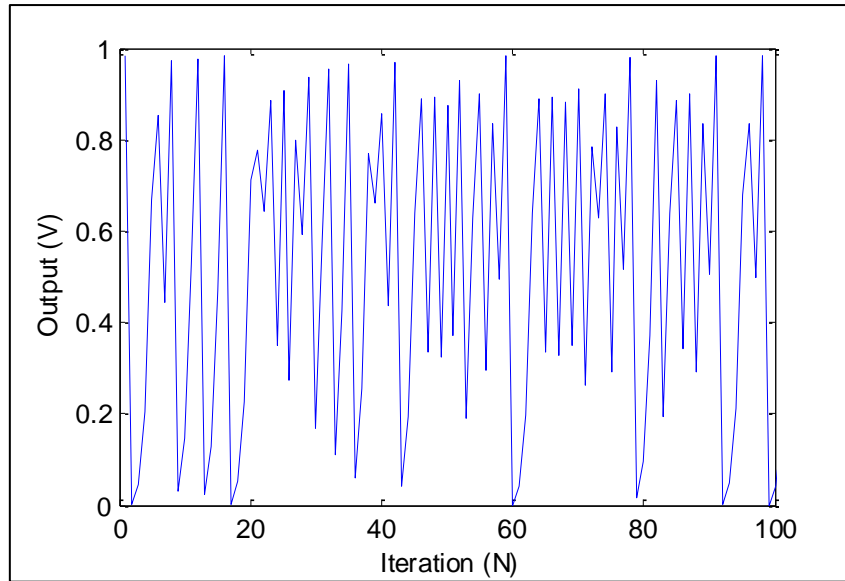


FIGURE 5-7 LOGISTIC MAP EXPERIMENTAL TIME SERIES

### 5.5.2 Tent Map Time Series

The time series of the TM output, in Figure 5-8, shows the evolution of the map under iteration with the parameter  $\mu$  set to 2, in order to obtain a chaotic behaviour; Figure 5-8 shows that the experimental time series occupies the entire output range going from 0 to 1 V which is expected for a parameter set to 2 as shown by the bifurcation diagram of the TM in Figure 2-15. The experimental time series obtained was used in the following section to ascertain the presence of chaos by estimating the LE value.

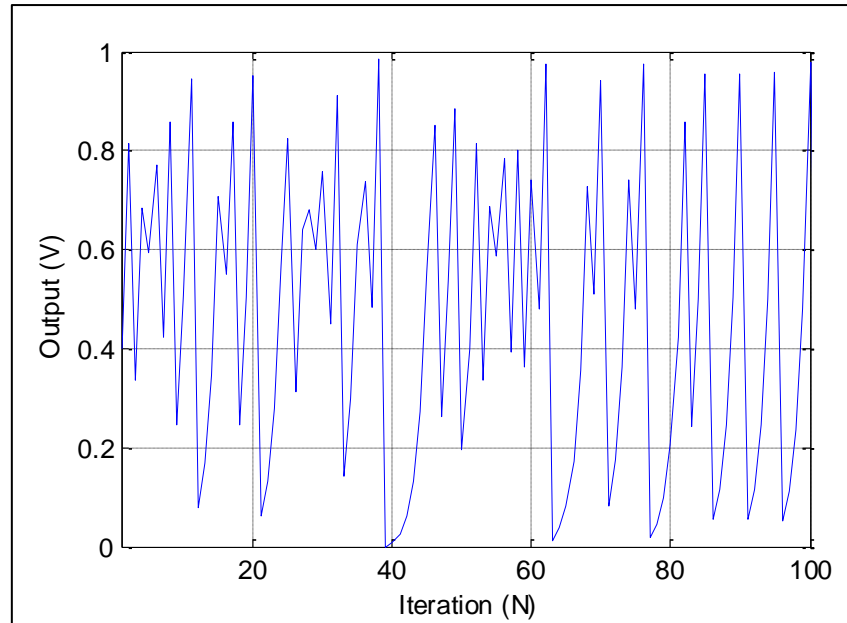


FIGURE 5-8 TENT MAP EXPERIMENTAL TIME SERIES

## 5.6 Lyapunov Exponent

A simple visual inspection of the time series is not sufficient to ascertain the chaotic behaviour of the electronic implementation; hence the LE method is used, as explained in section 2.5.1.

If the LE of a time series is positive then the system is chaotic (G.L.Baker and J.P.Gollub, 1990). To estimate the LE it is assumed that the equation emulated by the electronic implementation is unknown, thus the estimation will take into account any errors between the electronic implementation and the theoretical map. To demonstrate that the method used for the LE is valid, a non-chaotic time series was initially analysed. The map used was the LM and the parameter  $r$  was set to 3.35 to be in the region of non-chaotic behaviour. The measured time series is shown in Figure 5-9 and the estimated prediction error in Figure 5-10. It can be observed (in Figure 5-9) that after a short transient the output of the LM oscillates between two points, and also in Figure 5-10 it is not possible to estimate the value LE, since there

is no exponential separation between the two neighbouring points. Additionally, the LE is not consistently positive, which confirms that the system is not sensitive to initial conditions, and thus not chaotic.

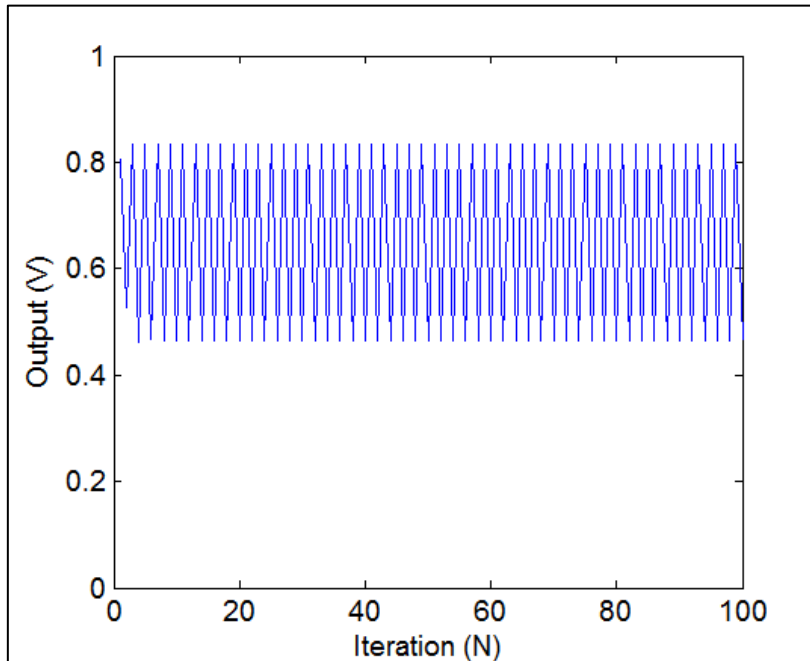


FIGURE 5-9 LOGISTIC MAP TIME SERIES FOR  $R = 3.35$

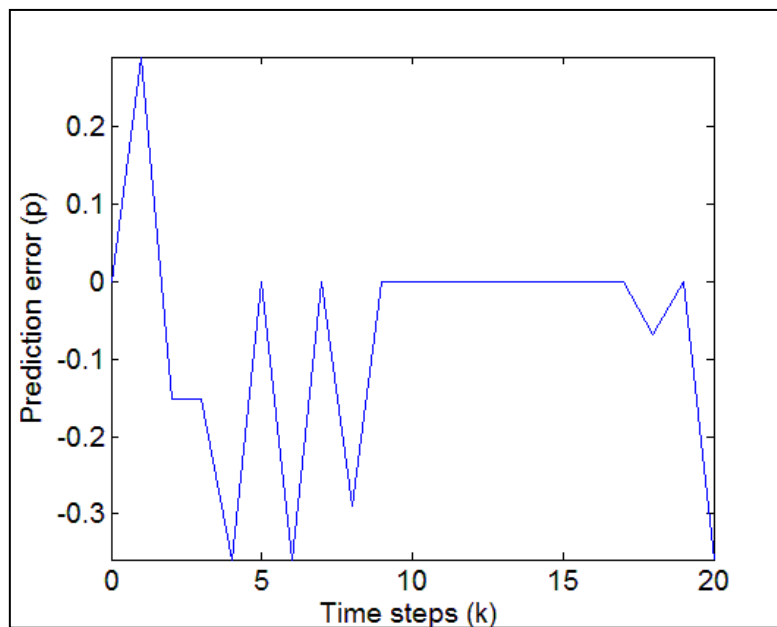


FIGURE 5-10 PREDICTION ERROR FOR A NON-CHAOTIC TIME SERIES

### 5.6.1 Logistic Map Lyapunov Exponent

The number of samples taken for the LE estimation was set to  $N = 500$  as recommended in literature (Rosenstein et al., 1992, Wolf et al., 1985), and analysed using MATLAB to generate the prediction error plot shown in Figure 5-11. After a transition from  $k = 0$  to  $k = 2$  ( $k$  is the number of time steps used for the estimation of the LE) the two neighbouring points start to diverge exponentially before plateauing and decreasing from  $k = 7$ , which separation is due to the folding of the map. The slope  $m$  is positive and the result obtained indicates that the LE of the electronic implementation is 0.79, for a parameter  $r$  of 3.99, as shown in Figure 5-11.

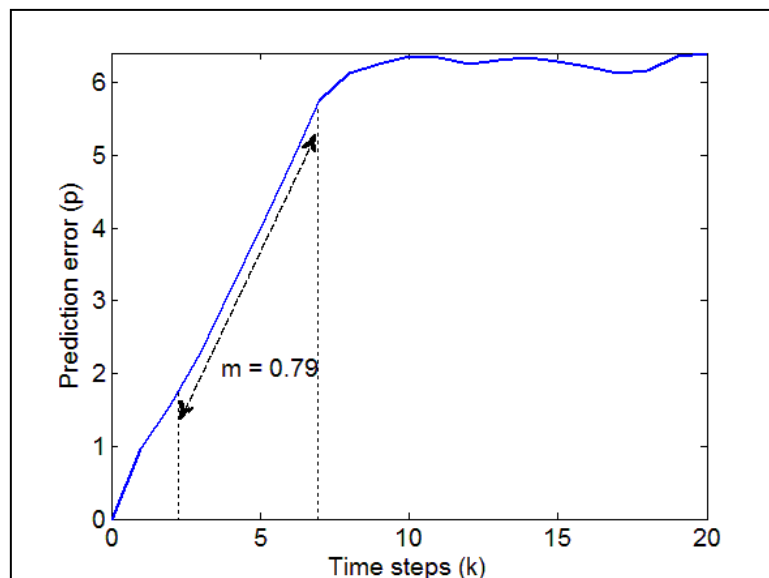


FIGURE 5-11 ESTIMATION OF THE LYAPUNOV EXPONENT FROM THE PREDICTION ERROR

TABLE 5-1 ESTIMATED AND THEORETICAL LYAPUNOV EXPONENT FOR THE LM

<b>Number Of Samples</b>	<b>Estimated Lyapunov exponent</b>	<b>Theoretical Lyapunov Exponent</b>	<b>% Error</b>
N = 500	$\lambda_1 = 0.79$	$\lambda_1 = 0.693$	13.9

The error between theoretical and estimated LE is 13.9%; this degree of accuracy is acceptable considering that the time series was obtained experimentally with limited data and measurement noise. Similar results were obtained in literature (Rosenstein et al., 1992). The estimated LE is positive which demonstrates that the electronic implementation of the LM exhibits high sensitivity to initial conditions and therefore that the system is chaotic.

### **5.6.2 Tent Map Lyapunov Exponent**

To ascertain if the TM implementation behaves chaotically the time series from Figure 5-8 was used to estimate the LE. The graph of the LE estimation is shown in Figure 5-12, where the slope of the prediction error equals 0.80 from  $k = 2$  to  $k = 10$  (linear region). After  $k = 10$  the folding of the map occurs causing the prediction error to fluctuate, this has no effect on the LE estimation as the measurement is taken on the linear region.

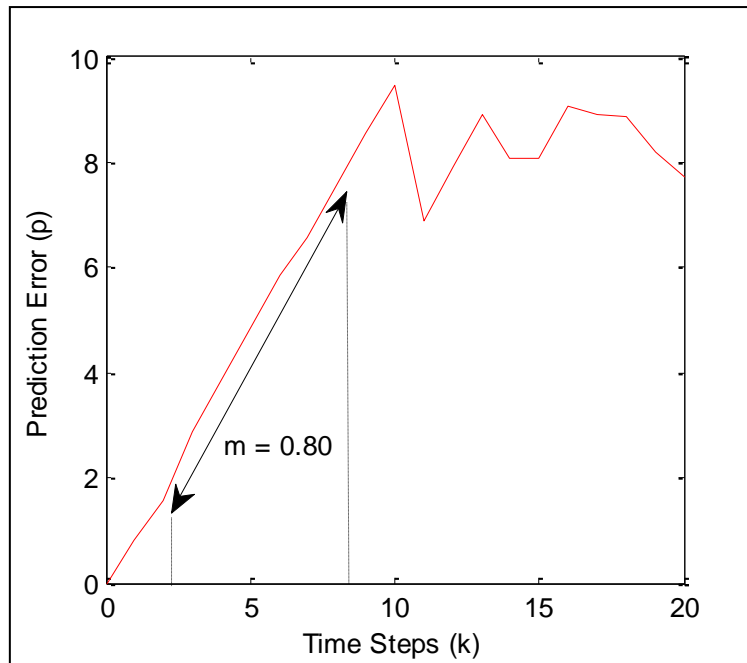


FIGURE 5-12 TENT MAP LYAPUNOV EXPONENT ESTIMATION

Table 5-2 shows the results error of the positive LE estimation, yielding an error of 15.4% which is also consistent with the results obtained in literature (Rosenstein et al., 1992) and defines the system as chaotic.

TABLE 5-2 ESTIMATED AND THEORETICAL LYAPUNOV EXPONENT FOR THE TM

Number Of Samples	Estimated Lyapunov exponent	Theoretical Lyapunov Exponent	% Error
N = 500	$\lambda_1 = 0.80$	$\lambda_1 = 0.693$	15.4

## 5.7 Noise Measurement

To assess the performance of the chaos map implementation the noise of the system was quantified, as the inherent noise will determine the sensitivity of the system.

The noise of the electronic implementations was measured using the following procedure;

- The input of the map under test was grounded and the noise at the output was measured using a HP 3562A Dynamic Signal Analyser (DSA) (Agilent, 1985).
- In order to minimise external noise sources the circuit under test was placed in an earthed metallic box to provide adequate shielding.
- To prevent any DC offset being generated by the map under test, a 20  $\mu\text{F}$  decoupling capacitor was connected between the circuit and the signal analyser.
- The measurement data was extracted using a General Purpose Interface Bus (GPIB) to USB interface cable.
- The noise floor of the DSA was measured by connecting a 50  $\Omega$  BNC terminator to the input of the DSA, and measured over 3 decades ranging from 10  $\text{H}_z$  to 10  $\text{kHz}$  (Figure 5-13).
- In order to obtain an accurate reading a separate measurement was taken for each decade and the results were combined into a single graph. The averaging process was set to 50 samples to obtain an accurate measurement whilst keeping the measurement time within a reasonable limit.

The noise floor of the 3562A DSA given in Figure 5-13, appears to have a step-like characteristic which is due to the use of different internal circuitry for each decade. In the low frequency region (10 – 100 Hz) some noise spikes are visible; the highest being due to the mains pickup at 50 Hz. The noise floor of the DSA is contained within  $100 \text{ nV}\sqrt{\text{Hz}}$  and thus for a noise measurement to be accurate the noise being measured should be at least  $1 \text{ }\mu\text{V}\sqrt{\text{Hz}}$  (an order of magnitude above the noise floor).

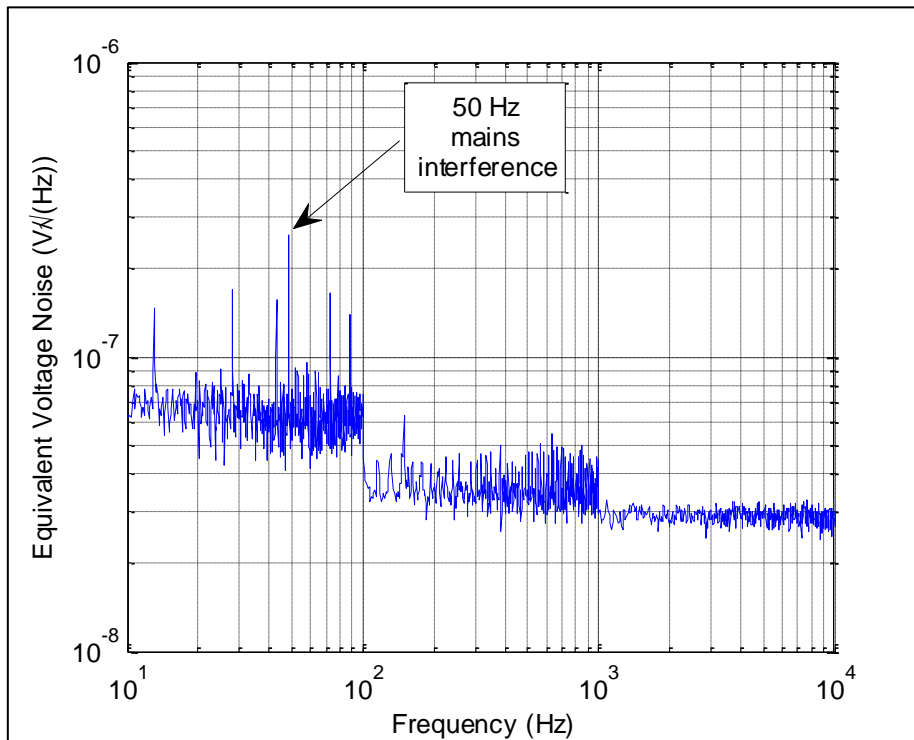


FIGURE 5-13 MEASURED NOISE FLOOR OF THE HP 3562A DSA

When the noise signal being measured was lower than  $1 \text{ }\mu\text{V}\sqrt{\text{Hz}}$ , a low noise preamplifier with a gain of 1000 was used to avoid any measurement errors due to the contribution of the DSA noise.

To calculate the overall noise  $V_n$  in terms of Voltage Root Mean Square ( $V_{n\text{RMS}}$ ) from the noise spectrum the formula in expression (5-1), can be applied.

$$V_{n_{RMS}} = \sqrt{\int_{f_{low}}^{f_{high}} (SD_f)^2 df} \quad (5-1)$$

Where  $f_{high}$  and  $f_{low}$  are the high and low frequencies of interest respectively and SD is the noise spectral density.

In the case when the value is relatively constant for all the frequencies, the expression (5-1) can be simplified as shown in expression (5-2).

$$V_{n_{RMS}} = SD * \sqrt{B} * K \quad (5-2)$$

Where B is the bandwidth and K the noise bandwidth coefficient which is set according to the order of filter used to limit the bandwidth (B) as shown in Table 5-3.

TABLE 5-3 EQUIVALENT NOISE BANDWIDTH COEFFICIENT

Filter Order	Equivalent noise bandwidth coefficient (K)
1 <sup>st</sup> Order	1.57
2 <sup>nd</sup> Order	1.11
3 <sup>rd</sup> Order	1.05
Ideal Filter (Brick Wall)	1

### 5.7.1 Logistic Map Noise Measurement

The equivalent voltage noise measurement for the LM is shown in Figure 5-14 with the noise centred between  $11 \mu V\sqrt{Hz}$  and  $10 \mu V\sqrt{Hz}$  and several harmonics from the mains (50 Hz) visible.

Applying expression (5-2) to the data within Figure 5-14, for a bandwidth of 1 kHz limited by a 2<sup>nd</sup> order filter gives:  $V_{n_{RMS}} = 351 \mu\text{V}$  which converts to  $V_{n_{pk-pk}} = 2.3 \text{ mV}$ , applying a factor of 6.6; (the standard deviation on the noise Gaussian distribution). The high sensitivity to initial conditions of the LM makes the detection, with certainty, of any signal changes lower in amplitude than the inherent noise of the system, difficult as the noise causes the time series to diverge before the input signal. In order to identify the major component noise contribution and thus reduce the noise of the overall system, the noise of each component has been evaluated given in Table 5-4. The information was determined from the datasheets or calculated using the relevant expressions (Analog-Devices, 2003, 2012, 2013). The resistors used are of low value (maximum 10 k $\Omega$ ) to maintain low Johnson voltage noise as given by expression (2-1) (Horowitz and Hill, 1989).

From Table 5-4 it is clear that the AD633JN is the main source of noise in the LM implementation; as explained in the section 4.1.1 the AD633JN divides the product of the two inputs by a factor of 10 before the output. This, therefore forces the use of an amplifier with a gain of 10 resulting in the noise being amplified by a value of 10. Hence, the AD633JN contributes  $185 \mu\text{V}_{pk-pk}$  which is of the same order of magnitude as the LM overall noise measured using the DSA ( $2.3 \text{ mV}_{pk-pk}$ ).

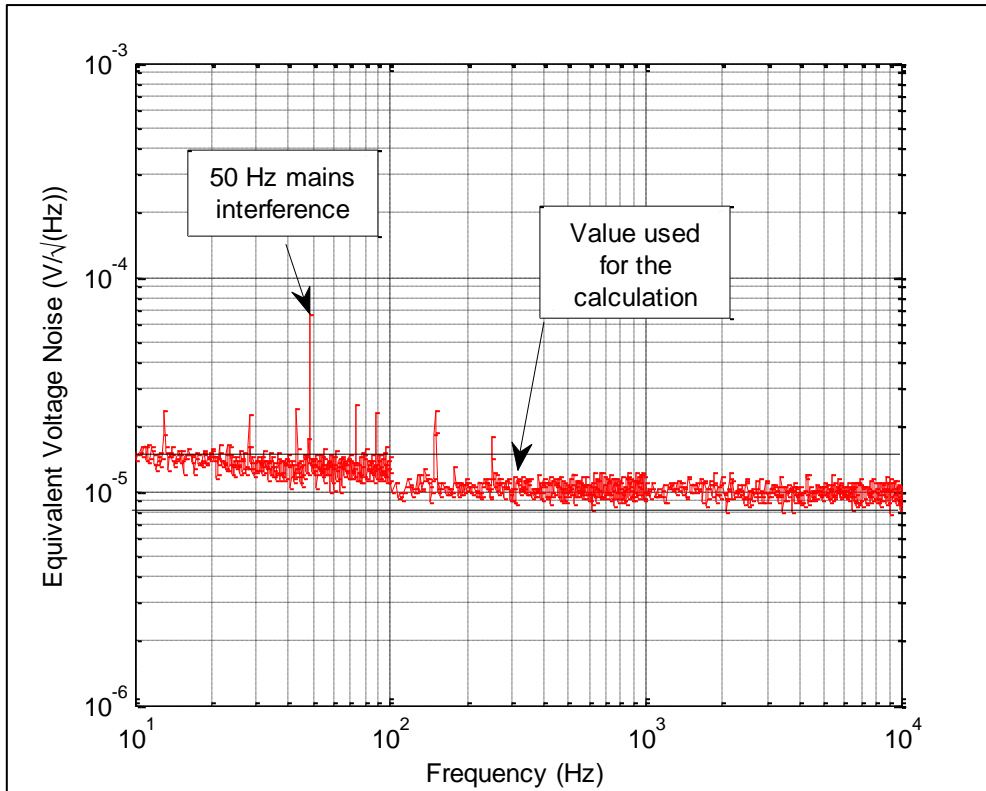


FIGURE 5-14 MEASURED NOISE OF THE LM

TABLE 5-4 NOISE FOR COMPONENTS USED IN THE LM IMPLEMENTATION.

Component Name	Equivalent noise voltage	Noise <sub>RMS</sub>	Noise <sub>pk-pk</sub>
		B = 1kHz	
OP27	3 nV/√Hz	0.1 μV	0.7 μV
AD633JN	0.8 μV/√Hz	28 μV	185 μV
10kΩ Resistor	12.8 nV/√Hz	0.45 μV	3 μV
AD587	-	-	4 μV

The noise measurement for the LM electronic circuit demonstrates that the overall noise of the implementation is predominantly due to the AD633JN analogue

multiplier, thus, in order to reduce the overall noise, the next section discusses an improved version of the TM implementation using discrete analogue multipliers.

### **5.7.2 Improved Logistic Map Implementation**

To improve the sensitivity of the LM, alternatives to the AD633JN were investigated in order to reduce the overall noise. Alternative analogue multiplier ICs are available but none presents a significant improvement in terms of noise over the AD633JN. However the fact that signals being multiplied in the LM are positive, allows the use of a simpler multiplier, namely the One-Quadrant (1Q) multiplier. Compared to the four-quadrant configuration, used by the AD633JN, where the input and output signals can be negative or positive the 1Q multiplier can only multiply positive signals. The main advantage of the 1Q multiplier is the simplicity of the circuitry. The solution adopted to replace the AD633JN is a semi-discrete 1Q multiplier implemented using two matched transistor pairs and four precision operational amplifiers; the simplest form of analogue multiplier shown in Figure 5-15. This configuration uses a Gilbert cell to compute the product of two numbers (Analog-Devices, 2009).

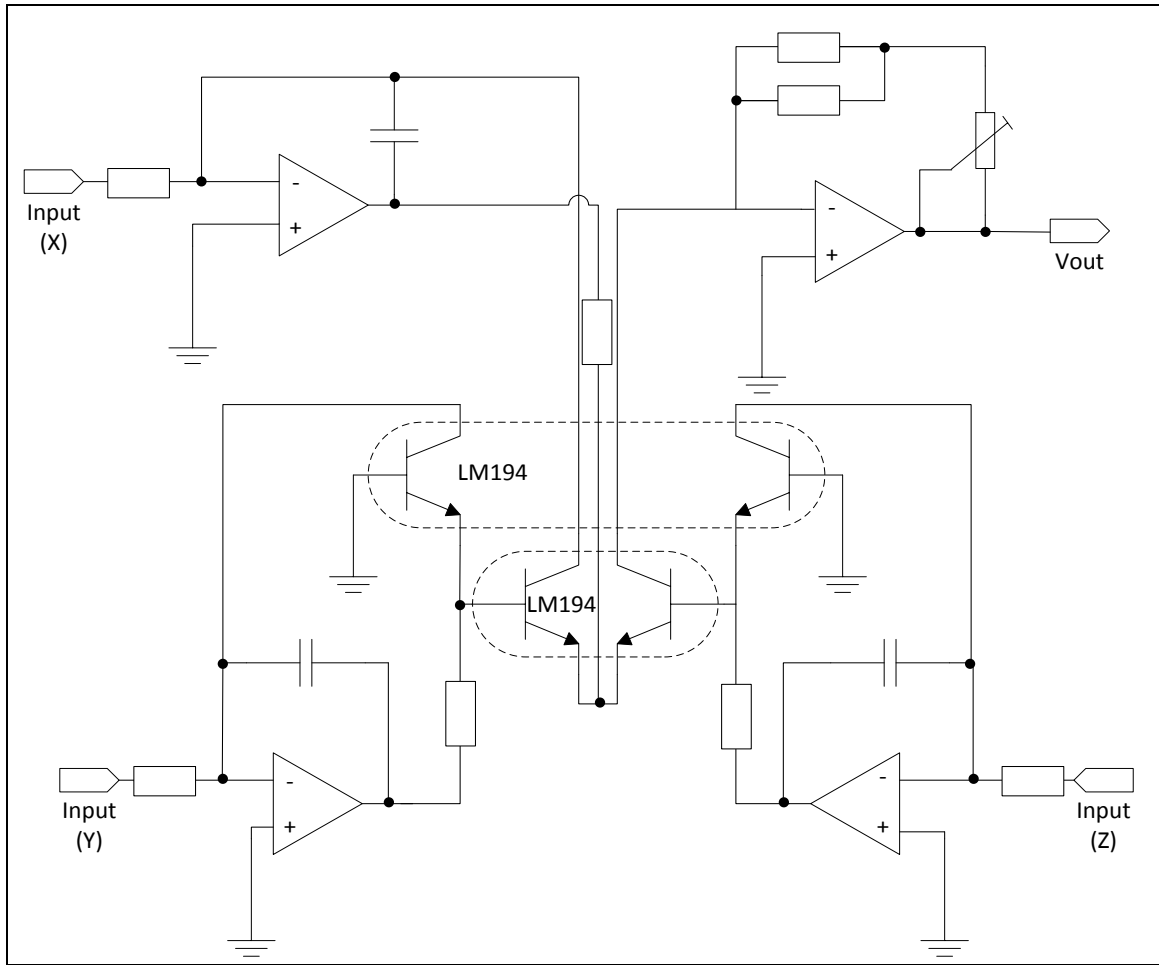


FIGURE 5-15 ONE-QUADRANT PRECISION ANALOGUE MULTIPLIER

The transfer characteristic for the multiplier in Figure 5-15 is given by expression (5-3) (National Semiconductors, 1994).

$$V_{\text{out}} = \frac{(X) * (Y)}{(Z)} \quad (5-3)$$

In the LM implementation, the input (Z) is connected to a 1V reference, therefore the transfer characteristic becomes the product of (X) and (Y). The noise of the multiplier was measured using the DSA and is shown in Figure 5-16, but as the noise floor was below that of the DSA, a low noise amplifier with a gain of 1000 was used to amplify the noise from the multiplier to reduce measurement error. A Low Pass Filter (LPF) with a cut-off frequency of 1 kHz was added to the multiplier to reduce

the overall noise. Besides harmonics due to the mains interference, the noise spectrum is constant from 10 Hz to 1 kHz which enables expression (5-2) to be used to calculate the rms noise voltage. The noise for a bandwidth of 1 kHz and a 2<sup>nd</sup> order LPF is approximately 35  $\mu\text{V}_{\text{RMS}}$  which is in the region of a fifth of the AD633JN noise. Another advantage of this multiplier is that the product is not divided by a factor of 10, thus eliminating the need for amplification, which further reduces the noise. Hence the overall noise floor has been reduced, compared to the AD633JN, by a factor of 50. Figure 5-17, shows the improved LM circuit implementation.

To demonstrate the gain in terms of noise performance the noise of the improved LM was measured as given in Figure 5-18. The noise floor is now equivalent to the noise of the one-quadrant multiplier, which means that the multiplier is still the main source of noise in the circuit. By applying expression (5-2) the noise is determined as 7  $\mu\text{V}_{\text{RMS}}$  or 46.3  $\mu\text{V}_{\text{pk-pk}}$ . Figure 5-19 shows the equivalent voltage noise of the two implementations (AD633JN multiplier against the 1Q multiplier).

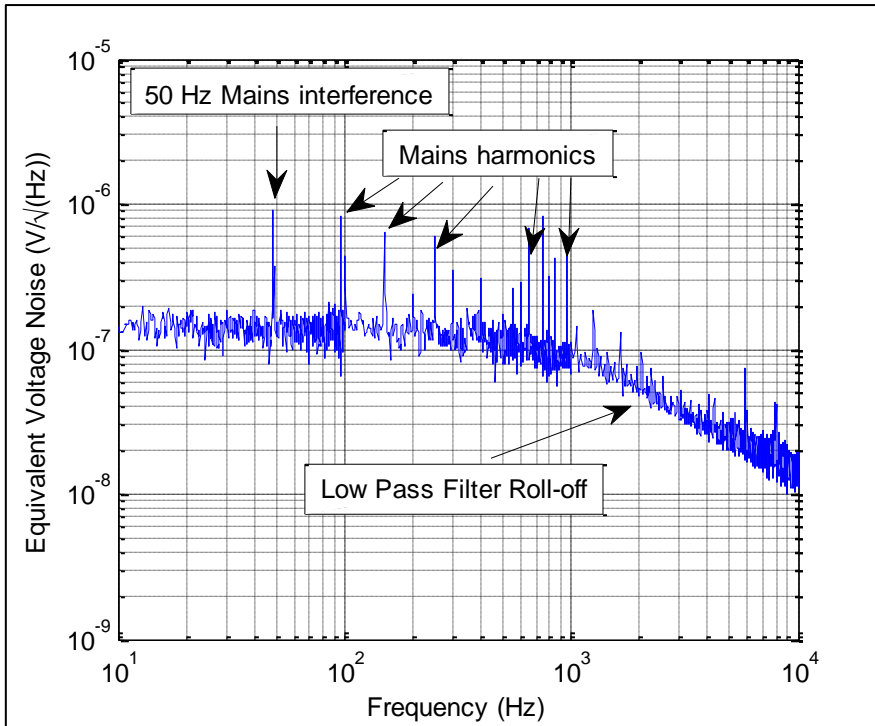


FIGURE 5-16 NOISE OF THE ONE-QUADRANT MULTIPLIER

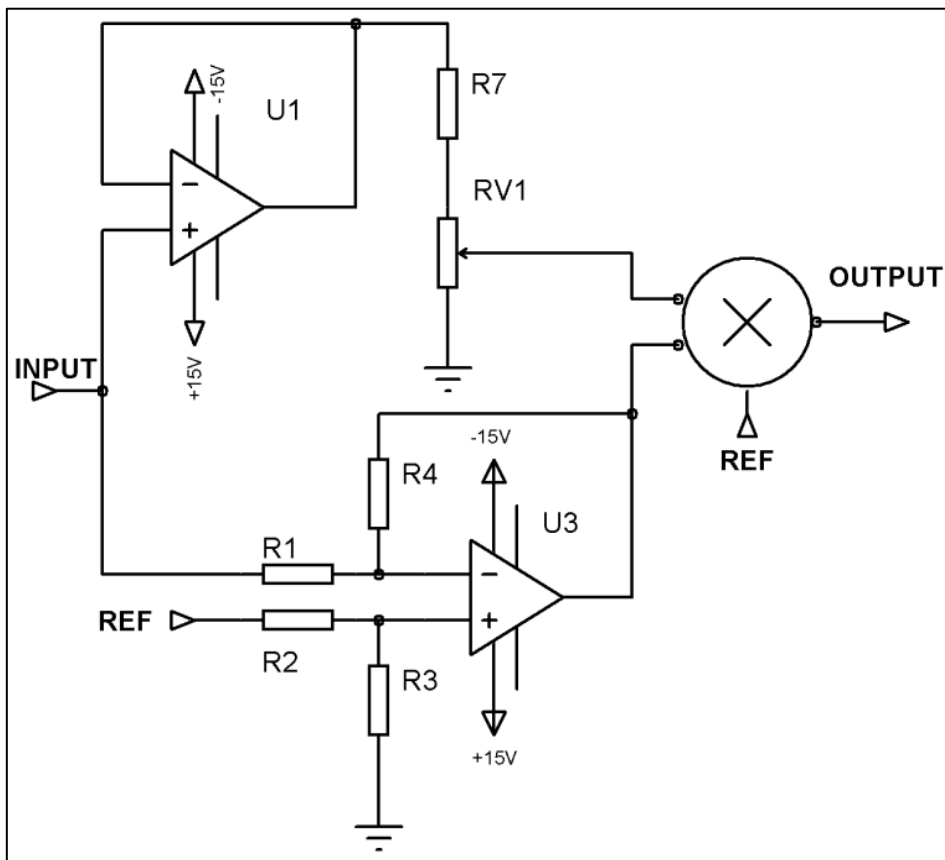


FIGURE 5-17 SIMPLIFIED SCHEMATIC OF THE IMPROVED LM

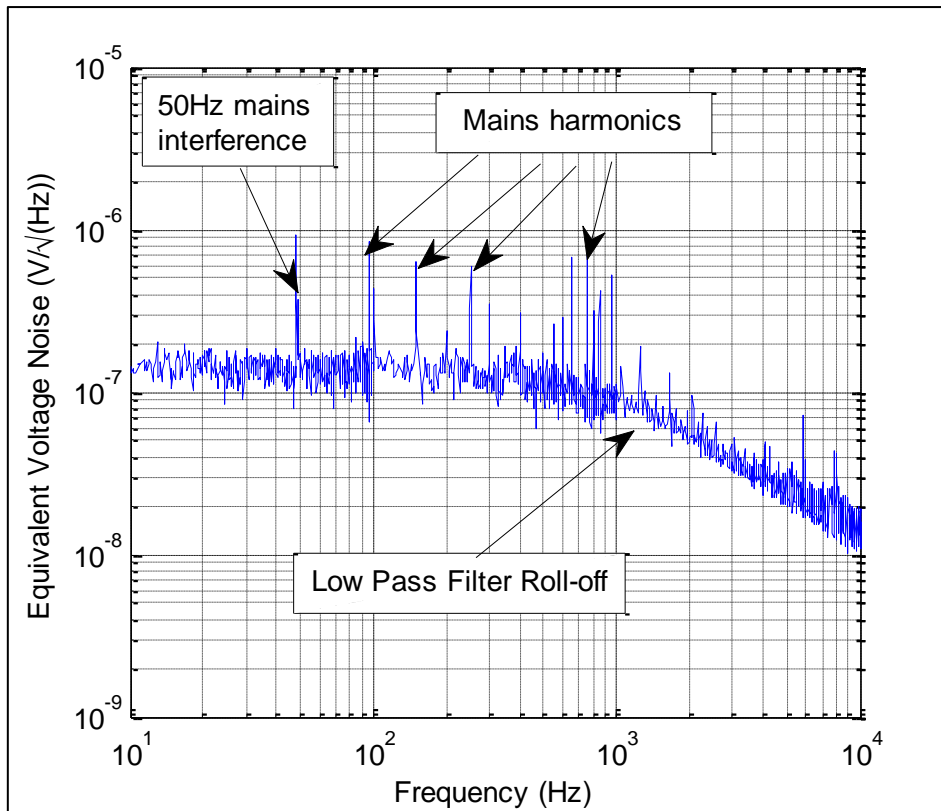


FIGURE 5-18 NOISE OF THE IMPROVED LM

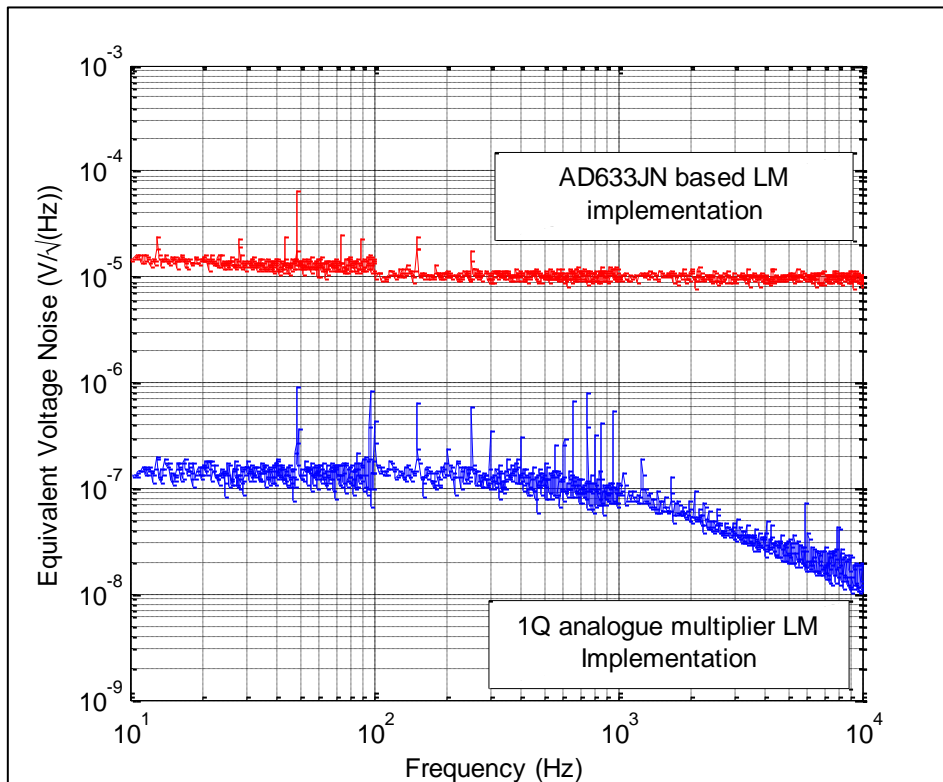


FIGURE 5-19 NOISE OF PREVIOUS IMPLEMENTATION VS IMPROVED IMPLEMENTATION

### 5.7.3 Tent Map Noise Measurement

The equivalent voltage noise spectrum of the TM is shown in Figure 5-20; by applying the expression (5-2) the noise at the output of the TM is  $1.4 \mu\text{V}_{\text{RMS}}$  or  $9.3 \mu\text{V}_{\text{pk-pk}}$ . This peak to peak noise figure is significantly lower than the noise of  $46.3 \mu\text{V}_{\text{pk-pk}}$  for the improved LM implementation by a factor of 5. This improvement is due to a circuitry used to implement the TM that does not require an analogue multiplier and the noise roll-off is due to low-pass filters implemented within the TM to reduce the overall noise. The lower noise will enable the TM to detect input signal change significantly lower than those of the LM.

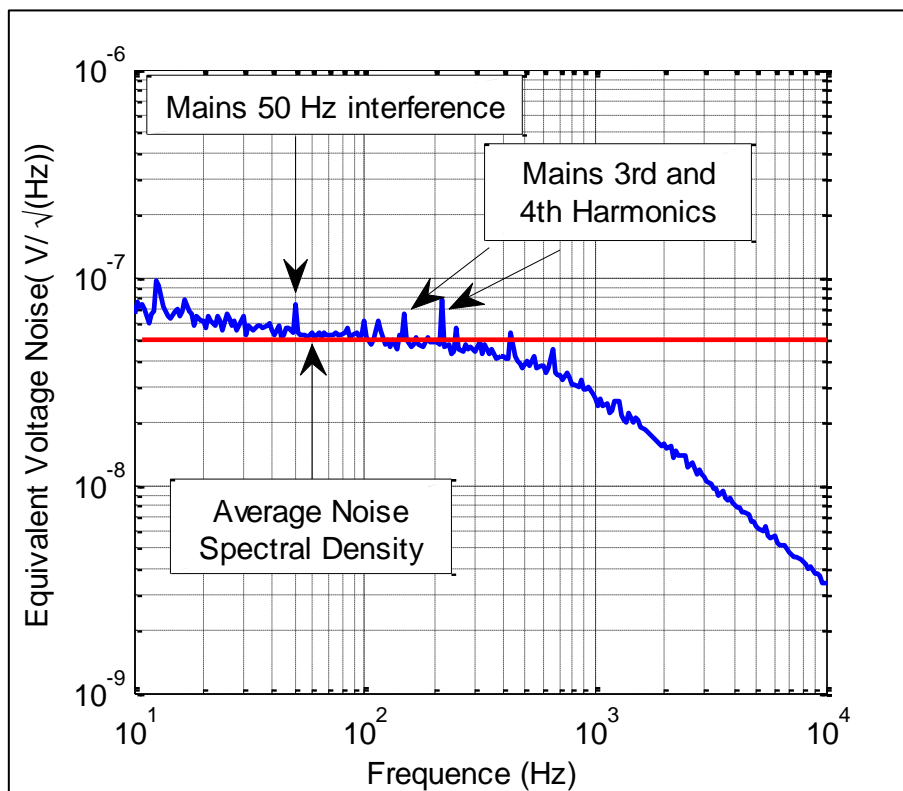


FIGURE 5-20 NOISE OF THE TM IMPLEMENTATION

## 5.8 Conclusion

The performance of the proposed implementations of the LM and the TM has been analysed and it has been shown that the practical performance closely matches the theoretical maps in terms of transfer characteristic, bifurcation diagrams, time series and LE.

The transfer characteristics for the LM and the TM are matched to the theory, within 1.5% and 1% respectively while the bifurcation diagrams display the same behaviour as the theoretical maps. The LE for each map was used to ascertain the presence of chaos and the results demonstrate a positive LE for each implementation, which proves the presence of chaos in the electronic circuits.

Finally, the noise measurements for, the original implementation of the LM, are relatively high at  $2.3 \text{ mV}_{\text{pk-pk}}$ . Hence, to reduce the overall noise, the main source of noise in the circuit was identified (AD633JN analogue multiplier) and an improved implementation of the LM was presented using a 1Q analogue multiplier. The overall noise was reduced by a factor of approximately 50 to  $46.2 \text{ }\mu\text{V}_{\text{pk-pk}}$ .

The noise measurement for the TM yields a noise value of  $9.3 \text{ }\mu\text{V}_{\text{pk-pk}}$  which is significantly lower than the noise of the LM due to the simplicity of the TM circuitry, where there is no requirement for an analogue multiplier. Therefore, the low noise of the TM circuit, compared to the LM implementation, enables the TM to measure input signal changes significantly lower than those of the LM.

The following chapter will discuss the measurement capability and the performance of the proposed Measurement System (MS).

# 6 Measurement System Results

In this chapter the Logistic Map (LM) and the Tent Map (TM) are integrated into the proposed MS to assess the overall performance in terms of divergence measurement, which is the basic criterion for small signal measurement and detection. The divergence measurements are as follows:

- **Divergence between two signals:** This measurement will verify the working principle of the MS as it will enable the ability of the different implementations of the MS to detect and/or measure small variations of the input signal to be evaluated.
- **Divergence through the entire input range:** This measurement will gauge the ability of the MS to maintain a consistent measurement for the same amount of input change throughout the entire input range. An ideal MS should have a perfect linearity throughout the whole input range.
- **Divergence for different magnitudes of input change:** This measurement will show the accuracy of the MS for different input signal amplitude changes.

For each input signal the MS system was iterated and the result of each iteration was sampled and stored using the  $\mu\text{C}$ . The same operation was then performed for each input signal with an additional input change. These system measurements were individually performed for each LM and TM implementation in a feedback based MS and then for a series implementation.

This chapter is divided in two main sections, firstly the LM is placed in the MS and the performance is measured. This is then followed by the performance of the MS based on the TM.

## 6.1 Divergence Between Two Signals

In order to measure the divergence between the input signals, and ensure consistency, repeatable and accurate signals are required, the input voltage was set using a DC voltage reference/calibrator (KROHN-HITE 511) with the following characteristics:

- Absolute accuracy of 10 ppm (0.001%)
- Voltage range from 100 nV to 10 V
- Resolution of 1 ppm of the range (0.0001%)
- $2 \mu\text{V}_{\text{pk-pk}}$  noise

The full specifications can be found in Appendix E.

The resolution of the 511 DC reference enables voltage increments of 100 nV, which is more than one order of magnitude lower than the smallest signal change being measured by the MS.

### 6.1.1 Logistic Map

To determine how the LM diverges for a known input change the LM was placed in the feedback MS as explained in section 3.2, the voltages were normalised, (i.e. scaled down by a factor of 10), to enable a direct comparison between the simulation and the practical results.

To test the LM implementation an arbitrary input value of 0.3430 V was set and after running (iterating) the system and recording the time series the input voltage was then increased by 500  $\mu\text{V}$  and the system was re-run and the data stored. In Figure 6-1(a) the two time series are displayed with the divergence displayed in (b). The divergence between the two time series is obtained by subtracting the second time series from the first. Two signals are considered to be divergent after a separation of more than 5 mV (for a 0-1 V normalised range). The divergence threshold was set so that the ADC (with a Least Significant Bit (LSB) of 1 mV) used can detect a divergence without any ambiguity due to noise and ADC errors. It can be observed that the two time series start to diverge from iteration 4, and the size of the divergence increases until iteration 8, at iteration 9 the two time series are uncorrelated and the information is irrecoverable.

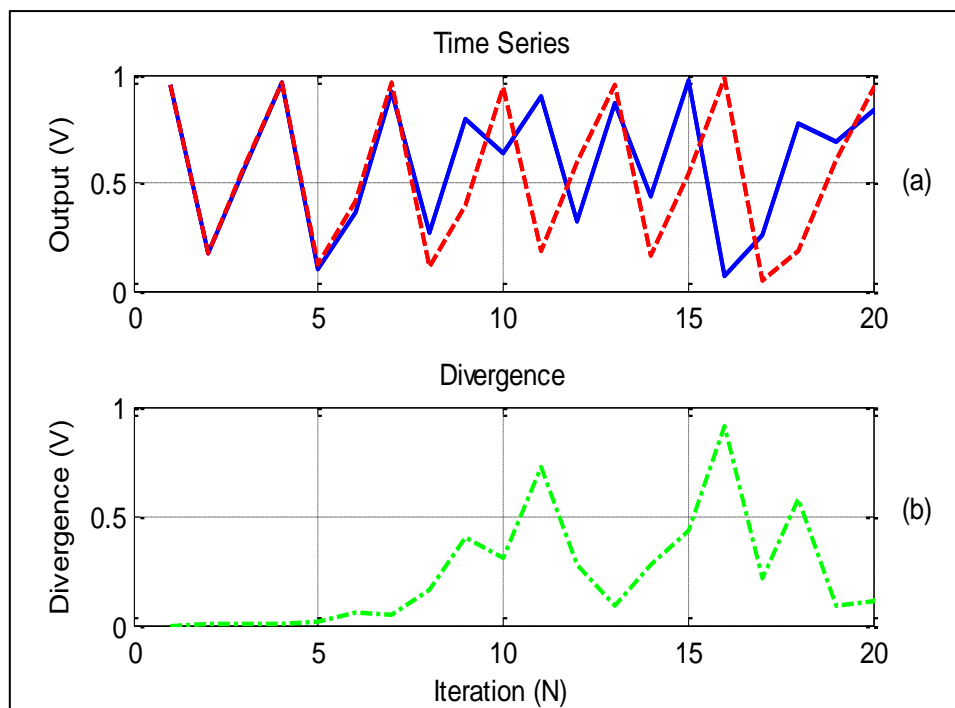


FIGURE 6-1 TIME SERIES AND DIVERGENCE FOR A 500MV CHANGE.

Figure 6-2 displays the divergence for a  $\Delta = 500 \mu\text{V}$  (green) along with the divergence for  $\Delta = 200 \mu\text{V}$  (red). As expected the time series diverge at an earlier iteration when the signal change ( $\Delta$ ) is increased. Table 6-1 shows the iteration at which the divergence occurs and also shows that practical results and theory yield the same results. To ascertain the minimum detectable change the LM was tested with the following procedure; the DC reference was set to a fixed value and the LM was run with the same sample multiple times. Ideally the time series obtained should match exactly but as discussed in the previous section (5.7) the noise will limit the LM sensitivity and the time series will diverge for a constant input signal, due to system noise. The amount of divergence between the time series enables the sensitivity of the system namely the minimum input change that can be detected, to be established.

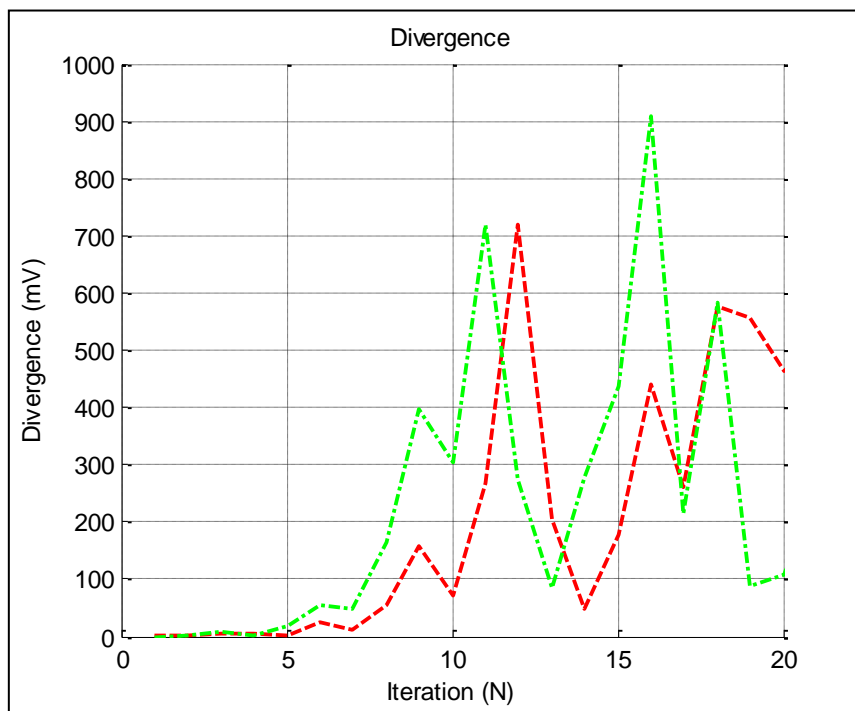


FIGURE 6-2 DIVERGENCE FOR TWO DIFFERENT INPUT CHANGES.

TABLE 6-1 PRACTICAL AND COMPUTED DIVERGENCE

<b>Input Change (<math>\Delta</math>)</b>	<b>Computed Divergence (Iteration Number)</b>	<b>Practical divergence (Iteration Number)</b>
200 $\mu$ V	5	5
500 $\mu$ V	4	4

Firstly, the LM was run 5 times with a fixed input and the respective time series obtained are shown in Figure 6-3. It can be observed that during the first 14 iteration there is no visible divergence between the time series but at iteration 15 the divergence becomes detectable i.e. above 5 mV. The minimum detectable change can be quantified by running the system multiple times for a fixed input, the two time series that are the most divergent can be taken in order to establish a “noise band”. Then a known change is applied to the input signal and if the resultant time series obtained is outside the “noise band” the input change can be detected. The change is reduced until the time series enters the “noise band” which means that the system is unable to discriminate between the input change and the noise. The amplitude of input change before the time series enters the “noise band” is defined as the sensitivity of the system as is illustrated in Figure 6-4.

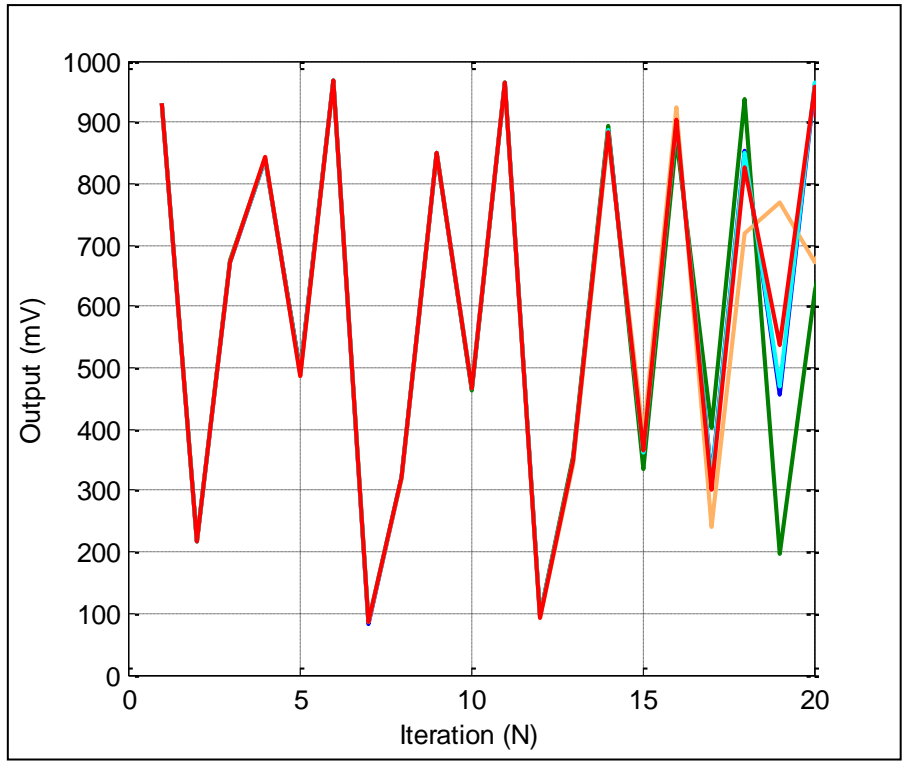


FIGURE 6-3 LM MULTIPLE RUNS FOR A FIXED INPUT

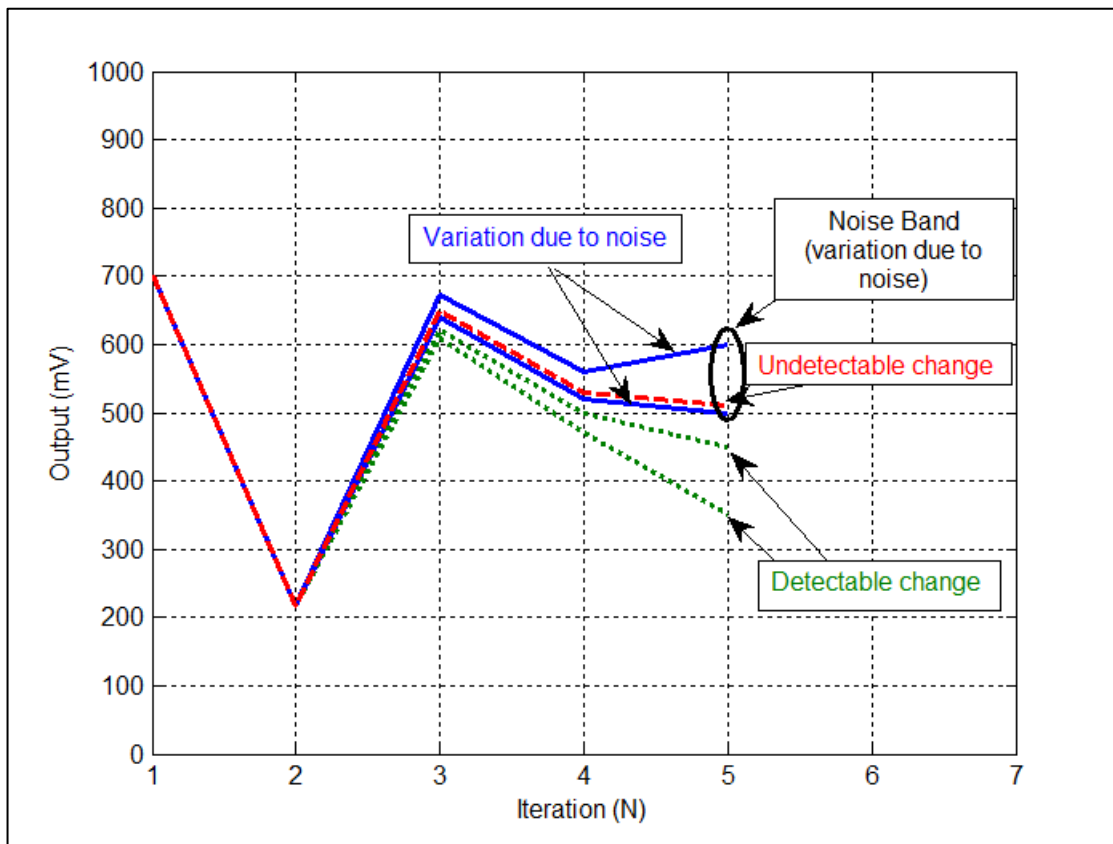


FIGURE 6-4 USE OF THE "NOISE BAND" TO MEASURE THE SENSITIVITY OF THE LM

To determine the sensitivity of the LM based MS using the “noise band”, the LM was iterated 8 times for 4 different input signals and the process was repeated 10 times for each input signal. A reference signal set at 0.2 V and three signals separated by a  $\Delta$  of 50  $\mu\text{V}$ , 100  $\mu\text{V}$  and 200  $\mu\text{V}$  yielding voltages of 0.20005 V, 0.2001 V and 0.2002 V respectively. The time series obtained are presented in Figure 6-5. To visualise the noise bands for each sample, Figure 6-6 shows an amplified section of the noise band for each sample at iteration 8. The clearance between the reference signal noise band and the noise band of the signal with  $\Delta = 200 \mu\text{V}$  is 24 mV, which is a greater amplitude than the noise bands contained within a 15 mV region. This indicates that the system can detect a  $\Delta$  of 200  $\mu\text{V}$  without any ambiguity. The clearance between the reference sample noise band and the noise band for  $\Delta = 100 \mu\text{V}$  is 8 mV which is lower than the noise band of 15 mV. In this case the system is unable to differentiate a divergence due to inherent noise from a divergence that occurred from a  $\Delta$  of 100  $\mu\text{V}$ . However, due to the clearance of 8 mV being in the region of the 15 mV noise band, the system can detect a  $\Delta$  of 100  $\mu\text{V}$  by the use of averaging. Moreover, a number of samples can be taken successively and averaged for each iteration, to reduce the noise band and enables the detection of  $\Delta = 100 \mu\text{V}$ . Finally, Figure 6-6 shows that for a  $\Delta$  of 50  $\mu\text{V}$  the noise band overlaps with the reference input voltage and the 100  $\mu\text{V}$   $\Delta$  which means that the detection of a 50  $\mu\text{V}$  change would require extensive use of averaging technique. However, the main drawback of averaging is that the time required for the system to perform one measurement is proportional to the number of samples taken. This means that a measurement taken at 1000 samples per second with 10 averaging samples is equivalent to a measurement at 100 samples per second. This is not an issue for

applications where the input signal is close to DC but it can be a problem for signals with frequencies of 1 kHz and above.

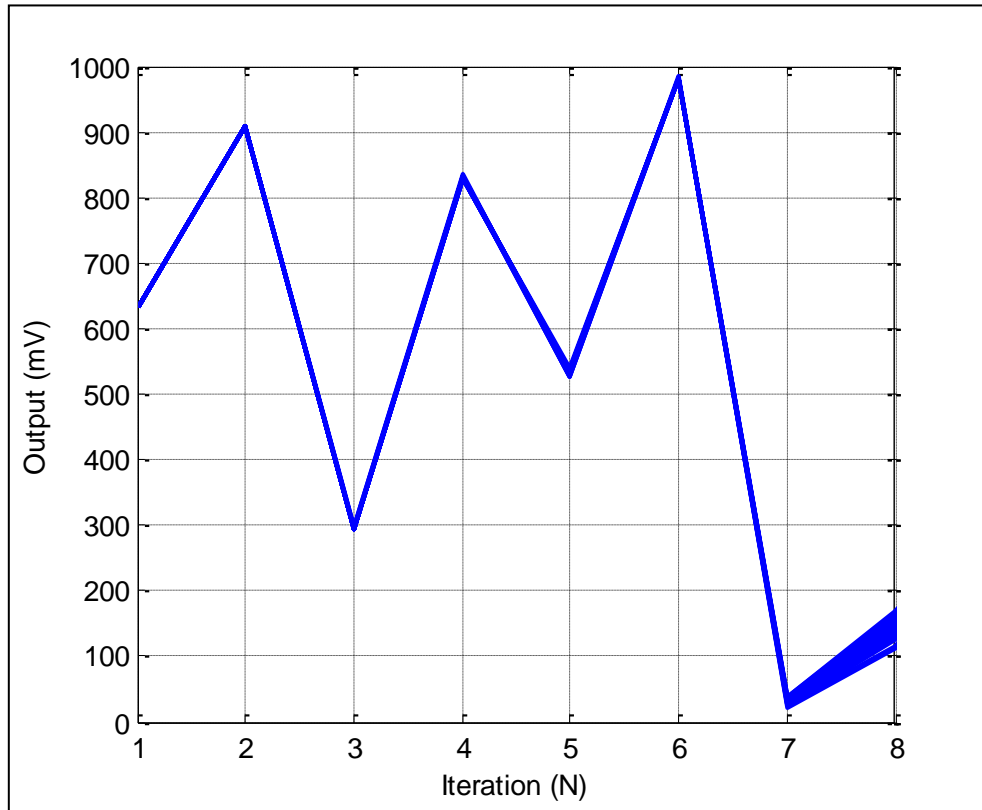


FIGURE 6-5 MULTIPLE TIME SERIES FOR DIFFERENT INPUT SAMPLES

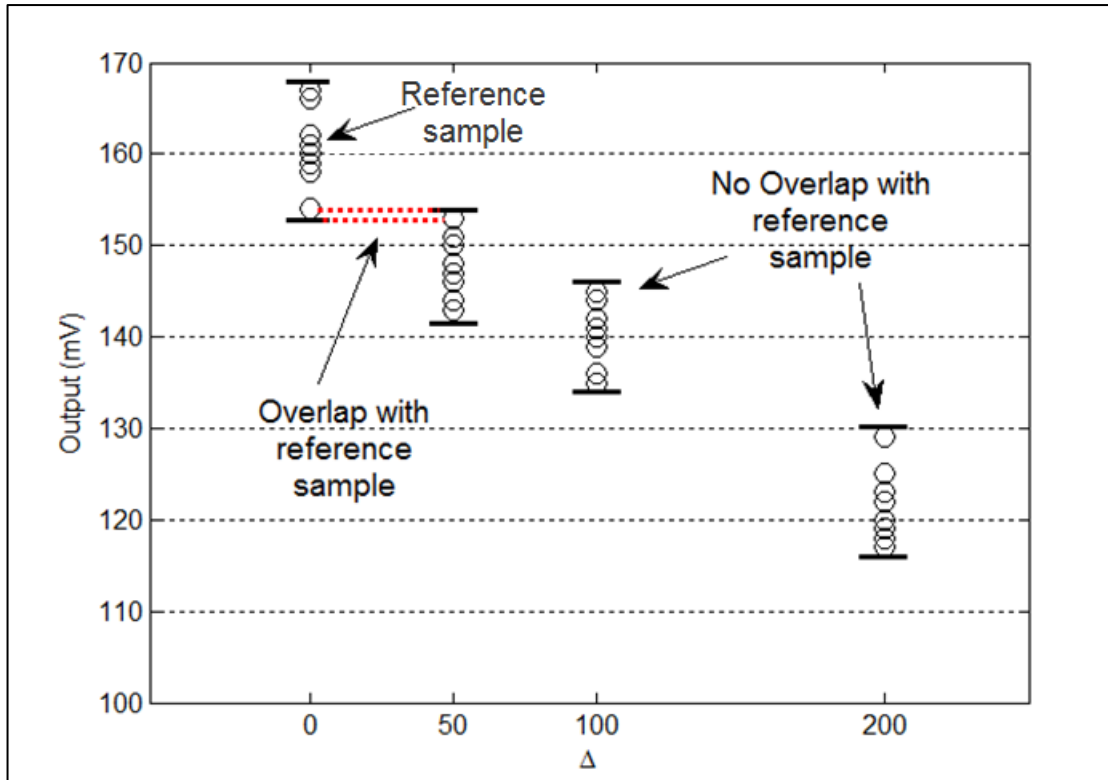


FIGURE 6-6 NOISE BAND AT ITERATION 8 FOR DIFFERENT INPUT SAMPLES

### 6.1.2 Tent Map

This section focuses on the divergence of two time series for two input samples for the TM and enables the proposed technique, developed in 3.1, to be tested experimentally. Samples are taken randomly across the input range for different input changes in order to test the theory, and particularly to test the performance of the feedback MS based on the TM by using equation (3-1). An example of two time series taken with a  $200 \mu\text{V}$  difference is shown in Figure 6-7(a) while the divergence between the two time series is displayed in (b). The exponential growth of the divergence is clearly visible from iteration 6 to iteration 12; however after iteration 12 the folding of the map occurs and the information is consequently irrecoverable.

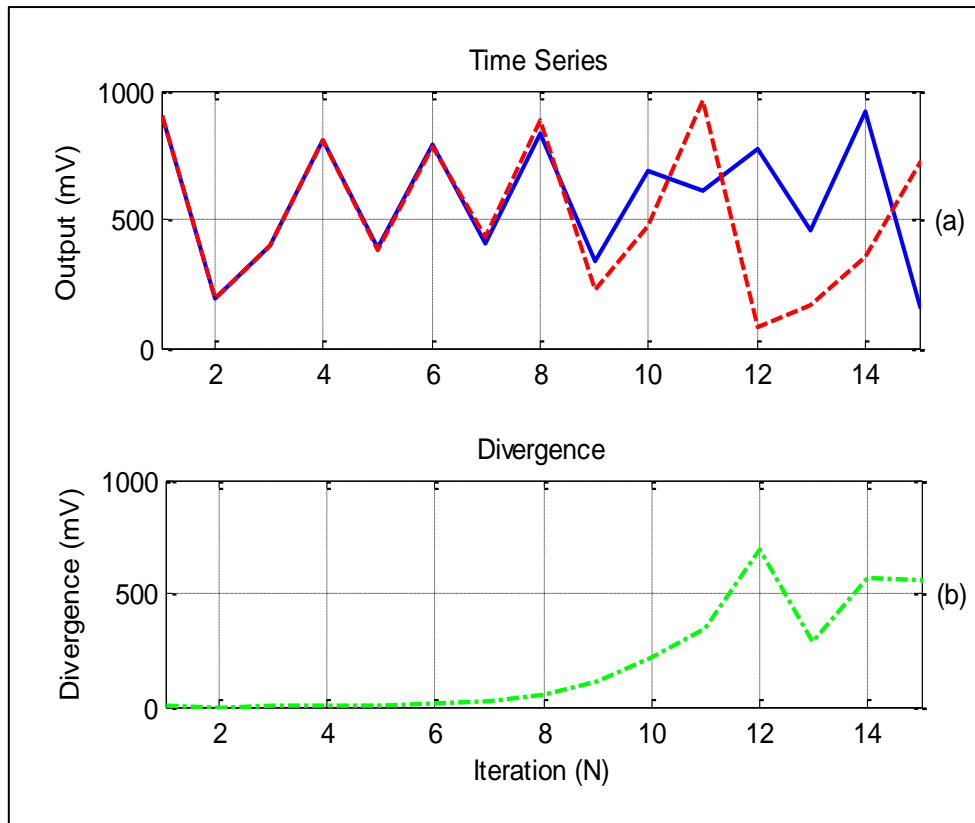


FIGURE 6-7 DIVERGENCE BETWEEN TWO TIME SERIES WITH A 200MV CHANGE

From the analysis carried-out in section 3.1, in order to minimize errors the equation (3-1) should be applied when divergence  $\geq 50$  mV, thus for the measurement in Figure 6-7 the divergence at iteration eight is equal to 54 mV which yield a calculated input change ( $\Delta$ ) of 210.9  $\mu$ V. An error of 10.9  $\mu$ V for a real change ( $\Delta$ ) of 200  $\mu$ V represents a 5.5% mismatch between the measured value and the real  $\Delta$ . To ascertain the overall performance of the TM, further results for different input samples were evaluated and shown in Table 6-2. For each value of  $\Delta$  two separate measurements were taken. It can be noted that for  $\Delta$  of 5 mV and 1 mV the error remains at zero since the noise of the system is significantly lower than the change being measured thus divergence occurs before the noise can be significantly amplified. With a  $\Delta$  of 500  $\mu$ V the error occurs as the  $\Delta$  being measured is closer to the noise of the system. The error reaches 120% for a  $\Delta$  of 20  $\mu$ V, which means that a change of that magnitude cannot be detected by the system. Thus according to the

noise measurement performed in the previous section the noise of the TM should not exceed 9.3  $\mu\text{V}$  but the measurement of  $\Delta$  shows much greater error than expected, which is due to the errors introduced by the feedback loop of the system. This feedback error is not measurable for the LM since the noise produced by the LM is of greater amplitude than the errors introduced by the sample and holds (S/H) used in the feedback loop.

TABLE 6-2 TM CHANGE MEASUREMENT WITH FEEDBACK SYSTEM

Real Change ( $\Delta$ )	Iteration of Divergence (N)	Measured Change ( $\Delta$ )	Error Between Real $\Delta$ and Measured $\Delta$
5 mV	4	5 mV	0%
	4	5 mV	0%
1 mV	6	1 mV	0%
	6	1 mV	0%
500 $\mu\text{V}$	8	510 $\mu\text{V}$	2%
	8	516 $\mu\text{V}$	3.2%
200 $\mu\text{V}$	8	211 $\mu\text{V}$	5.5%
	8	213 $\mu\text{V}$	6.5%
50 $\mu\text{V}$	10	70 $\mu\text{V}$	40%
	10	66 $\mu\text{V}$	32%
20 $\mu\text{V}$	11	44 $\mu\text{V}$	120%
	11	37 $\mu\text{V}$	85%

Since the errors introduced by the feedback system are significant in amplitude compared to the intrinsic noise of the TM, the next measurements performed on the TM MS will be completed using the series implementation of the MS, Table 6-3

shows the measurement results obtained with the series system: the error has decreased to 19 % for a  $\Delta$  of 20  $\mu\text{V}$  compared to 120% error on the system with feedback loop. The system can detect a input signal change of 50  $\mu\text{V}$  with a high degree of confidence as the error is limited to 8 %.

TABLE 6-3 TM CHANGE MEASUREMENT WITH SERIES SYSTEM

<b>Real Change (<math>\Delta</math>)</b>	<b>Iteration of Divergence (N)</b>	<b>Measured Change (<math>\Delta</math>)</b>	<b>Error Between Real <math>\Delta</math> and Measured <math>\Delta</math></b>
5 mV	4	5 mV	0%
	4	5 mV	0%
1 mV	6	1 mV	0%
	6	1 mV	0%
500 $\mu\text{V}$	8	504 $\mu\text{V}$	0.8%
	8	503 $\mu\text{V}$	0.6%
200 $\mu\text{V}$	8	202 $\mu\text{V}$	1%
	8	203 $\mu\text{V}$	1%
50 $\mu\text{V}$	10	54 $\mu\text{V}$	8%
	10	53 $\mu\text{V}$	6%
20 $\mu\text{V}$	11	24 $\mu\text{V}$	19%
	11	24 $\mu\text{V}$	19%
10 $\mu\text{V}$	12	14.3 $\mu\text{V}$	43%
	12	13.9 $\mu\text{V}$	39%

## 6.2 Divergence Against Input Signal Range

To evaluate the divergence of the practical implementation across the input signal range, the following procedure was carried out: the input signal was varied from 0 to 1 (normalised) with steps of 0.05 V and with a  $\Delta$  of 500  $\mu$ V. The two time series obtained for each step and for the step plus change were subtracted to obtain the divergence, which allows the absolute value of the divergence for the entire input range to be mapped.

### 6.2.1 Logistic Map

As shown in Figure 3-2; the divergence of the LM for a given input change is not uniform throughout the entire input range; the time series diverge earlier at the extremities of the input range. This feature of the LM map can be avoided by reducing the input range to 0.1-0.9 of the normalised input range. Figure 6-8(a) and (b) show the experimental data of the LM divergence where the whole input range is represented for an input change of 500  $\mu$ V. The iteration at which divergence occurs is constant (iteration seven) from 0.1 to 0.9 of the input range, and for input regions 0 to 0.1 and 0.9 to 1, divergence occurs at iteration five. Figure 6-8(a) and (b) represent the same data with two different angles in order to allow a better visualisation of the non-linearity at the extremities of the input range. From Figure 6-8(b) it can be seen that the LM present a high degree of linearity of divergence from 0.1 to 0.9 of the normalized input range. To further demonstrate this Figure 6-8(c) and (b) display the same experimental data but with a reduced input range (0.1 to 0.9).

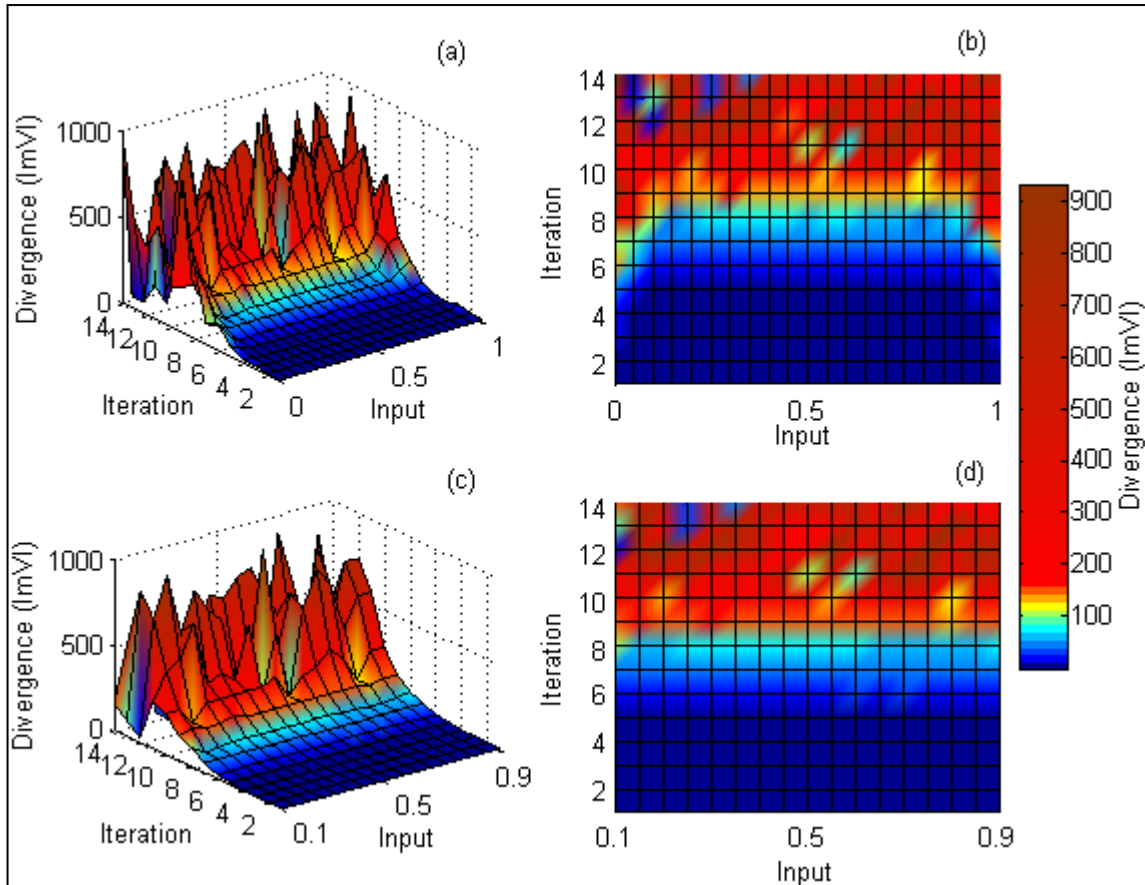


FIGURE 6-8 EXPERIMENTAL DIVERGENCE OF THE LM FOR A CHANGE OF  $500\mu\text{V}$ : (A) AND (B) FOR THE ENTIRE INPUT RANGE. (C) AND (D) FOR A RANGE LIMITED TO 0.1-0.9

## 6.2.2 Tent Map

In section 6.1.2, the measurements in Table 6-2 have shown that the errors introduced by the feedback in the iterated MS limits the performance of the TM, therefore the measurement of divergence for the entire input range has been carried-out only on a series configuration. This allows for improved performances by eliminating noise added by the S/H circuitry.

As shown in Figure 6-9, the divergence for a given input change is consistent throughout the entire input range which is ideal for a MS. This feature of the TM previously shown with the aid of computation in Figure 3-3, is a significant advantage over the behaviour of the LM. The divergence for a  $250\mu\text{V}$  change is

visible from iteration six and reaches more than 60 mV at iteration eight. The measurement for the estimation of the input change should be carried out at iteration seven or eight as this will be the most appropriate trade-off between estimation accuracy and probability of reaching a null reduction as explained in section 3.1.

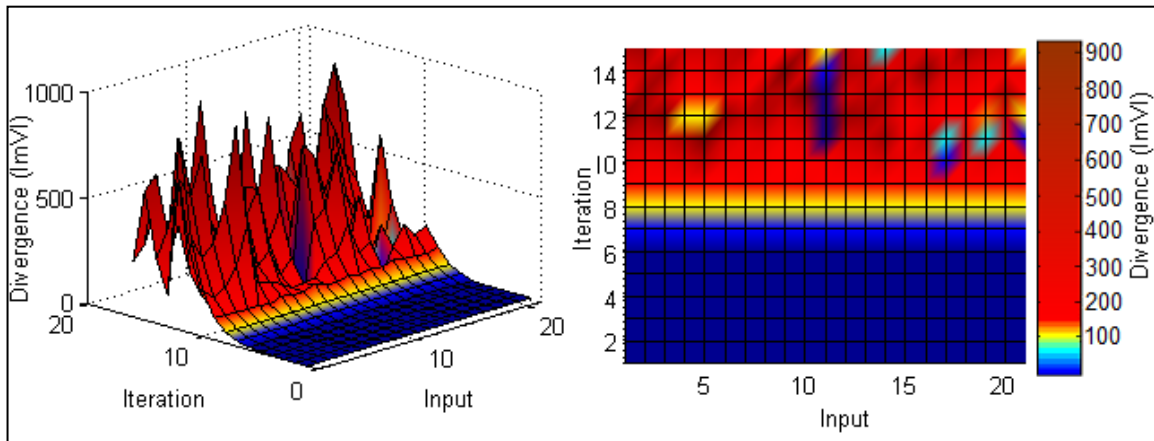


FIGURE 6-9 EXPERIMENTAL DIVERGENCE OF THE TM FOR A 200 $\mu$ V CHANGE FOR THE ENTIRE INPUT RANGE.

## 6.3 Divergence Against Input Signal Change

The final measurement carried out on each MS was the divergence against the amount of change between two input signals. The test procedure is different for each map as the method used to determine  $\Delta$  varies.

- LM based MS measurement procedure: the input was set to an arbitrary value within the linear range of the map (0.1 to 0.9). The time series obtained for the given input signal was stored then the signal was increased by a given amount ( $\Delta$ ) and resultant time series obtained and stored. The divergence between the two samples was calculated by subtracting the two time series and the iteration at which the absolute value of the divergence exceeded a set threshold was recorded and plotted on a graph. This process was repeated for

different input changes until a graph of the divergence against the amount of change was produced.

- TM based MS measurement procedure: different points were taken throughout the entire input range, with a  $\Delta$  ranging from 10  $\mu\text{V}$  to 1 mV and the error between the measured and real  $\Delta$  value was calculated for each input.

This will allow the sensitivity of the system to be determined.

### 6.3.1 Logistic Map

Figure 6-10 shows the iteration at which the divergence occurs for a given  $\Delta$ ; the full line represents the computed divergence whilst the dotted line shows the practical results. As the divergence is exponential the x axis is set to a logarithmic scale which means the “divergence versus change” data forms a straight line. Ideally the divergence of the practical implementation should follow that same line as the computed, however the practical results follow the computed divergence line until a change of approximately 100  $\mu\text{V}$  is applied. At this point the noise inherent to the systems makes the time series diverge before the signal change ( $\Delta$ ). This result is consistent with the “noise band” measurement discussed in section 6.1.1, where it has been shown that the LM is limited to approximately 100  $\mu\text{V}$  of detectable change due to the inherent noise of the electronic implementation.

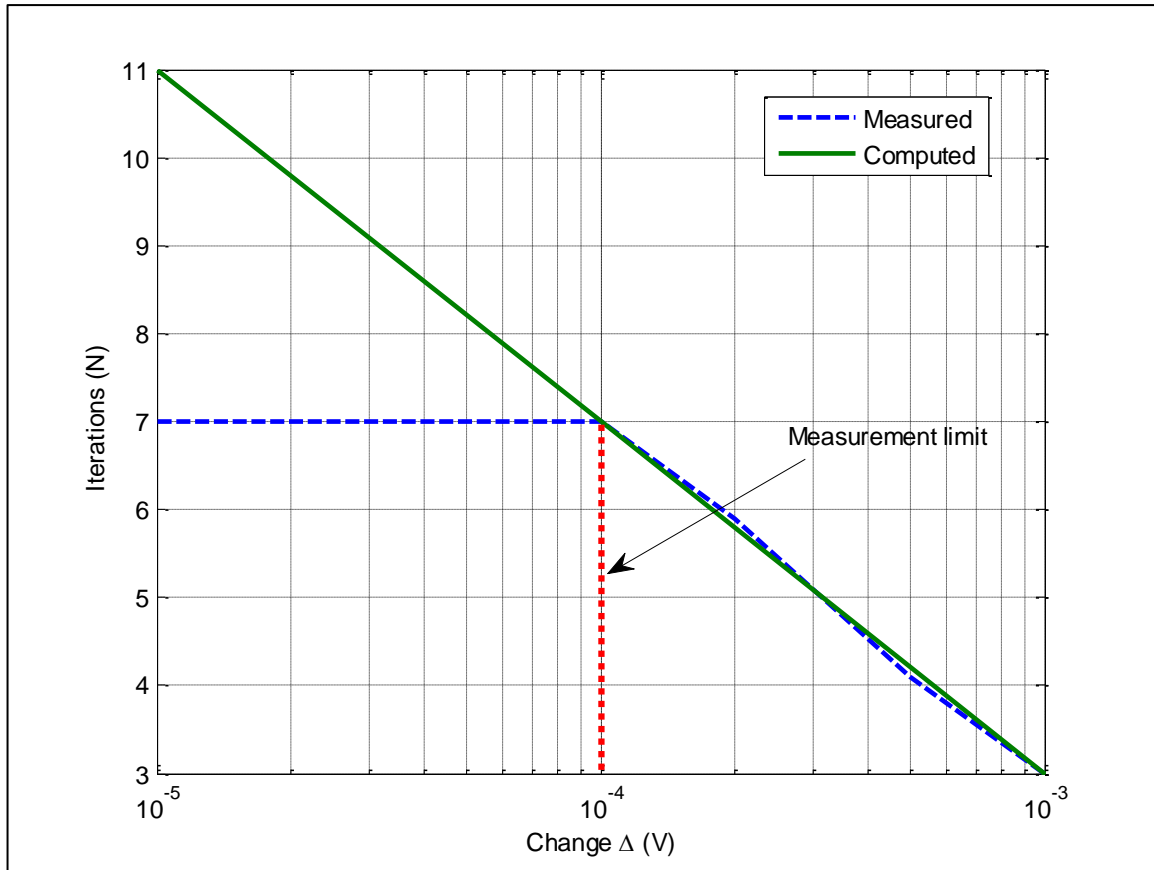


FIGURE 6-10 LOGISTIC MAP DIVERGENCE VS CHANGE

### 6.3.2 Tent Map

The proposed implementation of the TM has shown excellent divergence linearity throughout the entire input range hence the following measurements will determine the performance of the series based TM MS across different values of input change ( $\Delta$ ). Different points have been taken with  $\Delta$  ranging from 10  $\mu$ V to 1 mV and the error between the measured and real  $\Delta$  was calculated for each measurement and displayed as in Figure 6-11. The measurement error remains negligible for a  $\Delta$  of 1 mV as the noise of the system is insignificant compared to the  $\Delta$  being measured. For  $\Delta$  values lower than 1 mV the error starts to rise as the  $\Delta$  being measured is of a similar magnitude to the inherent noise of the TM implementation. The error remains below 19% for a  $\Delta$  of 20  $\mu$ V before rising to over 40% as  $\Delta$  is reduced to 10  $\mu$ V which represents a noise floor of approximately 4  $\mu$ V.

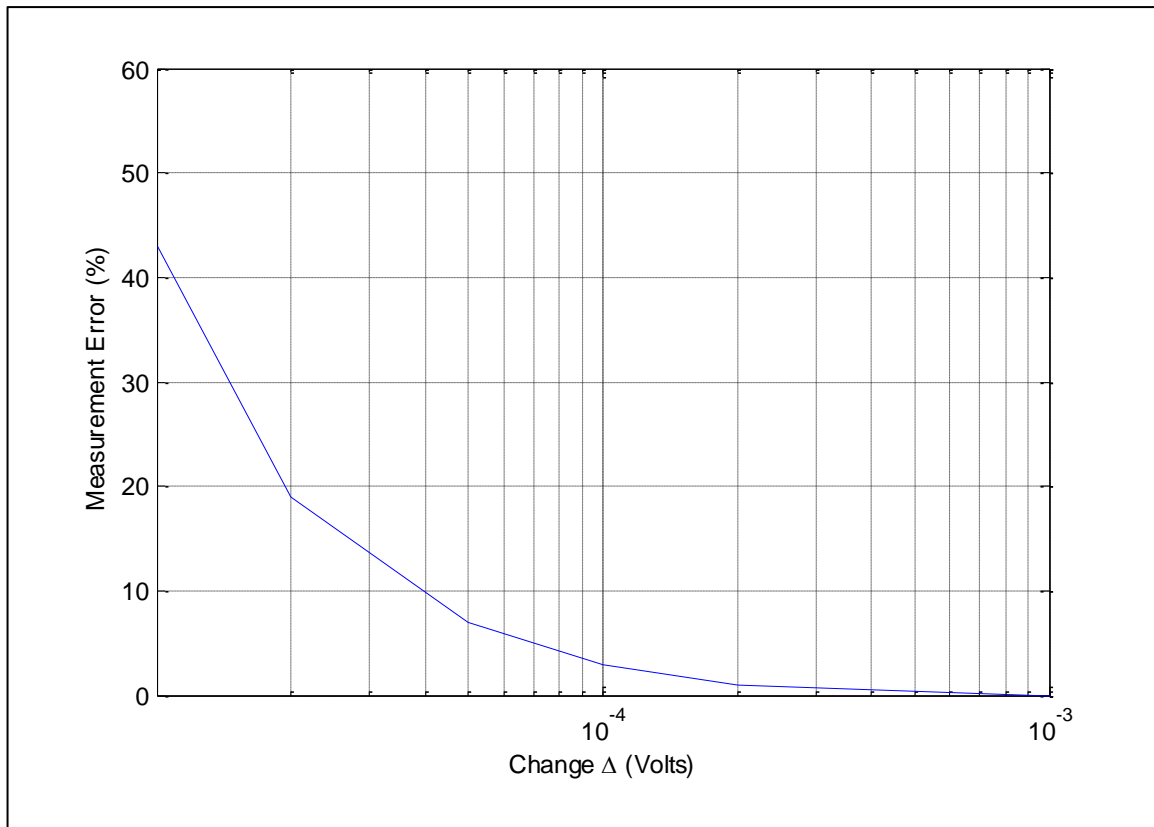


FIGURE 6-11 MEASUREMENT ERROR VS CHANGE FOR THE SERIES IMPLEMENTATION OF THE TM BASED MS

## 6.4 Conclusion

In this chapter the LM based MS was tested, followed by the TM MS and the results obtained were as follows:

- LM based system can detect an input signal change of 200  $\mu\text{V}$  without ambiguity and a 100  $\mu\text{V}$  signal change with the use of averaging. The input range has to be reduced to 0.1- 0.9 to obtain a linear divergence throughout the input range.
- The TM base system demonstrates a greater sensitivity to input signal change in the series configuration as the noise introduced in the feedback limits the performance of the MS. The results demonstrate that the MS based on the TM

can measure input signal changes of  $100\ \mu\text{V}$  with an error of 3% and  $20\ \mu\text{V}$  with an error of 19% with the use of the series implementation which represents a sensitivity of  $4\ \mu\text{V}$ .

- With a sensitivity of  $4\ \mu\text{V}$  independently of the input range, the voltage step size of the proposed chaos based MS is superior to an 20 bit ADC over a 10 V input range.

The next chapter will discuss the results obtained from the MS and the performance of the proposed implementations.

# 7 Discussion

The theoretical analysis of the one-dimensional chaotic maps demonstrates that the high sensitivity to initial conditions, which characterises chaotic behaviour, can be used to detect or measure small variation between signal samples. Two different approaches in order to quantify the change of input signal for two one-dimensional chaotic maps have been proposed. For the LM, the magnitude of change can be quantified by setting thresholds on the amount of divergence; this technique is more suitable for a detection system that would require only a few thresholds rather than a measurement system as the thresholds are set experimentally for each implementation which can be time consuming. For the TM; the equation (3-1), proposed by the author can be used to measure the difference between two signals which does not require any calibration making the MS based on the TM superior to the one utilizing the LM.

The results obtained from the newly developed electronic implementations of the two one-dimensional chaotic maps, demonstrate a  $\pm 1\%$  matching compared to the theoretical maps. The practical results show an identical behaviour in all aspects; transfer characteristics, bifurcation diagrams, and time series. The chaotic performance of each map was demonstrated by estimating the Lyapunov Exponent applying the Wolf method available in literature (Wolf et al., 1985).

The experimental results obtained for the proposed MS demonstrate that the LM and the TM can be used as part of a MS to detect or measure small changes of input signals. The LM implementation is capable of detecting signals in the order of hundreds of  $\mu\text{V}$  whilst the TM can measure signals changes higher than  $4 \mu\text{V}$ . The

sensitivity of the MS is independent of the input range which means that an increase in the input range does not affect the sensitivity of the measurement. This feature of the proposed MS makes it superior to the existing alternatives which are based on linear amplifier coupled to an ADC. In the classical approach to signal measurement, the sensitivity of the MS is directly proportional to the input range, for instance if the input range is doubled, the sensitivity of the system is reduced by the same factor. In general, to palliate the loss of sensitivity, the ADC is replaced by an ADC with higher resolution which increased the cost of the MS or requires the replacement of existing equipment. Alternatively, the suggested MS can be used with an input range as high as permitted by the power supply and components ratings without suffering any degradation of its performance.

The two topologies for MS investigated in the work were the feedback and series based system. The feedback system or iterated system uses feedback to iterate the initial input signal multiple times through the same electronic implementation of the map. This allows a flexible control over the number of iterations. In contrast the series implementation is configured so that the signal propagates through multiple circuit implementation of the same map. From the results for the prototype implementations using low cost electronics, the series implementation provides higher performance than the feedback system as the noise produced by the feedback limits the overall performance of the MS. The feedback error is not an issue when the LM is used as the inherent noise of the implementation is higher than the errors introduced by the feedback. To take advantage of the lower noise implementation of the TM, a MS based on the TM should be constructed using the series topology, the drawback for improved performance is the increased amount of components and the reduces flexibility when it comes to setting the number of iterations. The

performance of the MS could be further improved by different methods such as replacing some of the electronics with improved ICs or by integrating multiple maps on a single IC.

A novel signal measurement system (MS) based on one-dimensional chaotic map has been proposed for the measurement and detection of small signal changes. This thesis considers for the first time the electronic hardware implementation of a complete MS based on chaotic maps and develops the theory associated with such a system. The developed MS has led to a patent application (n° 1309585.4). The proposed MS is radically different from the classic approach to signal magnitude measurement as the measurement performed results in a measure of a signal change rather than an absolute value. Such a system could be used in many applications including:

- Relative value measurement: applications where the absolute value is not of importance but where a small difference between two signal samples needs to be measured. The main advantage over a classical approach is that the detectable change of signal (resolution) is independent of the input range thus allowing for greater dynamic range/ resolution ratio. For example, a strain gauge can be used to detect small strain variations over a wide initial signal range thus effectively increasing the resolution compared to a classic MS using the same ADC. Time series representing user defined strain thresholds can be set and the input signal monitored in order to detect when the strain drifts above or under the fixed limit. This example is not limited to strain measurement and can be applied to any physical quantity such as temperature or pressure. The proposed MS could also be used in safety applications where

thresholds are set on critical parameters in order to trigger an alarm or stop machinery when the working conditions are outside the set limits.

- Increased data acquisition capability: the proposed MS can be used to improve the detection capability of existing data acquisition systems. For example, an acquisition board equipped with an existing low resolution (8-bit or 12-bit) ADC can be expanded, with the addition the proposed MS, to obtain signal change detection levels in the order of 20-bits by effectively increasing the detectable step size of the system. The added advantage is that the relative resolution of the overall acquisition system will be increased as well as the approximate absolute measurement values still being available.

The results obtains are very promising and given further development could lead to a MS that offers significant performance and/or cost advantage over other measurement techniques for many applications.

# 8 Conclusion and Further Work

## 8.1 Conclusion

The main conclusions of this thesis are:

- a) One-dimensional chaotic maps as a mean of measurement have been successfully investigated using MATLAB.
- b) A novel 3D graphical representation of the high sensitivity to initial condition of one-dimensional chaotic map has been presented allowing a graphical visualisation of the phenomena. The developed visual representation is not limited to the Logistic and Tent maps and can be used to analyse the high sensitivity to initial conditions of any one-dimensional chaotic map.
- c) Two one-dimensional chaotic maps (Logistic map and Tent map) have been analysed and a novel low noise electronic implementation of the maps has been developed and presented.
- d) A mean of quantifying the change of input signal was proposed for each map and the advantages and drawback of using each map have been assessed.
- e) The proposed implementations have been tested using the transfer characteristic, bifurcation diagram, time series and Lyapunov Exponent showing a matching between theory and experimental results. The results

demonstrate a matching within  $\pm 1\%$  between theory and the practical implementations.

- f) Two measurement systems topologies have been proposed and designed; the series and the feedback topology. The two topologies were assessed and the following conclusions were drawn: the feedback topology develops higher inherent noise levels than the series topology. The series topology requires more hardware and offers less flexibility than the feedback topology.
- g) The developed electronic circuit representing the chaotic maps have been integrated into a measurement system.
- h) The sources of errors associated with the proposed measurement system have been identified and assessed. Means of mitigating some of the identified errors have been proposed.
- i) The proposed measurement systems have been assessed practically and the results shown that the small variation of input signals can be measured. The results demonstrate that the MS based on series implementation are superior in terms of detectable input signal change compared to a feedback system. The most favourable performance have been obtained using the TM based series topology: the measurement system was able to detect signal changes as low as  $4\mu\text{V}$  using a 10bit ADC with a step size (LSB) of 10mV for a 10V input range.

## 8.2 Further Work

The author of this thesis would like to propose the following further work:

- Investigate possible improvement to the electronics implementations of the TM in order to reduce noise which would increase the sensitivity of the proposed MS. Moreover, the possibility of implementing the MS using switched capacitor technique could be investigated; this could possibly lead to single IC integration thus reducing cost and potentially increase the sensitivity of the MS by lowering the noise for the feedback system.
- Further investigation regarding the behaviour of one dimensional chaotic map. This could potentially lead to alternative methods of using the high sensitivity to initial conditions as a mean of measuring small signals.
- Investigating the “nulls” that theoretically appear in the behaviour of the TM, and quantify the effects in the implemented system.
- Investigate the possibility of improving the performance of chaos based ADC using the proposed MS.

# References

- AGILENT. 1985. *3562A Dynamic Signal Analyzer Operating Manual* [Online]. Available: <http://cp.literature.agilent.com/litweb/pdf/03562-90001.pdf> [Accessed 08/06 2014].
- ALLIGOOD, K. T., SAUER, T. & YORKE, J. A. 1997. *Chaos: an introduction to dynamical systems*, New York [etc.], Springer.
- ANALOG-DEVICES. 2003. *OP27 Low-Noise, Precision Operational Amplifier Data Sheet* [Online]. Available: <http://web.mit.edu/6.301/www/OP27c.pdf> [Accessed 20/08 2013].
- ANALOG-DEVICES. 2007. *High Precision 10 V Reference AD587* [Online]. Available: [http://www.analog.com/static/imported-files/data\\_sheets/AD587.pdf](http://www.analog.com/static/imported-files/data_sheets/AD587.pdf) [Accessed 08/06 2014].
- ANALOG-DEVICES. 2008. *Sample-and-Hold Amplifiers MT-090 Tutorial* [Online]. Available: <http://www.analog.com/static/imported-files/tutorials/MT-090.pdf> [Accessed 20/08 2013].
- ANALOG-DEVICES. 2009. *MT-079 Tutorial: Analog Multipliers* [Online]. Available: <http://www.analog.com/static/imported-files/tutorials/MT-079.pdf> [Accessed 20/08 2013].
- ANALOG-DEVICES. 2012. *AD633 Low Cost Analog Multiplier Data Sheet* [Online]. Available: [http://www.analog.com/static/imported-files/data\\_sheets/AD633.pdf](http://www.analog.com/static/imported-files/data_sheets/AD633.pdf) [Accessed 20/08 2013].
- ANALOG-DEVICES. 2013. *ADR130 Precision Series Sub-Band Gap Voltage Reference Data Sheet* [Online]. Available: [http://www.analog.com/static/imported-files/data\\_sheets/ADR130.pdf](http://www.analog.com/static/imported-files/data_sheets/ADR130.pdf) [Accessed 20/08 2013].
- ARAYAWAT, S., THUBTONG, U., JULSEREEWONG, P., RIEWRUJA, V. & JULSEREEWONG, A. A voltage-mode Gray-code algorithmic ADC. 2008. IEEE, 605-608.
- ATMEL. 2005. *AVR121: Enhancing ADC resolution by oversampling* [Online]. Atmel Corporation. Available: <http://www.atmel.com/images/doc8003.pdf> [Accessed 20/08 2013].

- BRADLEY, E. 1993. Using chaos to broaden the capture range of a phase-locked loop. *IEEE transaction on circuits and systems fundamental theory and applications* 40, 808-818.
- CALLEGARI, S., ROVATTI, R. & SETTI, G. 2005. Embeddable ADC-based true random number generator for cryptographic applications exploiting nonlinear signal processing and chaos. *IEEE transactions on signal processing*, 53, 793-805.
- CAMPOS-CANTÓN, I., CAMPOS-CANTÓN, E., MURGUÍA, J. S. & ROSU, H. C. 2009. A simple electronic circuit realization of the tent map. *Chaos, Solitons and Fractals*, 42, 12-16.
- CHAIKLA, A., CHAIKLA, A., ARAYAWAT, S. & RIEWRUJA, V. OTA-based Gray-code Algorithmic ADC. 2006 2006. *IEEE*, 5787-5791.
- CHERNUKHA, E. Utilization of chaotic system properties to improve measurement quality. *IEEE Instrumentation and Measurement Technology Conference*, 1996 1996 Brussels. 1408-1411 vol.2.
- CRAIG, I. 1995. Analog-to-Digital and Digital-to-Analog Conversion Techniques (Second Edition) by David F. Hoeschele, John Wiley, New York, 1994, 397 pages including index (Hbk,£58). *Robotica*, 13, 321-321.
- CRISTINA, D. A., RADU, B. & CIPRIAN, R. A new pseudorandom bit generator using compounded chaotic tent maps. 2012 2012. *IEEE*, 339-342.
- DÍAZ-MÉNDEZ, A., MARQUINA-PÉREZ, J. V., CRUZ-IRISSON, M., VÁZQUEZ-MEDINA, R. & DEL-RÍO-CORREA, J. L. 2009. Chaotic noise MOS generator based on logistic map. *Microelectronics Journal*, 40, 638-640.
- DYER, S. A. 2001. *Survey of instrumentation and measurement*, Chichester, Wiley.
- EDANG, A. E., LEYNES, J. K. O., ELLA, R. L. A., LABAYANE, R. C. & SANTIAGO, C. M. 2011. Nonlinear maps from closed-loop tandems of A-to-D and D-to-A converters. *Communications in Nonlinear Science and Numerical Simulation*, 16, 1483-1489.
- EGUCHI, K., UENO, F., TABATA, T., ZHU, H. & INOUE, T. 2000. Simple design of a discrete-time chaos circuit realizing a tent map. *IEICE trans. Electron.*, E83-C.

- ERGULER, K. & STUMPF, M. P. H. 2008. Statistical interpretation of the interplay between noise and chaos in the stochastic logistic map. *Mathematical Biosciences*, 216, 90-99.
- G.L.BAKER & J.P.GOLLUB 1990. *Chaotic Dynamics: An Introduction*, Cambridge University Press.
- GLEICK, J. 1988. *Chaos: making a new science*, Penguin.
- HAI, N., HAI, N., NAIRN, D. G. & NAIRN, D. G. A low power 12-bit 10MS/s algorithmic ADC. 2010 2010. IEEE, 1-4.
- HARTH, E. Order and chaos in neural systems: An approach to the dynamics of higher brain functions. 1983. IEEE, 782-789.
- HERNANDEZ, E. D. M., GEEHYUK, L. & FARHAT, N. H. Analog realization of arbitrary one-dimensional maps. 2003 PISCATAWAY. IEEE-INST ELECTRICAL ELECTRONICS ENGINEERS INC, 1538-1547.
- HOROWITZ, P. & HILL, W. 1989. *The art of electronics*, Cambridge, Cambridge University Press.
- HU, W. & LIU, Z. 2010. Study of Metal Detection Based on Chaotic Theory. *Intelligent Control and Automation (WCICA)*. Jinan, Chinal.
- INGRAHAM, R. L. 1991. *A Survey of Nonlinear Dynamics*, World Scientific Publishing Company.
- J.-P. ECKMANN & D. RUELLE 1985. Ergodic theory of chaos and strange attractors. *Phys.* , 57.
- J.KURTHS & H.HERZEL 1987. An atractor in a solar time series. *Physuca*, 25D, 165-172.
- KANSO, A. & SMAOUI, N. 2009. Logistic chaotic maps for binary numbers generations. *Chaos, Solitons and Fractals*, 40, 2557-2568.
- KAPITANIAK, T., ZYCZKOWSKI, K., FEUDEL, U. & GREBOGI, C. 2000. Analog to digital conversion in physical measurements. *Chaos, Solitons and Fractals*, 11, 1247-1251.
- KATZ, O., KATZ, O., RAMON, D. A., RAMON, D. A., WAGNER, I. A. & WAGNER, I. A. A Robust Random Number Generator Based on a Differential Current-Mode Chaos. 2008 PISCATAWAY. IEEE, 1677-1686.
- KEITHLEY-INSTRUMENTS 2004. *Low level measurement handbook*. .
- KENG, L.-F. & SALAMA, C. A. T. Low-power current-mode algorithmic ADC. 1994 1994. 473-476 vol.5.

- KENNEDY, M. P. 1995. A Nonlinear Dynamics Interpretation of Algorithmic A/D Conversion. *International Journal of Bifurcation and Chaos*, 5, 891.
- KOCAREV, L. 2001. Chaos-based cryptography: a brief overview. *IEEE Circuits and Systems Magazine*, 1, 6-21.
- KOCAREV, L. & JAKIMOSKI, G. 2001. Logistic map as a block encryption algorithm. *Physics Letters A*, 289, 199-206.
- LAX, M., CAI, W. & XU, M. 2006. *Random Processes in Physics and Finance*, OUP Oxford.
- LEONARDO, P.-L., GONZALO ISAAC, D.-S., JOSÉ LUIS, A.-V. & RUBÉN, V.-M. 2012. Digital Noise Generator Design Using Inverted 1D Tent Chaotic Map. *VLSI Design*, 2012.
- LORENZ, E. N. 1963. Deterministic Nonperiodic Flow. *Journal of the Atmospheric Sciences*, 20, 130-141.
- LORENZ, E. N. 1972. Predictability; Does the flap of a butterfly's wings in brazil set off a tornado in texas. *American Association for the Advancement of Science 139th Meeting*
- LU, C.-C. 2011. A 1.5V 10 bit 5 MS/s CMOS Algorithmic ADC. In: IEEE (ed.) *4th International Congress on Image and Signal Processing*.
- LUCA, A., ILYAS, A. & VLAD, A. Generating random binary sequences using tent map. 2011. IEEE, 1-4.
- LYNCH, S. 2004. *Dynamical systems with applications using MATLAB*, Boston, [Mass.], Birkhäuser.
- MARTINEZ-NONTHE, J. A., CASTANEDA-SOLIS, A., DIAZ-MENDEZ, A., CRUZ-IRISSON, M. & VAZQUEZ-MEDINA, R. 2012. Chaotic block cryptosystem using high precision approaches to tent map. *MICROELECTRONIC ENGINEERING*, 90, 168-172.
- MAXIM. 2006. *Quad SPST CMOS Analog Switches* [Online]. Available: <http://datasheets.maximintegrated.com/en/ds/DG201A-DG211.pdf> [Accessed 08/06 2014].
- MAY, R. M. 1976. Simple mathematical models with very complicated dynamics. *Nature*, 26, 459-467.
- MINER, J. R. 1933. Pierre-François Verhulst, the Discoverer of the Logistic Curve. *Human Biology*, 5, 673.

- MORRIS, A. S. 1993. *Principles of measurement and instrumentation*, Prentice Hall.
- MORRIS, A. S. 2001. *Measurement and instrumentation principles*, Butterworth Heinemann.
- MORRIS, A. S., LANGARI, R. & BOOKS24X, I. 2012. *Measurement and instrumentation: theory and application*, Academic Press.
- MURALI, K., SINHA, S. & MOHAMED, I. R. 2005. Chaos computing: experimental realization of NOR gate using a simple chaotic circuit. *Physics Letters A*, 339, 39-44.
- NATIONAL-INSTRUMENTS. 2007. *NI 625x Specifications* [Online]. Available: <http://www.ni.com/pdf/manuals/371291h.pdf> [Accessed 08/06 2014].
- NEJATI, H., BEIRAMI, A. & MASSOUD, Y. 2012. A Realizable Modified Tent Map for True Random Number Generation.
- NEUBERT, H. K. P. 1975. *Instrument transducers: an introduction to their performance and design*, Clarendon Press.
- NORTON, H. N. 1969. *Handbook of transducers for electronic measuring systems*, Prentice-Hall.
- NOZAWA, H. 1992. A neural network model as a globally coupled map and applications based on chaos. *Chaos*, 2, 377–386.
- PAREEK, N. K., PATIDAR, V. & SUD, K. K. 2006. Image encryption using chaotic logistic map. *Image and Vision Computing*, 24, 926-934.
- PARLITZ, U. 1998. *Nonlinear Modeling: Nonlinear Time-Series Analysis*, Springer US.
- PATIDAR, V., PAREEK, N. K. & SUD, K. K. 2009. A new substitution–diffusion based image cipher using chaotic standard and logistic maps. *Communications in Nonlinear Science and Numerical Simulation*, 14, 3056-3075.
- PLASSCHE, R. V. D. 1994. *Integrated analog-to-digital and digital-to-analog converters*, Kluwer.
- POULIQUEN, P. O., BOAHEN, K. A. & ANDREOU, A. G. 1991. A Gray-code MOS current-mode analog-to-digital converter design. *IEEE International Symposium on Circuits and Systems*, 4, 1924 - 1927.
- QINGDU, L. & QIFENG, L. Simple chaos-based ADC with only one opamp. 2012 2012. *IEEE*, 824-827.

- R. H. SIMOYI, A. W., AND H. L. SWINNEY 1982. One-dimensional dynamics in a multicomponent chemical reaction. *Phys. Rev. Lett.*, 49, 245–248.
- RAZAVI, B. 1995. *Principles of data conversion system design*, IEEE Press.
- ROSENSTEIN, M. T., COLLINS, J. J. & LUCA, C. J. D. 1992. A practical method for calculating largest Lyapunov exponents from small data sets. *NeuroMuscular Research Center and Department of Biomedical Engineering*.
- SATO, S., SANO, M. & SAWADA, Y. 1987. Practical Methods of Measuring the Generalized Dimension and the Largest Lyapunov Exponent. *Pro. Theor. Phys*, 77.
- SCHMID, H. 1970. *Electronic analog/digital conversions*, Van Nostrand-Reinhold.
- SEMICONDUCTORS, N. 1994. LM194/LM394 Supermatch NPN Transistor Pair.
- SETTI, G., MAZZINI, G., ROVATTI, R. & CALLEGARI, S. Statistical modeling of discrete-time chaotic processes-basic finite-dimensional tools and applications. 2003 2002. 68-92.
- SIGNELL, S. Non-traditional architectures for AD- and DA- converters. 2005 2005. IEEE, 451-453.
- SIGNELL, S., BENGT JONSSON, HELGE STENSTROM & TAN, N. 1997. New A/D Converter Architectures Based on Gray Coding. *In: IEEE (ed.) International Symposium on Circuits and Systems*. Hong Kong.
- SINGH, N. & SINHA, A. 2010. Chaos-based secure communication system using logistic map. *Optics and Lasers in Engineering*, 48, 398-404.
- SONG, Y., CHEN, Z. Q. & YUAN, Z. Z. 2007. Neural network nonlinear predictive control based on tent-map chaos optimization. *Chinese Journal of Chemical Engineering*, 15, 539-544.
- SUNEEL, M. 2006. Electronic circuit realization of the logistic map. *Sadahana academy proceedings in engineering sciences*, 31, 69-78.
- TANAKA, H., SATO, S. & NAKAJIMA, K. 2000. Integrated Circuits of Map Chaos Generators. *Analog Integrated Circuits and Signal Processing*, 25, 329-335.
- TEXAS-INSTRUMENTS. 2000. *LF198/LF298/LF398, LF198A/LF398A Monolithic Sample-and-Hold Circuits* [Online]. Available: LF198/LF298/LF398, LF198A/LF398A Monolithic Sample-and-Hold Circuits [Accessed 20/08 2013].

- TEXAS-INSTRUMENTS. 2005. *TL071 Low-Noise JFET-Input Operational Amplifier Data Sheet* [Online]. Available: <http://www.ti.com/lit/ds/symlink/tl071a.pdf> [Accessed 20/08 2013].
- TEXAS-INSTRUMENTS 2009. Op Amp Noise MT-047 Application Note.
- USYCHENKO, V. G. 2011. Tent map as an abstract model of open system evolution. *Technical Physics*, 56, 885-888.
- VÁZQUEZ-MEDINA, R., DÍAZ-MÉNDEZ, A., DEL RÍO-CORREA, J. L. & LÓPEZ-HERNÁNDEZ, J. 2009. Design of chaotic analog noise generators with logistic map and MOS QT circuits. *Chaos, Solitons and Fractals*, 40, 1779-1793.
- WANG, CHEN, LIN & CHEN 1999. The application of chaotic oscillators to weak signal detection. *IEEE Transactions on Industrial Electronics*, 46, 440-444.
- WILAMOWSKI, B. M., SINANGIL, M. E. & DUNDAR, G. A Gray-Code Current Mode ADC Structure. 2006 2006. *IEEE*, 35-38.
- WOLF, A., SWIFT, J. B., SWINNEY, H. L. & VASTANO, J. A. 1985. Determining Lyapunov exponents from a time series. *Physica*, 16D, 285-317.
- ZELLER, M., BAUER, M. & MARTIENSSEN, W. 1995. Neural dynamics modeled by one-dimensional circle maps *Chaos Solitons & Fractals*, 5, 885-893.
- ZOU, F. & NOSSEK, J. A. 1993. Bifurcation and Chaos in Cellular Neural Networks. *IEEE Transactions on circuits and systems I - Fundamental theory and applications*, 40, 166-173.

# Appendices

## List of Appendices:

**Appendix A:** Tables of data used to generate graphs in Chapter 3.

**Appendix B:** MATLAB code developed to generate the 3D divergence graph for the LM along with divergence graphs for different input signal change.

**Appendix C:** MATLAB code developed to generate the 3D divergence graph for the TM along with divergence graphs for different input signal change.

**Appendix D:** Main C program developed for the PIC32MX460L using MPLAB.

**Appendix E:** Datasheet of the KROHN-HITE 511 DC voltage reference/calibrator.

**Appendix F:** Patent files submitted as part of the patent application n° 1309585.4.

**Appendix G:** Full schematics of the LM and TM electronic implementation.

## Appendix A

The data generate using MATLAB and used to create the graphs for the estimation error in section 3.1.1(Figure 3-5 , Figure 3-6 and Figure 3-7) and the time series for two different input signals are shown:

TABLE A-1 SIGNAL CHANGE ESTIMATION ERROR

Iteration Number (N)	1 <sup>st</sup> Sample	2 <sup>nd</sup> Sample	Divergence $\delta$	$\Delta$ Calculated using data rounded to the 3 <sup>rd</sup> decimal place	Error (%) between the real $\Delta$ and the calculated $\Delta$
0	0.37690	0.37691	0.00001	0	100
1	0.7500	0.75005	0.00002	0	100
2	0.49740	0.49739	0.00004	0	100
3	0.98990	0.98982	0.00008	0	100
4	0.02009	0.02025	0.00016	0	100
5	0.03998	0.04030	0.00031	0	100
6	0.07957	0.08019	0.00062	0	100
7	0.15835	0.15959	0.00124	8.091E-06	19.1
8	0.31513	0.31758	0.00246	8.132E-06	18.7
9	0.62710	0.63200	0.00489	1.022E-05	-2.16
10	0.74205	0.73231	0.00974	1.027E-05	-2.68
11	0.51331	0.53269	0.01938	9.803E-06	1.97
12	0.96849	0.92992	0.03857	1.011E-05	-1.12
13	0.06268	0.13944	0.07675	1.003E-05	-0.32
14	0.12475	0.27748	0.15274	1.002E-05	-0.17
15	0.24825	0.55220	0.30395	1E-05	-0.02
16	0.49403	0.89111	0.39708	6.564E-06	34.4
17	0.98312	0.21668	0.76644	6.364E-06	36.4

TABLE A-2 IDENTICAL TIME SERIES FOR TWO DIFFERENT INPUT VALUES

Iteration (N)	0	1	2	3	4	5	6	7	8	9
	0.49	0.98	0.04	0.08	0.16	0.32	0.64	0.72	0.56	0.88
	0.51	0.98	0.04	0.08	0.16	0.32	0.64	0.72	0.56	0.88

## Appendix B

MATLAB code developed to generate the 3D divergence graph (Chapter 3) of the LM is presented. The code was written using MATLAB 7.11 (R2010b). Some divergence graphs generated using the code are also shown.

### Matlab code:

```
clc; % Clear command window and workspace
clear;

%***** setting simulation parameters
*****

r=4; % set the parameter of the LM
change = 0.0002; % set the change
resolution = 100000; % set the number of points
addnoise = 0; % simulation with noise If 1
averaging = 1; % set to 1 for no averaging

loopvar = 1; %
n = 1; %
averageloop = 0; %
finalresult = zeros(51,100000); % initialise variables
finalresultsinglerun = zeros(51,100000); %
signatures = zeros(1,resolution); %
signaturesT = zeros(1,resolution); %

if addnoise
    noiseresult = zeros(1,resolution*40+1000);
    while (n < resolution*40+1000) % generate noise if
required
        x = (mean(randn(100,1))*0.000012);
        x = x';
        noiseresult(n) = x;
        n = n + 1;
    end
    n=1;
end

%***** Main Loop
*****

while(loopvar<=(resolution)-1) % set the main loop

    a1=[0:50];
    n=1;
    x= (loopvar/resolution);

    for averageloop = 1:averaging
        n=1;
```

```

    x = (loopvar/resolution);
    while(n<=51)

        if addnoise == 1;          %check if noise is to be added
            noise = noiseresult(loopvar*20-20+(n*averageloop)); %take
%noise from          %the noise          %matrix
        else
            noise = 0;
        end
        x = x+ noise;
        a1(averageloop,n) = r*(x)*(1-x); % iterate the equation and
add                                     % noise if required
        x = a1(averageloop,n);
        n = n + 1;
    end
end
if averaging > 1          % apply averaging if required
    a1 = mean (a1);
end
    a2 = [0:50];
    n=1;
    x= ((loopvar/resolution)+change);
    for averageloop = 1:averaging
        n=1;
        x= ((loopvar/resolution)+change);
        while(n<=51)

            if addnoise == 1;          %check if noise is to be
added
                noise = noiseresult(loopvar*20+(n*averageloop)); %take
noise          %from the          %noise          %matrix
            else
                noise = 0;
            end
            x = x+ noise;
            a2(averageloop,n) = delta*(x)*(1-x);
            x = a2(averageloop,n);
            n = n + 1;
        end
    end

    if averaging > 1
        a2 = mean (a2);
    end

%***** Add the iterations of the divergence
%*****

    end
    n=1;
    suma = a1-a2;
    suma = suma';
    finalresult(:,loopvar) = suma;
    finalresultsinglerun(:,loopvar) = a1;
    loopvar = loopvar + 1;
end

n=1;
resolution = resolution - 1;

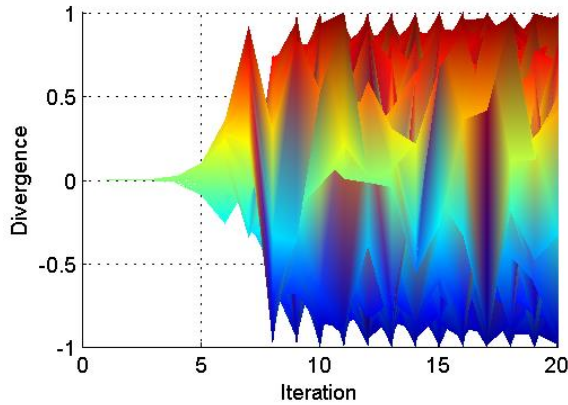
```

```

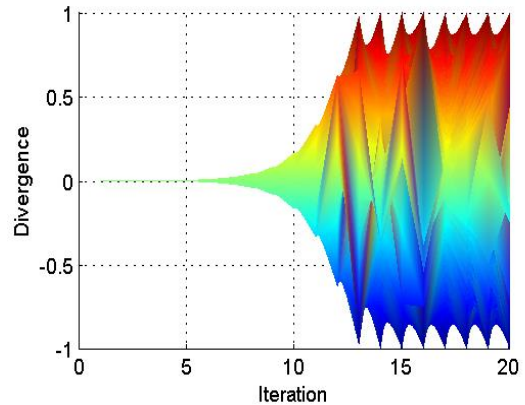
surf(finalresult(1:20,1:resolution-
10), 'DisplayName', 'finalresult(1:20,1:resolution)');figure(gcf)
% generate 3d graph of the divergence

```

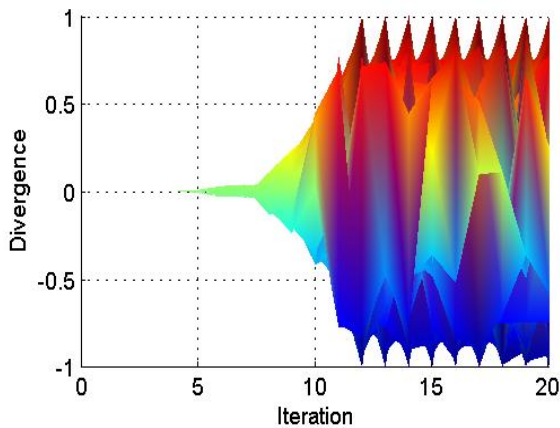
**Divergence Graphs for different values of  $\Delta$  and input ranges:**



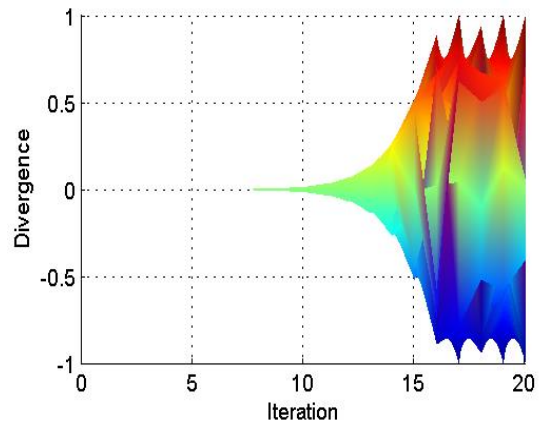
LM divergence full normalised range with  $\Delta = 0.0001$



LM divergence 0.1 to 0.9 normalised range with  $\Delta = 0.0001$



LM divergence full normalised range with  $\Delta = 0.00001$



LM divergence 0.1 to 0.9 normalised range with  $\Delta = 0.00001$

## Appendix C

MATLAB code developed to generate the 3D divergence graph of the TM (Chapter 3) is presented followed by 3D graphs representing the divergence of the TM.

### Matlab code:

```
clc; %clears the command window and the
clear; %workspace b4 every run

%***** setting simulation parameters
*****

delta=2; %sets the parameter of the tent map
change = 0.0001; %sets the change
resolution = 10000; %number of simulation points
addnoise =0; %0 = no noise/ 1 = with noise

loopvar = 1; %some variables used for the loops
n = 1;
testvariable = 1;

finalresult = zeros(40,200000); %declaration of tables
signatures = zeros(1,resolution);
StartingSignatures = zeros (40,resolution);
StartingSignatures2 = zeros (40,resolution);
%***** Generate noise and store it in a table (only if
addnoise = 1)*****
if addnoise
    noiseresult = zeros(1,resolution*80+1000);
    while (n < resolution*80+1000)
        x = (mean(randn(100,1))*0.000012);
        x = x';
        noiseresult(n) = x;
        n = n + 1;
    end
    n=1;
end

%***** Main Loop *****

while(loopvar<=resolution-1)

    a1=[0:39];
    n=1;
    x= (loopvar/resolution); %sets the input value

    while(n<=40)
```

```

    if addnoise == 1;           %check if noise should be added
        noise = noiseresult(loopvar*20-20+(n)); %take noise
from    %the noise matrix
    else
        noise = 0;
    end
        x = x ;
    if x < 0.5
        x1 = delta*x+ noise;
        x2 = 0;
    end

    if x >= 0.5
        x2 = delta*(1-x)+ noise;
        x1 = 0;
    end

    x = x1+x2;
    a1(n) = x;
    n = n + 1;

end

a2 = [0:39];
n=1;
x= ((loopvar/resolution)+ change);

while(n<=40)

    if addnoise == 1;           %check if noise is to be added
        noise = noiseresult(loopvar*20+(n)); %take noise from
%the noise matrix
    else
        noise = 0;
    end

    if x < 0.5
        x1 = delta*x+ noise;
        x2 = 0;
    end

    if x >= 0.5
        x2 = delta*(1-x)+ noise;
        x1 = 0;
    end

    x = x1+x2;
    a2(n) = x;
    n = n + 1;

end
    if loopvar == 3769;           % extract one signature for analysis
        signature(:,4) = a1; % loopvar sets the signature to be
analysed
        signature(:,5) = a2;
        signature(:,6) = a1 - a2;

```

```

signature(:,7) = abs(signature(:,6));
end

n=1;
StartingSignatures(:,loopvar) = a1;
StartingSignatures2(:,loopvar) = a2;
suma = a1-a2;
suma = suma';
finalresult(:,loopvar) = suma;           %storage of the
divergence
loopvar = loopvar + 1;
end

%*****Add the iterations of the divergence*****
while (n<resolution)
signatures(1,n) = sum (abs(finalresult(1:1,n)));
n=n+1;
end
n=1;

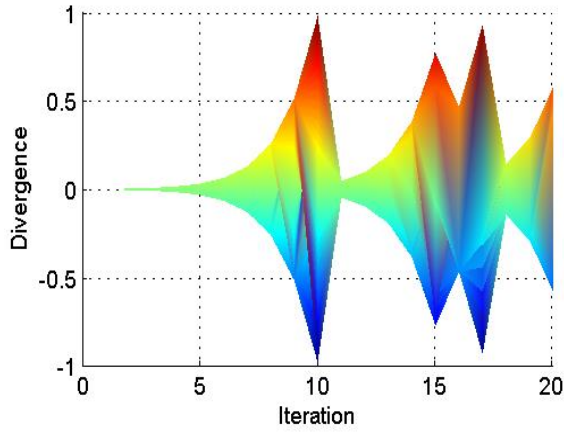
while (n<resolution)
signaturesIT(1,n) = (abs(finalresult(1,n)));
n=n+1;
end
n=1

%***** create the 3D divergence Graph*****

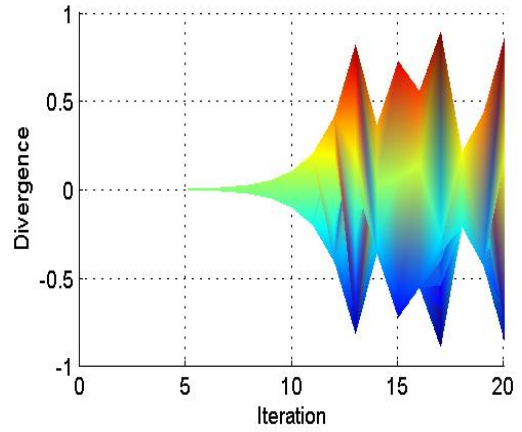
resolution = resolution - 1;
surf(finalresult(1:20,1:resolution-
10), 'DisplayName', 'finalresult(1:25,1:resolution)');figure(gcf)

```

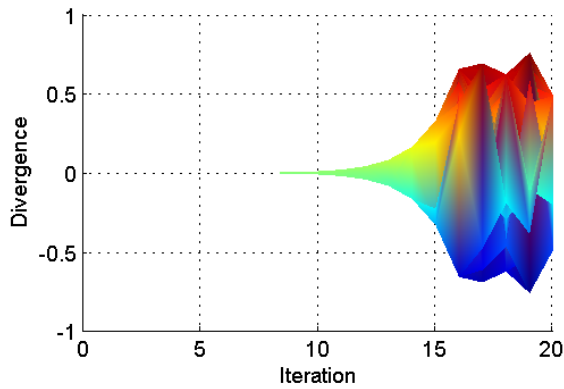
**Divergence Graphs for different values of  $\Delta$ :**



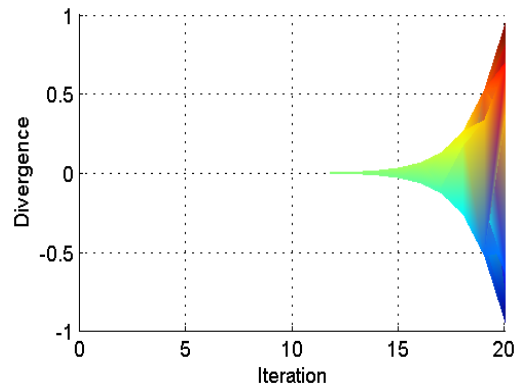
TM divergence full normalised range with  $\Delta = 0.001$



TM divergence full normalised range with  $\Delta = 0.0001$



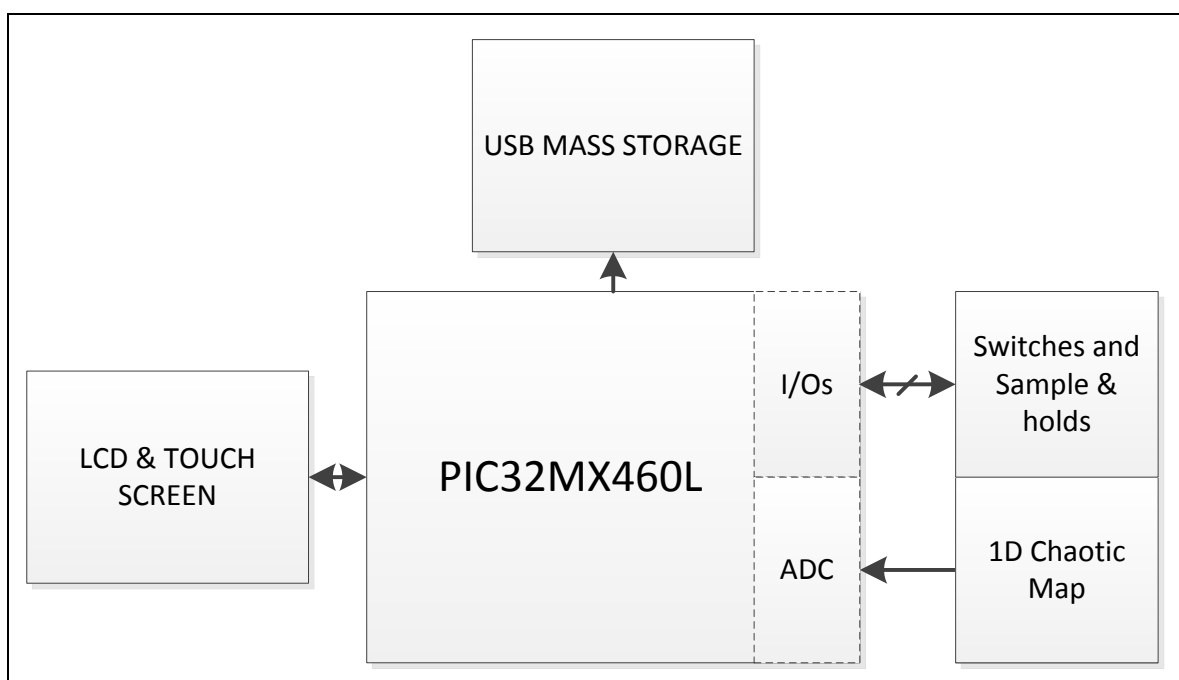
TM divergence full normalised range with  $\Delta = 0.00001$



TM divergence full normalised range with  $\Delta = 0.000001$

## Appendix D

The main C program developed for the PIC32MX460L using MPLAB is given. The program uses the I/Os to control the chaotic MS, the internal ADC to sample the data and the USB mass storage capability to store the data on an external USB memory. A colour LCD display with an integrated touch screen was used, to create a graphical user interface. The block diagram of the  $\mu$ C system is shown below.



### Main Program:

```
//List of incls
#include "MainDemo.h"
#include "MainDemoStrings.h"
#include "USB/usb.h"
#include "USB/usb_host_msd.h"
#include "USB/usb_host_msd_scsi.h"
#include "MDD File System/FSIO.h"

//////////////////// Configuration bits////////////////////////////////////
#pragma config FPLLODIV = DIV_1, FPLLMUL = MUL_20, FPLLIDIV = DIV_2, FWDTEN =
OFF, FCKSM = CSECME, FPBDIV = DIV_8
#pragma config UPLEN = ON // USB PLL Enabled
#pragma config UPLLIDIV = DIV_2 // USB PLL Input Divider
#pragma config OSCIOFNC = ON, POSCMOD = XT, FSOSCEN = ON, FNOSC = PRIPLL
#pragma config CP = OFF, BWP = OFF, PWP = OFF
```

```

////////////////////////////////////Variable declaration////////////////////////////////////
SHORT startscreen=0;
SHORT chaosscreen=0;
GOL_SCHEME* yellowScheme; // alternative yellow style
scheme
int channel8;// conversion result as read from result buffer
unsigned int channel15;
unsigned int offset;// buffer offset to point to the base of the idle buffer
int x;
int tempo;
int iteration;
int y;
int z;
int testvar;
char set,log=0,RUN=0,column=0;
char temp[10];
int signatur[500];
int NumberOfIterations=50;
int pbClk; // Variable for UART
FSFILE * myFile;
BYTE myData[512];
size_t numBytes;
volatile BOOL deviceAttached;

extern const FONT_FLASH GOLMediumFont; // medium font
extern const FONT_FLASH GOLSmallFont; // small font

void StartScreen(); // draws intro screen
void ChaosScreen(); // draws chaos screen

//////////////////////////////////// DEMO STATES //////////////////////////////////////
// DEMO STATES
////////////////////////////////////
typedef enum {

intro,
chaos

} SCREEN_STATES;
////////////////////////////////////
// GLOBAL VARIABLES FOR DEMO
////////////////////////////////////
SCREEN_STATES screenState = intro; // current state of main demo state
machine
SETTIME_STATES settimeState = defo; // current state of main demo state
machine
////////////////////////////////////
// IMAGES USED
////////////////////////////////////
// internal flash image
extern const BITMAP_FLASH batimage;
extern const BITMAP_FLASH bat2;
extern const BITMAP_FLASH sun;
////////////////////////////////////
/
// MAIN PROGRAM
////////////////////////////////////
/
int main(void)
{

```

```

    TRISD = 0x0000; ////PORT D set as output for the control of the Chaotic
map*****
    PORTD = 0;
#ifdef __PIC32MX__
    {
        int value;

        value = SYSTEMConfigWaitStatesAndPB( GetSystemClock() );

        // Enable the cache for the best performance
        CheKseg0CacheOn();

        INTEnableSystemMultiVectoredInt();

        value = OSCCON;
        while (!(value & 0x0000020))
        {
            value = OSCCON;    // Wait for PLL lock to stabilize
        }

        //PORTD=0xffff;
    }

#endif

deviceAttached = FALSE;
//Initialize the stack
USBInitialize(0);

GOL_MSG msg; // GOL message structure to interact with GOL
INTEnableSystemMultiVectoredInt(); // USE best performance
SYSTEMConfigPerformance(GetSystemClock()); // get clock and set best
performance
AD1PCFG = 0xccff; // ADC pins configuration
GOLInit(); // initialise graphics library &
TouchInit(); // initialise the touch panel
AD1PCFG = 0xccf8; // reconfigure ADC pins

yellowScheme = GOLCreateScheme(); // create yellow style scheme
yellowScheme->Color0 = BRIGHTYELLOW;
yellowScheme->Color1 = YELLOW;
yellowScheme->EmbossDkColor = RGB565CONVERT(0xFF, 0x94, 0x4C);
yellowScheme->EmbossLtColor = RGB565CONVERT(0xFD, 0xFF, 0xB2);
yellowScheme->TextColor0 = RGB565CONVERT(0xAF, 0x34, 0xF3);
yellowScheme->TextColor1 = RED;

PORTB=0x4000; //and set it at one to power the USB port (make sure that the
corresponding switch is one (SW12))

StartScreen(); // display the main screen

log=0;

while(1)
{
if (RUN==0)
{
//USB stack process function
USBTasks();
//if thumbdrive is plugged in
if(USBHostMSDSCSIMediaDetect())

```

```

    {
        deviceAttached = TRUE;
        //now a device is attached
        //See if the device is attached and in the right format
        if(FSInit())
        {
            //Opening a file in mode "w" will create the file if it
doesn't
            // exist. If the file does exist it will delete the old file
            // and create a new one that is blank.
            myFile = FSfopen("test.csv","w");

            //Write some data to the new file.

            FSfwrite("Signature",1,4,myFile);
            FSfwrite(",",1,1,myFile);
            FSfwrite("Signature",1,2,myFile);
            FSfwrite("\r\n",1,4,myFile);
            FSfclose(myFile);
            RUN=2;

        }
    }
} // end if (log=0)

if (RUN ==1)
{
    ////////////////////////////////////////////////////////////////////Start of iterations//////////////////////////////////////////////////////////////////
    PORTDbits.RD8 = 1; //FeedBack disconnected
    for(tempo=0;tempo<100;tempo++);
    PORTDbits.RD9 = 0; //input connected
    for(tempo=0;tempo<100;tempo++);

    PORTDbits.RD10 = 1; //Master S&H is sampling
    for(tempo=0;tempo<200000;tempo++);
    PORTDbits.RD10 = 0; //Master S&H is holding

    for(tempo=0;tempo<1000;tempo++);

    PORTDbits.RD11 = 1; //Slave S&H is sampling
    for(tempo=0;tempo<200000;tempo++);
    PORTDbits.RD11 = 0; //Slave S&H is holding

    for(tempo=0;tempo<80000;tempo++);

    channel8 = ADCGetPot();
    signatur[0] = channel8;
    for(tempo=0;tempo<100;tempo++);

    PORTDbits.RD9 = 1; //input disconnected
    for(tempo=0;tempo<100;tempo++);
    PORTDbits.RD8 = 0; //Feedback connected

    for(tempo=0;tempo<100000;tempo++);

    ////////////////////////////////////////////////////////////////////SETS the Number of Iterations for the Chaotic Map

```

```

for (iteration=0;iteration<NumberOfIterations;iteration++)
{
PORTDbits.RD10 = 1; //Master S&H is sampling
for(tempo=0;tempo<200000;tempo++);
channel8 = ADCGetPot();
signatur[iteration+1] = channel8;
for(tempo=0;tempo<100;tempo++);
PORTDbits.RD10 = 0; //Master S&H is holding

for(tempo=0;tempo<1000;tempo++);

PORTDbits.RD11 = 1; //Slave S&H is sampling
for(tempo=0;tempo<200000;tempo++);
PORTDbits.RD11 = 0; //Slave S&H is holding

for(tempo=0;tempo<50000;tempo++);

for(tempo=0;tempo<50000;tempo++);
}

PORTDbits.RD8 = 0; //Feedback disconnected
for(tempo=0;tempo<100;tempo++);
PORTDbits.RD9 = 0; //input connected
for(tempo=0;tempo<100;tempo++);

PORTDbits.RD15 = 1; //Discharge the Sample and Hold Capacitors
for(tempo=0;tempo<500000;tempo++);
PORTDbits.RD15 = 0;

//USB stack process function
USBTasks();
if(USBHostMSDSCSIMediaDetect()) //if thumbdrive is plugged in
{
deviceAttached = TRUE;

//now a device is attached
//See if the device is attached and in the //right format
if(FSInit())
{
myFile = FSfopen("data.csv","a");

FSfwrite("\r\n",1,4,myFile);

for (iteration=0;iteration<NumberOfIterations+1;iteration++)

{ //Write the data on the USB drive

signatur[iteration] = signatur[iteration]*3.22265625;
FSfprintf (myFile, "%#2u",signatur[iteration]);
FSfwrite("\r\n",1,4,myFile);

}
FSfclose(myFile);
RUN=2;
}
}

if(GOLDDraw()) { // Draw GOL objects
// Drawing is done here, process messages
TouchGetMsg(&msg); // Get message from touch screen
}
}

```

```

GOLMsg(&msg);
}

} // END while(1) Loop
} // END MAIN

/*****GOL Msg Callback
subroutine*****/
WORD GOLMsgCallback(WORD objMsg, OBJ_HEADER* pObj, GOL_MSG* pMsg)

WORD objectID,ident;
objectID = GetObjID(pObj);
ident = GetObjID(5); //get the static text ID

switch(objectID)
{

case 15 : // If button pressed go back to main
screen
if(objMsg == BTN_MSG_PRESSED)
{
screenState = intro;
}
return 1;

}
return 1;

case 10 : //chaos BUTTON IS PRESSED
if(objMsg == BTN_MSG_PRESSED)
{
screenState = chaos;
}
return 1;

case 56 : //Run BUTTON IS PRESSED
if(objMsg == BTN_MSG_PRESSED)
{
RUN = 1;
}
return 1;

case 60 : //iteration + BUTTON IS PRESSED
if(objMsg == BTN_MSG_PRESSED)
{
NumberOfIterations++;
}
return 1;

case 61 : // iteration - BUTTON IS PRESSED
if(objMsg == BTN_MSG_PRESSED)
{
NumberOfIterations--;
}
return 1;
break;
}
}

```

```

return 1;          // Process message by default
}
/*****End GOL Msg CallBack
subroutine*****/

WORD GOLDrawCallback()/****GOL Draw CallBack
subroutine*****/
{
    switch(screenState){
        case intro:
if (startscreen==0) {StartScreen();} // create window and buttons

x = GOLFindObject(5);          t
DmSetValue(x, voltage);
SetState(x,DM_DRAW);
voltage = (channel8*0.0322265625);

y = GOLFindObject(7);
DmSetValue(y, voltage2);
SetState(y,DM_DRAW);
voltage2 = (sec);

return 1; // draw objects created

case chaos:
if (chaoscreen==0) {ChaosScreen();
}
y = GOLFindObject(62);
DmSetValue(y, NumberOfIterations);
SetState(y,DM_DRAW);
return 1;

    }

return 1;

}

/*****End GOL Draw CallBack
subroutine*****/

void StartScreen()/****Main Screen
Subroutine*****/

{ GOLFree();
WndCreate(1, // ID
0,0,GetMaxX(),GetMaxY(), // whole screen dimension
WND_DRAW, // set state to draw all
NULL, // icon
"Chaos MS tool", // text
NULL); // use default GOL scheme

BtnCreate(10, // object's ID
5, 160, 210, 195, // object's dimension
0, // radius of the rounded edge
BTN_DRAW, // draw the object after creation
NULL, // no bitmap used
"Choatic Map", // use this text

```

```

yellowScheme);          // use yellow style scheme

DmCreate(5,              // ID
30,60,200,90,          // dimension
SLD_DRAW, // has frame and centre aligned
voltage,2,1,          // to display the value of voltage
NULL);                // use given scheme

DmCreate7,              // ID
30,90,200,120,        // dimension
SLD_DRAW, // has frame and centre aligned
voltage,2,0,          // to display 078.9
NULL);                // use given scheme

startscreen=1;

chaoscreen=0;

}
/*****END Main screen
subroutine*****/

/*****USB application
handler*****/
BOOL USB_ApplicationEventHandler( BYTE address, USB_EVENT event, void *data,
DWORD size )
{
switch( event )
{
case EVENT_VBUS_REQUEST_POWER:
// The data pointer points to a byte that represents the amount of power
// requested in mA, divided by two. If the device wants too much power,
// we reject it.
return TRUE;

case EVENT_VBUS_RELEASE_POWER:
// Turn off Vbus power.
// The PIC24F with the Explorer 16 cannot turn off Vbus through software.
//This means that the device was removed
deviceAttached = FALSE;
return TRUE;
break;

case EVENT_HUB_ATTACH:
return TRUE;
break;

case EVENT_UNSUPPORTED_DEVICE:
return TRUE;
break;

case EVENT_CANNOT_ENUMERATE:
**** USB Error - cannot enumerate device
return TRUE;
break;

case EVENT_CLIENT_INIT_ERROR:

```

```
USB Error - client driver initialization error
return TRUE;
break;

case EVENT_OUT_OF_MEMORY:
USB Error - out of heap memory return TRUE;
break;

case EVENT_UNSPECIFIED_ERROR: // This should never be generated.
USB Error - unspecified
return TRUE;
break;

default:
break;
}
return FALSE;
}
}
//END OF PROGRAM
```

# Appendix E

The datasheet of the KROHN-HITE 511 DC voltage reference/calibrator is presented.



## Model 511 DC Source/Calibrator

- Absolute Accuracy:  $\pm 10$ ppm
- Voltage Range:  $\pm 100$ nVdc to  $\pm 10$ Vdc
- Resolution: 1ppm of Range
- Wideband Noise:  $< 5\mu$ Vrms
- 3 Voltage Ranges
- Max. Current: 100mA
- Impedance:  $10\mu$  ohm all ranges
- Floating Output
- Certified to N.I.S.T.

### DESCRIPTION

Continuing with Electronic Development's (EDC) tradition, the NEW Krohn-Hite Model 511 Precision DC Source/Calibrator is a secondary standard that is highly stable and repeatable from  $\pm 100$ nVdc to  $\pm 10$ Vdc, providing N.I.S.T. traceable voltages for use in production, calibration labs, QA and QC departments, design labs, or any place where an accurate voltage is needed.

Using Krohn-Hite's state-of-the-art reference, the 511 provides extremely accurate ( $\pm 10$ ppm) and stable ( $\pm 2$ ppm for 24 hours) voltages over 3 ranges, allowing the output to be set from  $\pm 100$ nVdc to  $\pm 11.11110$ Vdc with a resolution of 1ppm of range.

The Model 511 is an extremely quiet source with  $< 5\mu$ V of noise measured from 0.1Hz to 100kHz. Maximum load current is 100mA on all ranges.

### RANGES

The 511 also provides 3 voltage ranges,  $\pm 100$ mV,  $\pm 1.0$ V and  $\pm 10$ V allowing the user to set the output from  $\pm 100$ nVdc to  $\pm 11.11110$ Vdc. Resolutions are 100nV,  $1\mu$ V and  $10\mu$ V respectively.

### APPLICATIONS

The Model 511 can be used in many applications including the calibration of precision A/D converters, strip chart recorders and calibration of Kaye Instruments Data Logging Systems.

### SPECIFICATIONS

#### OUTPUT

Specifications apply at  $23^\circ\text{C} \pm 1^\circ\text{C}$ ,  $< 70\%$  relative humidity.

Range (dc)	Full Scale (dc)	Resolution (dc)	Absolute Accuracy $\pm$ (ppm of setting + $\mu$ V)
			1Year
100mV	$\pm 111.11110$ mV	100nV	10 + 2
1.0V	$\pm 1.111110$ V	$1\mu$ V	10 + 6
10V	$\pm 11.11110$ V	$10\mu$ V	10 + 42
Above specifications include stability, line regulation and load regulation.			

#### Noise and Ripple:

Range	0.1Hz-10Hz	10Hz-100kHz	Max. Load	Zo
100mV	$2\mu$ Vp-p max.	$5\mu$ Vrms	100mA	$10\mu$ ohms
1V	$2\mu$ Vp-p max.	$5\mu$ Vrms		
10V	$2\mu$ Vp-p max.	$10\mu$ Vrms		
Above specifications include stability, line regulation and load regulation.				

**Temperature Coefficient,  $\pm$ (ppm of setting +  $\mu$ V)/ $^{\circ}$ C:**

0 $^{\circ}$ C to 10 $^{\circ}$ C	3 + 2
10 $^{\circ}$ C to 40 $^{\circ}$ C	2 + 1

**Stability:**

- 24hrs,  $\pm$ (2ppm of setting + 1 $\mu$ V).
- 1 year,  $\pm$ (10ppm of setting + 2 $\mu$ V).

**Settling Time:** 100ms max., typically 60ms.

**Load Regulation (all ranges):**  $\pm$ 1 $\mu$ V for a change from no load to full load.

**Line Regulation (all ranges):**  $\pm$ (1ppm + 1 $\mu$ V of range) for a  $\pm$ 10% change from normal line voltage.

**GENERAL**

**Calibration Interval:** 1 year for  $\pm$ 10ppm accuracy.

**Warm-Up Time:** 1 hour to rated accuracy.

**Isolation:** Floating 500V from chassis.

**Protection:** Will drive a short-circuit indefinitely.

**Temperature:**

<b>Calibration</b>	23 $^{\circ}$ C $\pm$ 1 $^{\circ}$ C.
<b>Operating</b>	0 $^{\circ}$ C to 50 $^{\circ}$ C. Accuracy is de-rated above 40 $^{\circ}$ C due to loss of oven control.
<b>Storage</b>	-30 $^{\circ}$ C to 70 $^{\circ}$ C.

**Power Requirements:** 105-125 or 210-250 volts ac, single phase, 50Hz-400Hz, 20 watts.

**Dimensions:** 3.5" (9cm) high, 14" (36cm) wide, 12.5" (32.1cm) deep.

**Weight:** 12 lbs (5.4kg) net; 14 lbs (6.3kg) shipping.

**Controls:** Six decade rotary switches with indicator knobs from 0 to 10 and 10% over-range; 3 position range and polarity rotary switches; push-button power on, sense and ground switches.

**Indicators:** LEDs indicate voltage range, power on and overload.

**Terminals:** Output terminals are safety, low thermal, gold plated type, mounted on the front panel. Terminal sets are configured for remote sensing of the output as follows:

- High Output and High Sense
- Low Output and Low Sense
- Case Ground
- Output terminals conform to European Standard Specifications.

**SAFETY**

The Model 523 is designed to meet the requirements of the following standards of safety for electrical equipment for measurement, control and laboratory use: IEC61010-1, EN61010-1.

**ELECTROMAGNETIC COMPATIBILITY**

Emissions and Immunity: EN61326-1, EMC, 61000-4-2; ESD, 61000-4-3; Radiated Immunity, 61000-4-4; EFT, 61000-4-5; Surge, 61000-4-6; Conducted Immunity, 61000-4-8; Magnetic Immunity, 61000-4-11; Voltage Interruption EN61010-1. CE Compliant for Class B Equipment.

**OPTIONS**

**Option 003:** Provides both front and rear panel terminals for instrument outputs. Only one output set of terminals may be used at one time.

**Option 004:** Provide CE regulation safety terminals.

**Rack Mount Kit:** Part number RK-314 permits installation of the Model 511 into a 19" rack spacing.

**Extended 1 Year Warranty:** Part No. EX511

**OPTIONAL ACCESSORIES**

**CAB-005:** Cable, Two Conductor Shielded Balance Line

**CAB-018:** Cable, Multi-stacking Double Banana plug

**CAB-023:** Cable Set, Low Thermal EMF Retractable Banana

**CAB-024:** Cable Set, Low Thermal EMF Spade Lug

Specifications are subject to change without notice.

## Appendix F

This Appendix contains the patent files submitted as part of the patent application.

### **British Patent Application n° 1309585.4**

Patent application:

#### Improved Method of Measuring Signal Change and System Including the same

The present invention relates to a high precision measurement system for measuring changes in one or more signals.

Although the following invention relates to measuring signal changes in relatively low value sensors, the person skilled in the art will appreciate that the present system can be applied to any device that generates an output signal.

In conventional measurement systems, low amplitude parameter change measurement is a challenge due to noise and inherent measurement system errors. The traditional approach to the problem is for the measurement system to include a sensor to convert the physical parameter into a signal, typically a voltage signal, followed by conditioning circuitry to adapt to the appropriate input range of a high resolution analogue to digital converter (ADC).

The practical limitation of accuracy for any measurement is determined by specific factors such as sensor sensitivity, intrinsic noise and ADC performance in terms of bit resolution and range.

Therefore, small changes in input signal can only be detected and/or measured using relatively expensive and sensitive equipment.

It is therefore an aim of the present invention to provide an improved method of measurement that addresses the abovementioned problems.

It is a further aim of the invention to provide a sensor apparatus or system that addresses the abovementioned problems.

It is a yet further aim of the invention to provide a method of signal change measurement that addresses the abovementioned problems.

In a first aspect of the invention there is provided a method of measuring signal change including the steps of:

- performing at least one calculation or iteration step based on one or more chaos functions on a first input signal, or sample of a signal, to produce a first iteration value;
- performing a second iteration step by repeating the at least one calculation or iteration step based on one or more chaos functions on the first iteration value to produce a second iteration value;
- performing a third and/or further iteration steps whereby the previous or earlier iteration value undergoes the at least one calculation or iteration step based on one or more chaos functions to generate the third and/or further iteration values;
- storing iteration values generated from the first input signal or sample of said first input signal; and
- performing at least one calculation or iteration step based on one or more chaos functions on at least a second input signal,

or sample of a second signal, to produce a first iteration value from the second input signal;

- performing a second iteration step for the second input signal by repeating the at least one calculation or iteration step based on one or more chaos functions on the first iteration value from the second input signal to produce a second iteration value;

- performing a third and/or further iteration steps for the second input signal whereby the previous or earlier iteration value undergoes the at least one calculation or iteration step based on one or more chaos functions to generate the third and/or further iteration values;

- storing iteration result values generated from the second input signal, or part of said second signal;

- subtracting one set of iteration values generated from either the first or second input signal from the corresponding iteration values generated from the other input signal wherein the number of iterations before the difference between the iteration result values increases is proportional to the relative difference between the first input signal and the second input signal and/or samples thereof.

Typically the stored iteration values generated from the first input signals, or portions thereof, form a first sample signature and/or the stored iteration values generated from the second input signals, or portions thereof, form a second sample signature.

Further typically, implementing the abovementioned method using electronic circuitry and/or an integrated circuit allows high detection resolution that is independent of the input range. As it is the difference between the inputs that is measured and not the absolute value of each input, relatively

low cost sensors can be modified to enable small signal changes, for example in the region of 20  $\mu\text{V}$ , to be accurately measured.

Preferably the iteration values and/or sample signatures are converted to digital data or a digital word. Typically the iteration values are converted to any one or any combination of digital words, binary codes, reflected binary codes (Gray codes) and then stored. Further typically an analogue to digital converter (ADC) is used to convert the values.

In one embodiment the stored digital words for each iteration form a signature or data set related to that particular input signal or sample of said signal.

Typically it is the number of iterations before the two signatures diverge that is proportional to the relative difference between the input signals or samples of said signals.

Typically, it is possible to obtaining a higher resolution than that which can be achieved using a standard, comparably priced, ADC based system. The ADC, in this system, is not directly sampling the input signal or data, but rather the data at the output of the chaotic function. This allows a detection of changes smaller than if the ADC was connected in a conventional way to the input, using a linear amplification and ADC combination.

In one embodiment the one or more chaos functions includes a one dimensional (1D) discrete chaotic map. Preferably the Chaos function is a Tent Map as shown below.

Tent Map Equation.

$$x_{n+1} = \begin{cases} \mu x_n & \text{for } x_n < \frac{1}{2} \\ \mu(1 - x_n) & \text{for } x_n \geq \frac{1}{2} \end{cases} \quad \text{equation (1)}$$

Where  $X_n$  represents the normalised input (typically 0 to 1),  $r$  is the fixed multiplying factor in the range (typically 1.8 to 2)

In one embodiment the chaos function includes the Logistic Map function.

### Logistic Map Equation

$$X_{n+1} = rX_n(1 - X_n) \quad \text{equation (2)}$$

Where  $X_n$  and  $X_{n+1}$  are the current and next input values respectively.  $r$  is the scaling factor set to make the function chaotic and avoid windows of periodicity, typically between 3.97 and 4.

The fundamental advantage of this signal measurement system, over typical ADCs, is that the size of the signal change that can be measured is independent of the range, thus increasing input signal range increases the overall resolution.

This high precision signal change detection and measurement system utilises the fundamental characteristic of high sensitivity to initial conditions, exhibited by the chaotic function. This normalised behaviour of the function means that an equivalent high detection resolution can be achieved that is independent of input range.

Typically the calculations or iteration steps are repeated ten times. Further typically the calculations are repeated for ten iterations to form the input signal/sample signature.

In a second aspect of the invention there is provided an apparatus to measure the difference between a first and at least a second signal and/or samples of a signal, said apparatus including circuitry to;

- perform at least one of calculation based on one or more chaos functions on a first input signal sample, to produce a first iteration value whereby said apparatus performs an iteration calculation by repeating the at least one calculation based on one or more chaos functions on the first iteration value to produce a second iteration result value, perform a third and/or further iteration steps whereby the previous or earlier iteration result value undergoes the at least one calculation based on one or more chaos functions to generate the third and/or further iteration result values,

- perform at least one of calculation based on one or more chaos functions on at least a second input signal sample, to produce a first iteration value from the second input signal, and to perform an iteration step for the second input signal by repeating the at least one calculation based on one or more chaos functions on the first iteration value from the second input signal to produce a second iteration result value, perform a third and/or further iteration steps for the second input signal whereby the previous or earlier iteration result value undergoes the at least one calculation based on one or more chaos functions to generate the second and/or further iteration result values; and further includes;

memory means to store the iteration result values generated from the first and second input signals; and

- either subtract the iteration result values from the first input signal sample from the corresponding iteration values generated from the second input signal sample, or vice versa wherein the number of iterations before the difference between the iteration values increases is proportional to the relative difference between the input samples.

In one embodiment the iteration steps are performed by circuits in series rather than repeating the calculation on the same circuit.

In one embodiment the data storage and/or subtraction is performed by a microcontroller. The person skilled in the art will appreciate that the data storage and/or subtraction steps can be performed with any device/component capable of data storage and simple mathematical operations. This includes any one or any combination of Field Programmable Gate Arrays (FPGAs), microcontrollers, microprocessors with additional memory, and specialised Integrated Circuits (IC).

In one embodiment the system is substantially integrated into a single IC and/or connected to a data acquisition board to store the signatures and/or perform the calculations using at least one computer means.

In one embodiment the apparatus is coupled to and/or integrated with a sensor output. An example of such a sensor is a strain gauge. Typically the gauge output is connected to the apparatus signal input.

In an alternative embodiment the apparatus is coupled to and/or integrated with a data acquisition board.

In a third aspect of the invention there is provided a measurement system comprising taking a first input sample and performs calculations based on a chaos function, said

calculations are repeated for a number of iterations with the result of each iteration being converted to a digital reference or word and stored, the stored digital words, for each iteration, form a signature or data set related to the input sample, and a second input sample is taken and iterated, and the data is stored giving a second signature wherein the signature from the first sample is subtracted to the signature from the second sample the result of which is then used to determine the difference between the two samples as the number of iterations before the two signatures diverge is proportional to the relative difference.

Specific embodiment of the invention are now described with reference to the following figures, wherein:

Figure 1 shows a system illustrating the iterations of a tent map function;

Figure 2 shows a schematic of a chaos function based measuring system with feedback in accordance with one aspect of the invention;

Figure 3 shows one embodiment of the implementation of a tent map in accordance with the invention;

Figure 4 shows one embodiment of the implementation of a logistic map in accordance with the invention;

Figure 5 shows a graph of determining sample difference in accordance with the invention;

Figure 6 shows the divergence of the tent map for a 50  $\mu\text{V}$  signal change across a full normalised input range;

Figure 7 shows the theoretical and practical divergence of the system versus the input change;

Figure 8 shows a series implementation of the Tent Map function in accordance with one embodiment of the invention;

Figure 9 shows a hybrid series/feedback implementation of the Tent Map function in accordance with one embodiment of the invention;

Figure 10 shows a schematic representing a strain gauge;

Figure 11 shows a circuit diagram for a Tent Map electronic circuit implementation.

Figure 12 shows a graph demonstrating sensitivity to initial condition change of  $1 \times 10^{-4}$  for the Logistic Map function;

Figure 13 shows a graph illustrating signature deviations for input signals and a  $1 \times 10^{-4}$  change for the Logistic Map;

Figure 14 shows a circuit diagram for a Logistic Map electronic circuit implementation.

Figure 15 shows a graph of measurement system input change detection compared to theoretical analysis.

Chaos theory is based on functions/systems that have widely diverging outputs for small differences in initial conditions, often termed the ‘butterfly effect’. This means that the long-term response of the system cannot be predicted with any degree of certainty due to very small parameter changes. However, the divergence between two chaotic responses can be used to accurately define the difference between that two input signals. The Tent Map (TM) function exhibits such behaviour and has been investigated and implemented, electronically, in this work.

There have been previous implementations of the TM and other chaotic functions using electronic circuits, however, some of these implementations are purely educational with no real

application. Figure 1 shows a system illustration of a TM function as used in associated literature.

The TM function, along with the Bit Shift/Doubling Map (BSM), has been used to measure signals in the form of an Analogue to Digital Converter (ADC). These methods rely on the piecewise-linear characteristic of the one dimensional (1D) maps to double and fold the signal on each iteration. After each iteration the digital output is shifted to the left until a binary word that represent the input signal is obtained (binary word for the BSM and Gray-code for the TM). However, inherent practical system errors grow exponentially limiting the resolution. A chaos function scaling factor above the ideal, due to noise, would cause the output to diverge to either supply rail - known as the 'exiting condition' or 'extinction'.

The fundamental aspect of the method, presented here, of signal measurement is that it relies on the difference between two input signals rather than the absolute value of a given signal, which makes it robust to any inaccuracy within the TM parameters.

This approach adopted herein is not to design an ADC but to detect small signal changes using an implementation that takes into consideration noise and errors encountered within practical systems. Rather than relying on producing a logic output of a 0 or 1 after each iteration (or stage) the output is sampled using a low resolution ADC. The digital word for each iteration is stored in the system memory so that after N iterations a unique N Bytes signature is obtained for a given input. This signature can then be compared with any other signature to determine the difference between them using the divergence. Errors introduced by the feedback loop can be eliminated by implementing the system in a cascaded/series configuration.

The present system takes the 1st input sample and performs calculations based on the chaos function, as shown in figure 2. These calculations are repeated, via the feedback loop, for a number of iterations (typically 10) with the result of each iteration being converted to a digital word and stored. The stored digital words, for each iteration, form a signature (data set) related to the input sample. A second input sample is taken and iterated, and the data is stored giving a second signature. The signature from the first sample is then subtracted from the second sample signature. The result obtained is then used to determine the difference between the two samples as the number of iterations before the two signatures diverge is proportional to the relative difference. The sample difference is measured and not the absolute value. The data storage and the subtraction are all performed by a microcontroller.

The discrete, 1D Chaotic map, implemented electronically and tested, was the Tent Map, containing the basic system functional blocks, as shown in figure 3

The main advantage, of this system, is the possibility of obtaining a higher resolution than that which can be achieved using a standard, comparably priced, ADC based system. The ADC, in this system, is not directly sampling the input data but rather the data at the output of the Tent map. This allows a detection of changes smaller than if the ADC was connected in a classic way, using a linear amplification and ADC combination.

In figure 4 5, a0 represents the Tent map behaviour over 20 iterations, for a normalised initial input condition of  $x = 0.6$ , a1 is the behaviour for an initial input condition of  $x = 0.60005$ , a2 is the difference between a0 and a1; showing the divergence. The number of iterations before a0 diverges from zero enables the initial sample difference to be determined.

Figure 5 6, shows that the number of iterations required, to measure a specified input signal change, is constant across the full input signal range. Hence, the measurement system is input signal amplitude independent.

The Tent map is not the only, one dimensional (1D), discrete chaotic map that can be use in the given system. Successful implementation of the 1D, discrete Logistic Map (LM) containing the basic system functional blocks, as shown in figure 6, for the same application, has also been achieved. However, the LM and other related functions generally require multiplication circuitry, in the practical implementation. The multiplication circuitry generates relatively large quantities of noise, compared to other system blocks used, and thus introduces high noise levels into the overall system. Consequently, the induced noise distorts the output and reduces the sensitivity of the system to small input signal changes. This means the system output signature divergence occurs earlier (fewer iterations) than predicted by theory, for a small input signal change.

The simplicity of the TM (no multiplication circuitry required) enables basic electronic circuitry to be used, which only introduces relatively low levels of noise into the system. Hence the achieved performance of the practical implementation is close to the ideal, mathematically simulated, response of the TM.

The current discrete component implementation of the system can detect changes in input samples of approximately 50  $\mu\text{V}$ , hence for a 10 V range (typical input voltage range for the system), the resolution is higher than that which can be achieved using a conventional 16-bit resolution ADC ( $10/2^{16} = 152.6 \mu\text{V}$  per step). This system requires only a lower resolution, low cost 8-bit ADC to convert the TM response to a digital signal for storages and processing.

Although the design is implemented using a microcontroller with a built-in ADC and discrete components, the full system could be designed on a single IC. This would further reduce induced noise from circuitry within the system, meaning that smaller input signal changes could be accurately determined. Figure 7 shows that the theoretical minimum signal change that can be measure, by the system, is limited by the noise of the practical implementation and not the TM function.

By removing the need for feedback the detectable input change as low as  $20 \mu V$  have been achieved. This was made possible by eliminating the errors introduced by the feedback, namely the sample and hold circuit. The circuit without feedback is shown in Figure 8. Multiple TM circuits have been placed in series so that the signal, instead of being iterated can propagate through the circuits. The signature is obtained by sampling between each TM circuit..

Hybrid series/feedback implementation: Combining the feedback and series systems into one system, shown in figure 9, using 2 to 8 series stages and feedback will enable flexibility and sensitivity to be optimised for different applications. The feedback system enables flexibility in iterations without the need to modify the circuitry, whilst the series stages, enables high levels of sensitivity to be achieved whilst operating at higher speeds.

Applications of the invention include:

#### Small Change Physical Parameter Measurement

A typical area of application for the signal change measuring system is that where a small variation in the output signal from a physical parameter sensor is required as opposed to absolute

values. For example, a strain gauge can be used to detect small strain variations over a wide initial signal range. The method normally used for this application is shown in Figure 10.

The change in strain, to be measured, creates a change of resistance at the terminals of the strain gauge, which is relatively small (typically in the order of tens of  $\text{m}\Omega$ ) compared to the typical nominal value of the strain gauge of  $350 \Omega$ , for example. The gauge is placed in a Wheatstone bridge resistor ( $R \Omega$  equal to the nominal strain gauge resistance) configuration in order to convert the strain gauge resistance variation, which is proportional to the strain applied, into a voltage. The voltage is then amplified by an instrumentation amplifier (low noise and high precision) before being adapted/conditioned to the input range of the ADC. This conditioning circuit is generally application and ADC dependent and requires relatively high cost precision amplifiers. However, the system is able to determine absolute value measurements to high precision levels but requires expensive high resolution ADCs.

If a small change in the strain, equivalent to an extension of  $0.00001\%$  over a  $\pm 10\%$  extension/compression range, occurs then the minimum resistance variation of  $0.0007 \Omega$  over a range of  $\pm 35 \Omega$  needs to be detected. The maximum voltage at the output of the Wheatstone bridge in the, given example, was calculated to be  $\pm 0.119\text{V}$ . Using a 16-bit ADC the minimum voltage change that can be detected is determined as being equal to  $76.3 \mu\text{V}$  for a  $5 \text{ V}$  reference ( $5/2^{16}$ ). Given the conditioning circuitry, the minimum ADC step sizes equates to  $3.66 \mu\text{V}$  bridge output voltage (minimum required to maintain full ADC range), which is equivalent to a  $1\text{m}\Omega$  change, which in turn is equivalent to a  $1.43$  micro strain change. However, since the measurement accuracy of the new system is  $20 \mu\text{V}$  a strain change of less than  $1$  micro strain can be detected. Hence, because of a need for detecting small changes over a wide

absolute range, the 16-bit resolution of the ADC is not high enough. In fact for the conventional system a more costly 18-bit ADC to attain the same level of accuracy (1 micro strain) would be required.

#### Increased Data Acquisition Capability.

Initial investigations indicate that the new signal change measurement system can be used to improve the detection capability of existing data acquisition systems. For example, an acquisition board equipped with an existing 8-bit or 12-bit ADC can be expanded, with the addition the new system, to obtain resolution levels in the order of 18-bits. The added advantage is that the resolution of the overall acquisition system will be increased as well as the approximate absolute measurement values still being available.

The skilled person will appreciate that the electronic circuit implementation of the Tent Map chaotic function, using low cost components, as shown by the simplified circuit in figure 13 enables signal changes in the region of 20  $\mu\text{V}$  to be accurately measured. The potential range of applications for this system is very large. The integration of the measurement systems onto a single IC will improve the level of accuracy and lower costs, thus increasing the scope of potential applications.

In a final example a high precision signal measurement system utilising the Logistics Map chaos function is presented.

Essentially a novel, high precision signal change measurement system based on the Logistic Map (LM) has been developed, analysed and tested. The measurement technique utilises the high sensitivity to initial conditions characteristic of the one dimensional Chaotic function. Investigations into the behaviour of the LM function, using Matlab, demonstrated that the

deviation between successive output iterations for two or more input signal samples is proportional to the size of the difference between them. An electronic prototype of the LM based measurement system has been developed, using low cost electronic devices, and the results demonstrate a strong relationship to the simulations, thus input signal changes can be accurately detected and quantified. Analysis of the measurement system has shown that input signal changes of  $100 \mu\text{V}$  can be determined, equivalent to 16-bit ADC resolution, over a 10V input range. The fundamental characteristic difference compared to typical ADC devices is that the size of the signal change that can be measured is independent of the input range, thus increasing the input signal range increases the resolution. This system is highly suited to applications where the detection of low amplitude signal sample change is of higher importance than the absolute value.

*Introduction:* To accurately observe, test and control any physical variable, a high resolution ‘measurement system (MS)’ is required. In most engineering systems, low amplitude parameter change measurement is challenging due to practical noise limitations and inherent measurement system errors. In the classical approach to the problem, the MS consists of a sensor to convert the physical parameter into typically a voltage signal, followed by conditioning circuitry to adapt to the appropriate input range of a high resolution ‘analogue to digital converter (ADC)’. The practical limitation of accuracy for any MS is determined by specific factors such as sensor sensitivity, intrinsic noise and ADC performance in terms of bit resolution and range. This high precision signal change detection and measurement system utilises the fundamental characteristic of high sensitivity to initial conditions, exhibited by the chaotic function. This normalised behaviour of the function means that an equivalent high detection resolution can be achieved that is independent of input range.

*Chaos:* Chaotic behaviour can be observed in many non-linear systems that exhibit irregularity and unpredictability and show high sensitivity to initial conditions, commonly known as the ‘butterfly effect’. Although, deterministic and commonly following simple algorithms, chaotic systems display complex behaviour, which in contrary to a linear system, the resultant divergence between two close starting parameter values is exponential. This property is thus used to detect small changes in the initial input conditions taken from a sensor. The simplest way of investigating this phenomenon is to use a discrete ‘one-dimensional (1D)’ chaotic map – ‘logistics map (LM)’.

*Logistics map:* The LM, is analogous to the logistics equation created by the mathematician Pierre François Verhulst and given by the difference equation (2).

The behaviour of one dimensional chaotic functions has been widely studied and a number of implementations and applications have been proposed, over a wide range of different disciplines, such as optics, communications and electronic engineering. In a simple electronic implementation of the LM has successfully been used to design a secure communication system.

The 1D tent map and dyadic functions have been used to measure signals in the form of an ADC, where the piecewise-linear characteristics are doubled and folded. The binary word is obtained from each successive iteration (logic 1 above the threshold and 0 below). These ADC signal measurement methods would only produce high resolution digital outputs, if the respective scaling parameter and the threshold are ideal values. However, inherent practical system errors grow exponentially limiting the resolution. Furthermore, a scaling

factor above the ideal, due to noise, would cause the output to diverge to either supply rail - known as the 'exiting condition' or 'extinction'.

This presented implementation is the first instance of a chaos function being used for signal change detection and is insensitive to system noise and parameter accuracy.

*Signal change measurement technique:* Matlab simulations were used to determine the validity of the measurement system based on the 1D LM chaos function. Firstly, the input value  $X_n$  is applied to the LM function and the resulting output fed back (iterated) a number of times, with the corresponding signature (output value per iteration) stored. A small change is applied to the input and the analysis re-run, where the resultant signature of the second analysis is subtracted from the first to obtain the difference signature. The iteration point where divergence occurs between the respective signatures was found to be proportional to the amplitude of the change in successive input signal samples.

In figure 12, the input  $X_n$  was set to 0.6 of the normalised input range and the map iterated 20 times (a1). The process was repeated for  $X_n = 0.6001$ , and iteration signature (a2) subtracted from (a1) giving the difference (a0). It can be observed that from iteration 1 to 6 there is no significant deviation in the two signatures a1 & a2; however divergence increases for subsequent iterations. By reducing the amount of deviation between successive input signal samples, it was noted that the iteration at which divergence occurs is proportional to the size of the sample difference. Simulations demonstrated that sample changes of magnitudes  $1 \times 10^{-12}$  or less, exhibit signature divergence proportional to the input sample change.

In order for this signal change, measurement technique to be valid, two successive samples taken at different times and at

different amplitudes, but with the same difference should diverge at the same iteration with the same magnitude range. To determine the consistency and repeatability of the technique, a three dimensional simulation graph was developed, as shown in figure 13, where the signature divergence over the full normalised input range, given a  $1 \times 10^{-4}$  change, is shown. It can be observed that the iteration where the divergence is above a specified threshold is constant in the normalised input signal range of 0.1 to 0.9. The non-linear regions  $\leq 0.1$  and  $\geq 0.9$ , exceed the threshold at an earlier iteration, hence these input ranges were avoided in the implemented signal measurement system.

*System implementation:* The LM function, given in equation 1, was implemented utilising readily available low cost electronic components, as shown by the simplified circuit in figure 14, using equation (3); the scaled LM equation for a 10 V input range.

$$X_{n+1} = rX_n(10-X_n) \quad \text{equation (3)}$$

This LM circuit is incorporated into a microcontroller based feedback system, which utilises a low 8-bit ADC to enable storage of the signatures but not used to detect the input signal change. Extensive analysis of the practical system demonstrates a strong correlation with the Matlab simulations, with the minimum change that can accurately be determined in the practical system, after 6 iteration, being  $1 \times 10^{-4}$ , as shown in figure 15. The computed and measured results in figure 15, show the number of iterations where the accumulated deviation

between successive signatures, due to input signal difference, exceeds a specified threshold.

The signal change of 100  $\mu\text{V}$  that can currently be detected, is limited by the practical system induced noise, which is dominated by the multiplier circuitry.

The theoretical Matlab analysis, shown in figure 15, demonstrates that by reducing induced signal noise through improved circuit implementation, signal change detection an orders of magnitude lower is possible. Further improvements in the multiplier design and increased signal range, should enable signal changes in the region of  $< 1 \times 10^{-5}$  – 20-bit resolution, to be achievable.

#### *Conclusions:*

A signal change measurement system based on the 1D LM chaos function has been successfully developed using low cost electronic devices. The system can accurately and consistently measure signal changes of 100  $\mu\text{V}$  in the region of 1 V to 9 V of a 10 V input range, equating to a 16-bit ADC resolution. The fundamental advantage of this signal measurement system, over typical ADCs, is that the size of the signal change that can be measured is independent of the range, thus increasing input signal range increases the overall resolution.

**Figures for the patent application:**

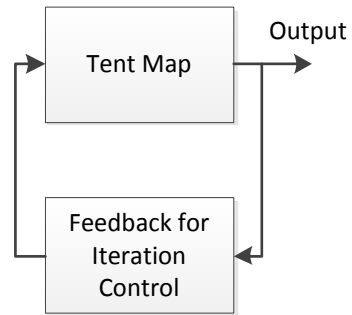


Figure 1

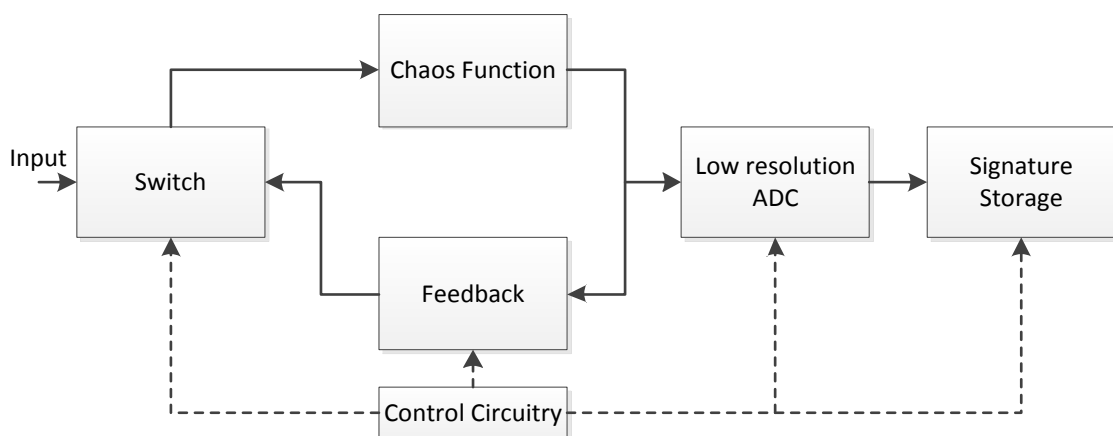


Figure 2

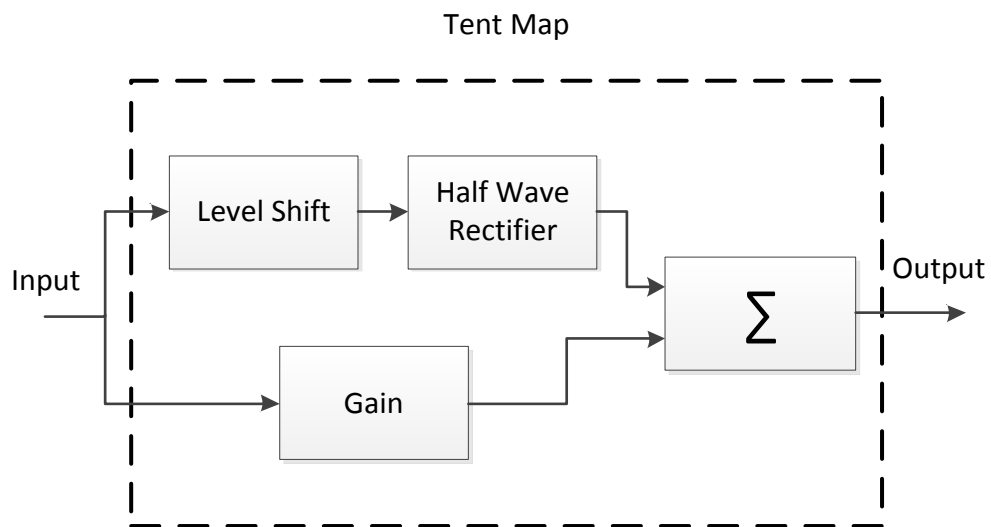


Figure 3

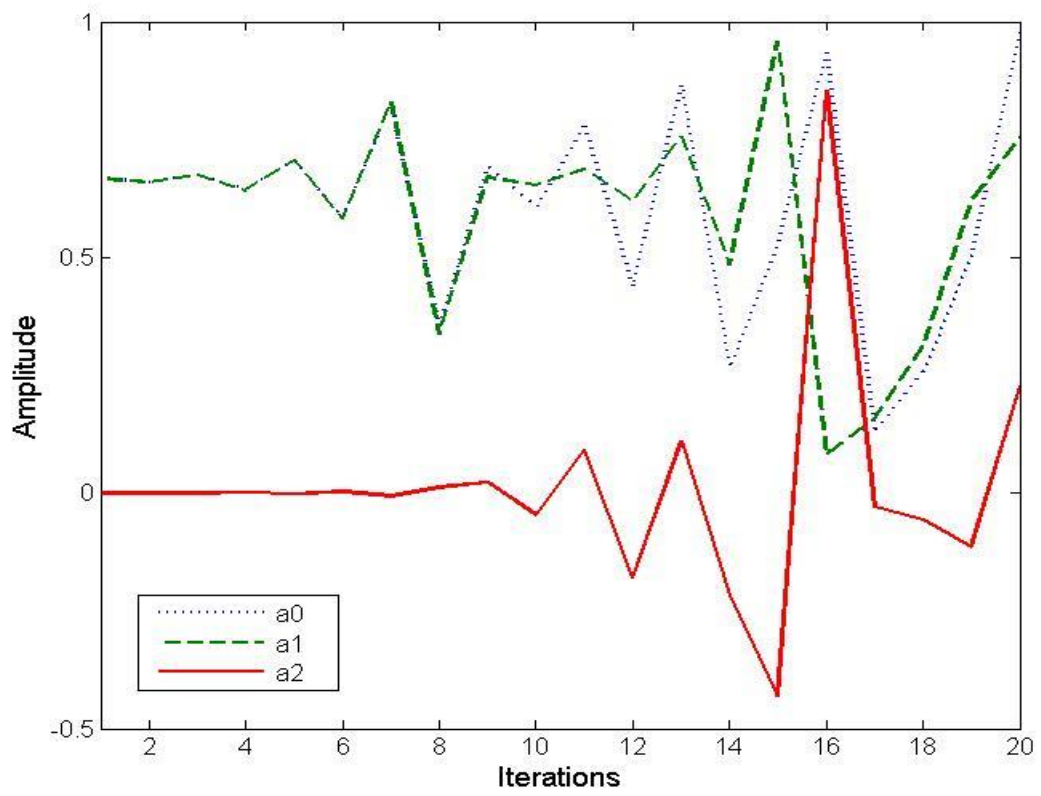


Figure 4

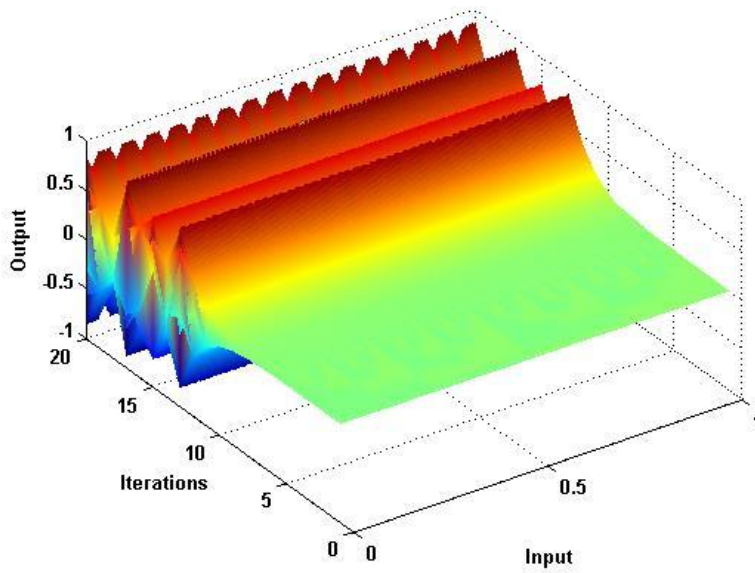
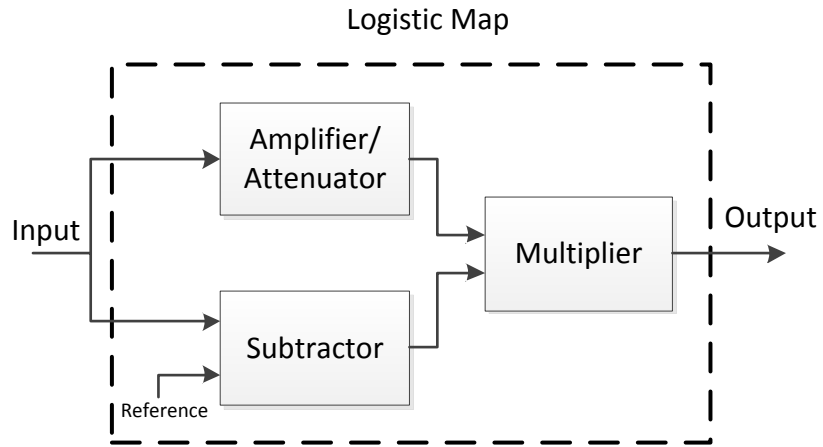
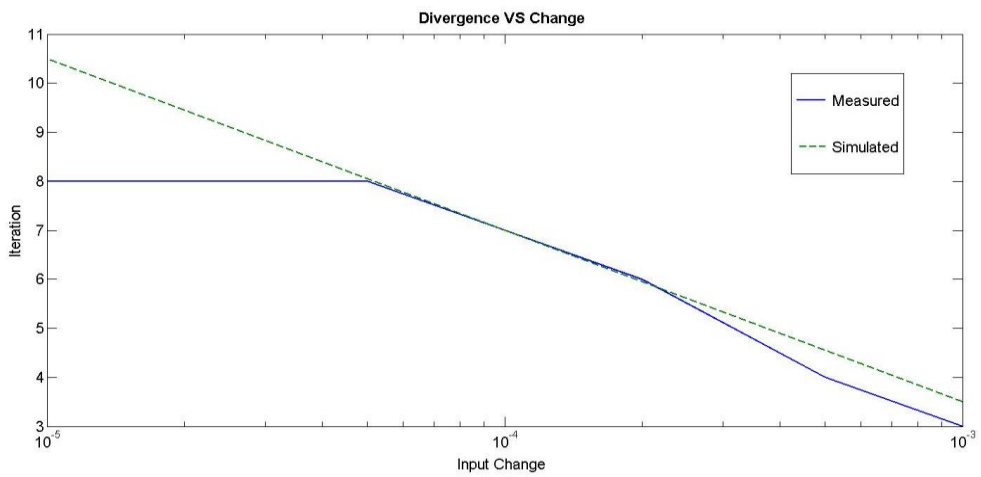


Figure 5



**Figure 6**



**Figure 7**

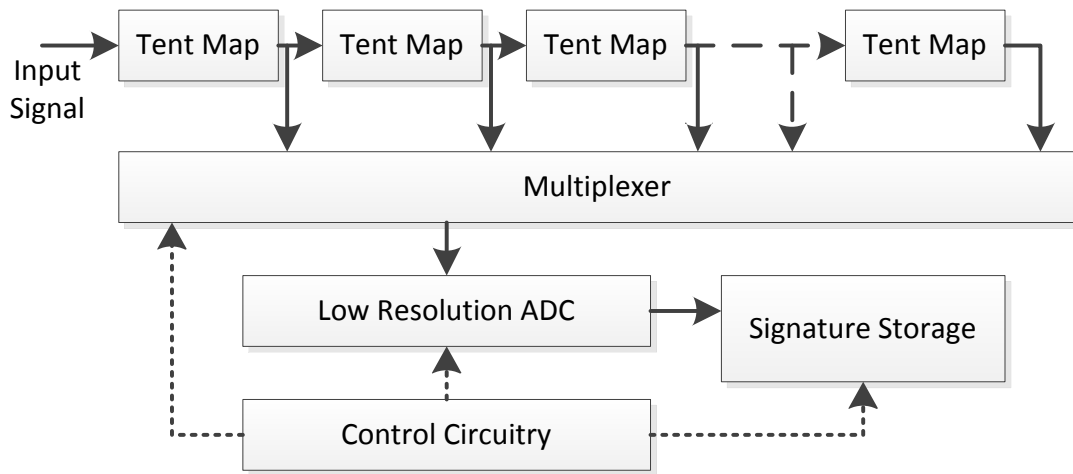


Figure 8

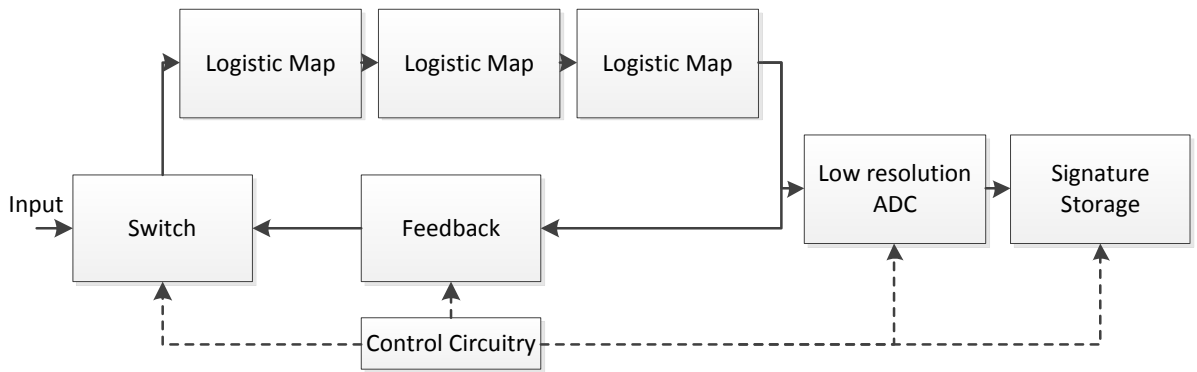


Figure 9

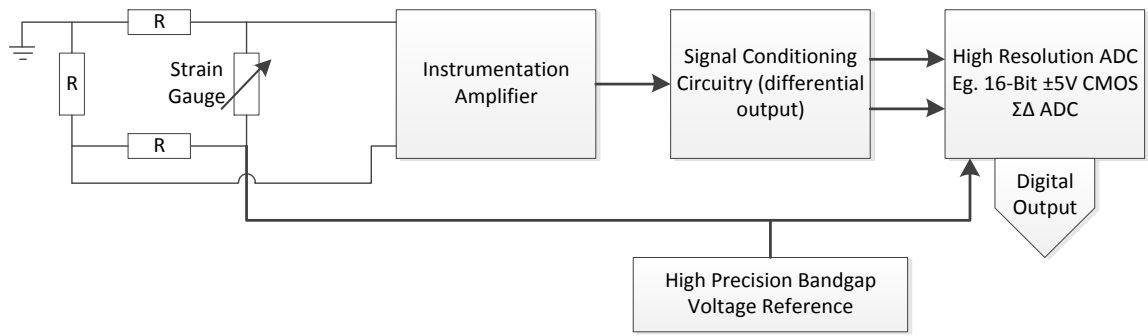


Figure 10

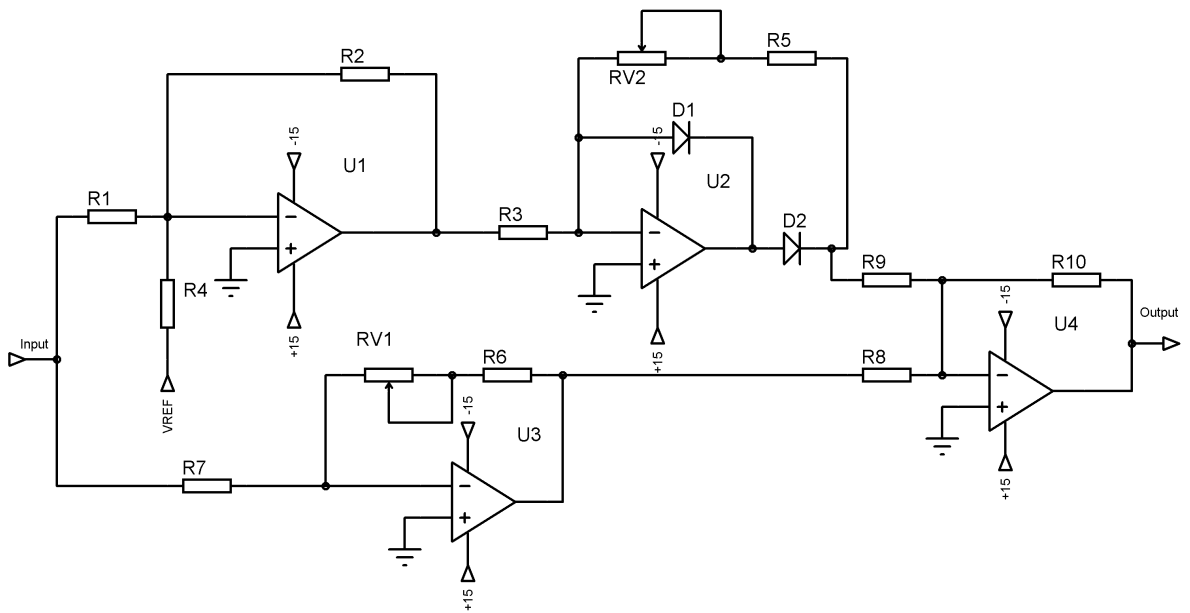


Figure 11

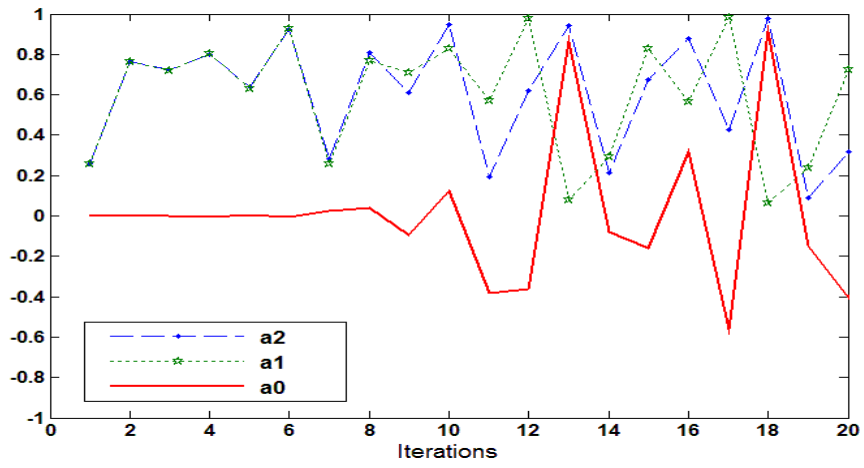


Figure 12

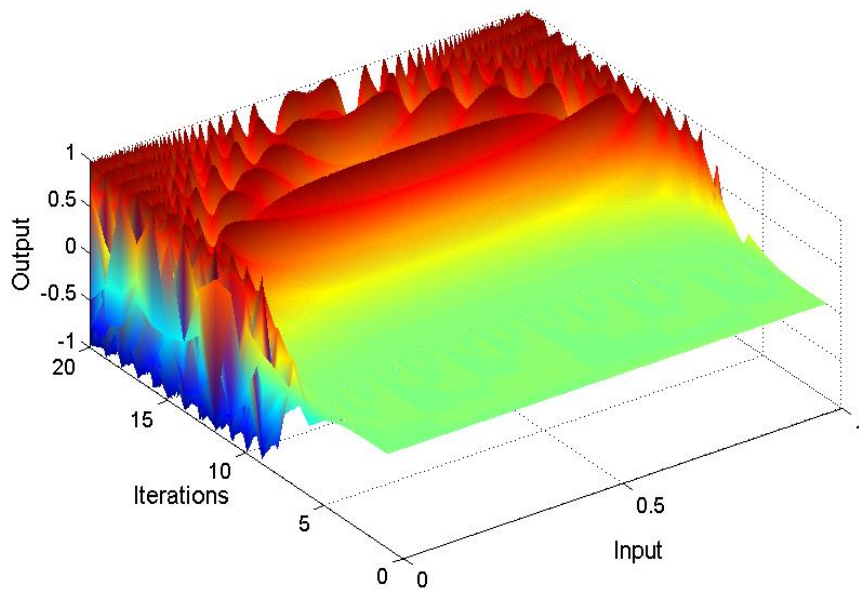


Figure 13

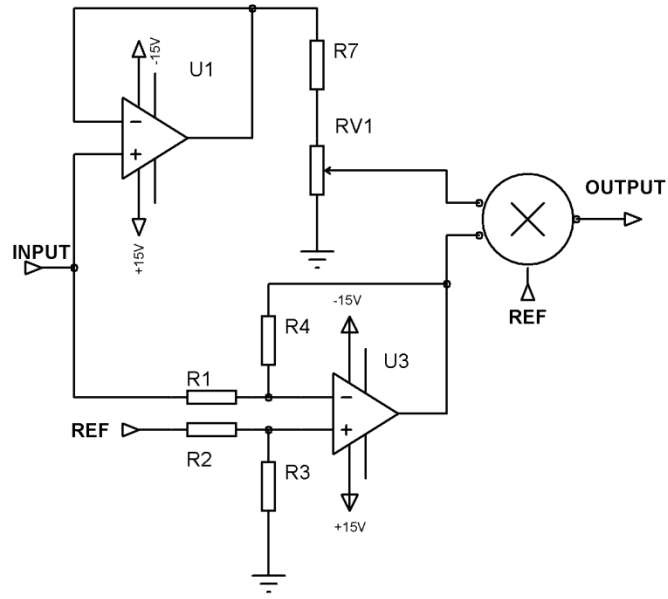


Figure 14

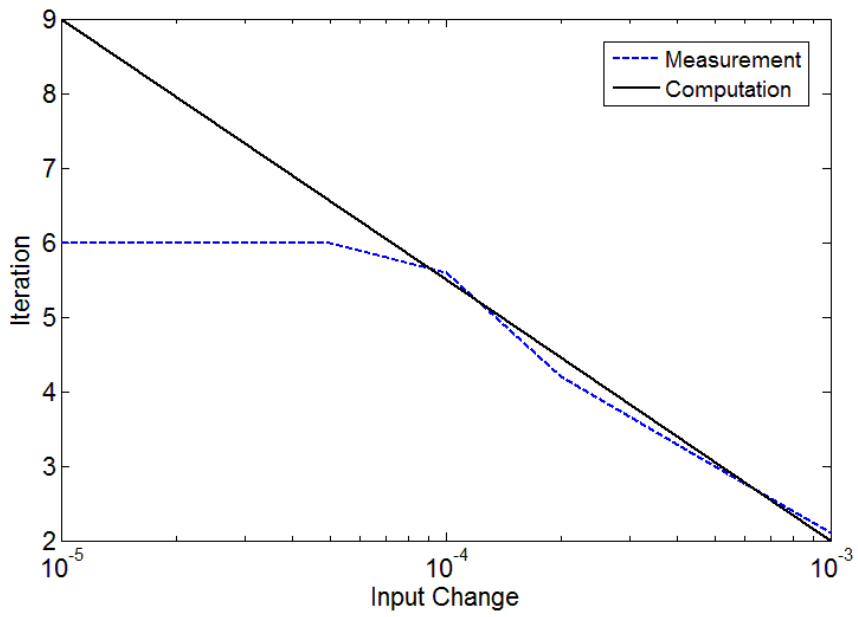
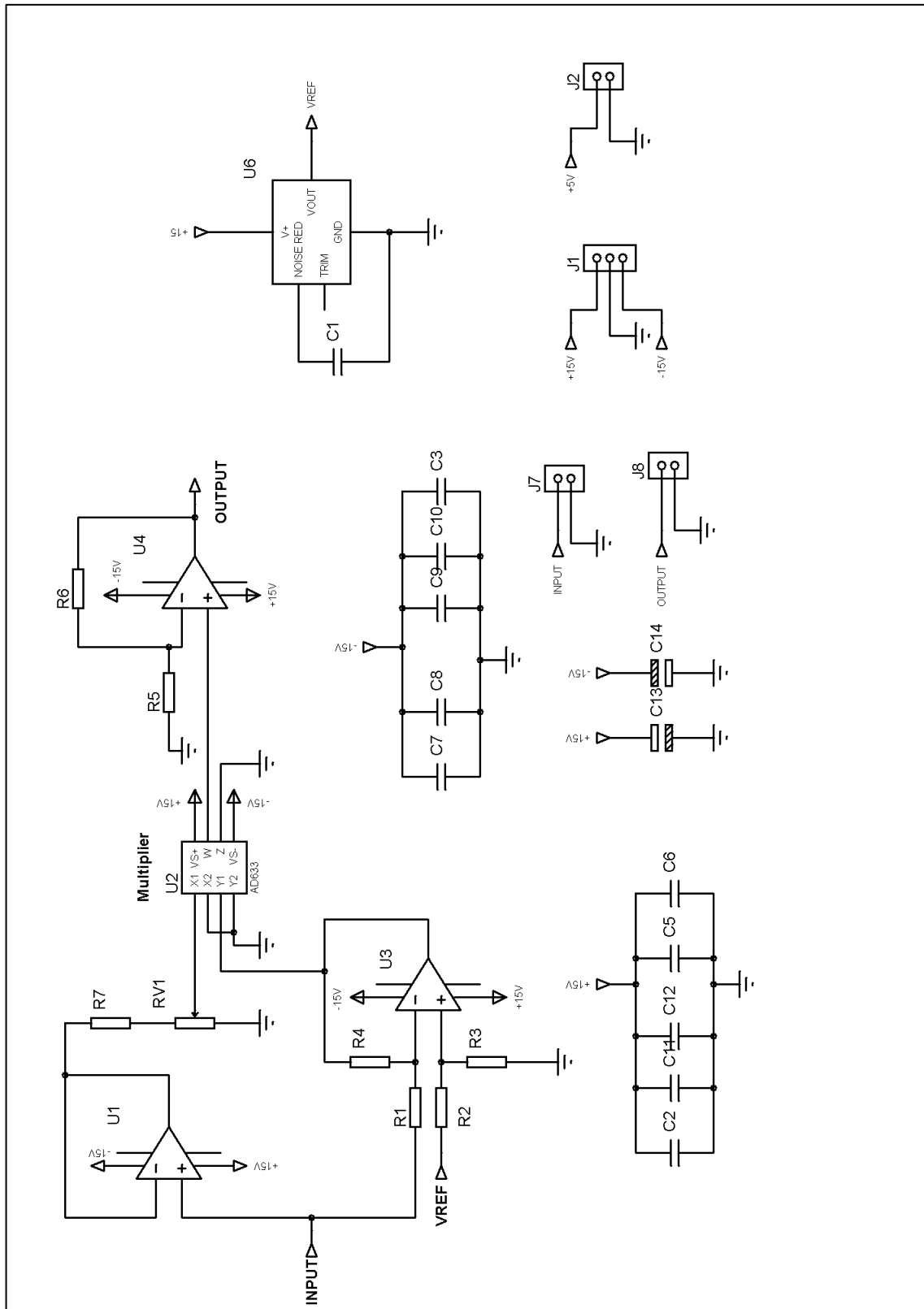


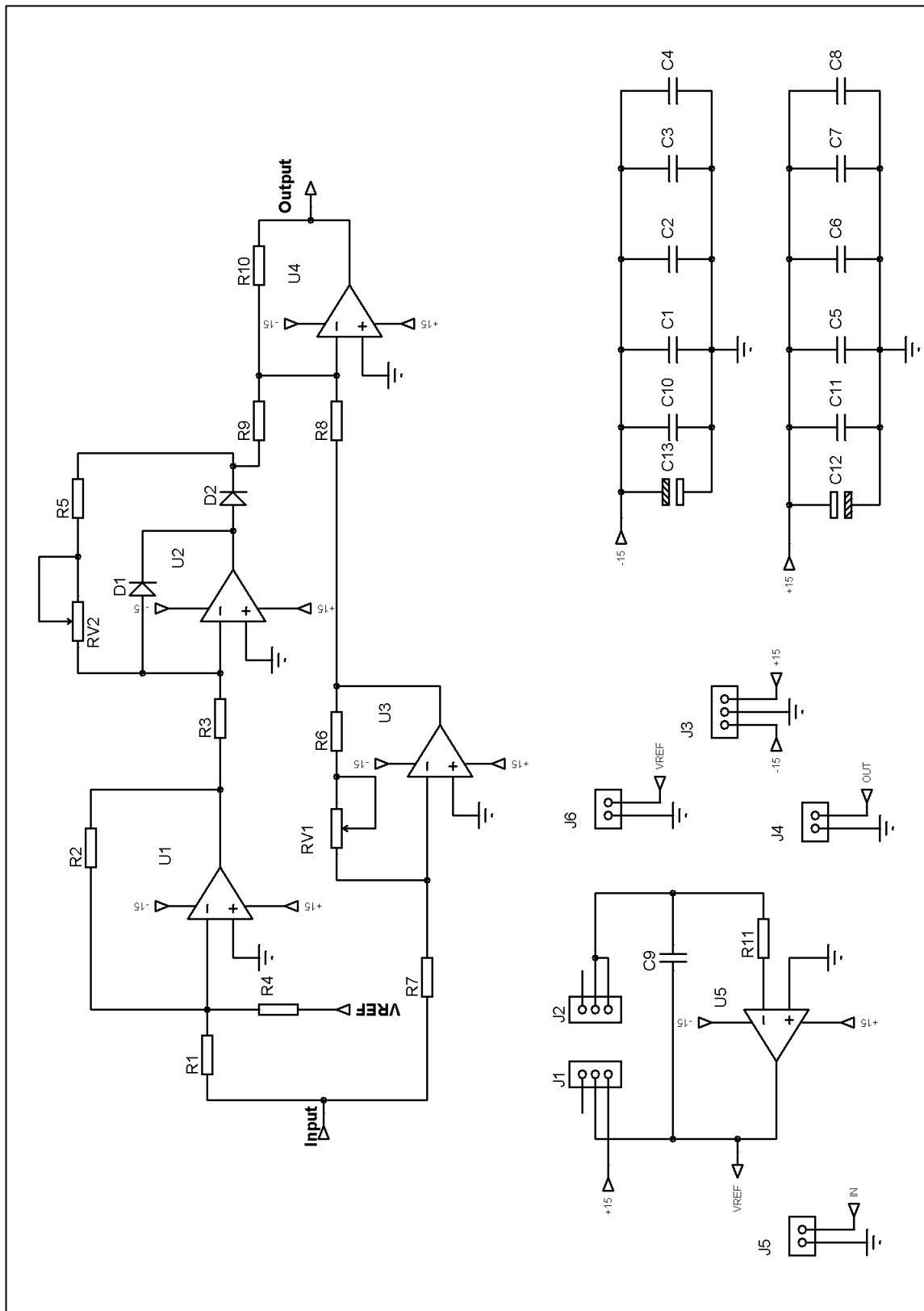
Figure 15

# Appendix G

The full schematics of the LM and the TM are shown, starting with the LM:



Schematic of the TM:



## Appendix H

The component selection process is shown.

### Operational amplifier:

The **OP27** was selected for the low input noise characteristic compared to FET input op-amps, the low voltage drift and high availability; the OP27 is easily sourced from any component supplier and is available in most labs. The table below shows the comparison of key parameter against another commonly found op-amp; the TL071.

Parameter	OP27	TL071
Input offset Voltage	10 $\mu\text{V}$	3 mV
Input Noise at 1kHz	3 nV/ $\sqrt{\text{Hz}}$	18 nV/ $\sqrt{\text{Hz}}$
Temperature Voltage Drift	0.2 $\mu\text{V}/^\circ\text{C}$	18 $\mu\text{V}/^\circ\text{C}$

### Analogue Multiplier:

Analogue multipliers are seldom used which limits their availability compared to other components such as op-amps. Besides being easy to find the **AD633JN** has similar performance compared to other analogue multipliers.

### Voltage references:

The voltage sources used for the electronic implementations of the chaotic maps are the **ADR130** and the **AD587**. The two main criteria of selection were; low noise and high precision. The ADR130 and AD587 have a typical output noise of only 3  $\mu\text{V}$

and 4  $\mu\text{V}$  respectively which is low compared to other voltage reference ICs. Additionally, both voltage references possess an optional noise reduction mechanism allowing for increased noise performance by the use of an external capacitor. Low noise performance combined with high accuracy ( $\pm 0.35\%$  for the AD130 and  $\pm 0.05\%$  for the AD587) makes the two voltage sources ideal for chaos map implementations.

#### Sample and Hold:

The sample and hold (S/H) **LF198** ICs were selected for their performance and availability. Some of the characteristics are;

- Low gain error (0.0002%)
- Low output noise

To increase the performance of the feedback system, polypropylene capacitors were used to reduce the error during sampling along with reset MOSFETS to reduce dielectric absorption errors.

#### Microcontroller:

The microcontroller used is the PIC32MX460L. The choice was mainly guided by practicability as a development board with the PIC32MX460L was already available in the laboratory. More information about the development board can be found in Appendix D. Any microcontroller with the following characteristics could be used instead of the PIC32MX460L to implement the proposed Measurement System (MS):

- At least 4 digital outputs for the feedback and switching control
- An internal low resolution ADC

- Internal RAM to store signal signatures

Additionally the microcontroller could have a user interface and external data storage if required.